# Imaging Cholinergic Function *In Vivo* In The Brain With Radioiodinated Stereoisomers of Quinuclidinyl Benzilate

**DAVID S. PATERSON**

A Thesis submitted for the degree of Doctor of Philosophy
to the Faculty of Medicine, University of Glasgow

Wellcome Surgical Institute and Hugh Fraser Neuroscience Laboratories
University of Glasgow
Garscube Estate, Bearsden Road, Glasgow, G61 1QH

**CONTENTS**.....**Page**

## CHAPTER 2: MATERIALS AND METHODS



## CHAPTER 3: RESULTS

**List Of Tables** **PAGE**

**List Of Figures** **AFTER PAGE**

## List Of Abbreviations

| | | |
|---|---|---|
| 1. | AChE: | acetylcholinesterase |
| 2. | Ach | acetylcholine |
| 3. | AChT | acetylcholine transporter |
| 4. | AD | Alzheimer's Disease |
| 5. | AF64A | ethylcholine aziridinium mustard |
| 6. | AFDX-116 | 11-[2-[(diethylamino)-methyl-1-piperidinyl] acetyl-5, 11 dihydro-6H-[2,3b] [1,4] benzodiazepine-6-one |
| 7. | AMPA | α amino-3-hydroxy-methyl-4-isoxazole proprionic acid |
| 8. | APP | amyloid precursor protein |
| 9. | ApoE | apolipoprotein E |
| 10. | α BgT | α bungarotoxin |
| 11. | n BgT | neuronal bungarotoxin |
| 12. | BA4 | amyloid B |
| 13. | BuChE | butyrylcholinesterase |
| 14. | CCL | cholecystikinin |
| 15. | ChAT | choline acetyl transferase |
| 16. | cChAT | cytoplasmic ChAT |
| 17. | mChAT | membrane bound ChAT |
| 18. | CNS | central nervous system |
| 19. | CT | computed tomography |
| 20. | DA | dopamine |
| 21. | DAG | 1, 2 diacyl-sn-glycerol |
| 22. | 4-DAMP | 4-diphenylacetoxy-N-methylpiperidine methoiodide |
| 23. | DMPP | 1, 1 dimethyl-4-phenylpiperazinium |
| 24. | EEG | electroencephalogram |
| 25. | GABA | γ amino butyric acid |
| 26. | HDB | horizontal limb of the diagonal band of Broca |
| 27. | HEP | heptylphysostigmine |
| 28. | HSSiD | hexahydrosiladifenidol |
| 29. | 5-HT | 5 hydroxy tryptamine |
| 30. | $IP_3$ | inositol 1, 4, 5 trisphosphate |
| 31. | LDT | lateral dorsal tegmental nuclei |
| 32. | mAChR | muscarinic acetylcholine receptor |
| 33. | MH | medial habenula |
| 34. | MLA | methyl caconitine |
| 35. | MRI | magnetic resonance imaging |
| 36. | fMRI | functional MRI |

| | | |
|---|---|---|
| 37. | nAChR | nicotinic acetylcholine receptor |
| 38. | NBM | nucleus basalis magnocellularis |
| 39. | NGF | nerve growth factor |
| 40. | NGFr | low affinity nerve growth factor receptor |
| 41. | NMDA | N-methyl-D-aspartate |
| 42. | NO | nitric oxide |
| 43. | NOS | nitric oxide synthase |
| 44. | NSTX | neosugarotoxin |
| 45. | PET | positron emmission tomography |
| 46. | PG | parabigeminal nucleus |
| 47. | $PIP_2$ | phosphatidyl inositol 4, 5 bisphosphate |
| 48. | PKC | protein kinase C |
| 49. | $PLA_2$ | phospholipase $A_2$ |
| 50. | PLC | phospholipase C |
| 50. | PPT | pedunculopontine tegmental nuclei |
| 51. | PrBCM | propyl benzilylcholine mustard |
| 52. | QNB | quinuclidinyl benzilate |
| 53. | SDHCAU | sodium dependent high affinity uptake system (choline) |
| 54. | SPECT | single photon emmission computed tomography |
| 55. | VDB | vertical limb of the diagonal band of Broca |

**Acknowledgements**

I would like to thank everyone at the Wellcome Surgical Institute for their kindness and generosity throughout the course of my studies.

My greatest thanks go to Professor James McCulloch for his expert guidance and encouragement throughout my time here. I am sure that the experimental thoroughness and attention to detail he has instilled in me will stand me in good stead in my future career.

I would also like to thank Dr Deborah Dewar and Dr Mhairi Macrae for their advice and help.

I am also extremely grateful to both Jonathan Owens and Andrew Tebbutt for supplying me with (R,S)- and (R,R)-[$^{125}$I]-QNB and for their help in performing the metabolite studies. Thanks are also due to Dr Jim Patterson for his help and advice with the kinetic modelling and with the printing of some of the images.

The excellent assistance received from all of the technical staff is gratefully acknowledged. In particular, I would like to thank Margaret Stewart for humouring even the vaguest of my requests and Gordon Littlejohn for putting up with the ever increasing radioligand deliveries.

Many thanks are extended to my colleagues Hilary Carswell, Manuela De Michele, Karen Horsburgh, Elaine Irving, Teresa Jover, Stephen Kelly, Amy Lam, Duncan MacGregor, Louise Marks, Ailsa McGregor, Eileen McCracken, Iain Murdoch, Elaine Peters, Marc Soriano, Omar Touzani and Philipa Yam who have made working here both socially and scientifically stimulating.

Thanks to everyone who knew me at Woodlands Drive, particularly Gav, Gayle, Karen and Liz who made staying in Glasgow a continual party and to everyone else who helped me get beer stains on my ceiling. Special thanks to my mate Andy for all the beers and for always getting the joke, even if he did steal all my patter!

Finally I would like to thank my parents for their constant support (not least financial!) and understanding throughout my entire career, and for feeding me with steak whenever I came home.

## SUMMARY

This thesis evaluates the ability of (R,S)- and (R,R)-[$^{125}$I]-QNB, two radioiodinated diastereoisomers of the high affinity muscarinic antagonist quinuclidinyl benzilate (QNB), to image dynamic changes in cholinergic function in the central nervous system using *in vivo* autoradiography.

The regional uptake and retention of (R,S)-[$^{125}$I]-QNB in the rat brain between 2 and 24 hours after intravenous administration was investigated to assess the utility of this technique to image muscarinic receptors in the central nervous system. The regional uptake and retention of tracer was compared to that of Sawada et al., (1990b) for (R)-[$^{125}$I]-QNB. Similarly, the uptake and retention of (R,R)-[$^{125}$I]-QNB was investigated between 30 mins and 6 hours after administration using *in vivo* autoradiography and was compared to that of (R,S)-[$^{125}$I]-QNB.

Secondly, the sensitivity of (R,S)- and (R,R)-[$^{125}$I]-QNB to dynamic changes in cholinergic neurotransmission *in vivo*, was assessed in conscious rats. The uptake and retention of.(R,S)- and (R,R)-[$^{125}$I]-QNB following a cholinergic challenge produced by administration of the long lasting AChE inhibitor heptylphysostigmine, was investigated. Regional brain levels of (R,S)- and (R,R)-[$^{125}$I]-QNB in heptylphysostigmine treated animals were compared to levels in saline treated animals by *in vivo* autoradiography. The ability of ACh to displace (R,S)- and (R,R)-[$^{125}$I]-QNB binding from rat brain sections *in vitro* in the presence of heptylphysostigmine was also investigated. Finally, the effects of heptylphysostigmine administration on regional cerebral blood flow were investigated using [$^{14}$C]-IAP autoradiography in conscious rats.

### Uptake and Retention Of (R,S)- and (R,R)-[$^{125}$I]-QNB

The *in vivo* uptake and retention of (R,S)-[$^{125}$I]-QNB in the brain of conscious rat was investigated up to 24 hours after tracer administration. At all time points the uptake of tracer was consistent with regional mAChR concentration. Highest levels of radioactivity were observed in the cortex and caudate nucleus, with intermediate levels observed in the thalamus and low levels observed in the cerebellum. Washout of tracer from brain appeared to be dependent upon regional mAChR concentration. Negligible loss of radioactivity was observed in the cortex between 2 and 24 hours (10% reduction) -an area of high mAChR concentration, while significant washout of activity occcurs from the mediodorsal thalamus (40% reduction) -an area of moderate mAChR concentration. These observations are consistent with those of Sawada et al., (1990b) for (R)-[$^{125}$I]-QNB and verify the validity of this methodology to image mAChRs *in vivo*.

The uptake and retention of (R,R)-[$^{125}$I]-QNB in the brain of conscious rat was investigated between 30 mins and 6 hours after administration of tracer. Regional distribution of radioactivity was similar to that of (R,S)-[$^{125}$I]-QNB at all time points and

was consistent with regional mAChR concentration. Retention of (R,R)-[$^{125}$I]-QNB in brain is significantly shorter than that of (R,S)-[$^{125}$I]-QNB. This is most notable in the thalamus where a proportionally greater amount of radioactivity is washed out over a much shorter period of time.i.e. a 70% loss of (R,R)-[$^{125}$I]-QNB over 6 hours compared to a 40% loss of (R,S)-[$^{125}$I]-QNB over 24 hours. Preliminary investigations confirmed that the washout of (R,R)-[$^{125}$I]-QNB occurs more rapidly than that of (R,S)-[$^{125}$I]-QNB from all brain regions.

These observations are consistent with those of a previous study where the *in vivo* dissociation rate of (R,R)-[$^{125}$I]-QNB ($k_1$=0.0654 min-1) from mAChRs was observed to be 13 fold faster than that of (R,S)-[$^{125}$I]-QNB ($k_1$=0.0049 min-1) (Gibson, et al., 1989).

The lower affinity and faster kinetics of binding displayed by (R,R)-[$^{125}$I]-QNB as determined *in vitro* in this thesis and in previous *in vitro* studies (Zeeberg, et al., 1991) support the observations made *in vivo*. It was therefore postulated that (R,R)-[$^{125}$I]-QNB would be more sensitive to changes in synaptic ACh concentration than (R,S)-[$^{125}$I]-QNB and thus a more suitable ligand than (R,S)-[$^{125}$I]-QNB for imaging dynamic changes in cholinergic function *in vivo*.

**Imaging Changes In Cholinergic Function With (R,S)- and(R,R)-[$^{125}$I]-QNB**

The ability to measure ACh release *in vivo* would allow assessment of neurotransmitter function in pathological conditions such as Alzheimer's disease. Quantification of changes in postsynaptic radioligand binding as a result of competition from increased levels of endogenous neurotransmitter would provide an indirect measure of synaptic concentration of neurotransmitter and a means to assess function. This has been successfully demonstrated with the dopaminergic system, where displacement of radioligand from dopamine $D_2$ receptors following amphetamine induced increases in endogenous dopamine, has been quantified non-invasively *in vivo*. using PET and SPECT. The ability to quantify synaptic neurotransmitter concentration in such a manner in the cholinergic system would have significant application for imaging neurotransmitter function in disease states. To this end the sensitivity of (R,S)- and (R,R)-[$^{125}$I]-QNB binding, to a cholinergic challenge produced by the administration of the long lasting AChE inhibitor heptylphysostigmine was assessed with *in vivo* autoradiography. It was postulated that increases in synaptic ACh concentration produced by heptylphysostigmine (which does not itself compete directly for mAChRs) would displace (R,S)- or (R,R)-[$^{125}$I]-QNB binding which could then be quantified.

Heptylphysostigmine administration (2mg/kg) did not induce displacement of (R,S)- or (R,R)-[$^{125}$I]-QNB binding *in vivo*. Similarly $10^{-6}$-$10^{-2}$M ACh failed to displace either (R,S)- or (R,R)-[$^{125}$I]-QNB binding from rat brain sections *in vitro* in the presence of $10^{-}$

$^{6}$M heptylphysostigmine. Contrary to this, heptylphysostigmine administration significantly increased brain levels of (R,S)- and (R,R)-[$^{125}$I]-QNB *in vivo*. Increases were observed predominantly in the cortex with both (R,S)- and (R,R)-[$^{125}$I]-QNB, although a number of sub-cortical regions were also affected. The most consistent and greatest increase with both tracers was observed in the auditory cortex, with an average increase across the time points of 66% and 58% observed respectively for (R,S)- and (R,R)-[$^{125}$I]-QNB.

It was postulated that the increased brain levels of radioactivity measured following heptylphysostigmine administration were the consequence of elevated levels of cerebral blood flow-a known effect of AChE inhibitor administration (Linville et al., 1992). An increased blood flow rate would deliver a greater supply of tracer to the brain and may account for the increases in radioactivity observed in the cortex of heptylphysostigmine treated animals. To this end rCBF was measured in conscious rats by [$^{14}$C]-IAP autoradiography 2 hours after administration of heptylphysostigmine (2mg/kg iv). Significant increases in rCBF were measured in a number of cortical regions including those which displayed increased levels of (R,S)- or (R,R)-[$^{125}$I]-QNB following heptylphysostigmine administration. Hypothetical concentration of radiotracer in the cortex of rat was observed to increase in a similar manner to that measured *in vivo* when the rate of blood flow was raised in a 3 compartment model of tracer uptake and retention. From these observations it was concluded that the increases in regional levels of (R,S)- and (R,R)-[$^{125}$I]-QNB observed following heptylphysostigmine administration are the result of elevated cerebral blood flow.

Three hypotheses were considered to account for the lack of radioligand displacement observed following heptylphysostigmine administration.:

1) Heptylphysostigmine was ineffective in inhibiting AChE and raising synaptic ACh levels at the dosage used in this thesis
2) A small amount of displacement occurred but was masked by the effects of increased cerebral blood flow
3) (R,S)- and (R,R)-[$^{125}$I]-QNB are of too high affinity for mAChRs to be displaced by endogenous neurotransmitter.

A number of factors suggest that the first hypothesis is unlikely. Semi-quantitative AChE histochemistry on sections of rat brain taken from *in vivo* studies with heptylphysostigmine indicate that AChE activity was significantly inhibited in the brain up to 24 hours. *In vivo* microdialysis studies support these results indicating that heptylphysostigmine at the dose used in this thesis significantly inhibits brain AChE activity for prolonged periods

(Messamore et al., 1993, Cuadra et al., 1994). The increases in cerebral blood flow measured following heptylphysostigmine administration-which are known to result from the action of excess ACh on the cerebrovasculature (Taylor, 1990), and the behaviour of animals receiving heptylphysostigmine (salivation, urination, muscle tremor, hypomobility etc) both indicate raised levels of ACh. Additionally, reports in the literature indicate that heptylphysostigmine at this dosage is effective in producing significant increases (i.e. 1000%) in synaptic ACh levels.

The third hypothesis is viewed as the most plausible. Consideration of the the relative affinities of endogenous neurotransmitter and radioligand for mAChRs (KD= 3.3μM and <1nM for ACh and [$^{125}$I]-QNB respectively) together with the resting synaptic concentration of ACh in the normal brain. (3-6nM) indicate that a substantial increase in synaptic ACh concentration would have been necessary to produce even a modest displacement of radioligand binding. It therefore seems unlikely that increasing synaptic ACh concentration with AChE inhibitors is an effective means of displacing (R,S) or (R,R)-[$^{125}$I]-QNB binding *in vivo*. This view is supported by a recent report indicating that a binding potential of between 3-10 for a radioligand is optimal for sensitivity to neurotrasnmitter changes and produces greatest displacement of ligand (Endres and Carson, 1998). Consideration of the binding potential of (R)-[$^{125}$I]-QNB as determined by Sawada et al., (1990b) for frontal cortex BP=1171, parietal cortex BP= 977, caudate nucleus BP=1116, thalamus BP= 247 and cerebellum BP= 51 indicates that both of the high affinity diastereoiosmers (R,S) and (R,R) of radioiodinated QNB will be extremely insensitive to changes in neurotransmitter concentration. In conclusion, (R,S)- and (R,R)-[$^{125}$I]-QNB are unsuitable ligands for the detection of cholinergic function *in vivo*.

## Preface and Declaration

This thesis reports the evaluation of two radioiodinated stereoisomers [(R,S) and (R,R)] of quinuclidinyl benzilate as potential ligands to image dynamic changes in cholinergic neurotransmission in the central nervous system *in vivo*. Results are presented from investigations in two broadly defined areas:

1) The uptake and retention of (R,S)-[$^{125}$I]-QNB in conscious rat brain compared to that of (R,R)-[$^{125}$I]-QNB and that of (R)-[$^{125}$I]-QNB described by Sawada et al., (1990b).

2) The ability of (R,S)- and (R,R)-[$^{125}$I]-QNB to image dynamic changes in cholinergic neurotransmission *in vivo* produced by administration of the cholinesterase inhibitor heptylphysostigmine.

This thesis comprises my own original work and has not been presented previously as a thesis in any form. The assistance of J. Owens in performing HPLC analysis of plasma and brain homogenate samples in metabolite studies is gratefully acknowledged.

# CHAPTER 1
# INTRODUCTION

## 1.1 ACETYLCHOLINE IN THE CNS

### 1.1.1 Cholinergic Pathways In The CNS

ACh is one of the most ubiquitous transmitters in the mammalian CNS. It is involved in the control of a variety of complex functions including learning, memory and modulation of behaviour. Cholinergic neurons exist as both projection neurons and interneurons in nearly all parts of the forebrain, midbrain and brainstem , although they are relatively few in number in the cerebellum. Specific cholinergic markers such as AChE, ChAT, mAChRs and nAChRs are used to identify neurons as cholinergic. Of these markers only ChAT is located pre-synaptically, with the others found both pre- and post-synaptically.

It is not possible to identify the presence of ACh itself by histochemical means, therefore cholinergic pathways in the CNS were originally identified by the presence of the of AChE, the catabolic enzyme for ACh by the pioneering work of Kolle and Shute and Lewis in the 1950s and 1960s (Shute and Lewis, 1967).

AChE is present at cholinergic synapses and can thus be used as a means to identify the location of cholinergic neurons in the CNS. On the basis of AChE histochemistry, Shute and Lewis (1967) identified two major ascending neuronal tracts containing AChE stained fibres. The first of these ascends from the brainstem, projecting dorsally into the thalamus, and ventrally up to the basal forebrain. The second ascends from the basal forebrain to the cerebral cortex (Krnjevic and Silver, 1965). This pattern of AChE distribution and of cholinergic innervation has been confirmed and expanded upon with the use of improved AChE histochemical assays (Butcher and Woolf, 1984).

The presence of AChE however, does not guarantee cholinergic innervation of a particular brain region. AChE is not exclusively located to cholinergic synapses in the CNS and therefore AChE histochemistry cannot be used as the definitive marker for the presence of cholinergic neurons. Not until the development of immunohistochemical and in situ hybridization techniques for ChAT (Crawford. et al., 1982, Ruggiero et al., 1990, Woolf, 1991) the synthetic enzyme for ACh, could neurons be unequivocally identified as cholinergic. Both of these techniques are highly specific for the identification of cholinergic neurons. The presence of ChAT mRNA as verified by in situ hybridization is now accepted as the definitive technique for the identification of cholinergic neurons (Butcher et al., 1993).

Comparison of the pattern of cholinergic neurons identified with each of the above techniques produces a pleasingly high degree of correlation. The results observed with AChE histochemistry (Talbot et al., 1988), ChAT in situ hybridization (Woolf,1991) and ChAT immunohistochemistry (Ruggiero et al., 1990) authenticate the observations of Shute and Lewis (1967) in identifying two main cholinergic pathways within the mammalian brain. These two pathways incorporate eight major cholinergic cell groups which project to a variety of CNS structures and are constitutive of the major cholinergic innervation of the

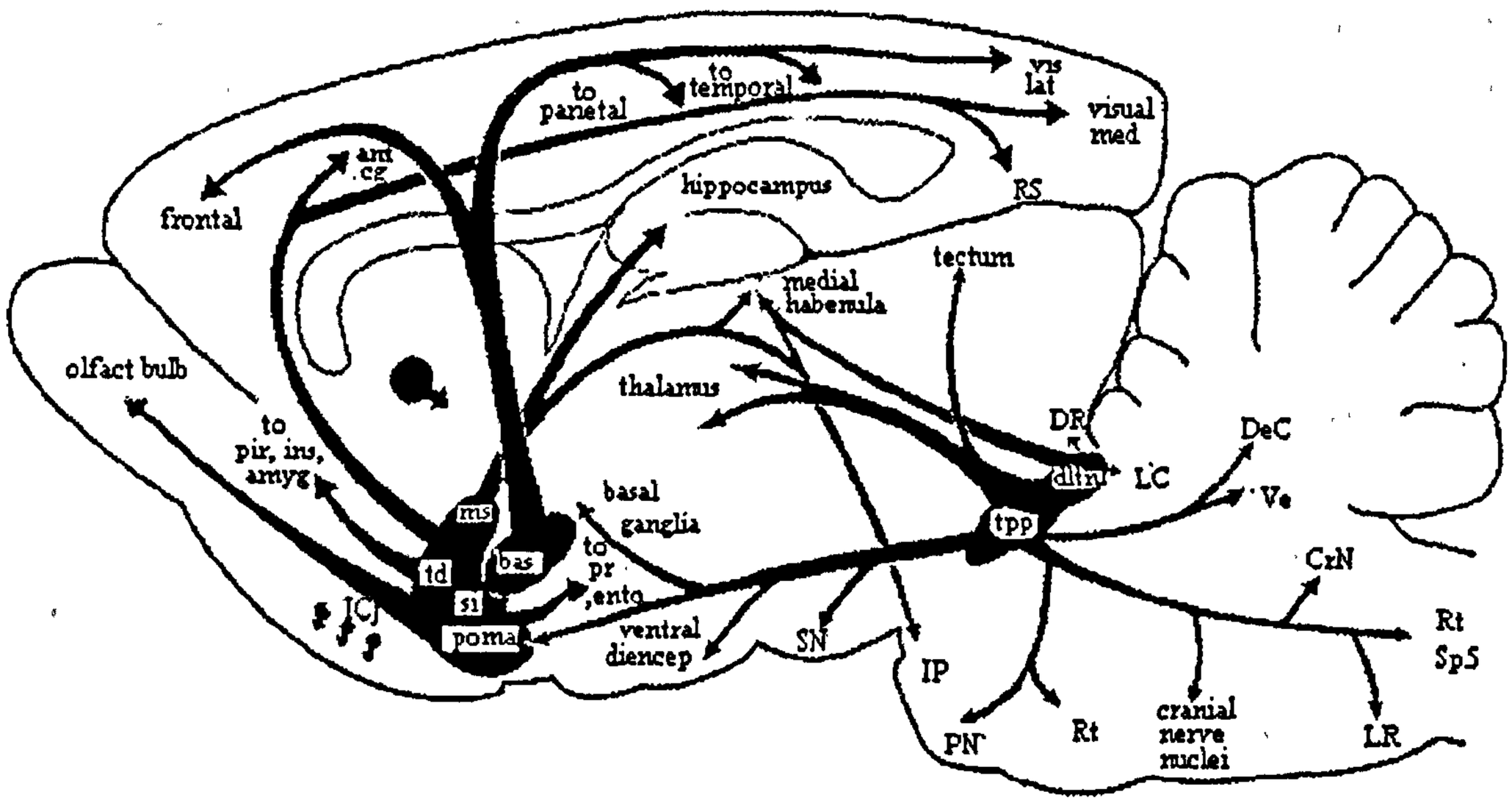


**Fig 1:** Schematic representation in the horizontal plane of the major cholinergic systems in mammalian brain. Illustration shows 2 major cholinergic projection pathways : the basal forebrain cholinergic complex consisting of the medial septum (ms), vertical and horizontal limbs of the diaginal band of Broca (td) , substantia inominata (si), and nucleus basalis (bas) which project to the cortex and hippocampus; and the pontomesencephalo-tegmental cholinergic complex consisting of the pedunculopontine (tpp) and laterodorsal (dltn) tegemental nuclei which project to the thalamus and descendingly to the pontine and medullary reticular reticular (Rt) formations. Additional abbreviations: amyg-amygdala, ant cg-anterior cingulate cortex, DeC-deep cerebellar nuclei, CrN-dorsal cranial nerve nuclei, diencep-diencephalon, DR-dorsal raphe nucleus, ento-entorhinal cortex, frontal-frontal cortex, ICj-Islands of Calleja complex, ins-insular cortex, LC-locus ceruleus, LR-lateral reticular nucleus, olfact bulb-olfactory bulb, pir-piriform cortex, PN-pontine nuclei, pr-perirhinal cortex, parietal-parietal cortex, SN-substantia nigra, Sp5-spinal nucleus of the cranial nerve 5, temporal-temporal cortex, Ve-vestibular nuclei, vis lat-lateral visual cortex, visual med-medial visual cortex.

CNS. The projecting cell groups include cholinergic neurons associated with the basal forebrain including the medial septal nucleus (MS), vertical and horizontal limbs of the diagonal band of Broca (VDB and HDB), and the nucleus basalis of Meynert (NBM). The other major cholinergic cell groups include the pedunculopontine tegmental nucleus (PPT) and the laterodorsal tegmental nucleus (LTD) of the rostral brainstem, the medial habenula (MH) and the parabigeminal nucleus (PG) [see Fig1]. The majority of these cell groups are not restricted to traditional nuclear boundaries and the neurons contained within them are not homogenous for ACh (Mesulam, 1988). Most notably GABAergic neurons are present within these nuclei (Gulyas et al., 1990).

With this in mind Mesulam (1988) devised the Ch1-Ch8 nomenclature to classify the cholinergic neurons within these cell groups -see Table 1 (Mesulam, 1988). When applied, this nomenclature refers only to the cholinergic neurons within a traditional neuroanatomical region. Tracer experiments in animals have indicated that the Ch1 and Ch2 cell groups (MS and VDB) provide the main cholinergic innervation for the hippocampus, projecting through the septo-hippocampal pathway. The neurons synapse mainly on hippocampal pyramidal and dentate gyrus granule neurons (Wainer et al., 1993). The Ch3 (HDB) projects mainly to the olfactory bulb, Ch4 (NBM) to the cortex and amygdala, CH5 and Ch6 (PPT and LDT) to thalamic nuclei, Ch7 (MH) to interpenduncular nucleus and Ch8 (PG) to the superior colliculus (Mesulam, 1990). Despite the identification of multiple cholinergic cell groups, the major ascending cholinergic projections conform to the original pattern identified by Shute and Lewis (1967) of two major cholinergic pathways. One originating in the magnocellular basal forebrain and a second arising from the mesopontine tegmental cholinergic cell group in the rostral brainstem. These two ascending cholinergic cell groups will now be discussed.

**Basal Forebrain Cholinergic Neurons Ch1-Ch4**

The basal forebrain is made up of a constellation of four groups of cholinergic projection neurons (Ch1-Ch4) consisting of the MS, VDB, HDB and the NBM which is the largest of the cell groups. All of the neurons in Ch1-Ch4 stain positively for AChE and ChAT, identifying them as cholinergic (Mesulam and Geula, 1988). A significant proportion of these neurons are immunoreactive for p75 NGFr, the low affinity nerve growth factor receptor (Mesulam et al., 1989). Nerve growth factor (NGF) is a neurotrophin that appears to be critical in the development and maintenance of cholinergic neurons (Levi-Montaclini and Angeletti, 1968, Kew and Sofroniew, 1997). With the exception of a few striatal interneurons, the cholinergic neurons of the basal forebrain are

**Table 1**

**Nomenclature and Major Projections of Cholinergic Cell Groups in the Brain**

| Cholinergic Cell Group | Anatomical Cell Group | Abbreviation | Major Projection |
|---|---|---|---|
| Ch1 | Medial septal nucleus | MS | Hippocampus |
| Ch2 | Vertical limb of the diagonal band of Broca | VDB | Hippocampus |
| Ch3 | Horizontal limb of the diagonal band of Broca | HDB | Olfactory bulb |
| Ch4 | Nucleus basalis of Meynert (Magnocellularis) | NBM | Cerebral cortex |
| Ch5 | Pedunculopontine tegmental nucleus | PPT | Thalamus |
| Ch6 | Lateraldorsal tegmental nucleus | LDT | Thalamus |
| Ch7 | Medial habenula | MH | Interpenduncular nucleus |
| Ch8 | Parabigeminal nucleus | PG | Superior colliculus |

Nomenclature and classification of cholinergic cell groups is based upon that of Mesulam, (1988) for human brain.

thought to be the main site of action of NGF in the CNS. Several lines of evidence are available to support this theory. Immunoreactivity for p75 NGFr co-localises with ChAT, the specific cholinergic marker, in neurons in the basal forebrain (Wainer et al., 1993). Injection of radiolabelled NGF into cortex or hippocampus results in the retrograde labelling of neurons in the basal forebrain (Schwab et al., 1979) and injection of NGF intraventricularly into neonate rats produces increased levels of ChAT in basal forebrain neurons (Gnahn et al., 1983).

Experimental lesion of neurons arising from the basal forebrain has highlighted the degree to which NGF is necessary to sustain the viability of cholinergic neuronal function. Studies involving transection of the fimbria-fornix, the pathway through which Ch1-Ch2 (MS and VBD) neurons project to the hippocampus, results in a marked reduction in the size and number of neurons in these areas of the basal forebrain (Gage et al., 1986). Injection of an immunotoxin specific for p75 NGFr into the hippocampus results in near total depletion of hippocampal cholinergic neurons, with a correlated significant decrease in cholinergic neurons in the MS and VDB (Ohtake et al., 1997). Destruction of the connection between the MS and VDB and the hippocampus in this manner appears to deprive the cholinergic neurons in the MS and VDB access to the high levels of NGF found in this structure resulting in their degeneration. By providing the neurons with a supply of NGF post-lesion via intraventricular injection, the neuronal degeneration normally observed can be prevented (Kromer, 1987). The ability of NGF to reverse neurodegeneration has led to its proposal as a therapeutic agent in the treatment of neurodegenerative conditions such as Alzheimer's disease. In this vein, infusion of NGF has been shown to ameliorate age related memory deficits and atrophy of the basal forebrain (Fischer, et al., 1987). NGF appears to be critical for the survival and function of cholinergic neurons in this region. The exact mechanism by which NGF exerts its trophic effects has yet to be elucidated, but the presence of NGFr is known to be necessary (Hempstead et al., 1989). Cholinergic neurons in the basal forebrain synthesise p75 NGFr in their perikaya. The receptor is then transported intraxonally into the cortex, where it binds with cortically produced NGF. The NGF-NGFr complex is then transported retrogradely back into the cell body of the basal forebrain cholinergic neuron where it exerts is trophic effect (Hefti et al., 1986). As the cholinergic neurons of the basal forebrain are the only neurons expressing NGFr in large amounts, its presence can be used to identify the neuron not only as cholinergic, but as a cholinergic neuron originating in the basal forebrain. The reverse case does not hold however, as not all cholinergic neurons in the basal forebrain express NGFr and thus its absence does not exclude the neuron from being cholinergic.

Recent investigations, however, have begun to question the role of NGF in maintenance of adult cholinergic neurons. In contrast to fimbria-fornix transection of hippocampal neurons, destruction of NGF synthesising neurons produced no subsequent degeneration of MS cells. This suggests that NGF is not required for the maintenance of adult neurons in this region,

that NGF is synthesised in novel sites outside of the hippocampus or that other trophic factors may be involved (see-Wainer et al., 1993 for discussion).

The Ch4 neurons of the basal forebrain provide the major cholinergic innervation of the cerebral cortex. The entire cerebral cortex receives a dense cholinergic innervation as mapped out by AChE histochemistry (Geula and Mesulam, 1989) ChAT immunohistochemistry (Mesulam et al., 1991) and NGFr immunoreactivity (Mesulam et al., 1992). In neurodegenerative diseases such as Alzheimer's, where there are severe cognitive deficits, there is a significant correlation between the loss of pre-synaptic cortical cholinergic markers and the loss of cell bodies in the NBM (Ch4) of the basal forebrain (Price, 1986).

In contrast to the cerebral cortex, cholinergic innervation of the thalamus by basal forebrain neurons is minimal, as evinced by NGFr immunoreactivity (Mesulam, 1995). The mediodorsal and reticular thalamic nuclei displaying the most dense innervation (Hallanger et al., 1987). As with thalamic nuclei, the basal ganglia receive minimal cholinergic input from the basal forebrain cholinergic complex, with the striatum displaying greatest NGFr immunoreactivity . The basal ganglia does however receive substantial cholinergic innervation (displaying intense ChAT staining), the majority of which is intrinsic, arising from numerous cholinergic interneurons (Mesulam et al., 1992).

**Mesopontine Tegmental Cholinergic Neurons Ch5-Ch6**

The cholinergic projection neurons of the mesopontine consist of the pedunculopontine (PPT) and lateral dorsal (LDT) tegmental nuclei, with both regions staining intensely for ChAT (Butcher et al., 1992). The LDT is located slightly more caudally than PPT, but as with other cholinergic projection nuclei, there is no confinement to traditional neuroanatomical boundaries and thus no precise delineation between the two nuclei. The PPT and LDT neurons have been found to express a rich NADPH diaphorase (NADPHd) content (Vincent et al., 1983), which is known to be analogous to nitric oxide synthase (NOS) (Hope et al., 1991). A combined NOS mRNA in situ hybridization and ChAT immunocytochemistry study revealed that these markers are colocalized in the majority of PPT and LDT neurons (Sugaya and McKinney, 1994). PPT and LDT neurons are also immunoreactive for several neuropeptides including atrial natriuretic peptide (ANP) and substance P, although their function in these brain regions has yet to be elucidated (Standaert et al., 1986).

The cholinergic neurons of the Ch5-Ch6 mesopontine tegmentum project to a variety of ascending and descending target nuclei. The most substantial ascending projections are to the thalamus, which receives its major cholinergic innervation from mesopontine projection neurons (Hallanger et al., 1997). Minor projections arising from the mesopontine cholinergic complex include those to cortical, extrapyramidal and limbic structures and to the basal forebrain (Preda et al., 1993). Descending projections provide innervation of the superior

colliculus and pontine and medullary nuclei (Hallanger and Wainer, 1988). The PPT projects to virtually all thalamic nuclei, whereas the LDT projects more selectively to the anterior, laterodorsal, central medial and mediodorsal thalamic nuclei which are closely associated with the limbic system (Hallanger et al., 1987). The PPT also has limited connections with extrapyramidal structures, particularly the SNc (Lee, et al., 1988). Innervation of basal forebrain structures is minor, with evidence suggesting that mesopontine projection neurons synapse only on non-cholinergic neurons in the NBM (Martinez-Murillo et al., 1990).

## 1.1.2 Functional Aspects Of Cholinergic Neurotransmission

### Synthesis, Storage and Release Of Acetylcholine

ACh is synthesised from choline and acetylcoenzyme A (acetylCoA) in the terminals of cholinergic neurons in a reaction catalysed by the enzyme choline-*O*-acetyltransferase (ChAT) (Tucek, 1985). Newly formed ACh is then transported into cholinergic synaptic vesicles in the nerve terminal by an energy dependent active transport mechanism (Parsons, S.M. et al., 1993). Depolarisation of the nerve terminal by the invasion of a propagating action potential results in release of ACh from vesicles by a calcium dependent exocytotic process. Once released, ACh is free to interact with postsynaptic cholinergic receptors (nicotinic or muscarinic) to produce a postjunctional response, before it is hydrolysed into choline and acetate by acetylcholinesterase (AChE), the degradative enzyme for ACh.

The most influential factor governing cholinergic neurotransmission is the supply of the precursor choline. The supply of choline is the rate limiting step in ACh synthesis and is strongly influential on the rate of release . The axoplasm of a cholinergic nerve contains only a small supply of choline (Potter, 1970) and the brain cannot synthesise choline de novo at a significant rate (Lakher and Wurtman, 1987). Therefore, the majority of choline needed for synthesis is supplied in diet and is obtained from the extracellular fluid surrounding the neuron . Choline is also obtained from the hydrolysis of previously released ACh (Potter, 1970 ).

A sodium dependent high affinity uptake system (SDHACU) present in the pre-synaptic membrane of cholinergic neurons exists to transport choline into the nerve terminal (Yammmamura, and Snyder, 1973). This transport system is intrinsically linked to ACh synthesis, with virtually all choline transported by this means converted into ACh. A low affinity carrier facilitated transport mechanism for choline also exists. This system is thought to be present in all neurons, however, and is involved in the transport of choline for phopholipid synthesis. Transport of choline by the high affinity system is potently inhibited by drugs such as hemicholinium-3 (HC-3) and troxypyrrolinium which in turn inhibit ACh synthesis and release.

The rate of choline uptake (and thus ACh synthesis) is accelerated following depolarisation of the nerve terminal and release of ACh (Potter, 1970, Collier and Katz, 1974). In this vein, it has been suggested that prior release of ACh is necessary for choline uptake (Murrin et al., 1977) and that the rate of choline transport is inversely proportional to the vesicular concentration of ACh in the presynaptic terminal (Yammamura and Snyder, 1973). Release and synthesis of ACh are thus intrinsically linked, ensuring that the rate of synthesis keeps pace with the demand for neurotransmitter (Browning and Schulman, 1968).

The activity of the synthesising enzyme ChAT is not a rate limiting factor in ACh synthesis(Salvaterra and Vaughn, 1989), Evidence suggests, however, that it may be indirectly involved. Two forms of the enzyme exist, cytosolic ChAT (cChAT) and membrane bound ChAT (mChAT). Cytosolic ChAT accounts for the majority of the enzyme in nerve terminals, with mChAT constituting the remaining 10-20% . Membrane bound ChAT forms part of a presynaptic membrane bound complex which is structurally or functionally associated with the SDHACU system. Thus mChAT activity may influence the rate of ACh synthesis by indirectly affecting choline uptake (Jope et al., 1979).

ChAT activity is regulated by a number of hormones and growth factors including thyroid hormone, oestrogen, interleukin-3, basic fibroblast growth factor, brain derived neurotrophic factor and nerve growth factor (Rylett and Schmidt, 1993). In particular, enzyme activity is sensitive to ionic conditions in the nerve terminal, the concentration of chloride ions having a major effect (Rossier et al., 1977). The enzyme is inhibited by a number of naphthylvinylpyridines, monohalogenated AChs and halogenoacetonyl-trimethylammonium compounds (Parsons et al., 1993).

Once synthesised in the cytosol, newly formed ACh is transported into synaptic vesicles in the nerve terminal for storage. An energy dependent active transport system located in the vesicle membrane exists to transport ACh from the cytosol into vesicles. ACh is stored in the vesicle at a concentration approximately 100 fold greater than that in the cytosol (Parsons et al., 1993). The vesicular ACh transporter (AChT) consists of two macromolecular components. The first is a proton pumping ATPase known as V-Type ATPase (Yamagata and Parsons, 1989). This pumps protons into the vesicle acidifying it creating a pH gradient across the membrane (Michaelson and Angel, 1980). The production of this pH gradient allows the AChT to concentrate ACh within the vesicle. The second component consists of the AChT itself, which exchanges vesicular protons for cytosolic ACh (Rebois et al., 1980). Storage of ACh in the vesicle can be blocked by the compound vesamicol, which in turn also inhibits ACh release (Marshall, 1970). Vesamicol prevents storage of ACh in vesicles by non-competitive inhibition of the AChT, binding to a site distinct to that of ACh (Bahr and Parsons, 1986).

ACh is released from cholinergic nerve terminals by a calcium dependent exocytotic process that usually occurs at the active zones in the pre-synaptic membrane(Parsons et al., 1993). Two forms of release exist. The first occurs in quiescent nerves where there is a spontaneous release of a single quanta of ACh that can be detected electrophysiologically as a spontaneously occurring miniature end plate potential (mepp). The frequency of this release is dependent on the intraterminal $Ca^{2+}$ concentration (Silinsky, 1985). The second form is evoked release of neurotransmitter. Evoked release occurs when a cholinergic nerve terminal is invaded by an action potential. Depolarisation of the terminal membrane occurs, causing voltage sensitive $Ca^{2+}$ channels to open, resulting in a transient rise in intraterminal

$Ca^{2+}$ ion concentration. This leads to the synchronous release of a large number of quanta of ACh ( For review of mechanism of release see Parsons et al., (1993).

This $Ca^{2+}$ dependent release of ACh from cholinergic neurons is modulated by a number of auto-, homo- and heteroreceptors located pre- and post-synaptically at cholinergic synapses (Pepeu et al., 1990). These receptors alter the intraterminal $Ca^{2+}$ ion concentration to either enhance or inhibit transmitter release. In each distinct brain region cholinergic neurons are equipped with different sets of these receptors making differential regional modulation of ACh release possible (Pepeu et al., 1990). Modulatory receptors include mAChRs, nAChRs, dopamine $D_2$, glutamatergic NMDA, cholecystekinin (CCK), opioid, GABA, adenosine $A_1$, 5-HT and $\alpha_2$ adrenoceptors (Table 2) .

Although the electrophysiological events resulting in ACh release are well understood, there is in contrast, divided opinion as to the mechanism by which transmitter is released from the nerve terminal. There are two main hypotheses, the vesicular exocytosis hypothesis and the membrane gate hypothesis. According to the former theory, all releasable ACh is stored within synaptic vesicles, with the readily releasable fraction of ACh stored in the vesicles nearest to the site of release. A larger reserve of transmitter is stored in vesicles lying further away from the release sites. Release of ACh occurs when there is a $Ca^{2+}$ dependent fusion of the vesicle membrane and the nerve terminal membrane, resulting in the expulsion of the vesicular contents by exocytosis (Silinsky, 1985).

The membrane gate hypothesis is based upon the supposition that ACh stored within vesicles represents transmitter reserve. Quantal release of ACh is produced by the opening of $Ca^{2+}$ sensitive membrane gates in the pre-synaptic terminal that allow fixed quantities of axoplasmic ACh to escape. Thus, according to this hypothesis, axoplasmic ACh represents the readily releasable store of transmitter and vesicular ACh represents transmitter reserve which can be released into the axoplasm as and when necessary. For a discussion of the relative merits of these hypotheses see Bowman, 1990 and Parsons, et al., 1993 (Parsons . et al., 1993).

Once released into the synaptic cleft ACh has a very short period of time in which to effect a response before it is hydrolysed by a cholinesterase enzyme. Hydrolysis is extremely rapid, one molecule of ACh being broken down by AChE every 80-100$\mu$s (Quinn, 1987). Vertebrates possess two cholinesterase enzymes, AChE (acetyl acylhydrolase, acetylcholinesterase or true cholinesterase) and pseudo- or butyrylcholinesterase (BuChE). These enzymes catalyse the hydrolysis of the ester bond in ACh, producing choline and acetate. AChE is highly specific for ACh and will hydrolyse it in favour of other choline esters (Massoulie' et al., 1993). BuChE is less specific for ACh, and is thought to regulate the synaptic level of ACh only when AChE is saturated. Both enzymes are present pre- and post-synaptically, and display a variety of different molecular forms (Massoulie and Bon, 1982). The catalytic site of an AChE molecule consists of two subsites. The anionic site, which attracts and holds the positively charged nitrogen group of ACh and the esteratic site,

## Table 2

### Pre- and Postsynaptic Receptors Influencing Release of ACh

| Region | Receptor | Location | Effect on release |
|---|---|---|---|
| **Forebrain** | $M_1$-$M_5$ | Presynaptic | Decrease |
| | $D_2$ | Postsynaptic | Increase |
| | CCK | Postsynaptic | Increase or Decrease |
| | GABA | Postsynaptic | Decrease |
| | Opioid | Postsynaptic | Decrease |
| | 5-HT | Postsynaptic | Decrease |
| **Striatum** | $M_1$, $M_2$ | Presynaptic | Decrease |
| | $D_2$ | Postsynaptic | Decrease |
| | NMDA | Postsynaptic | Increase |
| | 5-HT | Presynaptic | Decrease |
| | $A_1$ | Presynaptic | Decrease |
| | k-opioid | Presynaptic | Decrease |
| **Hippocampus** | $M_1$, $M_2$,$M_4$ | Presynaptic | Decrease |
| | GABA | Presynaptic | Increase |
| | $A_1$ | Presynaptic | Decrease |
| **Cortex** | $M_1$, $M_2$,$M_4$ | Presynaptic | Decrease |
| | $5\text{-}HT_{1F}$, $5\text{-}HT_2$ | Presynaptic | Decrease |
| | κ-opioid, δ-opioid | Presynaptic | Decrease |
| | Neurokinin-1 | Presynaptic | Decrease |
| | α2 | Presynaptic | Decrease |
| | GABA | Presynaptic | Decrease |

which catalyses hydrolysis. Once a molecule of ACh has bound to the enzyme, the reaction occurs in two stages. Firstly choline is split off, leaving an acetylated esteratic site on the enzyme, the latter then reacts with water releasing acetate and regenerating the enzyme. The activity of the enzyme is saturable and its action is inhibited by a variety of compounds that prolong the actions of ACh, such as physostigmine, tacrine, HEP and organophosphates.

## Muscarinic Cholinergic Receptors

Acetylcholine receptors were originally defined into two classes, muscarinic and nicotinic, on the basis of tissue responses to certain agonist and antagonist compounds. The presence of muscarinic cholinergic receptors in a tissue can be identified by a response to muscarine, an alkaloid derived from the poisonous mushroom *Amanita Muscaria* , that mimics the actions of ACh and which is selectively antagonised by atropine, an alkaloid derived from deadly nightshade (*Atropa belladonna*). Similarly, the presence of nicotinic cholinergic receptors in a tissue can be identified by a response to nicotine which is antagonised by *d*-tubocurarine. In 1914 Dale defined the two classes of cholinergic receptor on the basis of the tissue responses described above (Dale, 1914).

In the periphery muscarinic acetylcholine receptors (mAchRs) mediate a variety of well documented actions (for overview see Wess et al., 1990) including reduction of heart rate, vasodilatation, constriction of airways, increased secretions from sweat and lacrimal glands and constriction of the iris sphincter and ciliary muscles of the eye. Within the central nervous system they are present in relatively high densities as heteroreceptors and autoreceptors regulating neurotransmitter release. As such they are involved in a large number of physiological and psychological functions. These include involvement in sensory and motor functions, emotional and stress responses, and regulation of REM sleep. In addition they participate in the regulation of higher cognitive functions such as learning an memory (Raiteri et al., 1984; Akaike et al., 1988; Vizi et al., 1989, Raiteri et al, 1990 ).

### *Muscarinic Receptor Subtypes*

Until the early 1980s and the division of mAChRs into $M_1$ and $M_2$ on the basis of the binding properties of the novel ligand pirenzepine, mAChRs were thought to represent a fairly homogenous class of receptor. Pharmacological evidence to the contrary however, had existed since the 1950s. Gallamine, a neuromuscular blocking agent, used as an adjunct to general anaesthesia, was observed to produce sinus tachycardia as a side effect (Walton , 1950).

In isolated heart preparations, gallamine blocked the negative inotropic and chronotropic effects produced by the introduction of ACh, but was ineffective in antagonising the contractile actions produced by muscarinic agonists in isolated smooth muscle (Riker et al., 1951). Muscarinic receptors in heart therefore appeared to be different to those located in smooth muscle and exocrine glands.

Verification of multiple receptor subtypes came when the binding properties of the novel muscarinic antagonist pirenzepine were first described(Matsuo et al., 1979). Pirenzepine was initially used for treatment of gastric ulcers. It inhibited gastric acid and pepsinogen production at doses that had no effect on either heart rate or gastrointestinal motility; suggesting the presence of at least two subtypes of muscarinic receptor. Pirenzepine was subsequently used to define the presence of three subpopulations of muscarinic receptor. It binds with high affinity to mAChRs in the CNS and peripheral ganglia ($M_1$ receptors); with intermediate affinity to mAChRs in exocrine glands ($M_3$ receptors); and with low affinity to receptors in the heart [$M_2$ receptors] (Hammer et al , 1982).

The development of additional novel muscarinic antagonist compounds has aided the pharmacological classification of mAChRs into the three subtypes described above. The muscarinic antagonists 4-diphenylacetoxy-N-methlypiperidine methoiodide (4-DAMP) and hexahydrosiladifenidol (HHSiD) were found to antagonise $M_3$ mediated contractions of intestinal smooth muscle more potently than $M_2$ mediated cardiac responses and were thus define as $M_3$ selective (Barlow et al, 1976, Lambrecht et al, 1989).
However, these compounds are not strictly $M_3$ selective as they exhibit high affinity for $M_1$ receptors also. It is therefore more accurate to define them as non-$M_2$ antagonists. A group of compounds displaying $M_2$ selectivity are also available. These include 11-[2-[(diethylamino)-methyl]-1-piperidinyl] acetyl-5,11 dihydro-6H-pyrido-[2,3b] [1,4] benzodiazepine-6-one (AF-DX 116), which displays actions converse to those described for $M_3$ selective antagonists (Pedder et al ,1991).

None of the muscarinic antagonists currently available is highly specific for a single receptor subtype, with most exhibiting between a 2 and 10 fold difference in affinity between the subtype for which they are selective and the other subtypes (see Table 3). In this regard, there are also no true subtype selective muscarinic agonists available, with only McN-A-343 displaying a moderate $M_1$ selectivity (Hu J. and El-Fakahany,1990). However, the recent discovery of neurotoxins (isolated from snake venom) displaying a high degree of selectivity for $M_1$ and $M_4$ receptors provides some optimism for the future development of subtype selective muscarinic ligands (Adem and Karlsson, 1997).

*Cloning Of Muscarinic Receptor Genes*

Unequivocal evidence for the heterogeneity of mAChRs came in the late 1980s when 5 different subtypes were identified using molecular biological techniques

## Table 3

## Affinity of Muscarinic Antagonists at Five muscarinic Receptor Subtypes

| Antagonist | m1 | m2 | m3 | m4 | m5 |
|---|---|---|---|---|---|
| Pirenzepine | 6 | 223 | 138 | 37 | 89 |
| HHSiD | 22 | 131 | 15 | 15 | 93 |
| 4-DAMP | 0.58 | 3.8 | 0.52 | 1.17 | 1.05 |
| Methoctramine | 50 | 13 | 213 | 32 | 135 |
| AF-DX 384 | 31 | 6 | 66 | 10 | 537 |

Table shows Ki (nM) values for 5 muscarinic antagonists for binding to human m1-m5 mAChRs. Affinity values were derived from [$^3$H]-N methyl scopolamine displacement experiments (Dorje et al., 1991).
HHSiD= hexahydrosiladifenidol, 4-DAMP= 4-diphenylacetoxy-N-methylpiridine methoiodide, AF-DX 384= 5,11-dihydro-11-{[(2-{2-[(dipropylamino)methyl]-1-piperidinyl}ethyl)amino]carbonyl}-6H-pyrido(2,3-b)(1,4)benzodiazepine-6-one.

Bonner et al., 1987a, Kubo et al., 1986a, Kubo et al., 1986b; Peralta et al., 1987). Muscarinic $m_1$ and $m_2$ receptors were first cloned from cDNA libraries extracted from porcine brain and heart (Kubo et al.,1986a, Kubo et al, 1986b). Three more muscarinic receptors were cloned shortly afterwards ($m_3$, $m_4$, and $m_5$) by screening cDNA and genomic libraries under low stringency conditions with oligonucleotide probes corresponding to regions of high homology between $m_1$ and $m_2$ sequences (Bonner et al, 1987, Peralta et al., 1987b, Lioa et al., 1990).

The convention of designation for mAChRs is to use an uppercase "M" or a lowercase "m" for receptors identified pharmacologically (M) or by molecular biology (m) respectively. On the basis of the pharmacological properties of the expressed recombinant receptors and the relative distribution of their mRNA , the $m_1$ , $m_2$ and $m_3$ cloned receptors appear to correspond to the $M_1$, $M_2$ and $M_3$ receptors identified solely by pharmacological means (Maeda et al., 1988). In this thesis, both conventions will be used and should be interpreted as being interchangeable.

Of the cloned receptors $m_1$ is abundantly expressed in the forebrain and sympathetic ganglia and exhibits high affinity for pirenzepine ( Ehlert and Tran, 1990; Giraldo et al, 1987, Hammer et al., 1982; Kashihara et al., 1992; Yasuda et al., 1993). The $m_2$ receptor exhibits high affinity for AF-DX 116 and gallamine (Kashihara et al., 1992) and accounts for almost the entire mAChR population in the heart. Compared to the $m_1$ receptor it is expressed in a low uniform density throughout the brain (Ehlert et a l., 1990, Yasuada et al, 1993).The $m_3$ receptor displays high affinity for the $M_3$ (non-$M_2$) antagonists HHSiD and 4-DAMP and is the major mAChR in the exocrine glands (Kashihara et al., 1992, Pedder et al., 1991). It is expressed in low levels through out the brain (Yasuda et al., 1993). The $m_4$ receptor exhibits high affinity for 4-DAMP and himbacine (Kashihara et al.,1992). It is abundantly expressed in the forebrain, particularly the corpus striatum and olfactory tubercle (Yasuda et al., 1993). The $m_5$ receptor also shows high affinity for HHSiD and 4-DAMP and is typified by its low affinity for AF-DX 116 (Yasuda et al, 1993). Out of the five cloned receptors it is expressed in the lowest density throughout the brain, representing less than 2% of the total density of mAChRs (Yasuda et al., 1993).

*Muscarinic Receptor Structure*

Analysis of the primary sequences of mAChRs shows that they are members of the superfamily of genes which are G-Protein coupled (Bonner et al., 1987, Kubo et al., 1986). This family of receptors is typified by the presence of 7 hydrophobic domains in their sequence which span the membrane (Fig 2). The transmembrane (TM) segments of mAChRs represent the regions of highest homology between the different subtypes of receptor. There is a 63% continuity of identity among the amino acid residues making up the 7 TM regions in the human $m_1$-$m_5$ receptors. The main sequence differences between the subtypes exist in

**Fig 2:** Structure of a membrane bound G-protein coupled mAChR.

**A** shows 7 transmembrane segments typical of G-protein receptors, the cytoplasmic carboxy terminus (COOH), the extracellular amino terminus ($NH_2$) and the 4 intracellular amino acid loops (i1-i4). **B** is a helical wheel model of depicting the likely orientation of the 7 transmembrane segments which from a barrel like structure with a central pore containing the binding site for mAChR ligands.

## Muscarinic Receptor Structure

### A: Transmembrane Sequence Disposition

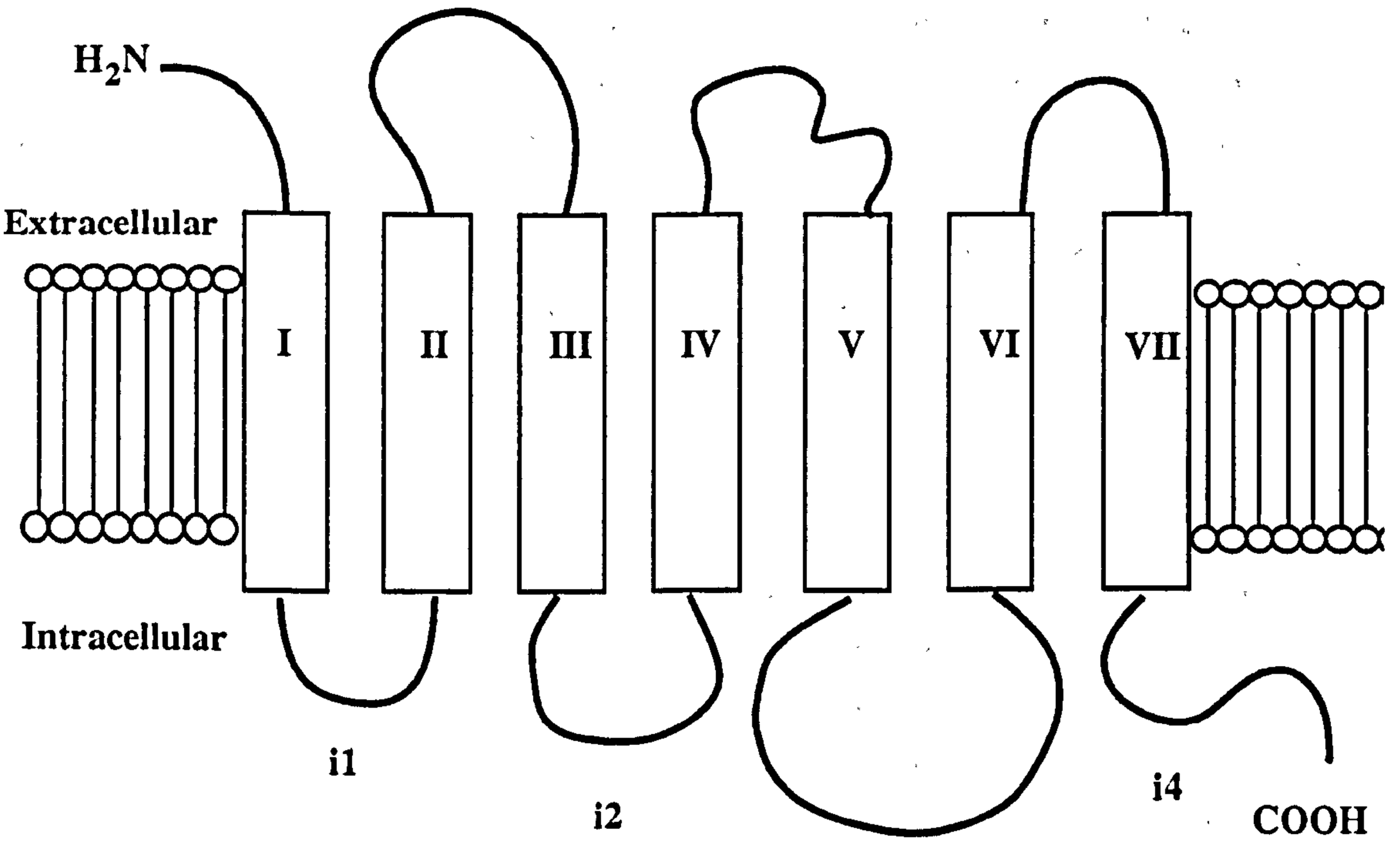


### B: Helical Wheel Model

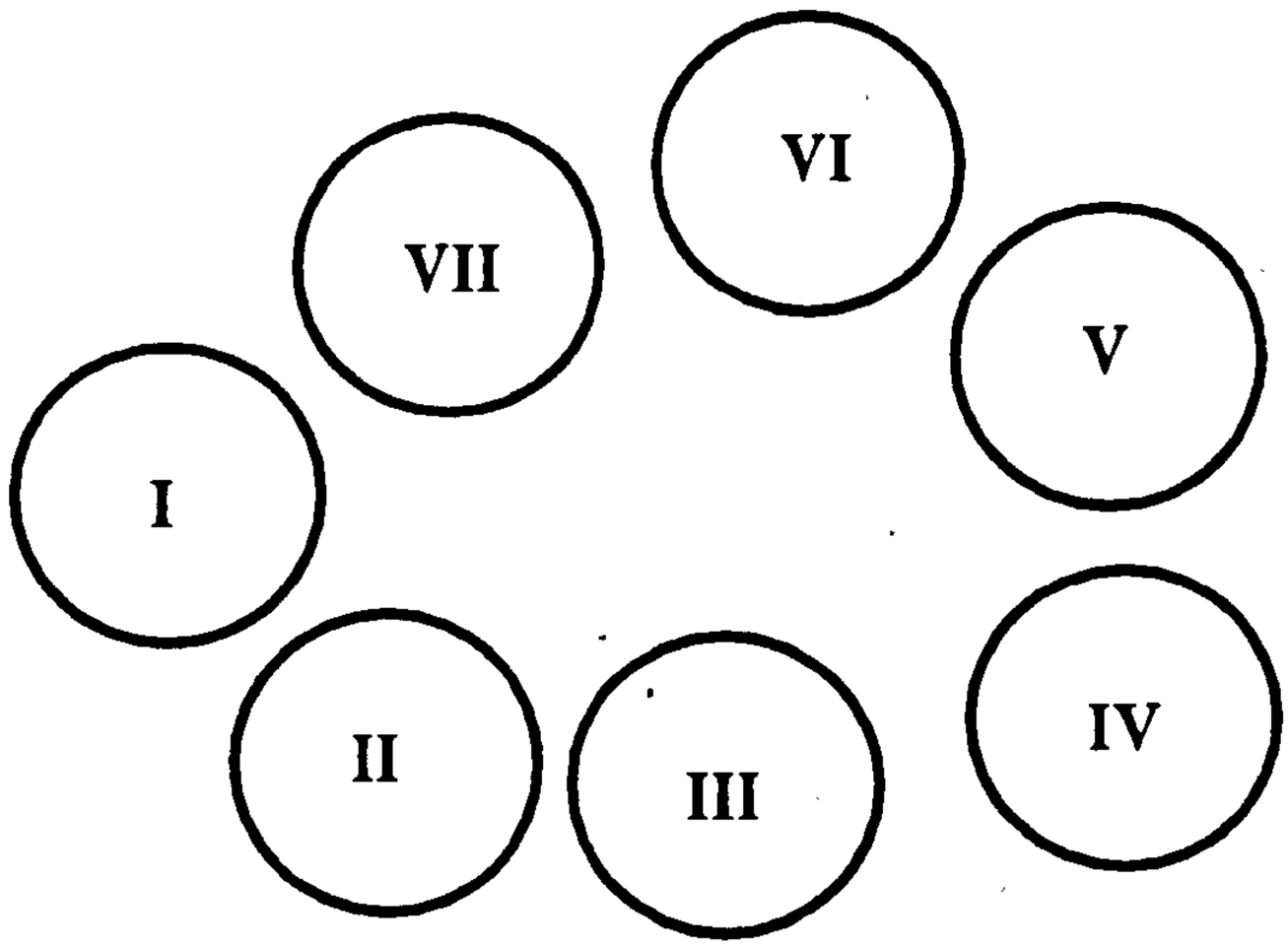


**Fig 2:** Structure of a membrane bound G-protein coupled mAChR.

the amino acid residues making up the extracellular amino acid termnis, the third intracellular loop and the cytoplasmic carboxy terminis of the receptor structure. Of these regions the third intracellular loop displays the greatest divergence. This region varies from 156 ($m_1$) to 239 ($m_3$) amino acid residues in length and accounts for 35-45% of the total number of residues in the entire receptor sequence. A comparison sequences shows that $m_1$, $m_3$ and $m_5$ receptors show homology with each other, while $m_2$ and $m_4$ constitute a separate homologous group. The 7 TM regions are thought to form a barrel like structure in the membrane, with a central pore. Acetylcholine and other muscarinic ligands are proposed to bind at a site within this pore. Hulme et al., (1990) predict that the most conserved residues in the receptor sequence form the inner surface of this pore and have suggested that this may be responsible for the lack of highly selective subtype specific muscarinic antagonists and agonists available.

*Ligand Binding Site*

The binding site on mAChRs is thought to exist on a highly conserved aspartic acid residue, which is anionic in nature, in the third intracellular TM region, (Ehlert et al, 1980). The anionic nature of the proposed binding site conforms with knowledge that all effective muscarinic antagonists are cationic. Peptide mapping and sequencing studies with [$^3$H] propylbenzilycholine mustard ([$^3$H] PrBCM) have provided further evidence to support the proposed location of the binding site. Results indicate that [$^3$H] PrBCM covalently binds to aspartic acid residues 105 and 111 in human $m_1$ and $m_4$ sequences respectively (Hulme et al, 1990). In addition, the chemically reactive aziridinium site on [$^3$H] PrBCM is structurally similar to the quaternary ammonium head group of many muscarinic ligands. Further evidence supporting the anionic aspartate residue as the ligand binding site comes from site mutation studies. Mutation of the aspartate 105 to asparagine in the third TM region in the $m_1$ receptor abolishes ligand binding and transduction mechanism activation (Fraser et al., 1989). Other site mutation studies have shown that threonine and tyrosine residues in the fifth TM region are necessary for agonist but not antagonist binding (Wess et al., 1991, Wess et al., 1992).

*Allosteric modulation Of mAChRs*

Considerable evidence now exists for the presence of allosteric interactions between muscarinic drugs and other agents acting on mAChRs (Birdsall et al., 1987, Hulme et al., 1990, Mithcleson, 1988; Tucek and Proska, 1995). All five mAChRS are known to be sensitive to allosteric modulation (Ellis et al., 1991). The neuromuscular blocking agents gallamine, alcuronium and pancuronium all act allosterically at mAChRs . In general these compounds have a negative allosteric effect. That is they inhibit the binding of competitive

muscarinic ligands to the orthosteric (primary) binding site in a non-competitive manner. Gallamine, the most studied allosteric ligand, characteristically slows down both the association and dissociation kinetics of ligands binding to the orthosteric site (Stockton et al., 1983). In contrast, alcuronium is known to enhance the binding of [$^3$H]-NMS to mAChRs by increasing the affinity of the binding sites for the radioligand (Tucek et al., 1990). It should be noted however, that the positive allosteric effect of alcuronium is observed only with m2 and m4 receptors (Jakubik and Tucek, 1994). Of the five muscarinic receptor subtypes the m2 receptor displays the greatest susceptibility to allosteric modulation. In transfection studies with Chinese hamster ovary cells expressing the individual mAChR subtypes the affinity of the uncoupled receptors for alcuronium was as follows m2> m4> m1> m3> m5 (Jakubik et al., 1996).

Consideration of the binding kinetics suggests the allosteric binding site on mAChRs is located in a position close to the orthosteric binding site but at a more extracellular location (Proska and Tucek, 1994; Tucek et al., 1993). Allosteric ligands are generally large charged molecules and when bound to the allosteric site are thought to create a steric hinderance to competitive muscarinic ligands binding to the orthosteric site. The allosteric effects of these compounds are observed in intact cells and tissues, suggesting that the allosteric binding site is located on the extra cellular surface of the receptor. Site directed mutagenesis studies on the mAChR sequence support this theory (see Tucek and Proska, 1995 and Wess, 1996).

*Signal Transduction Mechanisms*

Binding of ACh or any other muscarinic agonist to a mAChR stimulates signalling by initiating binding of the receptor to a G-protein complex, which provides the specificity for coupling to an appropriate receptor. The G-protein consists of a heterotrimer of three different proteins, Gα , Gß and Gγ , in order of molecular weight . Upon binding to the activated receptor, the α subunit of the G-protein separates from the ßγ subunits and then interacts with the appropriate effector protein or ion channel to stimulate or inhibit the release of intracellular second messengers. Coupling of the mAChR to the α subunit occurs primarily through interaction at the third cytoplasmic loop (Wess et al, 1989, Wess et al., 1990). Recent evidence indicates that the ßγ subunits may also be involved in the activation of second messenger systems (Camps et al, 1992).

Muscarinic receptors can be broadly divided into two categories depending upon the effector systems which they employ; those which inhibit adenylate cyclase activity and those which stimulate phosphoinositide hydrolysis. Results from transfection studies involving the individual receptor genes have demonstrated that m2 and m4 receptor activation produces a pertusis toxin sensitive inhibition of adenylate cyclase and m1, m3, and m5 receptor

activation produce a pertusis toxin insensitive stimulation of phosphoinositide hydrolysis (Lai et al, 1988; Peralta et al, 1988, Lai J. et al, 1991, Liao, 1990).However, it should be noted that pertusis toxin sensitive $m_1$ activation of phosphoinositide hydrolysis has also been identified (Mei et al., 1989).

The effector systems that individual receptors employ is primarily determined by the type of G-protein with which it is able to interact. The $m_1$, $m_3$ and $m_5$ receptors preferentially couple to G-proteins of the $G_{q/11}$ family (Berstein et al., 1992, Offermans et al., 1994, Wong and Ross, 1994). These G-proteins mediate the activation of various isoforms of phospholipase $C_\beta$ ($PLC_\beta$), that catalyse phosphoinositide hydrolysis (Peralta et al., 1988 Smrcka et al., 1991, Berstein et al., 1992). The $m_2$ and $m_4$ subtypes are selectively linked to G-proteins of the $G_{i/o}$ class which, with the exception of $G_z$, are inactivated by pertusis toxin (Parker et al., 1991, Offermans et al., 1994). It should be noted however, that one receptor subtype can couple to both effector systems. Thus, $m_2$ and $m_4$ receptors can couple to phosphoinositide hydrolysis, although only weakly and at high receptor levels and agonist doses (Ashkenazi et al., 1987). In fact it appears that a single receptor can activate multiple effector systems by interaction with different G-proteins.
The predominant effector systems that interact with mAChRs are briefly described below.

*Adenylate Cyclase*

The negative coupling of $m_2$ and $m_4$ receptors to adenylate cyclase is well documented (see Caufield et al, 1993 for review). It is now also recognised that under certain conditions $m_1$, $m_3$ and $m_5$ receptors may also inhibit enzyme activity (Peralata et al., Nature 1988, Lai et al., 1992). In contrast however, mAChR activation has been shown to stimulate adenylate cyclase activity in a variety of expression systems, (Baumgold and Fishman, 1988; Regunathan et al, 1990; Olianas et al., 1992). Several regulatory mechanisms are likely to be responsible for muscarinic receptor mediated activation of adenylate cyclase including a $Ca^{2+}$/ protein kinase C (PKC) dependent mechanism (Jansson, et al., 1991, Baumgold et al, 1992). Muscarinic receptor activation can also increase (Brandi et al., 1987) and decrease (Hughes et al, 1986) levels of cAMP by activation and inhibition respectively, of cyclic AMP phosphodiesterase, the catabolic enzyme for cAMP.

*Phospholipase C*

Receptor mediated phospholipase C (PLC) activation is the first step in a cascade of events resulting in phosphoinositide hydrolysis. Increased PLC activity is historically associated with stimulation of $m_1$, $m_3$ and $m_5$ mAChRs. However, as with adenylate cyclase, activation of this enzyme is by no means exclusive to these receptors, as the $m_2$ and $m_4$ subtypes may also stimulate PLC (Ashkenazi et al, 1987, Peralata et al., 1988).However,

PLC activation and hydrolysis of membrane phospholipid is greater following m1 , m3 or m5 than m2 or m4 receptor activation (Peralta et al, 1988, Ashkenazi et al,1989).

Upon activation, PLC hydrolyses the membrane phospholipid phosphatidylinositol 4,5-bisphosphate ($PIP_2$) into 1,2-diacyl-*sn*-glycerol (diacylglycerol, DAG) and D-*myo*-inositol 1,4,5-trisphosphate ($IP_3$) (Berridge, 1983, Fisher et al., 1987). DAG then binds to and stimulates protein kinase C (PKC) and $IP_3$ liberates $Ca^{2+}$ stored in the endoplasmic reticulum by binding to the $IP_3$ receptor, an $IP_3$ sensitive $Ca^{2+}$ channel. Activated PKC is then able to phosphorylate proteins, thereby regulating their functions.

*Phospholipase A2*

Activation of m1, m3 and m5 has been shown to stimulate the release of arachidonic acid by activating the enzyme phospholipase A2 (Conklin et al., 1988, Felder, et al, 1990). Arachidonic acid is released by the action of $PLA_2$ on membrane phospholipid, it can then be converted into a number of eicosanoid compounds and activates PKC. Muscarinic m2 and m4 receptors do not stimulate $PLA_2$ at physiological levels of expression (Conklin et al, 1988).

*Phospholipase D*

Phospholipase D (PLD) hydrolyses the membrane phospholipid phosphatidyl choline into phosphatidic acid and choline (Chalifour et al., 1980, Exton , 1990). Posphatidic acid , after interaction with the enzyme phosphotidate phosphohydrolase, produces DAG which is then able to activate PKC (Gustavsson et al., 1990). As with PLC, all five mAChR subtypes are coupled to PLD with m1, m3 and m5 receptors producing a more robust activation than m2 and m4 receptors (Sandmann et al, 1991). The coupling of mAChRs to PLD may be of general importance to cholinergic transmission in so far as it results in the production of choline, a precursor for ACh.

*`Distribution Of Muscarinic Receptors Within The CNS*

The distribution of mAChRs within the CNS has been mapped out using a variety of techniques. Binding sites were first visualised in the 1970s with *in vitro* autoradiography studies using [$^3$H] radioligands (Yamamura, et al., 1974; Kuhar and Yamamura, 1975). More recently, the development of immunoprecipitation (using subtype selective antibodies) and in situ hybridization techniques, has provided unequivocal evidence of the distribution of muscarinic sites within the brain. In general, there is excellent agreement between the different techniques as to the distribution of mAChRs.

Radioligand binding studies have identified a high density of $M_1$ receptors in the hippocampus, cortex and striatum (Spencer et al., 1986, Cortes and Palacios,Brain 1986, Mash and Potter, 1986; Frey and Howland, 1992). Lower population density is observed in the thalamus and hypothalamus and in the brainstem nuclei. This distribution of $M_1$ receptors is supported by immunoprecipitation (Levey et al., 1991, Wallet al., 1991) and in situ hybridization studies (Buckley et al., 1988, Vilaro et al., 1994).

$M_2$ receptors show a more widespread distribution with mRNA present in nearly all brain regions (Vilaro et al., 1992). Autoradiography studies indicate a low uniform distribution throughout the CNS, with $M_2$ receptors placed most predominantly in thalamic nuclei, striatum, superior colliculus, pontine nuclei, and brainstem (Regenold et al., 1987; Wang et al., 1987; Frey and Howland, 1992). Results of immunoprecipitation studies support this distribution (Levey et al., 1991). In general, the distribution of $M_2$ sites is similar to that of the cholinergic markers AChE and ChAT, i.e. high density in striatum, thalamic nuclei, and superior colliculus (Fibiger, 1982; Quirion and Boska, 1986; Woolf, 1991). In contrast the distribution of $M_1$ sites is very different to that of the cholinergic markers. These observations suggest a presynaptic location for $M_2$ receptors and a postsynaptic location of $M_1$ receptors. Functional evidence has suggested the presence of $M_2$ receptors on presynaptic cholinergic terminals where they act as autoreceptors regulating the release of ACh (Lapchak et al., 1989; Hoss etal., 1990). Although $m_2$ receptors are thought to be the predominant subtype of autoreceptor in areas such as the striatum (Billard et al., 1995) evidence exists to suggest that all five subtypes of receptor may have roles as presynaptic autoreceptors on projecting cholinergic neurones (Vilaro, et al., 1994, Vannucchi et al., 1995; Stillman et al., 1996).

Distribution of $M_3$ sites within the CNS has been mapped with autoradiography (Michael et al., 1989; Michael and Whiting, 1990), immunoprecipitation (Levey, 1993; Levey, et al., 1994) and in situ hybridization (Buckley et al., 1988; 8:4646-4652, Vilaro et al., 1994). The pattern observed is similar to that of $M_1$ receptors, with high density in the cortex, striatum and hippocampus and lower density in the thalamic, hypothalamic and brainstem nuclei . $M_3$ receptors however, are present in higher density in certain thalamic and brainstem nuclei and possibly also in some deeper cortical layers (Quirion et al., 1993). The functional role of the $M_3$ receptor in the CNS is yet to be established, although evidence exists for their role as autoreceptors (Vilaro et al., 1994).

The visualisation of $M_4$ and $M_5$ receptors has been hampered by the lack of subtype selective ligands . However, recent labelling strategies utilising *in vitro* autoradiography, have allowed their distribution in the CNS to be mapped (Ferrari-Dileo et al., 1994, Flynn et al., 1997, Reever et al., 1997). $M_4$ receptors are found in greatest density in the caudate nucleus, nucleus accumbens, and olfactory tubercle. Areas of lower density are found in the cortex, hippocampus and the laterodorsal and pedunculopontine tegmental nuclei (Buckley

et al., 1988, Vilaro et al., 1991). The distribution profile of the $M_5$ receptor is distinct from the other four subtypes. Of the mAChRs, it is expressed in the lowest density in the CNS, although recent evidence suggests its level of expression may be higher and more widespread than originally thought (Reever et al., 1997).Brain regions which are relatively enriched with $M_5$ receptors include the outer layers of the cerebral cortex, the hippocampus, the caudate nucleus, and the nucleus accumbens. As with the $M_3$ and $M_4$ subtypes little is known about its physiologic role.

## Nicotinic Cholinergic Receptors

Nicotinic acetylcholine receptors (nAChRs) are a family of ligand gated cation channels belonging to a larger superfamily including 5-HT, $GABA_A$ and glycine receptors (Ortells and Lunt, 1995). They are comprised of hetero-oligomers consisting of five membrane spanning subunits which form a barrel like structure in the membrane around a central ion channel (Fig 3) (Cartaud et al., 1973 ). Molecular cloning studies in chick, rat and human have identified multiple genes that encode various subtypes of subunit that allow assembly of a wide variety of receptor oligomers with different distribution and distinct pharmacological profiles (Sargent et al., 1993). Peripheral nAChRs, such as those found at the neuromuscular junction or in electric organ tissue, are made up of α1, ß1, γ and δ or ε subunits in the fixed stoichiometry of 2.1.1.1.( e.g. 2α1, 1ß1, 1γ, and 1δ or 1ε). Neuronal nAChRs differ from those in the periphery in that they have no γ, δ or ε subunits in their make up, and consist of various complements of α2-α9 and ß2-ß4 subunits. In mammalian brain two major neuronal populations of nAChR can be delineated using radioligand binding: those recognising α-bungarotoxin (α-BgT) and neuronal bungarotoxin (n-BgT) with high affinity and those that do not (Clarke, et al., 1985 Sugaya et al., 1990). The major brain species of nAChR constitutes the receptor population with low affinity for α- and -BgT. These receptors are composed of two α4 and three ß2 subunits (Whiting and Lindstrom, 1986) and bind [$^3$H]-nicotine and [$^3$H]-ACh with high affinity (Clarke et al., 1985). Neuronal nAChRs with high affinity for α- and n-BgT do not display the same high affinity for nicotine or reflect ACh binding in terms of kinetics, pharmacological profile or distribution. Recent evidence suggests that these receptors are composed of homo-oligomers consisting predominantly of subunits of the α7 subtype (Breese et al., 1997). Additional multiple forms of neuronal nAChR exist, composed of different combinations of both α and ß subunits which form a wide variety of functional hetero-oligomers with distinct pharmacological and physiological properties. Furthermore, each neuronal subpopulation displays a distinct pattern of distribution within the brain as will be described in a later section (Sargent et al., 1993 )

**Fig 3:** Structure of ligand gated nicotinic ion channel-receptor

Figure shows five membrane spanning subunits (**A**) which form a barrel like structure in the membrane around a central ion channel (**B**) . The stoichiometry of peripheral and neuronal nicotinic receptors is shown in **C**. Peripheral nAChRs, such as those found at the neuromuscular junction or in electric organ tissue, are made up of a1, ß1, γ and δ or ε subunits in the fixed stoichiometry of 2.1.1.1.( e.g. 2α1, 1ß1, 1γ, and 1δ or 1ε). Neuronal nAChRs differ from those in the periphery in that they have no g, d or e subunits in their make up, and consist of various complements of α2-α9 and ß2-ß4 subunits.

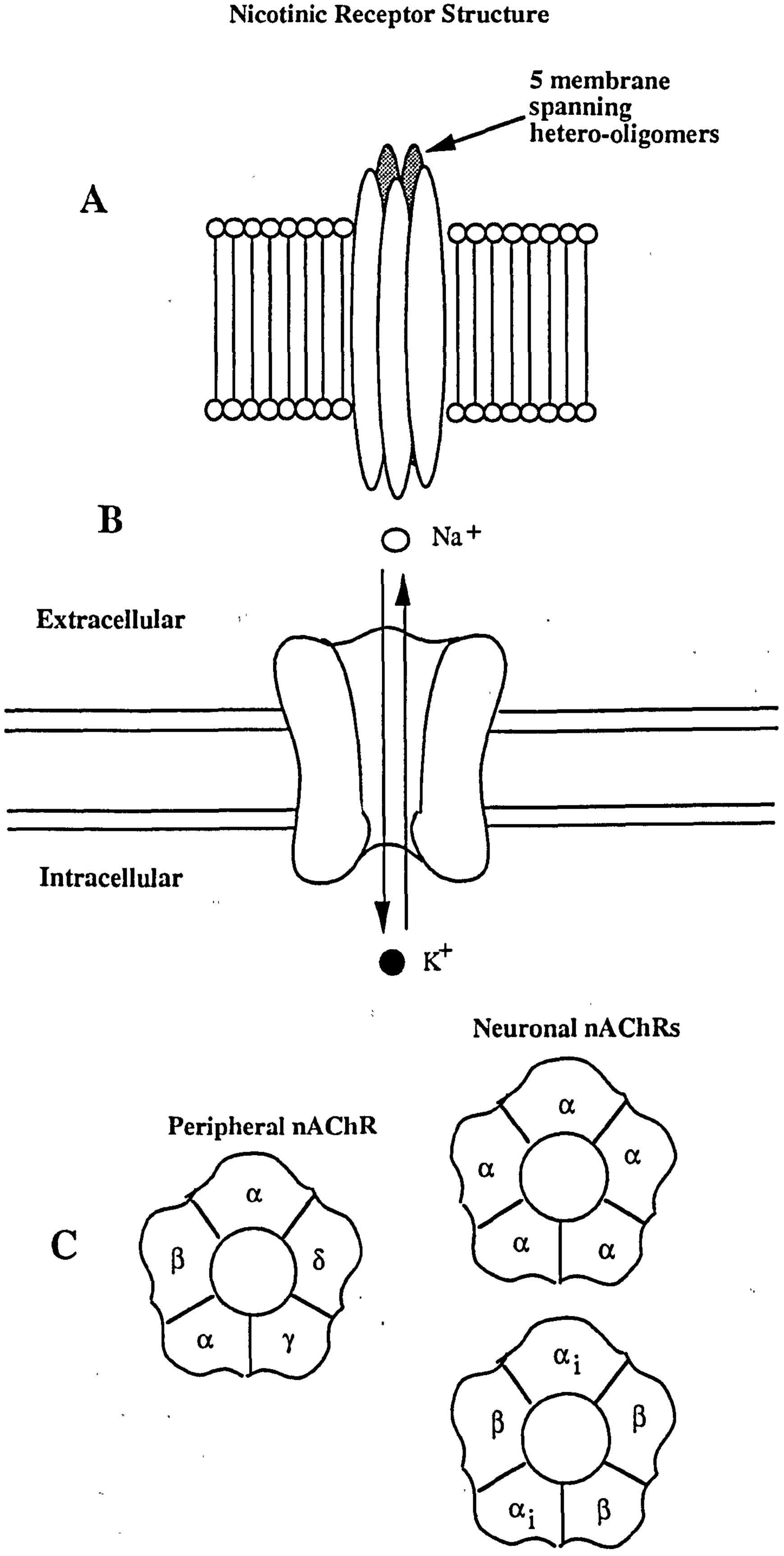


**Fig 3:** Structure of ligand gated nicotinic ion channel-receptor

*Nicotinic Receptor Structure and Ligand Binding Site*

Analysis of the amino acid sequence of nAChRs reveals significant sequence homology between receptor subtypes with similar distribution of hydrophillic and hydrophobic regions within their length (Galzi and Changeux, 1995). The receptor sequence consists of a large hydrophillic amino terminal domain, a compact hydrophobic domain split into three segments of 19-27 amino acids termed M1-M3, a small highly variable hydrophillic domain and a hydrophobic C-terminal domain of approximately 20 amino acids termed M4. It is thought that the large hydrophillic domain is exposed to the synaptic cleft and plays some role in the binding of ligands. The small hydrophillic domain is exposed to the cytoplasm and the four hydrophobic domains comprise the transmembrane segments of the protein, some of which line the ion channel ( Galzi and Changeux, 1995).

From studies on *Torpedo* electric organ it was elucidated that the nAChR in this tissue and that in muscle, carried two ACh binding sites (Reynolds and Karlin, 1978). The binding sites were originally thought to reside solely upon the α-subunit but evidence from site-directed mutagenesis studies on muscle nAChR has indicated that the ligand binding sites exists at the interfaces between the α and ß and α and ∂/ε subunits. In hetero-oligomeric neuronal nAChRs of the $\alpha i_2 \beta j_3$ type(e.g. $\alpha 4_2 \beta 2_3$) the binding sites are formed in a similar manner (Alkondon et al., 1993). However, in the homo-oligomeric α7 or α8 subtypes of nAChR, five identical ACh binding sites are formed due to the identical nature of the subunits making up the receptor protein (Sargent et al., 1993).

The subtype composition of the receptor is very important in determining sensitivity to agonists and antagonists. Expression of different subunit combinations in oocytes has allowed direct comparison of the binding properties of the receptor subtypes.
For example, α4ß2 receptors display the greatest sensitivity to ACh and (-) nicotine, with an EC50 of 0.7 $\mu$mol/L for both compounds. The α3ß2 receptor subtype displays lower affinity for ACh and (-) nicotine with an EC50 of 5 $\mu$mol/L. Both of these receptor subtypes are insensitive to α-BgT. In contrast α7 nAChRs which are blocked by both α- and n-BgT are relatively insensitive to ACh and (-) nicotine, with EC50s of 155 $\mu$mol/L and 10 $\mu$mol/L respectively (Court and Perry, 1994). The rank order of potency of the nAChR agonists ACh, (-)-cytisine, 1,1-dimethyl-4-phenylpiperazinium (DMPP) and tetraethylammonium on nAChRs formed from ß2 or ß4 subunits combined with α2, α3 or α4 subunits has established the importance of both α and ß subunits in defining the binding properties of nAChRs (Luetje and Patrick, 1991). Receptors containing the ß4 subunit were most sensitive to (-)-cytisine whereas those containing the ß2 subunit were (-)-cytisine insensitive. Currently no subtype selective nAChR agonists are available, although development of α4ß2 selective compounds is on going as potential therapeutic agents for the treatment of Alzheimer's disease (Abreo et al., 1996). The alkaloid epibatidine, a natural product in frog

skin , is the most potent nicotinic agonist ligand reported to date. It binds with high affinity at [$^{3}$H]-cytisine and [$^{125}$I]- α-BgT sites and is functionally more potent than nicotine (Qian et al., 1993). It also appears to be an excellent ligand for *in vitro* and *in vivo* labelling of nAChRs (Perry and Kellar, 1995).

In comparison, several nAChR antagonist compounds are available that allow a certain degree of delineation between receptor subtypes. For example, while having no effect on α2ß4 and α4ß2 subtypes, n-BgT is a potent inhibitor of α3ß2 nAChRs (Luetje et al., 1990 ). In addition, the neurotoxin neosugurotoxin (NSTX), potently blocks α2ß2, α4ß2 and α3ß2 but not α7 or α1ß1∂γ/ε (muscle) nAChRs subtypes (Martin et al., 1993). Furthermore, the nAChR antagonist methylcaconitine (MLA) an inhibitor of [$^{125}$I]-α-BgT binding, blocks the ion channel response at α7 but not α4ß2 , α3ß2 or muscle type nAChRs , thus making it the only antagonist that can clearly distinguish between neuronal and muscle type BgT sensitive nAChRs.

*Alternative Ligand Binding Sites*

Evidence indicates that a number of ligand binding sites distinct from the classical ACh binding site may exist which allosterically modulate nAChR ion-channel function. Alternative "Channel Activator" sites are thought to be present on the α-subunit of nAChRs . Compounds such as the AChE inhibitors physostigmine and galanthamine act at these sites in a positive allosteric manner resulting in increased neuronal nAChR ion conductance (Pereira et al., 1993). Evidence also indicates that the neurotransmitter 5-HT binds to the same site on the α subunit and increases ion conductance by increasing the frequency of channel opening (Schrattenholz et al., 1996).

A number of pharmacologically and chemically diverse compounds such as chlorpromazine, phencyclidine, MK801, local anaesthetics, detergents, fatty acids, barbiturates and alcohols can produce a negative allosteric effect on nAChR ion channel function (Lena and Changeux, 1993). These compounds are non-competitive (negative allosteric) channel blockers which are thought to interact with two distinct sites that differ from those of competitive blockers. The first high affinity site, which binds ligands in the nanomolar range, is thought to be located within the ion channel and is composed of amino acid residues of the M2 segment in each of the five subunits making up the nAChR protein. Binding of ligands to this site is facilitated by agonist activation of the receptor and produces a rapid reversible channel blockade, with ion conductance blocked simply by steric hindrance (Valenzuela et al., 1994). The second binding site binds ligands with low affinity and is thought to accelerate desensitisation of the ion-channel receptor. There are thought to be numerous (10-20) sites of this type on each nAChR molecule which are postulated to be

located at the interface between the lipid membrane and the receptor protein (Lena and Changeux, 1993).

Steroids can inhibit neuronal nAChR function by binding to a receptor site distinct from both the classical ACh site and the ion-channel site (Inoue and Kuriyama, 1989). Progesterone and testosterone coupled to bovine serum, have been observed inhibit neuronal α4ß2 nAChRs in a voltage sensitive manner. In addition, corticosterone administration to mice following adrenalectomy, produces a reversible increase in sensitivity to (-)-nicotine . Furthermore, high steroid concentrations ($\mu$molar range) have been observed to displace [$^{125}$I]-α-BgT from rat brain membranes and to reduce the affinity of (-)-nicotine for this site (Lena and Changeux, 1993). Calcium ions also appear to have a role in modulation of nAChR ion-channel function. Calcium ions produce a negative allosteric effect by binding to a large number of sites on the nAChR protein, some of which are very likely to be located within the ion channel as suggested by voltage sensitive decreases in conductance observed (Fairclough et al., 1986). This binding site is also known as the dihydropyridine binding site, as L-type $Ca^{2+}$ channel blockers of this class of compound have been observed to have effect at this site (Lopez et al., 1993). Calcium ion may also produce a positive allosteric effect by binding to another category of site carried only by neuronal nAChRs, potentiating the response to agonists in a voltage sensitive manner (Mulle et al., 1992).

*Transitional States of nAChR*

Nicotinic AChRs follow a "concerted allosteric" scheme in which they can exist in any one of four functionally distinct interconvertible transition states at any one time. The activation and desensitisation transition states have been analysed in detail electrophysiologically *in vivo* and *in vitro* (Heidmann and Changeux, 1979).
The receptor can be in a resting state (R), an activated state (A) where the channel opens on a microsecond to millisecond timescale when activated, but has low affinity (10$\mu$M-1mM) for agonists, or in one of two desensitised closed channel states I and D. In the sensitised states the channels are refractory to activation on microsecond and minute timescale respectively, but display high affinity (1 nM-1 $\mu$M) for agonists (Glaze and Change, 1995). Desensitisation of the receptor is characterised by the slow progressive decline in response amplitude following a prolonged period of receptor-ion channel activation

The classical ACh binding site together with the distinct classes of allosteric binding site described above, co-operatively modify the equilibrium between the receptor states thus affecting the number of receptors existing in any one of the four states at any time. As with the ligand binding profile of individual receptor subtypes the subunit composition of each receptor has great influence upon the kinetics of activation and desensitisation , with the

homo-oligomers (e.g. α7 and α8) exhibiting most rapid desensitisation (see Galzi and Changeux, 1995).

*Distribution of nAChRs in the CNS*

The distribution of nAChRs has been extensively mapped using radioligand binding and in situ hybridization techniques in rodent brain. The topographical distribution of nAChRs corresponds well with the effects elicited by (-)-nicotine and the known functions associated with each brain region. Studies with [$^3$H]-(-)-nicotine have revealed abundant high affinity sites in the cerebral cortex (layers III and IV), thalamus, medial habenula, superior colliculus and interpenduncular nucleus (Clarke et al., 1985 ). A second class of sites revealed by radioligand binding studies with [$^{125}$I]-α-BgT display a distribution pattern distinct to that of [$^3$H]-(-)-nicotine, with high a density of binding observed in the hippocampus, cortex (layers I and IV), amygdala and certain brainstem nuclei (Clarke et al., 1985).

The distribution of nAChR subunit mRNA detected by in situ hybridization generally correlates with the distribution of the [$^3$H]-(-)-nicotine and [$^{125}$I]-α-BgT binding sites. The distribution of α4ß2 mRNA generally reflects the pattern of [$^3$H]-(-)-nicotine binding, supporting the theory that receptors of this subunit composition compose the majority of the high affinity nicotine sites in the CNS (Wada et al., 1989). The other subunits generally display a more circumscribed pattern of distribution. The α3 subunit constitutes the major α subunit present in the medial habenula and cortical layer IV. It is also found in the thalamus, hypothalamus and brainstem. The α2 subunit is concentrated in certain interpenduncular nuclei, the lateral dorsal tegmental nucleus of the brainstem, hippocampus and inferior colliculus (Wada et al., 1989). The α5 is present in significant levels in distinct layers of the subicular complex, substantia nigra pars compacta, interpenduncular nucleus and dorsal motor nucleus of the vagal nerve (Wada et al., 1990). The distribution of α7 mRNA closely resembles the binding pattern of [$^{125}$I]-α-BgT and is distinct from that of [$^3$H]-(-)-nicotine. It is present in highest density in the cerebral cortex (layers I and IV) and in the hippocampus, particularly he CA4 region . Little or no α7 mRNA is present in the thalamus, striatum or substantia nigra (Seguela et al., 1993). Of the ß subunits, ß2 and ß4 are most widely distributed in the brain and are present in nearly all areas. The ß3 subunit expression is more limited but is present in highest density along with ß4, in the medial habenula (Dineley-Miller et al., 1992).

Topographical analysis of nAChR distribution in human brain has yet to be completed to the same degree as that in rodent brain. However, radioligand binding and in situ hybridization studies indicate broad agreement with the distribution of receptors in rodent brain. Binding of [$^3$H]-(-)-nicotine was observed to be greatest in the thalamus , particularly the lateral geniculate nucleus (Perry et al., 1989). A high density of binding was

also observed in the subicular complex, specifically the pre-subiculum with a general low level of binding observed in the hippocampus. The exception being the CA2-3 region. Human cortex also displays a distinct pattern of nAChR distribution. In somato-sensory and occipital visual cortex binding is highest in upper and lower cortical layers while layer IV is relatively low in nAChR binding site density (Perry et al., 1992). As in rodent brain, the distribution of α7 [$^{125}$I]-α-BgT sites is distinct to that of receptors with high affinity for (-)-nicotine. Binding sites are concentrated in dentate and CA1-3 regions of the hippocampus (Court and Perry, 1994).

Although displaying widespread distribution, the pattern of nAChR expression does not correlate to any distinct cholinergic projection pathway within the CNS. However, concentrated nAChR binding observed in the thalamus, substantia nigra and superior colliculus suggests location of nAChRs immediately postsynaptic to brainstem Ch5-Ch6 projection neurons where they may act to modify function . Therefore, these nAChRs are likely to have a role in arousal, attention and modulation of thalamic sensory control (Court and Perry, 1994). The identification of nAChRs in the substantia nigra, together with the well known presynaptic modulation of dopamine release by nAChRs, indicates a role for these receptors in the modulation of the extrapyramidal motor system (Rapier et al., 1988).

Considerable evidence exists for modulation of neurotransmitter release by pre-synaptic nAChRs (see Wonnacott et al., 1996 for review). They exist as autoreceptors on motor, cortical and hippocampal cholinergic neurons where they have been shown to increase the release of ACh. The loss of nAChR in these regions (see later section) parallels the degeneration of cholinergic terminals in Alzheimer's disease and is consistent with a pre-synaptic location of these receptors. Evidence suggests that these autoreceptors are of predominantly α4ß2 subtype. Neuronal nAChRs are also present as heteroreceptors where they increase the release of a variety of neurotransmitters including dopamine, noradrenaline, GABA and excitatory amino acids . Of the heteroreceptor actions of nAChRs, the most well characterised is the nicotinic stimulation of striatal dopamine release (Rapier et al., 1988).

In addition to modulatory actions on neurotransmitter release, nAChRs are involved in a number of physiological and behavioural functions. In particular nAChRs are implicated in learning and memory processes. Administration of nicotine is known to enhance learning and memory performance in a variety of cognitive ability tests (Buccafuso and Jackson, 1991, Levin, 1992, Gray, 1994 ). Nicotine also reverses deficits in cognitive impairment produced by cholinergic lesion, an effect which persists even after the withdrawal of nicotine (Levin, 1992). The presence of nAChRs in the subiculum complex of the hippocampus, are thought to be associated with the perforant pathway projecting from the subiculum to dentate granule cells. Therefore, stimulation of these nAChRs may mediate the effects of nicotine on learning and memory. Nicotine administration also produces EEG

desynchronisation, indicating that nAChRs have a role to play in arousal and attentional processes (Soldatos et al., 1980 ).

## ACh In The Cerebral Circulation

There is a considerable body of evidence indicating that ACh mechanisms play a significant role in the regulation of cerebral blood flow. Systemic administration of ACh increases cerebral blood flow (Aubineau et al., 1977). Application of ACh or ACh agonists such as carbachol to isolated perfused cerebral arteries and arterioles produces vasodilatation in vessels in a resting state and additionally produces relaxation in pre-contracted vessels (Edvinsson et al., 1977, Dacey and Bassett, 1987). Furthermore systemic administration of cholinesterase inhibitors such as physostigmine, that increase extracellular levels of ACh, have been observed to increase CBF without concomitant metabolic activation (Scremin et al., 1982). Anatomic AChE and ChAT studies have identified a network of ACh fibres innervating the cerebrovasculature (Arneric et al., 1988). Additionally, high levels of AChE and ChAT are preferentially associated with cerebral arteries in comparison to peripheral arteries and specific choline uptake and release mechanisms, systems closely associated with ACh nerve terminals have been identified in major cerebral arteries (Arneric et al., 1988) . These observations indicate that cerebral blood flow is at least in part regulated by ACh innervation. A neurogenic basis for ACh regulation of cerebral blood flow is enhanced by evidence from studies involving stimulation of cholinergic projection neurons. Electrical stimulation of the nucleus basalis in the basal forebrain and the fastigial nucleus of the cerebellum increases cerebral blood flow in the cortex of rats in a stimulation dependent manner (Arneric et al., 1987). The importance of ACh in regulation of cerebral blood flow has recently been confirmed by the observation that ACh neurons provide the major innervation of the cortical microvasculature-an important vascular segment for regulation of cerebral blood flow (Vaucher and Hamel, 1995).

The vasodilatory responses of cerebral vessels to cholinomimetic administration or to stimulation of ACh neurons can generally be blocked in a competitive and reversible manner by the administration of atropine. Responses are therefore elicited through action at mAChRS. Under physiological conditions the vasodilatory action of ACh is endothelium dependent and is produced by stimulation of mAChRs on the vascular endothelium (Furchgott and Zawadzki, 1980). Activation of endothelial mAChRs stimulates synthesis and release of an endothelial derived relaxing factor , believed to be nitric oxide which then acts to modulate vascular tone (Paler et al., 1987). Nitric oxide is produced from l-arginine by the synthetic enzyme nitric oxide synthase, the action of which can be inhibited by a number of l-arginine analogues such as L-NOARG (More et al., 1990). Administration of L-NOARG inhibits cortical vasodilatation following electrical stimulation of the ACh basal forebrain, implicating nitric oxide release in ACh mediated vasodilatation (Biesold et al., 1989).

Recent evidence has identified the presence of a population of cortical nitric oxide synthase containing neurons associated with the vascular bed receiving cholinergic input from the basal forebrain (Voucher and Lintel, 1997). This observation indicates that ACh regulation

of cerebral blood flow is partly controlled via direct action on mAChRs of the vascular endothelium and partly via stimulation of local nitric oxide releasing relay neurons associated with the vascular bed. The evidence outlined above indicates a significant role for ACh in the control of cerebral blood flow.

## Behavioural Aspects Of Cholinergic Transmission

### *ACh and Arousal*

The concept of arousal as a general state of CNS activity is classically related to the different stages of sleep and wakefulness (Morass and Meagan, 1949). During the waking state, cortical electroencephalogram (EEG) is dominated by a pattern of low voltage, high frequency discharge known as EEG de synchrony, which is characteristic of an aroused state. The concept of arousal has since been developed into the notion of a state of CNS activity that optimises the processing of sensory stimuli in the cerebral cortex. A process which is now construed as a form of attentional function (Hebb, 1955). The level of arousal, consciousness and the regulation of the sleep waking cycle was originally proposed to be under the influence of an ascending reticular activating system controlled by the reticular formation (Moruzzi and Magoun, 1949). It is now known that arousal is controlled by a diffuse network of cholinergic and monoaminergic (NA, DA and 5-HT) pathways which innervate wide areas of the forebrain and cortex (Robbins, 1997).

The involvement of cholinergic mechanisms in the control of cortical activation dates from the well known ability of systemically administered muscarinic antagonists to block EEG desynchronisation during normal waking periods (Longo, 1966). This observation was tied to the concept of a reticular activating system by the identification of a projecting cholinergic cell group (mesopontine cholinergic complex) in the rostral brainstem by Shute and Lewis (1967). This system was proposed to mediate the major activating effects on cortical EEG, with the observation that cholinergic neurons in this region increased their firing rate during periods of EEG desynchronisation.

The theory of cholinergic mesopontine control of cortical activation was consolidated with the confirmation of a major cholinergic pathway connecting the mesopontine cholinergic complex and the thalamus, and was enhanced by the observation that depolarisation of cholinergic thalamic neurons was associated with EEG desynchronisation (McCormick, 1989). The thalamus itself is now known to play an important role in cortical activation and information processing (Riekkinen et al., 1991). However, control of cortical activation by the mesopontine cholinergic complex was discredited to a significant degree with the demonstration that cholinergic neurons of the basal forebrain provide the main cortical innervation as well as the major afferent input to the reticular nucleus of the thalamus (Levey et al., 1987). Furthermore, a diffuse network of

intrinsic cholinergic neurons within the cortex was identified which may also be involved in cortical activation. A considerable body of evidence now exists supporting basal forebrain regulation of cortical EEG activity. Increased firing of cholinergic neurons of the NBM display inverse correlation with the power of cortical slow delta activity (Buzsaki et al., 1988a). Selective lesioning of NBM cholinergic neurons produces cortical cholinergic deafferentiation and slowing of EEG (Buzsaki et al., 1988b) which can be partially alleviated by administration of muscarinic agonists or anticholinesterase drugs (Riekkinen et al., 1991).

These ascending cholinergic projections from the NBM play an important role in attentional function. Following lesion of NBM, rats with approximately a 70% loss of cortical ChAT activity , display impaired performance in a 5 choice continuous performance test of attention, involving location of randomly presented light flashes. (Muir et al., 1995). This behaviour is not thought to be the consequence of the loss of motor or sensory function but a direct deficit of attentional performance. The deficit in performance is exacerbated when the duration of stimulus is shortened, and is mimicked by pharmacological manipulations that reduce cholinergic function (Robbins, 1997). In addition, the effects of both lesioning and pharmacological intervention can be reversed by administration of the anticholinesterase physostigmine, thus defining the deficit as primarily cholinergic in nature (Muir et al., 1995). Impairment of performance in this task has recently been identified as functional deficit of the cholinergic frontal cortex (Muir, 1996,). It is now apparent that different regions of the basal forebrain are involved in control of distinct cortical functions. Lesion of the VDB produces cholinergic deafferentiation of the parietal cortex and a functional impairment associated with conditional discrimination. Furthermore, loss of cholinergic input to the hippocampus, produced by lesion of the MS results in impairment of performance in working memory tasks (Robbins, 1997).

*Learning and Memory*

There is a large body of evidence to suggest the involvement of central cholinergic systems in learning and memory. Different fields of research have provided the empirical bases for the cholinergic hypothesis of learning and memory. These are behavioural pharmacology- the effects of cholinergic drugs on cognitive performance, behavioural neuroscience-the effect of brain lesions on cognitive performance and aging and dementia research. The last field providing the most convincing evidence, with a correlation between reduced cognitive performance in aging and dementia as observed in Alzheimer's disease, and loss of cholinergic markers in the brain (Bartus et al., 1982).

The amnesiac effect of the cholinergic antagonist scopolamine provided some of the first pharmacological evidence of a role for the cholinergic system in learning and memory (Drachman and Leavith, 1974). Systemically injected scopolamine was observed to produce

amnesia in young healthy adults in a manner comparable to that observed in aged untreated adults. The effects could be reversed by the subsequent administration of a cholinesterase inhibitor. These results indicated that the cognitive deficit observed was cholinergic in nature. In addition, administration of pirenzepine, mecamylamine and hemicholinium all produced similar impairments in memory . Many subsequent experiments have been performed (often involving scopolamine) showing that cholinergic antagonists mediate impaired performance in tasks of learning and memory. More recent studies however, have indicated that the cognitive impairment observed with scopolamine does not directly affect mnemonic function but produces this deficit by inhibition of sensory, attentional and motor functions. For example, in young healthy monkeys intramuscular administration of scopolamine produced a deficit in a delayed matching to sample task (Rupniak et al., 1991). The impairment showed a similar profile when the delay was lengthened or irrelevant stimuli were presented during the delay interval, and was similar to the performance observed in untreated aged rats. Administration of physostigmine enhanced the performance of scopolamine treated rats in the standard test but not in the prolonged delay or irrelevant stimuli trials. In addition, physostigmine did not enhance the performance of aged rats. These results suggest that the cholinergic system does not mediate short term memory in this task, or at least that the anti-cholinergic action of scopolamine does not affect short term memory. Disruption of attentional processing by scopolamine is a more likely explanation for these data. Further evidence is available to support the theory that mnemonic deficits observed following systemic administration of scopolamine may not primarily affect the learning and memory process but is actually the result of impaired sensory and attentional function (Kirk et al., 1988). The cholinergic specificity of scopolamine in producing cognitive deficits is also in question. Compounds such as d-amphetamine, fluoxetine and nootropic drugs such as piracetam, aniracetam and diazepam have all been observed to attenuate memory impairment produced by scopolamine, indicating the involvement of other non-cholinergic neurotransmitter (Smith, 1988). A further problem with the interpretation of the studies detailed above concerns the specificity of action of cholinergic compounds following systemic injection. Systemic injection of cholinergic drugs produces undifferentiated effects -i.e. the entire central cholinergic system will be affected. Individual cholinergic pathways control qualitatively different psychological functions and therefore any behaviour observed following systemic administration of a cholinergic compound is likely to be the result of drug action on a number of different cholinergic pathways. Studies involving local infusion or injection of cholinergic drugs into specific brain regions circumvent this problem and allow a more controlled analysis of cholinergic involvement in learning and memory.

Several studies have been performed in which local infusion of drugs into the hippocampus has been observed to impair performance in learning and memory tasks (Blozovski and Hennocq, 1982, Brito et al., 1983, Blokland et al., 1992). These studies

however, did not take into account possible impairment of attentional and motor functions and should be regarded as far from conclusive evidence with regard to hippocampal cholinergic involvement in learning and memory. Further studies involving the bilateral injection of scopolamine and pirenzepine into the hippocampus of rats have been performed (Messer et al., 1987). Scopolamine was observed to produce accuracy impairment and also increase the latency of response in a T-maze alternation task, whereas pirenzepine only caused accuracy impairment. These observations lend support to the theory of a more specific action of pirenzepine and involvement of the $M_1$ receptor in learning and memory. Additional support for this theory comes from another study in which a unilateral intraventricular infusion of pirenzepine impaired performance in a spatial learning task in rats (Hagan et al., 1987). Thus, drugs with more specific cholinergic actions appear to produce more specific effects on learning and memory. Further evidence involving muscarinic receptors in the control of learning and memory comes from the study of Andrews et al., (1994) in which pirenzepine, AF-DX 116 and UH-AH 37 each impaired performance in cognitive tasks.

The non-specificity of systemically administered scopolamine on cholinergic pathways was further demonstrated by the observation that injection of scopolamine into selective brain regions produced different effects on memory performance. Bilateral injections into the hippocampus produced a delay dependent performance in a delayed matching to position task, while similar injections into the pre-frontal cortex produce a delay independent deficit in the same task. These results suggest a role for the hippocampal cholinergic system in short term memory with the pre-frontal cholinergic system appearing to affect memory by a non-specific mechanism. In this regard scopolamine appears to have a greater effect on working memory than on reference memory (Ingles et al., 1993). Intrahippocampal injections of both pirenzepine and methoctramine have been observed to produce deficits in working memory without appearing to have any effect on reference memory. In a similar study, injections of mecamylamine also produced cognitive impairment indicating the involvement of nicotinc receptors in working memory (Ohno et al., 1993). As in previous studies, however, the non-specific effects of treatment on attentional processes, motor function and motivation were not taken into consideration. Further studies with scopolamine involving intraventricular infusion in monkeys support the theory of cholinergic disruption of attentional function in producing cognitive deficits as opposed to a direct effect on working memory. In a continuous performance task scopolamine reduced the number of responses noted with no associated decrease in accuracy. This effect was exacerbated when stimulus duration was shortened (Callahan et al., 1993).

From the studies outlined above it is apparent that different cholinergic pathways within the brain are associated with different psychological functions and that systemic administration of cholinergic drugs such as scopolamine provide relatively little evidence to

support a specific role for cholinergic systems in learning and memory processes. In addition, the mnemonic deficits observed upon systemic administration of cholinergic drugs are more likely to be due to disruption of attentional function. Studies involving the injection of cholinergic drugs into specific brain sites have much greater value and support a less direct role of ACh in learning and memory.

The hypothesis that cholinergic degeneration of the basal forebrain is responsible for geriatric memory dysfunction and dementia in Alzheimer's disease gave rise to studies of the involvement of the cholinergic system in mnemonic functions in experimental animals. Animal models of Alzheimer's were developed by lesioning brain cholinergic nuclei. As the cortical and hippocampal regions receive their major innervation from the cholinergic nuclei of the basal forebrain these areas were targeted for lesion studies.

The majority of studies performed have employed the use of axon sparing neurotoxic excitatory amino acids, particularly ibotenic and kainic acid, to produce basal forebrain lesions . These compounds produce general cell body destruction in the basal forebrain including cholinergic cells of the NBM and are thought to be more selective than electrolytic or radiofrequency induced lesions. Kainic or ibotenic acid lesions of the basal forebrain have been found to impair memory function in a number of learning and memory tasks including passive avoidance including active avoidance , spatial navigation and spatial delayed matching to sample tasks . For review of these studies see Dunnett et al., (1991). These observations have been interpreted as lesions disturbing learning and memory processes and as evidence for the involvement of cholinergic systems in these processes. However, the cognitive deficits displayed may be the result of disruption of other cognitive or non-cognitive processes and may be attributable to the destruction of other non-cholinergic cell groups within the basal forebrain. In this regard, ibotenic acid lesions of the basal forebrain have been observed to produce a high mortality rate and cause a wide range of somatosensory and motor deficits. The location of the lesion also appears to have important effects on memory performance. For example, excitotoxic lesion of rat NBM results in impairment of reference memory leaving working memory intact while bilateral lesion of the hippocampus selectively disrupts working memory leaving reference memory intact . Evidence also suggests that the memory deficits observed are more likely to be the result of disruption of attentional processes (Robbins. et al., 1989). The specificity of the lesion for cholinergic cells has also been brought into question. In basal forebrain lesion studies comparing four excitotoxins, *N*-methyl-D-aspartate (NMDA), kanic, ibotenic and quisqualic acid, all four toxins produced comparable cortical ChAT depletions. However, quisqualate produced fewer side effects than the others and showed greater specificity to cholinergic neurons. In addition, quisqualic acid produced severe deficits in a passive avoidance test but only ibotenic acid produced deficits in a spatial navigation test, a standard test for cognitive deficits induced by basal forebrain lesions (Dunnett et al., 1987). In several further studies these observations have been repeated(See Dunnett, et al., 1991 for review). Quisqualic acid

produces greater destruction of NBM-cortical cholinergic neurons than ibotenic acid as assayed by cortical ChAT activity, while producing significantly milder deficits in cognitive performance.

An excitotoxin even more effective in destroying cholinergic NBM neurons, α-amino-3-hydroxy-5-methyl-4-isoxazole proprionic acid (AMPA), has also been studied. AMPA can produce greater than 70% depletion of cortical ChAT activity while having minimal or no effect on cognitive performance. Although AMPA produces a more specific and greater cholinergic cell loss than ibotenic acid it should be noted that a significant loss of non-cholinergic cells in the basal forebrain still occurs (Page et al., 1995).

The studies detailed above would appear to indicate that the cholinergic involvement in cognitive deficits observed following basal forebrain lesion has been overestimated. As the cholinergic specificity of the lesion increases the deficits in learning and memory are reduced. Therefore, while AMPA would appear to be the neurotoxin of choice to induce cholinergic basal forebrain lesions, a highly selective cholinergic toxin would provide further elucidation of the cholinergic involvement in learning and memory.

Initial developments on a selective cholinergic neurotoxin centred on ethylcholine mustard aziridinium (AF64A). This compound was shown to be a selective neurotoxin for septo-hippocampal neurons (Fisher et al., 1982). Intraventricular injection of AF64A produced destruction of cholinergic neurons and reduced ChAT and ACHE activity in the hippocampus (Hanin, 1990). However, AF64A has been discredited as a selective cholinergic neurotoxin as it was found to cause gross tissue damage when injected intraparenchymally (Jarrard, et al., 1984 ).

The coupling of 192 IgG, a monoclonal antibody specific for the p75 low affinity NGFr, to saporin, a ribosome inactivating factor, provided the first highly selective cholinergic neurotoxin (Wiley et al., 1991). Intraventricular infusion of 192 IgG Saporin produces high levels of basal forebrain cholinergic cell loss associated with minimal effects on monoaminergic and other cholinergic systems. In addition, intracortical injection was observed to produce loss of cortical cholinergic neurons as evinced by reduced AChE staining, without affecting non-cholinergic systems (Holley et al., 1994). Initial studies involving intracortical injection of 192 IgG Saporin produced impaired performance in spatial awareness tasks and associated reduction of ChAT activity (Nilssson et al, 1992). These observations lend support to cholinergic involvement in learning and memory. In contrast however, specific lesion of the basal forebrain produced a high degree of cholinergic cell loss, with minimal non-cholinergic cell loss but no associated deficits in memory and learning (Wenket al., 1994). A further study with 192 IgG saporin induced lesion of the NBM supports the above observations, with virtually no learning and memory deficits shown (Torres et al., 1994).

From the above data it is apparent that the more specific the lesion is for cholinergic cells, the less dramatic the effect is on learning and memory. Extrapolation of these data would

suggest that a completely selective cholinergic lesion would have no effect on learning and memory. It does however appear that the cholinergic system in the basal forebrain is involved in attentional rather than mnemonic processes (see previous section *ACh and Arousal* for details).

### 1.1.3 Cholinergic System In Alzheimer's Disease

Alterations in cholinergic function, particularly the loss of mAChRs has been reported in a number of neurological and psychiatric conditions. These include schizophrenia (Tandon et al., 1991), Huntington's disease (Penney et al., 1982), Progressive Nuclear Palsy and Parkinson's disease (Palacios et al., 1990). However, the most consistent and well documented neuropathological condition associated with cholinergic degeneration is Alzheimer's disease.

Alzheimer's disease (AD) is a progressive neurodegenerative condition affecting almost 1 in 10 individuals over the age of 65 (Evans, 1989). It accounts for over 50% of the senile dementia and the majority of pre-senile dementia cases and is characterised progressive deterioration of higher cognitive functions including the loss of memory (Octave, 1995). Postmortem AD brains display two distinctive neuropathological features which constitute conclusive diagnostic markers for AD: intracellular neurofibrillary tangles and extracellular neuritic senile plaques. Intracellular neurofibrillary tangles accumulate in neuronal perikarya and consist of paired helical filaments containing the microtubule associated protein tau (Delacourte and Defossez, 1986). The presence of tau in neuronal cell bodies represents a highly aberrant localisation of the protein, as compared to the axonal localisation observed in normal neurons (Kowall et al., 1987). In AD brains , tau is present in tangles in a hyperphosphorylated form (Grundke-Iqabal et al., 1986). The amount of phosphorylated tau in AD brain is several hundred fold greater to that in normal brains, making tau an excellent disease marker (Vandermeeren et al., 1993).

The neuritic plaques observed extracellularly in AD brains contain amyloid peptide fibrils in their core. These fibrils consist of the amyloid ß or A4 (ßA4) peptide (Glenner et al., 1984). The ßA4 peptide is derived from a larger precursor peptide termed the amyloid precursor peptide/protein (APP) , a glycosylated transmembrane protein with a single membrane spanning domain (Kang et al., 1987). APP is normally cleaved within its transmembrane domain yielding a secretory form , the exact physiological role of which is not entirely understood. Processing in this manner normally involves cleaving APP in the ßA4 domain, which consists of 15 transmembrane and 28 extracellular amino acids. However, an alternative processing pathway exists in which APP is cleaved at abnormal transmembrane and extracellular sites, generating a soluble form of ßA4 which may then go on to form amyloid plaques.

In addition to these specific neuropathological features AD brains exhibit extensive cellular atrophy and cell loss, shrinkage of cortical thickness, enlargement of sulci and ventricles and changes in multiple neurochemical systems including ACh, glutamate, GABA and 5-HT.

However, the most consistent and severe neurochemical abnormality associated with AD is the loss of cholinergic innervation of the cerebral cortex and hippocampus (Coyle et al., 1983). ChAT activity is significantly reduced in the cortex and hippocampus of AD

brains (Reisine et al., 1978). Post-mortem analysis of AD brains reveals that the NBM, the major source of cortical and hippocampal cholinergic innervation, is degenerated in AD (Whitehouseet al., 1982). In addition, a linear correlation between reduced cortical ChAT activity and degree of dementia has been observed (Perry et al., 1978). Observations such as these prompted Bartus et al., (1982) to propose the cholinergic hypothesis of AD in 1982, which specifically attributed the cognitive deterioration associated with the disease to the degeneration of the cholinergic basal forebrain .

**Muscarinic Receptors in Alzheimer's Disease**

The observation that the muscarinic antagonist scopolamine produces cognitive deficits in young healthy humans (see *ACh in Learning and Memory*) promoted interest in the expression levels of muscarinic receptors in dementia and AD. Pharmacologically defined binding sites have been analysed in detail in both AD and control brains post-mortem (see Levey, 1996 for review). Initial results were somewhat conflicting, with several groups reporting decreases and other groups reporting no change in receptor density. The reason for these discrepancies is not certain, but may be due to the use of non-subtype selective radioligands in the performance of the binding assays. More recently, the general consensus was that neither the total population of receptors (as detected by N-methyl scopolamine or quinuclidinyl benzilate) nor the $M_1$ or $M_2$ subtypes (detected using pirenzepine), undergo any marked change in number or affinity in AD (Perry et al., 1990). However, several inconsistencies in these results still exist, as these ligands do not have the necessary specificity to accurately distinguish between the individual mAChR subtypes or to spatially resolve their pre- or post-synaptic location. Several studies indicate that $M_1$ receptors, which are generally regarded as primarily postsynaptic, undergo no change in AD as determined pharmacologically by radioligand binding studies. In contrast, "pre-synaptic" $M_2$ receptor levels are reduced in cortex and hippocampus in AD (Mash et al., 1985).

The recent identification of five distinct molecular mAChR subtypes has made interpretation of the above results difficult with regard to the distribution of the molecular subtypes within the brain. A recent immunoprecipitation study has provided information on the expression of the molecular mAChR subtypes in AD. A significant reduction in the level of $m_1$ receptor protein was observed in the cortex and hippocampus of AD brains compared to controls, despite unchanged levels of $M_1$ binding sites observed in the same tissues as detected by [$^3$H] pirenzepine (Flynn et al., 1995). These observations are in conflict with the previous theory which suggests that $m_1$ receptor levels are unchanged in AD. The authors suggest that although the number of $M_1$ ligand binding sites is unchanged an altered form of receptor protein may be present in AD which results in reduced antibody recognition and the reduction in $m_1$ sites observed. In addition, they propose that the existing receptor-binding sites may be non-functional or functionally impaired, as the antibodies bind to the

third intracellular loop of the receptor a site which is critical in G-protein interaction. Therefore, a specific alteration at this site may have severe consequences on signal transduction and signal amplification following receptor activation.

In agreement with previous ligand binding studies Flynn et al., observed reduced $m_2$ immunoreactivity in cortex and hippocampus, correlated with reduced $M_2$ ligand binding site density. A further observation from this study was a significant increase in $m_4$ immunoreactivity in cortical regions. This increase in $m_4$ sites may be responsible for the findings of previous ligand binding studies in which levels of $M_1$ receptor binding was unchanged. The ligand binding specificity for the $m_1$ and $m_4$ receptors overlap, in that they are both "$M_1$-like" . The opposing directions of change in the levels of these receptors in AD could therefore feasibly account for the apparent lack of change in $M_1$ receptor numbers in ligand binding studies (Levey, 1996).

## Cholinergic Therapy of Alzheimer's Disease

The cholinergic hypothesis of Alzheimer's disease attributes the cognitive deficits of the disease and their severity to the degeneration of the cholinergic pathways from the NBM to the cortex and hippocampus. For this reason therapies aimed at the treatment of AD have been generally based upon cholinergic replacement, with the aim of alleviating the symptoms or to slow down deterioration by attenuating the progression of the disease. Initial therapies were based upon the success of L-DOPA in the treatment of Parkinson's, with precursor loading of patients with choline or lecithin in an attempt to boost ACh synthesis( Wurtman, 1985). This approach was unsuccessful however, possibly due to the need to simultaneously increase release and inhibit breakdown of ACh. Thus far, four other cholinergic strategies have been investigated, including increasing ACh release, reducing breakdown of ACh , activating postsynaptic mAChRs and stimulation of second messengers (Lamy, 1994). To date, with the exception of AChE inhibitors, all of these strategies have met with no success, although research is on going in the development of CNS penetrative subtype specific mAChR agonists (Iverson, 1993).

Cholinesterase inhibitors such as physostigmine and tacrine have been reported to have produced limited improvements in cognition and memory in clinical studies in some AD patients (Lamy, 1994). Physostigmine, one of the oldest and most studied AChE inhibitors, produces a small improvement in cognition of less severely demented AD patients (Stern et al., 1988). However, its short duration of action and common adverse side effects preclude its use as a major therapeutic agent for AD. Tacrine has displayed the most promising therapeutic effects of all AChE inhibitors studied for the treatment of AD. It has a longer duration of action and fewer side effects than physostigmine and produces not only a symptomatic improvement in AD but may also slow disease progression (Giacobini, 1994).

Compared to physostigmine it is a relatively weak AChE inhibitor. Therefore its ability to alleviate symptoms of AD is not simply a result of its ability to inhibit AChE and is due to other effects of the drug. Indeed tacrine is known to have multiple actions on mammalian brains (Lamy, 1994). A possible mechanism to explain the slower deterioration of AD patients resulting from tacrine treatment comes from data indicating that cholinergic agonist may regulate the processing and secretion of ßA4 by increasing PKC levels of target cells (Nitsch et al., 1992). Increasing the levels of ACh in AD close to those in normal brains may activate normal APP processing, thus reducing ßA4 deposition and the neurodegeneration associated with it (Giacobini, 1994). In agreement with this hypothesis is the observation that chronic treatment with the mAChR antagonist atropine (mimicking cholinergic de-nervation in AD) increases ßA4 content in rat cerebral cortex (Beach et al., 1996). From the above observations it appears that AChE inhibitors have limited efficacy in the treatment of AD, with limited beneficial effect in some patients with mild to moderate symptoms. They are however the only viable therapy presently available for the disease. For a review of AChE inhibitors in AD see Lamy, (1994).

**Nicotinic Receptors in Alzheimer's Disease**

With the lack of success of previous cholinergic therapies for AD generally aimed at increasing mAChR function , research interest turned towards nAChRs. In contrast to mAChRs, there is clear evidence from numerous ligand binding studies that there is a significant loss of nAChRs from the cortex and hippocampus in AD along with parallel reductions in ChAT activity (Whitehouse et al., 1986). For a review on nAChRs in AD see Court and Perry, (1994).

Nicotinic receptors exist as pre-synaptic autoreceptors, activation of which enhances ACh release from cholinergic neurons in the cortex and hippocampus, and as such they present novel targets for cholinergic therapy in AD (Araujo et al., 1988). Administration of nicotine is observed to enhance cognitive performance (Sahakian et al., 1989) and a reduced occurrence of AD has been reported in populations of smokers and former smokers as compared to non-smoking population. These observations indicate the possible therapeutic and neuroprotective actions of nAChR stimulation. Problems exist with the use of nicotine as a therapeutic agent itself concerning the prevalent undesirable side effects associated with the drug, such as addiction and adverse cardiovascular effects. However, research is on going into the development of novel subtype selective therapeutic drugs with action at central nAChRs, with particular interest in the α4ß2 nAChR which is thought to represent the population of pre-synaptic receptors lost in AD (Abreo et al., 1996).

## ApoE: Selective Vulnerability of Cholinergic Neurons In Alzheimer's Disease

Although other neurochemical systems in the brain degenerate in AD, cholinergic neurons appear to be the most vulnerable. This selective vulnerability may be due to the unique nature of ACh neurons in that they use choline for two purposes: ACh synthesis and membrane phosphatidyl choline synthesis. The enzymes involved in both processes are dependent upon the concentration of choline as their rate limiting step in the formation of phosphatidylcholine and ACh. Therefore, in a situation where choline is in short supply and ACh neurons are physiologically active, synthesis of ACh transmitter will take precedence over membrane building, in order to sustain neurotransmission (Ulus et al., 1989). If this situation persists, phosphatidylcholine will be removed from the membrane to supply choline for transmitter synthesis-a process known as "autocannabilism" , which may lead to cell shrinkage and even death. From postmortem studies it has been found that phosphatidylcholine turnover is accelerated and choline availability reduced in AD brains (Blusztain et al., 1990). Changes in membrane composition such as this could result in the abnormal exposure of the transmembrane domain of APP and could feasibly be the cause of its abnormal processing and the production of ßA4 (Wurtman et al., 1992).

Recently, the role of apolipoprotein E (ApoE) a lipid carrier molecule playing a key role in mobilisation and redistribution of cholesterol and phospholipid during membrane remodelling associated with synaptic plasticity and CNS injury, has been implicated in the pathology of AD (Poirier et al., 1991). Three major isoforms of ApoE exist, E2, E3 and E4. These isoforms are expressed from multiple alelles on a single gene and give rise to three common homozygous phenotypes ε2/ε2, ε3/ε3, ε4/ε4 and three heterozygous phenotypes ε2/ε3, ε2/ε4 and ε3/ε4 (Poirier et al., 1994). Evidence strongly suggests that possession of the Apoε4 allele is a pre-disposition to development of AD and an indicator of poorer response to cholinergic therapy. The frequency of the Apoε4 allele has been shown to be markedly increased in AD patients (Poirier et al., 1993). A gene dosage effect has also been observed, in that as the age of onset of AD increases, Apoε4 allele copy number decreases . In addition, ApoE mRNA levels have been shown to be reduced in the cortex and hippocampus of AD brains post-mortem, with subjects of Apoε4/ε4 genotype expressing approximately 50% of the level of ApoE compared to Apoε3/ε3 or control brains (Bertrand et al., 1995). It is therefore reasonable to assume that ApoE associated lipid transport is severely compromised in AD, resulting in inefficient cholesterol and phospholipid transport and ultimately loss of synaptic integrity (Poirier, 1994). This loss of function may selectively damage the cholinergic system which, as described above, relies heavily upon intact phospholipid metabolism. The theory of the selective vulnerability of cholinergic neurons in AD is enhanced with the observations that the characteristic reductions in ChAT activity in the cortex and hippocampus of AD brains is proportional to the E4 allele copy number, i.e. as E4 copy number increases, ChAT activity decreases (Poirier, 1994 ). However, in conflict

with the above observations, a recent study has indicated that reductions in ChAT activity and nAChR number observed in AD were independent of ApoE genotype (Svensson et al., 1997). In addition, a study with ApoE knockout mice, no deficit in central cholinergic activity (e.g. ChAT activity, receptor number) or cognitive performance was observed between knockout and wild type mice (Anderson and Higgins, 1997) despite previous report to the contrary (Gordon et al., 1995).

The evidence described above indicates that the ApoE4 genotype influences the integrity and function of the cholinergic system in AD, with E4 carriers being at greater risk for the loss of cholinergic neurons and therefore also less capable of responding to cholinergic therapies based upon enhancing the function of remaining cholinergic neurons.

## 1.2 IMAGING OF THE CNS *IN VIVO*

Techniques for brain imaging can be broadly divided into two categories: structural and functional. Structural techniques such as computed tomography (CT) and magnetic resonance (MRI) imaging, generally provide purely neuro-anatomical and pathological information on the brain, while functional imaging techniques such as positron emission tomography (PET) and single photon emission computed tomography (SPECT) allow compilation of functional maps reflecting the biochemistry and physiology of the brain.

### 1.2.1 Structural Imaging

*Computed Tomography (CT) and Magnetic Resonance Imaging (MRI)*

Computed tomography is a method of x-ray examination of the CNS in which a thin slice or planar volume of tissue is examined. In contrast to conventional radiography, the x-ray is collimated to a linear beam, allowing measurement of absorbance in a thin slice or planar volume of the brain. This decreases the superimposition of tissues and the scatter effects of wide-beam x-rays upon the image as in conventional radiography (Orison, 1989). The x-ray source coupled with detectors surrounding the head measure the amount of x-ray transmission passing through the region of interest, enabling calculation of the attenuation of the x-ray beam occurring at specific points within the brain. Digital storage and processing using mathematical algorithms is then accomplished with the aid of computers to re-construct the radiographic image. In certain instances, where a more detailed image of a specific area of interest is needed, the technique of contrast enhanced CT is employed. Contrast enhanced CT involves the intravenous injection of a radio-opaque medium that will absorb x-rays. The contrast medium is of high electron density and is usually iodine based. Contrast enhanced CT is used to increase the contrast between areas of high and low absorbance of x-rays on the radiographic image. It can be used to increase the image contrast between areas of normal and abnormal tissue that are not well defined prior to contrast medium infusion, such as breakdown of the blood brain barrier.

In contrast to CT, MRI is a relatively new technique with a significantly different method of image production. MRI manipulates the physical phenomenon of spinning subatomic particles (nucleons) present in the nucleus of any atom. The intrinsic magnetic properties of a nucleus of any atom (and also their magnetic resonance parameters ) are dependent upon the proton density within the nucleus. Nuclei with even numbers of protons and neutrons display no significant magnetic properties as they tend to cancel each other out. However unpaired nuclei, with an odd number of protons, such as the hydrogen nucleus (single proton) are highly magnetic and also extremely useful for MRI. The hydrogen nucleus which is present in natural abundance in biological tissues can be manipulated for

MRI. When placed in a magnetic field protons will orient their spin in alignment with the magnetic field. Pulsing of the tissue with a radiofrequency wave at the correct frequency, excites the spinning protons causing them to move out of alignment with the magnetic field. When the radiowave pulse ends, they will revert their spin to a position of equilibrium within the magnetic field while simultaneously losing energy which can be detected as a radiofrequency or transverse magnetic field signal. This signal is then amplified and processed by computer to reconstruct an image. A specific area of tissue emitting a signal can be identified by creating gradients within the magnetic field allowing the x, y and z co-ordinates of given value to be generated which in turn allows three dimensional reconstruction of the image. Images can therefore also be constructed in any plane desired.

MRI displays several advantages over CT as a method of imaging the CNS. It makes use of natural non-radioactive nuclei without the use of ionising radiation to generate images. The images themselves are of high resolution with the absence of bone or dental artefacts commonly observed with CT (see Chakeres and Schmalbrock, 1992).

Both CT and MRI are conventionally concerned with the imaging of brain pathology and neuroanatomy and are routinely used diagnostically for a number of CNS conditions. These include visualisation of cerebral contusions, oedema and haemorrhage following head trauma, cerebrovascular infection (e.g. meningitis), cerebral infarction of various types and diagnosis of cerebral neoplasms. Additionally they are both used to image the pathology of a number of neurodegenerative diseases including Alzheimer's disease (for review see Smith, 1996). However, relatively recently MRI techniques have been expanded to visualise brain function. Using a blood oxygenation level dependent (BOLD) contrast mechanism for MRI, cerebral blood flow and oxygen utilisation in rat was measured. The technique is based upon the levels of deoxyhaemoglobin (which acts as a natural paramagnetic agent) which are altered by oxygen consumption and the metabolic activity of neurons during elevated function. Experiments such as these were subsequently repeated in cats (Turner et al., 1991) since which time functional MRI (fMRI) has been successfully used to map functional activity in the human brain in numerous studies (for review see Kim and Ugurbil, 1997 ) including Alzheimer's disease (Smith, 1996).

As a functional imaging technique, fMRI offers advantages over the more conventional functional imaging techniques of PET and SPECT. Theoretically fMRI offers higher resolution both temporally and spatially as well as allowing repeated scanning in a single subject without concern for the cumulative effect of multiple doses of ionising radiation. Furthermore, fMRI allows highly accurate comparison of functional and anatomical maps of the brain as both types of data may be acquired simultaneously during a single imaging session.

### 1.2.2 Functional Imaging

*Autoradiography*

*In vivo* receptor autoradiography involves the selective labelling of CNS receptors by the intravenous administration of a radioligand with high affinity and specificity for the target receptor. The first studies of *in vivo* receptor labelling with autoradiography utilised radioligands for the mapping of mAChRs with [$^3$H] quinuclidinylbenzilate (QNB) (Kuhar and Yammamura, 1975), [$^3$H] diprenorphine for opiod receptors (Pert et al., 1975) and [$^3$H] spiperone for dopamine receptors (Kuhar, et al., 1978). These radioligands have several characteristics that allow them to be used for *in vivo* receptor labelling including rapid penetration into the brain from the circulation, high receptor affinity, very slow dissociation kinetics, antagonist activity that allows them to label all receptor affinity states high specific/non-specific binding ratio and ability to quantifying target by modelling its interaction with the radioligand. The high affinity of the ligand for the receptor results in retention of ligand at or on receptor molecule, allowing generation of autoradiograms which provide information on receptor distribution within the CNS (Kuhar et al., 1986).

Mapping of neurotransmitter receptors in this manner has a number of important applications such as providing insight into mechanism of drug action, and the chemical organisation of the brain as well as neuropathological applications. Additionally, *in vivo* autoradiographic studies are essential for the development of PET and SPECT tracers which allow non-invasive imaging of CNS function in man. The ability of this technique to elucidate mechanisms of drug action can be illustrated by considering the well known effects of opiate drugs. Drugs acting at opioid receptors are known to produce a variety of effects including analgesia , cough suppression and respiratory depression as well as their characteristic addictive effects. Investigation of the distribution of opioid receptors among central neuronal circuits allows understanding of these drug effects and how they are produced. A significant number of autoradiographic studies mapping opioid receptor distribution have been performed (see Knapp et al., 1993). Opioid receptors are widely distributed throughout the CNS, with differential distribution between the receptor subtypes ($\partial$, $\mu$, $\kappa$) observed. The nucleus tractus solitarius in the brainstem , which is crucial in respiratory control, is know to contain high densities of $\mu$ and to a lesser extent $\partial$ opiod receptors. Drug action on these receptors is therefore very likely to be responsible for respiratory depression associated with opioid drugs. Other regions of high density include laminae I and III of the dorsal horn of the spinal cord, regions that are proposed to be involve in the analgesic actions produced by opiates (Dubner and Bennet, 1983).

*In vivo* receptor mapping also has applications in assessing the neurotoxic action of drugs. Amphetamines are routinely used in research in psychiatric disorders, producing their beneficial effects by altering monoaminergic neurotransmission. However, over-use or

abuse of these drugs results in neurotoxicity. The extent of neurotoxicity can be estimated by measurement of the high affinity uptake sites situated on monoaminergic nerve terminals. Reduction of uptake binding site density is specifically attributed to the loss of neurons. The neurotoxic actions of amphetamines such as fenfluramine and the amphetamine based drugs 3,4-methylenedioxyamphetamine (MDA) and 3,4-methylenedioxymeth-amphetamine (MDMA) on monoaminergic (particularly 5-HT) neurons has been investigated in some depth using *in vivo* autoradiographic techniques (Appel et al., 1989, De Souza et al., 1990, Battaglia et al., 1991). Repeated administration of MDMA was observed to produce profound reductions in [$^3$H]-paroxetine labelled 5-HT uptake sites in 5-HT pathways ascending to the cortex, striatum and hippocampus, while having no effect on [$^3$H]-mazindol binding, measuring DA uptake sites, thus demonstrating a neurotoxic specificity to 5-HT neurons. In addition to opioid and 5-HT receptors several CNS receptor systems have been mapped with *in vivo* autoradiography. These include mAChRs with [$^3$H] and [$^{125}$I] labelled quinuclidinylbenzilate (QNB), nAChRs with [$^3$H] and [$^{125}$I]-α-bungarotoxin , dopamine $D_2$ receptors with [$^3$H]-spiperone, and benzodiazepine receptors with [$^3$H] Ro15-1788 and Ro15-4513 (for review see Kuhar et al., 1986).

Aside from functional mapping of specific neurotransmitter receptors and elucidation of drug action upon these receptors, *in vivo* autoradiographic techniques can be applied to map metabolic activity in the CNS. The [$^{14}$C]-iodoantipyrine (IAP) and [$^{14}$C]-2-deoxyglucose (2-DG) autoradiographic techniques have made it possible to map regional cerebral blood flow and local cerebral glucose utilisation, respectively, within individual brain regions (Sokoloff et al., 1977, Sakurada et al., 1978). These techniques demonstrate highly localised activity dependent changes in cerebral blood flow and glucose utilisation with a high degree of spatial resolution, with coupling of flow and metabolism to relevant anatomical structures.

The conceptual basis for metabolic mapping with [$^{14}$C]-2-DG is founded upon some basic features of brain biochemistry. The brain is dependent almost entirely upon aerobic catabolism of glucose for its energy requirements, with function in any brain region directly related to the energy consumption within that region. As the brain can store only a very limited amount of carbohydrate, and its energy requirement is dependent upon the level of function, the energy demands must be met by aerobic catabolism of glucose continuously supplied by the cerebral circulation. It follows that increased metabolic activity is often accompanied by increased cerebral blood flow, which is necessary to meet the increased glucose requirements. The above techniques are therefore extremely useful tools as a measure of CNS function.

Functional mapping with [$^{14}$C]-2-DG has been applied to numerous areas of neuropharmacology, including the functional effects of stimulation or blockade of neurotransmitter systems such as glutamate, 5-HT, GABA and ACh. In tune with the theme of this thesis, some examples of functional changes induced by modulation of cholinergic

transmission will be discussed. Administration of the mAChR antagonist scopolamine depresses cerebral glucose utilisation in an anatomically selective manner (Helen and London, 1984). In contrast, the effects administration of the mAChR agonist oxotremorine produces pronounced increases in glucose metabolism primarily in brain structures associated with motor function, e.g. motor cortex, nigrostriatal system, globus pallidus. Oxotremorine produces marked tremor in experimental animals , and it appears that the increased glucose metabolism in brain motor control regions is associated with this motor dysfunction rather than as a result of drug action on cholinergic receptors (Dow-Edwards et al., 1981). The cholinergic agonist arecoline produces similar increases in glucose utilisation to oxotremorine in motor regions of the brain, but also produces significant increases in the hippocampus. The differences in metabolic activation induced by the two compounds are suggested to be the result of their differential effects on mAChR subtypes (Sonancrant et al., 1985). Administration of nicotine also produces significant increases in glucose metabolism, with correlation to brain regions such as the subiculum and superior colliculus, that display a high density of nAChRs (London et al., 1988). Furthermore, glucose metabolism is significantly reduced in the cortex of animals following basal forebrain lesions (London et al., 1984).

The acute and chronic functional consequences of unilateral intracerebral injection of excitatory amino acids into the basal forebrain has been mapped using [$^{14}$C]-2-DG autoradiography in conscious rats (Browne et al., 1998). Acute stimulation of NBM neurons by injection of AMPA significantly reduced glucose use in 9 cortical regions innervated by NBM efferents, including the frontal, sensory-motor and cingulate cortices. Acute stimulation of NBM neurons by NMDA injection reduced glucose use in only two cortical regions, however, NMDA injection was additionally observed to reduce glucose utilisation in a number of cortical regions (including frontal and parietal cortices) contralateral to the injection site. In contrast, injection of the $GABA_A$ agonist muscimol into the NBM had no effect on glucose utilisation in any of the associated cortical regions. Assessment of excitotoxic lesions 3 weeks after injection of AMPA, NMDA, ibotenic acid or quisqualic acid into the NBM indicated no significant alterations in glucose use, suggesting long term compensatory functional adaptation occurs following cortical de-nervation. These observations support the view that AMPA receptors are co-localised with basal forebrain cholinergic neurons to a greater extent than other glutamatergic receptor subtypes.

*PET and SPECT*

Quantitative imaging of functional and pathological processes in the living mammalian brain has recently become feasible through the development of PET and SPECT imaging techniques. PET and SPECT are non-invasive tomographic methods for imaging the

emitting radionuclides such as [$^{11}$C], [$^{13}$N] and [$^{18}$F] which allows them to be substituted into compounds of biological interest without altering their basic pharmacology. This is of distinct advantage when using radiotracers to describe the chemistry of a biological process. However, these radionuclides have a very short half-life (e.g. [$^{13}$N] $t_{1/2}$ = 9.96 mins) which necessitates on site cyclotron and radiochemistry facilities to produce the radionuclides and synthesise the tracers. PET scanners detect the brain distribution of radioactivity by means of externally placed banks of paired detectors that register co-incidental energy (in form of 2 γ rays) from the annihilation of emitted positrons with electrons. Tomographic techniques similar to those employed in CT are then used to reconstruct an image from the γ rays produced. Because of the simultaneous emission of two γ rays in exactly opposite directions, images of high resolution can be constructed.

SPECT employs similar principles to those used in PET, with the main difference being the nature of the radioisotope used to label tracer compounds. SPECT utilises γ or photon emitting radioisotopes such as [$^{123}$I] and [$^{99m}$Tc] in conjunction with a rotating γ camera or multiple detector rings to register emitted activity. In contrast to PET, the synthesis of radioligands is relatively simple as the half life of the compounds is considerably longer (e.g. [$^{123}$I] $t_{1/2}$ = approx. 13.2 hours) which also facilitates ease of scanning. The radioisotopes are also available commercially making SPECT scanning considerably cheaper. However, addition of these large radioisotopes into biological compounds may alter the pharmacology and biodistribution kinetics of the labelled ligand. Therefore a great deal of effort is employed in the synthesis of chemical structures that are lipophilic while retaining pharmacological action. One other disadvantage of SPECT is its reduced spatial resolution compared with PET, due to incomplete correction for attenuation and scatter of activity signal. With the use of the correct collimator, resolution can be improved at the expense of sensitivity, resulting in longer scanning time. Therefore it is necessary to obtain a balance between sensitivity and spatial resolution.

Radioligands for PET and SPECT have to satisfy a number of criteria, very similar to those for ligands used in vitro homogenate binding studies, before they are acceptable for use in human studies. These include: (1) Saturability of the receptor site of interest by radioligand such that increasing doses of unlabelled ligand will displace binding of radioligand. (2) Appropriate competition by various radioligands known to bind to the receptor of interest. (3) Regional distribution of radioligand consistent with the known pattern of neurorceptors. In addition the ligands must be of sufficiently high specific activity to aid detection as receptor densities in the CNS are very low.

A number of ligands for imaging neuroreceptor systems, neurotransmitter precursors, neurotransmitter enzymes and transporters are now available for use with both PET and SPECT . These techniques have a number of clinical applications including measurement of cerebral blood flow, glucose metabolism, neuroreceptor mapping and

monitoring of drug treatment, allowing investigation of the physiology and pathophysiology of the human brain.

The use of [$^{11}$C] N-methylspiperone to label dopaminergic $D_2$ receptors with PET was among the first reports of *in vivo* receptor visualisation in humans (Wagner et al., 1983). Subsequent studies, combined with mathematical modelling, in which the experimental paradigm involved prior administration of neuroleptic drugs to inhibit radioligand binding, followed by a second scan in the control state (no drugs), allowed calculation of receptor density and affinity (Wong et al., 1986a , Wong et al., 1986b). Dopamine $D_2$ receptors have also been mapped successfully in humans with $^{123}$I-(S)-N-(1-ethyl-2-pyrrolidinyl) methyl-2-hydroxy-3-iodo-6-methoxy benzamine ($^{123}$IBZM) and SPECT (Kung et al., 1990). The $D_2$ receptor is implicated in a number of neurologic and psychiatric conditions such as schizophrenia, manic depression, Parkinson's disease, Huntington's disease, and in drug abuse, thus imaging of this receptor is of clinical importance. The clinical utility of functional imaging with PET and SPECT has been demonstrated by visualisation of dopaminergic transmission in conditions such as schizophrenia and Parkinson's disease. For example, clinically effective doses of chemically distinct neuroleptic drugs known to produce their beneficial effects at $D_2$ receptors were observed to display 85-90% occupancy of $D_2$ receptors in the putamen of schizophrenic patients (Farde et al., 1986). Additionally, the loss of $D_2$ receptors in Parkinson's sufferers has been quantified with the use of [$^{18}$F]-spiperone (Hantraye et al., 1986). Dopamine synthesis, the dopamine transporter and $D_1$ receptors can also be imaged with a variety of radioligands with both PET and SPECT.

A number of other neuroreceptor systems can be visualised with both PET and SPECT. These include 5-$HT_2$ receptors with [$^{11}$C]- ketanserin and N-1-[$^{11}$C]-methyl-2-Br-LSD ([$^{11}$C]-MBL) with PET (Baron et al., 1985, Wong et al., 1987). SPECT ligands for 5-$HT_2$ receptors are based upon LSD analogues such as [$^{123}$I]-ethyl-LSD which displays high levels of specific binding in animal models. These receptors are implicated in neuropsychiatric disorders, behavioural dysfunction and drug abuse and are therefore of clinical importance.

PET imaging of opioid receptors was first demonstrated with the use of [$^{11}$C]-carfenatil which is highly selective for the $\mu$ receptor subtypes (Frost et al., 1985). Based on animal studies implicating opioid receptors in epilepsy, a PET scanning study on epileptic patients with this radioligand revealed increased ligand uptake in cortical sites ipsilateral to seizure focus, suggesting that epilepsy could be related to upregulation of opioid receptors (Frost et al., 1988). Benzodiazepine receptors have been imaged in primate and man using [$^{123}$I]-iomazenil with SPECT and with PET using [$^{11}$C]-flunitrazepam and [$^{11}$C]-Ro-15-1788 .

Much interest has centred upon imaging of the central cholinergic system and in particular mapping of cholinergic receptors, due to the associated degeneration of this neurotransmitter system in Alzheimer's disease. Muscarinic cholinergic receptors were first

imaged in man with SPECT using [$^{123}$I] -QNB and a few years later with [$^{11}$C]-scopolamine in PET ( Eckelman et al., 1984a,b, Frey et al., 1987). Distribution of binding was consistent with data from autoradiographic studies and the known cholinergic pathways within the CNS. Since then a great deal of effort has been applied to the development of novel mAChR ligands for use with PET and SPECT, with particular emphasis on the development of subtype selective mAChR ligands. Recently however, interest has moved towards development of nAChR ligands which have been successfully imaged with [$^{11}$C]-nicotine for PET in animals (Nordberg et al., 1989). Imaging of the cholinergic system will be discussed in greater detail in the next section.

PET and SPECT techniques can also be applied to measure cerebral blood flow and glucose utilisation in discrete brain regions within man. Measurement of rCBF with PET and SPECT is based upon the same principles as the autoradiographic technique of Sakurada et al, (1978) using the freely diffusible tracer [$^{14}$C]-IAP (see Methods: Theory of rCBF). With PET radioactive water $H_2$[$^{15}$O] or [$^{15}$O]-butanol are used to measure blood flow (Fox et al., 1984, Berridge, et al., 1991). With SPECT, rCBF may be measured using the [$^{133}$Xe] clearance technique, which involves inhalation of the inert radioactive Xe (Celsis et al., 1981) or by use of more conventional injectable radioactive tracers such as [$^{123}$I]-isopropyl-p-iodoamphetamine (1IMP), [$^{99m}$Tc]-d-L-Hexamethylpropyleneamine (HMPAO) and [$^{99m}$Tc]-Ethylcysteinate Dimer (ECD) (Hill, et al., 1984, Neirinckx et al., 1987, Holman et al., 1989). Glucose utilisation has also been mapped in man using ligands such as [18F]-fluorodeoxyglucose with PET, which is based upon the same principles as [$^{14}$C]-2-DG (Phelps et al., 1981). These techniques have been applied to mapping of cerebral function in a number of physiological and pathological conditions in man including Alzheimer's disease (for review see Waldemar, 1995).

### 1.2.3 Imaging Of Cholinergic Neurotransmission *In Vivo*

#### ACh, Acetylcholinesterase and the Vesicular ACh Transporter

During the past decade considerable effort has been made in the development of radiopharmaceuticals for the *in vivo* study of cholinergic neurotransmission with PET and SPECT. The synthesis of more selective and specific radioligands, together with the development of more efficient PET and SPECT cameras have provided new possibilities for clinical investigation of cholinergic neurotransmission in the physiology and pathology of the human brain (Maziere et al., 1995). Ligands are available or are in development that allow in vivo imaging of nearly all aspects of cholinergic neurotransmission from the synthesis of endogenous ligand to distribution and activity of the catabolic enzyme AChE.

Direct labelling and visualisation of ACh itself is not possible due to the high dilution that occurs with endogenous unlabelled ligand, however attempts have been made to study the ACh synthesis *in vivo*. PET studies performed in monkeys with the ACh precursor choline labelled with [$^{11}$C] have have been successful to a limited degree. A low uptake of radioactivity by brain (less than 1% of injected dose) along with a very rapid metabolism of newly synthesised [$^{11}$C]-ACh was observed. These observations combined with a lack of specificity for cholinergic brain regions indicate limited clinical applications for this technique.

Imaging of the distribution and activity of AChE, the catabolic enzyme for ACh, has met with greater success. Interest in the localisation and function of this enzyme is based upon the dramatic decrease of enzyme activity observed in the brains of patients with neurodegenerative diseases such as Huntington's and Alzheimer's. The therapeutic use of AChE inhibitors such as tacrine (THA) in AD provides a clinical basis on which visualisation of enzyme function is desirable, as this would enable determination of drug efficacy and elucidation of mechanism of action. Autoradiographic studies with [$^{3}$H] and [$^{14}$C] labelled THA demonstrated distinct binding sites of high and low affinity for THA in the brain, with neither of these sites co-localised with AChE activity . PET studies in baboon using an [$^{11}$C] methylated derivative of THA (MTHA) displayed a similar divergence of localisation from that of AChE. High levels of binding were observed in the cortex and basal ganglia compared to the cerebellum, with binding inhibited or displaced by administration of non-radiolabelled THA (Tavitian et al., 1993). [$^{11}$C]-MTHA should therefore be useful in determining the sites and method of action of THA. An [$^{11}$C] labelled form of the classical AChE inhibitor physostigmine has also been developed for imaging of AChE distribution in the brain . In a combined AChE histochemistry and autoradiographic study in rat, the distribution of [$^{11}$C]-physostigmine was superimposable on the pattern of AChE staining in the same sections (Planas et al., 1994). In PET studies in primates [$^{11}$C]-physostigmine displayed blood flow dependent uptake into the brain followed by redistribution of

radioactivity to AChE-rich brain regions (Tavitian et al., 1993). These studies indicate the potential of this compound as a marker for alterations in cholinergic transmission observed in neuropathological conditions. Activity and distribution of AChE has also been mapped in man with [$^{11}$C] -methylpiperidinyl propionate (PMP) (Frey et al., 1997).

Cholinergic neurons and specifically cholinergic nerve terminals, can be mapped with ligands that selectively radiolabel the vesicular ACh transporter. The vesicular ACh transporter removes newly synthesised ACh from the cytoplasm in nerve terminals and concentrates it in synaptic vesicles ready for release. This process is inhibited by the compound vesamicol. Autoradiographic studies with 2-(4-phenylpiperidino-cyclohexanol (AH 5183) have demonstrated vesamicol binding sites highly localised to cholinergic nerve terminals (Marien et al., 1987). Ligands for both PET and SPECT based upon the non-toxic trozamicol, a pharmacologically inactive precursor of vesamicol have been developed. Two SPECT ligands are available [$^{123}$I]-HIPP and [$^{123}$I]-m-iodobenzyltrozamicol and one PET ligand [$^{18}$F]-fluorobenzyltrozamicol (Efange et al., 1993a, Efange et al., 1993b , Efange et al., 1993c). Results indicate that these radiotracers can be successfully used as markers of presynaptic cholinergic innervation (Maziere, 1995).

**Nicotinic Receptors**

Nicotinic receptors are widely distributed in the mammalian brain and fulfil a number of physiological roles including pre-synaptic modulation of ACh release and an involvement in learning and memory. In addition, loss of nAChR number is implicated in the pathology of AD. They can be labelled *in vivo* with high affinity in mice by injection of [$^{3}$H]-nicotine which displays rapid brain uptake and a pattern of distribution similar to that of [$^{3}$H]-ACh (Brouselle et al., 1989). Nicotine has also been labelled with [$^{11}$C] for use in PET and nAChRs have been visualised in monkeys and in man with this ligand (Nyback et al., 1989). In AD patients uptake of [$^{11}$C]-nicotine is reduced in cortical areas compared to the uptake observed in age matched controls (Nordberg et al., 1990). This reduction in uptake is thought to be related to the loss of nAChRs observed in AD brains post-mortem. Although uptake into the brain is good and distribution is similar to that of [$^{3}$H]-nicotine following intravenous administration, [$^{11}$C]-nicotine displays high levels of non-specific binding, very rapid loss of radioactivity from brain tissues and rapid metabolism (Nyback et al., 1994). It is therefore less than ideal for imaging of nAChRs. Considerable effort is currently being invested in the development of nAChR ligands suitable for use in PET and SPECT which display a greater specific/non-specific binding ratio and a more favourable kinetic and metabolic profile. A PET study evaluating the high affinity nAChR agonists N-[$^{11}$C]-ABT 418 and N-[$^{11}$C]-methylcytisine was attempted in baboons. However, both ligands displayed low levels of uptake into the brain combined with rapid washout of radioactivity from brain tissues and rapid metabolism of tracer making visualisation of

receptors impossible (Valette et al., 1997). More favourable results were forthcoming with a series of [$^{3}$H] labelled nicotine analogues including [$^{3}$H]-(R,S)-5-isothiocyanonicotine and [$^{3}$H]-(R,S)-5-aminonicotine, which have been evaluated *in vitro* and *in vivo* and appear to possess the appropriate attributes for potential PET and SPECT ligands (Kim et al., 1996). A lot of interest is currently centred upon developing the high affinity nAChR agonist epibatidine, an alkaloid naturally occurring in frog skin, as a ligand for *in vivo* use with PET and SPECT. Epibatidine has been labelled with [$^{3}$H] and evaluated *in vitro* where it displays very high affinity for nAChRs and extremely low non-specific binding (Perry and Kellar, 1995). A [$^{3}$H] labelled analogue (+)-norchloroepibatidine has also been developed and evaluated in vitro and in vivo in mice where it displays similar high specificity and low non-specific binding with a similar distribution to [$^{3}$H]-nicotine *in vitro* (Scheffel et al., 1995). [$^{125}$I] and [$^{123}$I] radiolabelled forms of IPH, an epibatidine analogue, have been studied in vivo as a potential SPECT ligand for nAChRs (Musachio et al., 1996). Epibatidine and its analogues appear thus far to be the most promising candidate ligands for the visualisation of nAChRS *in vivo*. However, other nAChRs such as [$^{18}$F]-Exo-2-(2-fluoro-5-pyridyl)-7-azabicyclo [2.2.1] Heptane for PET and [$^{125/123}$I]- (-)-iodonicotine for SPECT are additionally available (Horti et al., 1996, Saji et al., 1993).

**Muscarinic Receptors**

Many investigations have pursued the imaging of mAChRs in the brain (for review see Maziere, 1995). Potent mAChR antagonists, many of which are ligands commonly used for in vitro autoradiographic studies have been labelled as potential tracers for PET and SPECT. In particular quinuclidinyl, piperidinyl and tropanyl esters of benzillic acid which display high affinity for mAChRs have been used. In man, mAChRs were first visualised by external means with the use of [$^{123}$I]-QNB (Eckelman et al., 1984a). This ligand was subsequently used to study mAChRs in AD where a moderate loss of mAChR function was reported compared to an age matched control (Holman et al., 1985).

Since then a number of ligands have been used successfully for both PET and SPECT to image mAChRs in the living brain, including [$^{11}$C] and [$^{18}$F]-QNB, [$^{11}$C]-benztropine, [$^{11}$C]-scopolamine, [$^{11}$C]-n-methyl-4-piperidinyl benzilate (NMP) and [$^{123}$I]-iododexetimide (Prenant et al., 1989 , Wilson et al., 1989, Dewey et al., 1990, Frey et al., 1992, Mulholland et al., 1995). PET studies with [$^{11}$C]-QNB in baboon demonstrated distribution of tracer in the brain corresponded to the pattern of mAChR localisation as evinced from *in vitro* and *in vivo* binding studies, with high concentrations of radioactivity located in the cortex and striatum and low levels of residual activity, indicative of non-specific binding, observed in the cerebellum (Varastet et al., 1992). Additionally, administration of mAChR antagonists such as atropine or dexetimide resulted in displacement of binding from the cortex and striatum while no changes were observed in the

cerebellum. These observations support the utility of this ligand in the accurate imaging mAChR distribution within the CNS.

Quantitative estimation of cerebral mAChRs was investigated in AD with [$^{11}$C] (+)2$\alpha$-tropanyl benzilate ([$^{11}$C]-TRP) and PET. Observations suggested a selective loss of mAChR in cortex of AD patients. However, the kinetic properties of the ligand, high binding rate relative to transport and slow dissociation kinetics make accurate regional estimation of mAChR density difficult, limiting the clinical use of this ligand (Koeppe et al., 1994 ). A similar problem is seen with [$^{11}$C]-scopolamine (Frey et al., 1992) and with [$^{123}$I]-QNB (Wyper et al., 1993) prompting the search for a ligand with more suitable kinetics which would attain equilibrium conditions more rapidly. To this end, [$^{11}$C]-NMP was developed and evaluated as potential ligand for imaging of mAChRs (Mulholland et al., 1995). NMP displays greater brain uptake than TRP combined with more favourable kinetic parameters for quantifying mAChR number in the brain.

The potent mAChR antagonist dexetimide and its inactive enantiomer levetimide have been radiolabelled for use with both PET and SPECT with [$^{11}$C] and [$^{123}$I] respectively (Dannals et al., 1988, Wilson et al., 1989). Furthermore, two [$^{18}$F] labelled fluorine analogues, 2-fluoro- and 4-fluoro-dexetimide and a bromine analogue [$^{76}$Br] 4 -bromodexetimide, have also been synthesised (Hwang et al., 1991, Kassiou et al., 1995). In rats both of the fluorine analogues and the bromine labelled compound displayed high specificity for mAChRs in the brain. However, 2-fluoro-dexetimide also displayed rapid de-fluorination *in vivo* making it unsuitable as a PET ligand. In contrast the bromo-compound is very stable in the brain. In baboons, [$^{76}$Br]-4-bromodexetimide shows rapid brain uptake, with high retention of tracer in cortical regions compared to a rapid washout of tracer from cerebellum during the experimental period. In addition, radioactivity could be displaced from cortical regions following intravenous administration of cold dexetimide indicating high specificity of the tracer for mAChRs. Evaluation of [$^{123}$I]-iododexetimide in mice indicated its suitability as a mAChR ligand for SPECT including stereospecificity for mAChRs (Wilson et al., 1989). An advantage of using [$^{123}$I]-iododexetimide with SPECT to image mAChRs in human brain is that the distribution of the ligand represents almost entirely specific binding to mAChRs. In contrast, the distribution of [$^{123}$I]-iodolevetimide the inactive enantiomer, represents non-specific binding. This allows subtraction of data from images obtained with levetimide from those obtained with dexetimide permitting an extremely accurate measurement of specific binding. This is of obvious benefit when attempting to quantify small changes in receptor number such as those apparent in AD.

The majority of the tracers discussed above, while having good brain penetration and retention and distribution consistent with the known pattern of mAChRs in the brain, display poor selectivity for the mAChR subtypes. With the loss of $M_2$ receptors observed in AD development of tracers with this subtype selectivity are highly desirable as they would be likely to provide data useful for the diagnosis and monitoring of this disease. Considerable

effort is therefore being channelled into development of $M_2$ selective ligands for use in PET and SPECT. The mAChR antagonist QNB although a non-selective ligand has four diastereoisomers displaying different affinities and kinetic parameters for binding to mAChRs . It has been proposed that with careful protocol design preferential imaging of $M_2$ mAChRs should be possible with proper manipulation of the kinetics of the diastereoisomers (Gibson et al., 1989). However, more direct strategies have been used to develop subtype selective mAChR ligands. These include attempts to increase the blood-brain barrier permeability for existing subtype selective analogues (Gitler et al., 1992, Doods et al. 1993) and modifying more permeable ligands to have higher selectivity (Baumgold et al., 1991). Attempts were made to synthesise a series of novel mAChR ligands with subtype selectivity. This resulted in a number of 3-(3-substituted-1, 2, 5-thiadiazol-4-yl)-1, 2, 5, 6-tetrahydro-1-methylpyridines (substituted -TZTP) including xanolemine and butylthio-TZTP which demonstrated $M_1$ selectivity. These compounds have subsequently been labelled with [$^{11}$C] and evaluated in monkeys with PET (Farde et al., 1996). Both ligands displayed high uptake into brain and localised predominantly in the cortex and striatum. An analogue of QNB, in which the phenyl ring has been replaced with an iodopropenyl substituent (IQNP) has also been prepared (McPherson et al., 1994) IQNP displays high specificity for $M_1$ mAChRs in vitro and in vivo, and is a potentially useful ligand for SPECT. An $M_2$ selective ligand 3-(3-(3-[$^{18}$F] fluoropropyl) thio)-1 2, 5 thiadiazol-4-yl)-1, 2, 5, 6-tetrahydro-1-methylpyridine ([$^{18}$F] FP-TZTP) has been synthesised and evaluated *in vitro* and *in vivo* (Kiesewetter et al., 1995). The ligand displays greater than 3 fold affinity for $M_2$ over $M_1$ receptors and the biodistribution of tracer is consistent with that of $M_2$ rather than $M_1$ receptors. [$^{18}$F] FP-TZTP is therefore a very promising ligand for the visualisation of $M_2$ receptors in man with PET.

### 1.2.4 3-Quinuclidinyl-4-Iodobenzilate (IQNB)

Quinuclidinyl benzilate (QNB) is a high affinity mAChR antagonist. In a non-radiolabelled form it is non-subtype selective and displays a Ki value of between 0.032nM and 0.2nM *in vitro* with individual receptor preparations [see Table 4].The iodinated form of QNB was originally developed for use as a radioligand for the imaging of myocardial mAChRs (Rzeszotarski et al., 1982). In a subsequent competition study with [$^{3}$H]-QNB, iodo-QNB was observed to display high affinity for mAChRs in the caudate of rabbit brain as well as for mAChRs in the heart, indicating its potential as a ligand for the imaging of central mAChRs (Gibson et al., 1983). Iodo-QNB radiolabelled with [$^{123}$I] and [$^{125}$I] was successfully synthesised and evaluated. Distribution of radioactivity in rats was confined to organs known to have high densities of mAChRs (Rzeszotarski et al., 1982). Subsequent studies have provided evidence to suggest receptor-mediated localisation of radioactivity. Following intravenous administration in rats [$^{125}$I]-QNB shows high tracer uptake in the cortex and cerebellum with maximum concentration reached after 30 mins. In the caudate no washout of radioactivity is observed up to 4 hours after administration, correlating with the high density of mAChRs known to exist in this brain region. In contrast greater than 90% of radioactivity is lost from the cerebellum by 4 hours, consistent with the low level of mAChRs present in this region, suggesting initial tracer uptake into this brain region corresponds to non-specific binding (Gibson et al., 1984a). Additionally, with *in vivo* competition studies, co-injection of cold tracer or another mAChR ligand, blocks tracer localisation in target tissues such as the cortex and caudate (Gibson et al., 1984a, Eckelman et al., 1984b).

Both the non-iodinated parent compound QNB and iodo-QNB exhibit stereoisomerism.QNB has one chiral centre about the 3-carbon atom in the quinuclidinyl moiety of the compound (Fig 4.), creating two stereoisomers (R)- and (S)-QNB. The (R) isomer displays approximately 100 greater fold affinity for mAChRS than the (S) isomer (Meyerhoffer, 1972). Introduction of an iodine to one of the phenyl rings in the QNB structure results in a second chiral carbon in the benzillic acid moiety (see Fig 4.). Therefore, iodo-QNB has four diastereomeric forms each of which displays different affinity and binding kinetics for mAChRs. The chiral centre on the quinuclidinyl moiety has greatest influence on the kinetic parameters of the individual diastereoisomers and is therefore always quoted first when assigning stereochemistry to iodo-QNB. As with QNB the (R) configuration at the quinuclidinyl centre confers greatest affinity for mAChRs, thus iodo-QNB has two high affinity (R,S) and (R,R) and two low affinity (S,S) and (S, R) diastereoisomeric forms (Rzesotarski et al., 1988). The binding kinetics and affinities of the diastereoisomers (particularly the high affinity (R,S) and (R,R) forms) have been characterised in a number of *in vitro* and *in vivo* binding studies. *In vitro* (R, R,S) [$^{125}$I]-QNB (i.e. compound is of undefined/racemic stereochemistry at benzillic chiral centre)

## Structure Of 3-quinuclidinyl 4-iodobenzilate

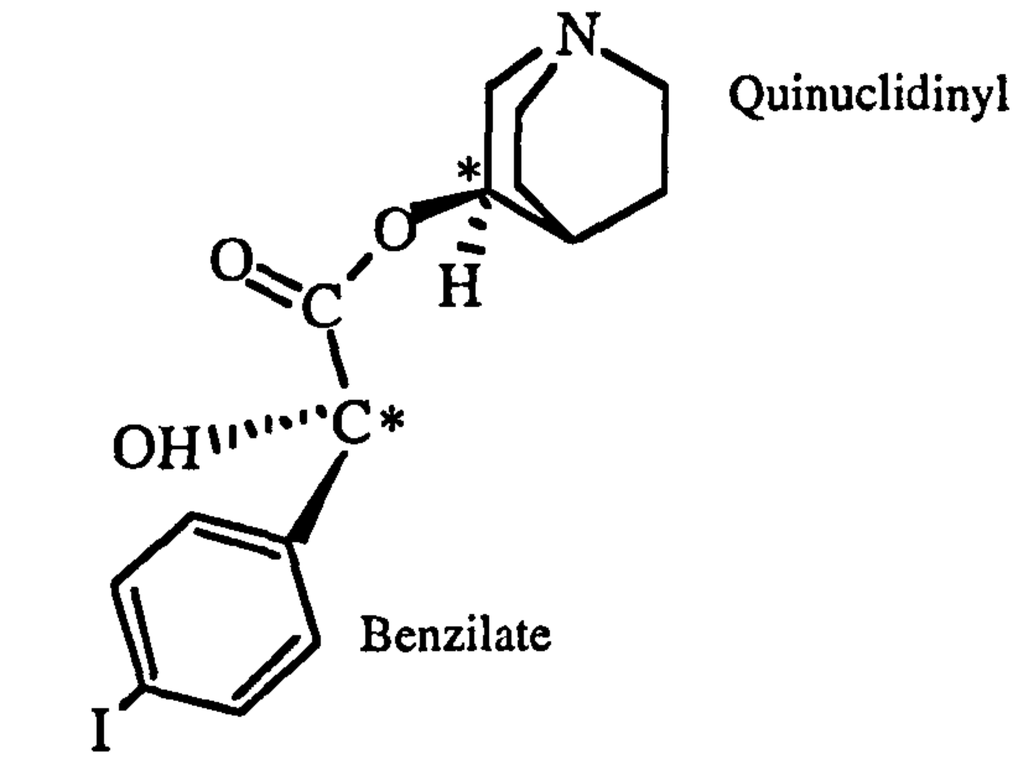


**(R,R)-IQNB**

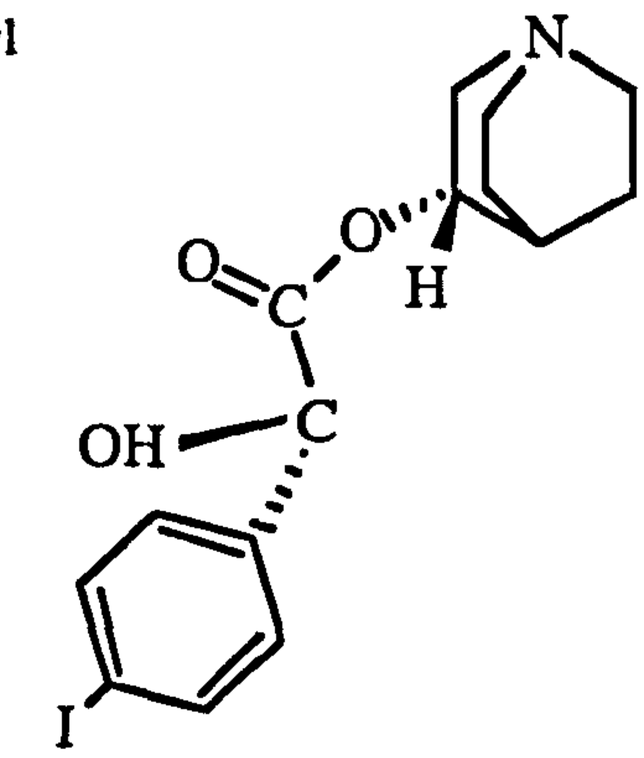


**(S,R)-IQNB**

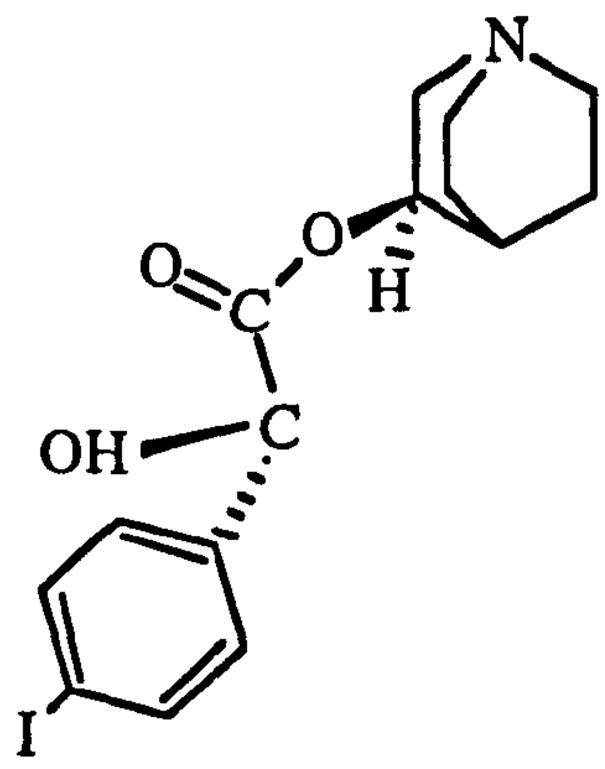


**(R,*S*)-IQNB**

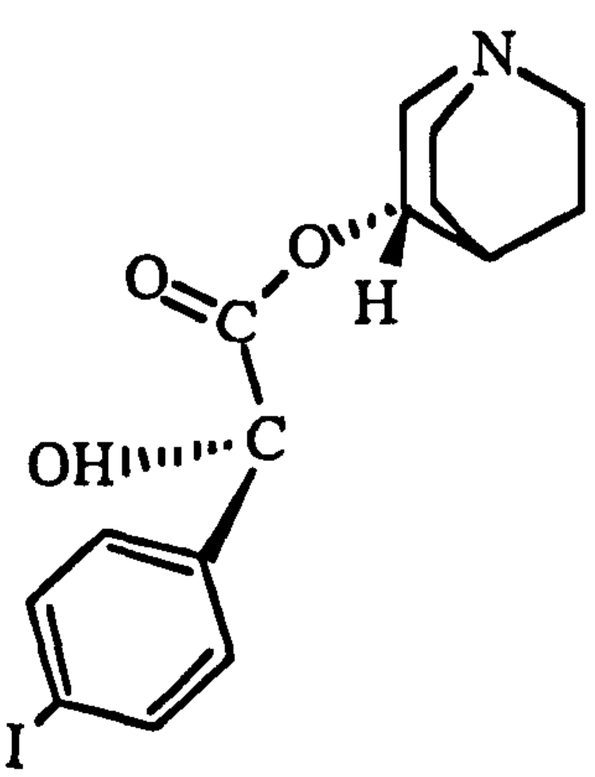


**(S,*S*)-IQNB**

**Fig 4:** Structure of four diastereoisomers of IQNB. Each diastereoisomer displays different affinity and binding kinetics for mAChRs. (R) configuration at the quinuclidinyl moiety confers greatest affinity for mAChRs, therefore IQNB has two high affinty diastereoisomers (R,S) and (R,R) and two low affinity diastereoisomers (S,S) and (S,R) with the rank order of affinity for mAChRs (R,S)> (R,R)> (S,S)> (S,R). * indicates chiral carbon atom.

## Table 4

## Affinity Of QNB Compared To Other Muscarinic Antagonists

| | $M_1$ | $M_2$ | $M_3$ |
|---|---|---|---|
| **Antagonist** | $K_i$ (nM) | $K_i$ (nM) | $K_i$ (nM) |
| | | | |
| **R-QNB** | 0.032 | 0.13 | 0.2 |
| **Atropine** | 0.2 | 0.7 | - |
| **Pirenzepine** | 0.37 | 7.1 | 2.5 |
| **AF-DX 384** | 31 | 6 | 66 |
| **4-DAMP** | 0.58 | 3.8 | 0.52 |

Table shows the affinity constant for a number of mAChR antagonists derived from displacement of [$^3$H]-N methyl scopolamine binding to bovine striatal membrane , rat myocardium membrane and rat pancreatic membrane preparations (R-QNB, for $M_1$, $M_2$ and $M_3$ receptors and atropine for $M_1$ and $M_2$ receptors) and displacement of [$^3$H]-N methyl scopolamine binding to $M_1$, $M_2$ and $M_3$ receptors expressed in Chinese hamster ovary cells (pirenzepine, AF DX 384 and 4-DAMP). $K_i$ values for R-QNB are in the subnanomolar range for all mAChR subtypes indicating high affinty for each receptor.
$K_i$ values are taken from Rzeszotarski et al., (1988) and Dorje et al., (1991).

displayed high affinity for mAChRs in membrane receptor preparations of rat and dog caudate-putamen and of dog heart (Gibson et al., 1984b). In a combined *in vitro* and *in vivo* study, the binding parameters and regional distribution of the two high affinity diastereoisomers were examined (Gibson et al., 1989). Following intravenous injection into rats, distribution of both (R,S) and (R,R) [$^{125}$I]-QNB was consistent with pattern of mAChRs in the CNS, with high uptake of radioactivity in the cortex, hippocampal and caudate and low uptake in the cerebellum. In contrast however, (R,R)-IQNB displayed a considerably faster washout from brain tissues than (R,S) indicating lower affinity for mAChRs. The *in vivo* behaviour of the ligands was reflected *in vitro*, with the ligands displaying considerably different binding kinetics. Estimation of the *in vitro* equilibrium association constant ($K_A$) indicates that (R,S)-IQNB has approximately 3 fold higher affinity for mAChRs than (R,S), with $K_A$ of $8.9 \times 10^9$ $M^{-1}$ and $2.9 \times 10^9$ $M^{-1}$ respectively. This in itself is a relatively small difference in affinity, but the estimated rate constants are markedly different. The calculated dissociation rate of (R,S) ($k_{-1}$ =0.0049 min-1) is 13 fold slower than that for (R, R) ($k_{-1}$ = 0.0654 min-1). The calculated association rate of (R,S) ($k_{+1}$ =1 1.9 x 10-8 M-1 min-1) 2.5 fold slower than (R,R) ($k_{+1}$ =4.4 x 107 M-1 min-1). A similar study was performed to estimate the binding parameters of (R,S)- and (R,R)-IQNB to transfected cell membranes expressing individual mAChR subtypes (Zeeberg et al., 1991). In this study the equilibrium dissociation constant ($K_D$) and association ($k_{+1}$) and dissociation ($k_{-1}$) rates were estimated for both diastereoisomers for binding to $m_1$, $m_2$ and $m_3$ receptors. Both ligands displayed a similar degree of high affinity for all receptor subtypes and in general $k_{+1}$ and $k_{-1}$ values for binding to $m_1$ and $m_3$ receptors were similar. In contrast however, both ligands displayed faster dissociation rate from $m_2$ receptors, indicating a slight specificity for $m_1$ type receptors. A further study characterising the *in vitro* and *in vivo* behaviour of (R,S)-IQNB reported similar results to the study above, with a more rapid washout of tracer associated with brain regions expressing $M_2$ receptors. The authors suggested that the difference in dissociation kinetics observed may be of use when designing imaging protocols to allow selective imaging of $M_2$ receptors (Gibson et al., 1992). The data outlined above confirm that the (R,S) diastereoisomer of IQNB displays the highest affinity for mAChRs. Sawada et al., (1990b) performed a complete kinetic analysis of (R,RS) and (S,RS)-[$^{125}$I]QNB *in vivo* in rats . Two sets of experiments were performed evaluating the washout of ligands from brain following intracarotid injection and brain uptake and retention of ligands following intravenous injection. Data was analysed using 4 compartmental models incorporating blood-brain barrier transport , non-specific binding to tissue and high and low affinity binding to mAChRs. Results indicate that (R) and (S) ligands have similar transport rates into the brain and therefore IQNB is not subject to stereospecific transport. Uptake and retention of (S)-IQNB in brain structures was considerably less than that of (R)-IQNB. A fairly low uniform distribution of radioactivity was observed throughout the brain indicative of low affinity for mAChRs. Washout of (S)-

IQNB from brain structures is also considerably more rapid than that observed with (R)-IQNB. (R)-IQNB displays high uptake and retention in brain structures relative to their mAChR concentration, with high levels observed in the cortex and caudate, intermediate levels in the thalamus and low levels in the cerebellum. The concentration of ligand observed in the cerebellum, although considerably lower than in cortex or caudate, was higher than that of (S)-IQNB. This observation is consistent with the higher affinity of (R)-IQNB for mAChRs and indicates binding to a population of low affinity sites which are possibly of the $M_2$ subtype. The intermediate level of binding observed in thalamic regions is reflected in the washout out of ligand from this region, which is more rapid than cortex or caudate but slower than cerebellum. This is consistent with the presence of a mixed population of high and low affinity binding sites within this region. The observations above indicate that the stereochemistry of IQNB confers a degree of subtype selectivity for mAChRs (i.e. $M_1$ selectivity) as well as influencing the affinity of the ligand for receptors.

It should be noted at this point that the stereochemical designation employed in this thesis and when referring to previous publications is in accordance with the corrected stereochemistry for iodo-QNB of Kiesewetter et al., (1996) and Zeeberg et al., (1997). In recent years a degree of confusion has existed as to the correct stereochemical assignment of the diastereoisomers of iodo-QNB in papers published before 1993. The original stereochemical assignment of the benzillic acid centre was incorrect, resulting in (R,S)-IQNB being wrongly identified as (R,R)-IQNB. This error has since been identified and the stereochemical assignment corrected, based upon x-ray crystallography and the *in vivo* behaviour of the ligands. Thus, the rank order of affinity of the 4 diastereoisomers of IQNB for mAChRs is (R,S) > (R,R) > (S,S) > (S,R).

Since the first report of imaging of mAChRs in man with SPECT the technique has been applied in a number of studies attempting to quantify changes in mAChRs in dementia (Eckelman et al., 1984a). The first study performed with an AD patient compared regional brain uptake of [$^{123}$I]-QNB and cerebral blood flow measured with [$^{123}$I]-IMP (Holman et al., 1985). In AD reductions in blood flow were observed in the temporal and parietal cortex compared to age matched control. The uptake and retention of IQNB in both control and AD was consistent with the pattern of mAChR density, with a moderate reduction in activity in the temporal-parietal cortex observed in AD brain, suggesting a reduction in mAChR binding. The authors reject the theory that the reduction in IQNB retention in this brain region is a blood flow mediated event on the basis that the radioactivity observed in the cerebellum is considerably lower than in the cortex at this time point, despite the two regions having relatively similar rates of blood flow. Data from the scans was obtained up to 15 hours after intravenous administration of the tracer, with the IQNB content of the brain observed to rise slowly over this time. Information on the subtype selectivity of IQNB could not be determined as no dissociation from putative $M_2$ receptors could be observed. A number of other studies with AD patients have confirmed the focal reduction in IQNB

uptake in the temporal-parietal cortex of AD with an associated increase in striatum/cerebellum ratio with time (Weinberger et al., 1990a,b). A further study by Weinberger et al., (1991) reports similar deficits in IQNB uptake into temporal-parietal cortex of AD brain, while control brains display high uptake in the basal ganglia and cortex, low uptake in the thalamus and negligible uptake of radioactivity in the cerebellum after 21 hours. The lack of radioactivity present in the cerebellum at this time is consistent with the relatively sparse localisation of mAChRs in this region and re-inforces the receptor-mediated theory of tracer retention in the brain. From this study it is uncertain whether IQNB labels any mAChR subtype selectively, but the negligible amount of tracer in the cerebellum a region which contains mostly $M_2$-like receptors combined with the faster dissociation rate of the ligand for this receptor, suggests an $M_1$-like selectivity for the ligand *in vivo*. However, accurate modelling of tracer kinetics with a suitable compartment model will be necessary for quantification of mAChR density. In contrast, a similar study of (R,S) [$^{123}$I]-QNB uptake into brain was examined at 21 hours in relation to cerebral blood flow (Wyper et al., 1993). Results from this study indicate that although blood flow deficits are apparent in the majority of AD cases, a selective reduction in mAChR density is only apparent in the more severely demented patients where disease progression is advanced. These observations support the view that alterations in local cerebral blood flow have little impact on IQNB concentration in any brain region.

Further evidence to support this view comes from a combined [$^{18}$F]-FDG PET and IQNB SPECT study. This study reports similar reductions in metabolic activity and IQNB uptake in AD patients, although abnormalities in IQNB uptake were generally greater (Weinberger et al., 1992).

The studies outlined above provide powerful evidence of the utility of SPECT to image mAChRs with [$^{123}$I]-QNB in man. However, several problems still exist with this technique such as the lack of a suitable mathematical model allowing accurate quantification of receptor number. Additionally, the lack of subtype selective radioligands is preventing visualisation of $M_2$ mAChRs which are the subtype most likely to be lost in AD. However, conflicting reports on the loss of mAChR populations combined with the relatively low homogeneous distribution of mAChRs in the brain make accurate determination of $M_2$ receptor number difficult. Additional evidence has recently indicated loss of nAChRs in AD resulting in an effort to develop *in vivo* ligands specific for this receptor. These observations indicate that the ability to measure ACh function *in vivo* (i.e. ACh release) may be of greater importance than absolute quantification of receptor number. This view is supported by the loss of cholinergic function associated with AD and the current cholinergic replacement treatments aimed at the enhancement of ACh transmission (e.g. cholinesterase inhibitors) which form the basis of Alzheimer's therapy. The ability to measure ACh release *in vivo* would provide a means of assessing deficits in ACh function in AD and also provide a means to assess the efficacy of any replacement therapy. As it is not possible to measure

ACh release directly, quantification of changes in postsynaptic receptor-radiotracer binding following increased ACh outflow may provide a means to measure *in vivo* synaptic ACh concentration and thus the ability to assess cholinergic function in the brain.

A number of PET and SPECT studies have indicated that it is possible to measure displacement of dopamine $D_2$ receptor ligands from receptors *in vivo* by increasing synaptic concentrations of endogenous neurotransmitter. Amphetamine induced increases in synaptic AD levels have been observed to displace [$^{18}$F]-N-methylspiroperidol, [$^{11}$C]-raclopride and [$^{123}$I]-IBZM binding from $D_2$ receptors in the striatum of baboons, non-human primates and man (Brucke et al., 1991, Logan et al., 1991, Innis et al., 1992, Carson et al., 1997). Furthermore, studies in man have indicated that altered dopaminergic function can be measured by this technique in pathological conditions such as Parkinson's disease and schizophrenia. In un-medicated Parkinsonian patients no change in [$^{123}$I]-IBZM binding to $D_2$ receptors in the striatum was observed compared to controls. However in L-Dopa medicated patients a significant reduction in binding was observed., indicating that pharmacologically induced changes in dopaminergic function can be detected by postsynaptic radioligand binding (Brucke et al., 1991). Amphetamine induced displacement of [$^{11}$C]-raclopride is greater in schizophrenic patients than in controls (Breier et al., 1997). These observations provide evidence to suggest that altered neurotransmitter function in pathological conditions is measurable with radioligands *in vivo*. At the commencement of the investigations constituting this thesis no such studies had been attempted for the cholinergic system. The *in vivo* characteristics of the stereoisomers of IQNB indicate that they would be well suited to such studies in the cholinergic system. Quantification of changes in postsynaptic receptor-IQNB binding induced by agents that alter ACh release but do not themselves bind to cholinergic receptors, would provide an indirect measure of *in vivo* synaptic ACh concentration and thus the ability to assess cholinergic function in a particular brain region .

# CHAPTER 2

# MATERIALS AND METHODS

## 2.1 [$^{125}$I]-QNB *IN VIVO* AUTORADIOGRAPHY

### Basic Principles of *In Vivo* Brain Receptor Imaging

During the past two decades the study of neuroreceptors and their interactions with neurotransmitters and drugs has been of prime interest in the field of neuroscience. Important findings on the biochemical and pharmacologic aspects of these sites and their anatomic distribution has been made through the development of potent and selective radioligands, receptor binding assays and autoradiographic techniques. In *vitro* receptor studies are typically performed by incubating radioligands with brain tissue homogenate preparations and determining the amount of binding after removal of un-bound radioactivity . From the data the number of sites and their affinity for a particular ligand can be estimated[see section 2.2]. Quantitative *in vitro* autoradiographic techniques have the added advantage of providing an image of the density and distribution of receptors. With the extension of these techniques it is now possible to image receptor function *in vivo* in the living mammalian brain.

*In vivo* receptor imaging is based upon the principle that an intravenously injected radioligand or inhaled radioactive gas can pass from the blood into the brain and bind to target receptors with high specificity and selectivity allowing mapping of neuroreceptor distribution and number either by external detection of emitted radioactivity as in SPECT and PET or by autoradiographic means in experimental animals. With autoradiography, PET and SPECT the anatomical location and time course of ligand receptor interactions can be observed and quantitative information on regional receptor concentrations can be obtained. A correlation is sought between image information and normally occurring processes in the brain or to abnormalities that may reveal underlying neurologic or psychiatric diseases.

Before use as *in vivo* imaging agents radioligands must satisfy a number of selection criteria similar to those for ligands used *in vitro* . A ligand must display high affinity and pharmacologic specificity for receptor, binding to receptors should be saturable and reversible and should display appropriate regional distribution. However, conditions *in vivo* are considerably different to those *in vitro*. Blood flow, permeability of ligand to blood brain barrier, ligand metabolism and the presence of endogenous neurotransmitter all affect receptor binding *in vivo*. Furthermore, conditions *in vitro* can be manipulated (e.g. ionic concentration and temperature of incubation medium) to maximise binding and reduce non-specific binding (e.g. post incubation washing). In contrast, non-specific binding *in vivo* increases linearly with plasma tracer concentration. Therefore to reduce non-specific binding plasma tracer concentration must be kept to a minimum.

An ideal radioligand for use as an *in vivo* imaging agent would therefore have the

following attributes:

- Freely diffusible across the blood-brain barrier
- Rapid clearance from the blood following administration
- High affinity and specificity for target receptor
- Rapid clearance from non-specific sites in the brain
- Forms no lipophilic radiolabelled metabolites that may enter the brain
- May be radiolabelled to high specific activity

The aim of receptor mapping *in vivo* with such ligands is to provide evidence of receptor-specific accumulation of radioligand and also to gain quantitative information on receptor density and affinity (i.e. KD and $B_{max}$). However, absolute quantification of KD and $B_{max}$ in the same manner as that employed *in vitro* is not appropriate *in vivo* . Due to the factors described above and to the fact that the free ligand pool in the brain cannot be measured directly, the conditions and assumptions of the law of mass action do not apply. It is therefore necessary to develop a model that permits quantification of receptor density and affinity *in vivo*. To this end there are two types of experimental approach:

**1) Equilibrium Binding Studies**

This technique is a direct extension of *in vitro* equilibrium binding assays. It is based upon relatively few assumptions with regard to mechanisms of ligand distribution and produces ligand distribution proportional to regional receptor density.

Following administration tracer is considered to exist in two major anatomic compartments, the intravascular compartment ($C_B$) and the extravascular compartment ($C_E$). Tracer in $C_E$ may be free ($L_E$), non-specifically bound ($NS_E$) or bound specifically to receptors ($S_E$). It is assumed that following introduction of tracer the system reaches equilibrium and the concentrations in the non-saturable compartments $C_B$, $L_E$ and $NS_E$ are linearly proportional to one another.

Thus: $L_E+NS_E= \lambda C_B$

where $\lambda$ is a constant representing regional tissue to blood partition coefficient for free and non-specifically bound tracer.

From the above, total tracer concentration ($C_T$) can be defined as:

$$C_T= C_BV_B + C_EV_E \qquad (1)$$

$$=C_BV_B + (L_E+NS_E+S_E)V_E$$

Where $V_B$= volume of intravascular compartment

$V_E$= volume of extravascular compartment

Assuming that $L_E$,$NS_E$ and $S_E$ are distributed uniformly in the tissue and

$$V_B + V_E = 1 \qquad (2)$$

Solving for $S_E$:

$$S_E = \frac{C_T - C_B V_B}{V_E} - L_E - NS_E \qquad (3)$$

Substituting for equation (1):

$$S_E = \frac{C_T - C_B V_B}{V_E} - \lambda C_B \qquad (4)$$

and by elimination of $V_E$ using equation (2):

$$S_E = \frac{C_T - C_B V_B}{(1 - V_B)} - \lambda C_B \qquad (5)$$

Equation (5) may be used to determine specific binding from total tissue levels of tracer by PET or SPECT when regional values of $V_B$ and l are known and CB is determined by temporal analysis of tracer content in peripheral arterial blood.

In practice, an experiment of this kind is initiated by injection of a bolus dose of radioligand followed by an infusion protocol previously determined to produce a constant arterial concentration of radioligand. Equilibrium in various tissue compartments is then inferred from observation of the measured time-activity curves in various regions of interest in the brain. A single experiment of this kind determining regional radioligand distribution is sufficient to determine regional levels of specifically bound ligand when intravascular and non-specific binding corrections are made. Additionally, when total tissue ligand concentration reflects predominantly specific binding a single equilibrium image will directly yield a regional map of receptor density (Frey et al., 1985a,b).

### 2) Kinetic Binding Studies

This method of *in vivo* receptor quantification is based upon analysis of the distribution of radioligand in the blood and tissue (Frey et al., 1984).
A similar compartment model to the one described for equilibrium binding is considered, with tissue compartment consisting of free, non-specifically bound and specifically bound radioligand.

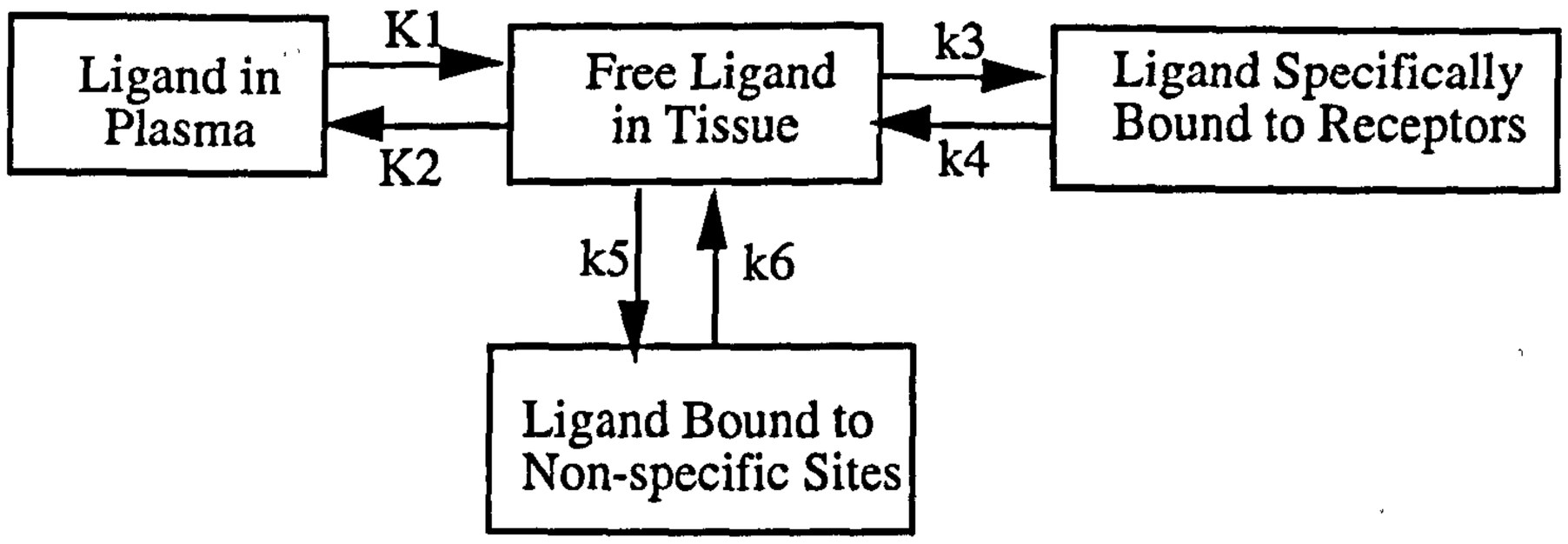


The exchange rates of tracer between compartments are described by transfer coefficients $K_1$, $K_2$, $k_3$, $k_4$, $k_5$ and $k_6$. Tracer entry to and exit from tissue are determined by regional cerebral blood flow and capillary tracer concentration [see section 4.3 for more detail]. Transport constants $K_1$, $K_2$ describing blood-brain and brain-blood transfer of tracer and constants $k_5$ and $k_6$ describing binding and un-binding of tracer to non-specific sites within the brain, can be defined as first order rate constants since the processes represent simple diffusion and non-saturable binding respectively. $k_3$ and $k_4$ describe interaction of free tracer in tissue with the free receptor population , that is $k_4$ = dissociation of bound ligand from receptor and $k_3$= association of free ligand to receptor.

$k_3$ is related to the concentration of free ligand in tissue and the free receptor concentration thus:

$$k_3 = k_a R \qquad (6)$$

Where $k_a$ is the association rate constant and R is the free receptor population. Under conditions where R is constant $k_3$ becomes a pseudo first order rate constant, and an expression describing the relationship between the blood and tissue tracer time courses in terms of the model parameters can be derived. For this relationship to hold the tracer must not occupy a significant proportion of the free receptors.

In practice, a tracer kinetic experiment involves a single intravenous bolus injection of radioligand with continuous determination of arterial tracer concentration and regional tissue tracer concentration for imaging with PET or SPECT. For autoradiography in experimental animals, continuous determination of arterial tracer concentration is combined with determination of regional tissue concentration at multiple time points in multiple animals. Arterial blood and tissue time activity curves can then be analysed by non-linear least squares curve fitting procedures to determine estimates of the model parameters (Frey et al., 1984).

An important issue for tracer kinetic modelling is the relationship between receptor density and experimental derivation of $k_3$. Free receptor concentration is related to total receptor concentration $R_T$, as: $R_T = R + S_E + LR_E$ (7)

Where $LR_E$= receptor bound to endogenous neurotransmitter. Thus, alterations in specific binding may reflect changes in total receptor density and also synaptic levels of endogenous neurotransmitter. Only when $k_a$ is regionally invariant and constant between individuals will k3 determination permit inference of changes in receptor density (equation 6). Similarly, KD cannot be estimated by this method, instead a combined measure of affinity and density, the Binding Potential (BP=k3/k4) for receptor populations is employed (Mintun et al., 1984). However, assessment of absolute values for KD and $B_{max}$ utilising this technique is possible with use of complex mathematical models (Gjedde and Wong, 1990).

### 2.1.1 Uptake and Retention Of (R,S)- And (R,R)-[$^{125}$I]-QNB In Rat Brain

#### Surgical Preparation

Male sprague dawley rats were placed in a perspex chamber and anaesthetised with 5% halothane in a nitrous oxide and oxygen mixture (70%/30%). Anaesthesia was subsequently maintained by administration of 0.5-1% halothane in the gas mixture via a face mask. Right femoral vessels were exposed by blunt dissection through a small incision in the skin in the groin of the rat. Polyethylene catheters (Portex, exterior diameter 0.96mm, interior diameter 0.58mm) attached to a larger polyethylene catheter (Portex, exterior diameter 1.40mm, interior diameter 0.63mm) were inserted approximately 2cm into both the femoral artery and vein and tied in place with surgical silk. The surgical ties were then secured in place by means of a small amount of cyanocrylate glue.

A hollow stainless steel rod was then passed under the skin, through the incision in the groin, along the line of the leg and up out through a small incision in the back of the neck. The arterial and venous catheters were then passed up through the steel rod and exteriorised through the incision in the neck. The steel rod was then removed. Both the wound in the groin and in the back of the neck were then infiltrated with antiseptic xylocaine gel (2%) and sutured closed with surgical silk. The catheters were then secured in place with a small amount of cyanocrylate glue. Anaesthesia was discontinued, and animals were allowed a minimum period of 1 hour of recovery before any further manipulations were performed.

#### Experimental Procedure

Male Sprague-Dawley rats weighing 300-350g were used in all experiments. Following recovery from anaesthesia animals received an intravenous injection of 200μCi (0.7mls in 0.9% saline) of either (R,S)- or (R,R)-[$^{125}$I]-QNB (specific activity 1480 MBq/mmol) at a constant rate over 30 seconds. Following administration

of tracer timed arterial blood samples (100µl) were collected, with up to 14 samples taken over the initial 45 mins of the experiment. The regime for subsequent sampling of arterial blood was dependent upon the experimental end point for the individual animal as follows:

Animals sacrificed at 1 hour: further sample collected at 1 hour

" 2 hours: further samples collected at 1 and 2 hours

" 6 hours: further samples collected at 1, 2, 4, and 6 hours

" 12 hours: further samples collected at 1, 2, 4, 8 and 24 hours

" 24 hours: further samples collected at 1, 2, 4, 8, 12, and 24 hours

All arterial blood samples were immediately centrifuged and 20µl plasma samples taken to determine [$^{125}$I] content and glucose concentration by means of liquid scintillation analysis and semi-automated glucose oxidase enzyme assay (Beckman) respectively. Arterial plasma samples were also taken at predetermined intervals before and after isotope administration for analysis of $pCO_2$, $pO_2$ and pH using a blood gas analyser (168 or 288 pH/Blood Gas System, CIBA. Corning). In all animals arterial blood pressure and core temperature were monitored at predetermined intervals before and after isotope administration, by means of a pressure transducer (P23ID Gould Stratham, Model 2202) connected to the femoral artery catheter and a rectal temperature probe respectively. Throughout the duration of the experiment animals had free access to food and water.

At the end of the experimental period animals were sacrificed by an intravenous injection of pentobarbitone sodium (Euthatal, 200mg/ml) and decapitated at 2, 6, 12 and 24 hours for (R,S) [$^{125}$I]-QNB experiments (n=5 for 2 and 24 hrs and n=3 for 6 and 12 hrs) and 0.5, 1, 2 and 6 hours for (R,R) [$^{125}$I]-QNB experiments (n=5 for each time point). Brains were then rapidly removed and frozen in isopentane at -42$^0$C for 10 mins. The frozen brains were then mounted onto swivel headed microtome chucks with plastic embedding matrix (Lipshaw) over solid $CO_2$.

## Preparation Of [$^{125}$I] Autoradiograms

Triplicate serial 20µm coronal sections of frozen brain were cut in a cryostat microtome at 200µm intervals throughout the brain and thaw mounted onto glass coverslips and then dried rapidly on a hot paté at 60$^0$C. The coverslips were then glued onto thin card and autoradiograms generated by exposing the brain sections along with pre-calibrated [$^{125}$I] standards (0.66 - 313.02µCi/g tissue equivalents) to [$^{125}$I] sensitive film (Kodak BioMax MR) in light - tight cassettes for 3 days. Films were then processed according to the manufacturers instructions.

## Quantification Of Autoradiograms

[$^{125}$I] autoradiograms were analysed using a computer based image analysis system

(M4 MCID, Imaging Research Inc.). Films were analysed densitometrically for radioisotope content in discrete brain regions by grey level comparison with pre-calibrated standards. Images captured by the video camera are digitised into an array of image points (pixels), each with a grey level in the range of 0-256. The grey level measured is refered to the dynamic range of the sensor and is converted to a relative optical density (ROD) value. For example, if an image of grey level 64/256 produces a ROD of 0.25, then a grey level of 128/256 would produce a ROD of 0.5. The ROD produced has no intrinsic biological value, it is merely the value the video image is assigned by the systems internal measurement scale. The system was therefore calibrated against [$^{125}$I] tissue equivalent standards in the range of 0-313.02 $\mu$Ci/g, with a zero value produced by taking a background reading from the film. This generates a calibration curve of ROD values versus isotope concentration, allowing subsequent quantification of tissue isotope concentrations in discrete brain regions. Measurements of isotope concentration were made by placing a measuring frame over each anatomical region of interest. The size of the measuring frame was variable but was kept constant for anatomical regions of interest between individual studies. For all *in vivo* studies with (R,S)- and (R,R)-[$^{125}$I]-QNB 33 distinct anatomical regions were analysed, with bilateral readings taken from 6 consecutive sections for each region of interest. Structures in the rat brain were defined anatomically by reference to the stereotaxic atlas of Paxinos and Watson (1986).

Data generated from autoradiograms were expressed as mean ± S.E.M % Dose per 100g brain normalised to the caudate nucleus to reduce the impact of inter-animal variability.

## 2.1.2 Metabolic Fate of (R,S)- and (R,R)-[$^{125}$I]-QNB *In Vivo* in rat

The purpose of this study was to analyse rat brain and plasma samples by high performance liquid chromatography (HPLC) for the presence of tracer breakdown products following intravenous injection of (R,S)- or (R,R)-[$^{125}$I]-QNB into the conscious rat.

All HPLC work was carried out with the following solvent system Solvent A: 0.1% trifluoroacetic acid in acetonitrile, Solvent B: 0.1% aqueous trifluoroacetic acid. Analytical work was carried out using an LKB 2000 series binary pump system with an LKB UV spectrophotometer at 230 nm and a Packard Radiomatic 500TR flow monitor. A Jones C18 Genesis column (4.6 x 250 mm) with 10 mm guard cartridge was used with 50% solvent A, 50% Solvent B at a flow rate of 1ml/min. Data were collected and analysed using Packard FLO-ONE software. The background signal was subtracted from each trace and the start and end points of each trace were assigned manually. Peak areas were recorded as a percentage of total peak area.

**Surgical Preparation**

Animals were prepared surgically as described in section 2.1.1.

**Experimental Procedure**

Experiments were performed in male Sprague dawley rats (300-350g) injected intravenously with 200μCi (R,S)- or (R,R)-[$^{125}$I]-QNB(specific activity 1480 MBq/mmol) in 0.7 mls 0.9% saline. Arterial blood samples (1ml) were taken at time intervals ranging from 1 min to 12 hours following tracer administration. The blood volume removed at each time was replaced by a slow intravenous injection of saline (0.9%). Samples were immediately centrifuged and the plasma removed and stored on ice. A 20 μl aliquot of plasma was removed from each sample for liquid scintillation counting. 250 μl of acetonitrile was added to 250 μl of plasma from each time point. The mixture was vortexed then centrifuged at 2000 rpm for 10 min and the supernatant removed. A 150 μL sample of the supernatant was injected on to the analytical HPLC system detailed previously. Animals injected with (R,S)-[$^{125}$I]-QNB were decapitated at 2, 6, 12 and 24 hours after administration of tracer. Animals injected with (R,R)-[$^{125}$I]-QNB were decapitated 30, 60, 120 and 360 mins after administration of tracer. Each brain was rapidly removed and homogenised in 1ml saline (0.9%) using a small hand held glass homogeniser. Equal volumes of homogenate and acetonitrile were mixed and centrifuged at 2000 rpm for 10 min to give a clear supernatant. The supernatant was injected directly on to the analytical

HPLC system detailed previously.

In addition to investigation of the metabolism of (R,S)- and (R,R)-[$^{125}$I]-QNB *in vivo*, the degree of degradation occurring following re-constitution of tracer in saline was examined. HPLC analysis of an ethanolic solution of [$^{125}$I]-QNB injectate removed from the injecting syringe was performed as detailed above for plasma.

## 2.1.3 Effect of Heptylphysostigmine Administration on Uptake and Retention of (R,S)-and (R,R)-[$^{125}$I]-QNB in the Brain of Conscious Rat

### Surgical Preparation

Surgical preparation of animals was performed as described as in 2.1.1.

### Experimental Protocol

Experiments were carried out in 20 male sprague dawley rats weighing 300-350g as described in 2.1.1 with the following alterations. Heptylphysostigmine tartrate 2mg/kg (0.7mls in 0.9% saline) or vehicle (0.7mls 0.9% saline) was administered as an intravenous infusion at a constant rate over 30 mins, one hour before injection of (R,S)- or (R,R)-[$^{125}$I]-QNB (specific activity 1480 MBq/mmol). Animals were sacrificed by an intravenous injection of pentobarbitone sodium (Euthatal, 200mg/ml) and decapitated at 2 and 24 hours (n= 5 at both time points for heptylphysostigmine and vehicle treated animals) following tracer administration for (R,S)-[$^{125}$I]-QNB experiments, with 24 hour animals receiving a second intravenous infusion of 2mg/kg heptylphysostigmine or vehicle 8 hours following the initiation of the first infusion. In (R,R)-[$^{125}$I]-QNB experiments animals were decapitated 30 mins, and 1, 2 and 6 hours following tracer administration (n=5 for each time point for both heptylphysostigmine and vehicle treated animals). Brains were then rapidly removed and frozen in isopentane at -42$^0$C for 10 mins. The frozen brains were then mounted onto swivel headed microtome chucks with plastic embedding matrix (Lipshaw) over solid $CO_2$.

### Preparation Of [$^{125}$I] Autoradiograms

Autoradiograms were prepared as described in 2.1.1 except that additional 20$\mu$m coronal sections were taken and thaw mounted onto glass slides and rapidly dried on a hot plate at 60$^o$C. Triplicate sections were taken at pre-determined levels of the caudate nucleus, dorsolateral hippocampus and cerebellum. These sections then underwent histochemical staining for acetylcholinesterase activity as described in section 2.4.

### Quantification of Autoradiograms

Autoradiograms were analysed as described in section 2.1.1.

### Data Analysis

At each time point the data from the two experimental groups, heptylphysostigmine and vehicle were analysed using a two tailed Student's unpaired *t* - test. The data were expressed as mean ± S.E.M. of % Dose per 100g brain normalised to the caudate nucleus.

## 2.2 [$^{125}$I]-QNB *IN VITRO* AUTORADIOGRAPHY

### General Principles of *In Vitro* Ligand Auotradiography

*In vitro* ligand binding autoradiography is based upon the principle that radiolabelled ligands, which are highly selective for particular recognition sites, emit energy which will produce a photographic image when placed in contact with radiation sensitive film. The optical density of the image is related to the amount of radioligand bound and hence to the density of the binding sites in any given area and can be quantified by reference to calibrated radioactive standards. Thus *in vitro* autoradiography techniques allow anatomical mapping of the distribution of ligand binding sites within the CNS with a high degree of spatial resolution and sensitive quantification of ligand binding densities in discrete brain regions.

### Receptor Theory and Ligand - Receptor Complex Interactions

As an integral part of the *in vivo* characterisation of the stereoisomers [$^{125}$I]-QNB, it is necessary to determine their *in vitro* binding kinetics . The behaviour of these stereoisomers *in vitro* provides parameters by which they may be described pharmacologically and valuable background information which may be utilised to define differences in their performance as *in vivo* imaging agents.

In this section the basic principles behind *in vitro* binding studies will be discussed along with a more detailed examination of the theory involved in kinetic and equilibrium binding assays from which binding data for a particular ligand and receptor can be derived.

### Law Of Mass Action

Ligand-receptor interactions generally follow kinetics very similar to those of classic enzyme-substrate interactions and are based upon the Law of Mass Action:

Unbound ligand reversibly binds to unbound receptor at a rate dependent upon the concentration of the two reactants, and the resultant ligand-receptor complex breaks down at a rate proportional to the concentration of the complex. At equilibrium or steady state, the rate of association is equal to rate of dissociation, that is, the rate of formation of the complex is equal to the rate of its breakdown.

These rules form the basis for ligand-receptor interactions but are only valid as long as the following conditions apply.

The interaction of the ligand and receptor must be completely reversible. The reactants can only exist in one of two states, either completely free or completely bound.

Measured products do not include elements unavailable for binding(e.g. degraded or

non-specific ligand). All receptor sites have unitary affinity and are independent of each other.

Thus, in a simple bimolecular reaction , where the rate limiting step is the collision of the ligand with the receptor site:

$$[L] + [R] \underset{k_{-1}}{\overset{k_{+1}}{\rightleftharpoons}} [LR]$$

Where:

$[L]$ = concentration of free ligand

$[R]$ = concentration of free receptor

$[LR]$ = concentration of ligand-receptor complex

$k_{+1}$= Association Rate Constant (*On rate*), and defines the rate at which the ligand receptor complex is formed.

$k_{-1}$= Dissociation Rate Constant (*Off rate*), and defines the rate at which the ligand receptor complex breaks down.

Therefore, Association rate= $k_{+1}[L][R]$

and Dissociation rate= $k_{-1}[LR]$

and at equilibrium or steady state: $k_{+1}[L][R] = k_{-1}[LR]$.

This can be rearranged to: $$\frac{k_{-1}}{k_{+1}} = \frac{[L][R]}{[LR]} = K_D \qquad (1)$$

Where $K_D$ is the Equilibrium Dissociation constant and is expressed in moles per litre. It is equal to the concentration of ligand which occupies 50% of receptors at equilibrium. A low $K_D$ denotes high affinity of the ligand for binding to the receptor.

Ligand - receptor interactions also show saturability, that is, only a finite number of specific receptor sites exist per unit of tissue . This number of specific receptor sites is termed $B_{max}$ and is usually expressed in pmoles per mg protein.

Therefore, according to the above: $[LR]+[R] = B_{max}$

Multiply by [L] : $[L][LR]+[L][R] = B_{max}[L]$

$$[LR][L]+\frac{[LR]}{[LR]}[L][R] = B_{max}[L]$$

Substituting for equation (1): $[LR]([L]+K_D) = B_{max}$

$$[LR] = \frac{B_{max}[L]}{[L] + K_D} \qquad (2)$$

This is the classic law of mass action for enzyme-substrate interactions adapted for ligand-receptor interactions. If we now define [RL] as bound ligand B and [L] as free ligand F: $B = \frac{B_{max}}{F + K_D}$ and $BF + BK_D = B_{max}F$

Dividing by F: $B + \frac{B}{F}K_D = B_{max}F$

$$\frac{B}{F} = \frac{B_{max} - B}{K_D} \qquad (3)$$

This is the Scatchard Equation. This equation allows the calculation of the Equilibrium Dissociation Constant $K_D$ and the maximum number of specific binding sites $B_{max}$, if the concentrations of free and bound ligand are known at equilibrium.

## Kinetic Analysis: Ligand Association and Dissociation

Initial experiments performed in the characterisation of ligand-receptor interaction are likely to be exploratory studies of the kinetics of association and dissociation. An important aim is to establish the time needed for equilibrium binding to be achieved. During kinetic analysis the formation and breakdown of product over time is measured and the association or dissociation rate constants for the reaction can be calculated from data derived from such experiments.

The rate of formation of [LR] is described by: $\frac{d[LR]}{dt} = k_{+1}[L][R] - k_{-1}[LR]$

At equilibrium: $\frac{d[LR]}{dt} = 0$ and $k_{+1}[L][R] = k_{-1}[LR]$

Experimental derivation of $k_{+1}$ (the association rate constant) involves measuring the formation of [LR] under conditions where [L] is in excess. This is known as an Association Time Course Experiment. Binding assays of this type, using membrane homogenate preparations requires the addition of radioligand in a single concentration to fixed level of receptor protein in a single tube, removing aliquots and filtering at time intervals until equilibrium is reached. This methodology is not compatible with *in vitro* autoradiographic analysis. Instead, individual brain sections are incubated in a fixed amount of a single concentration of radioligand. The starting times are staggered and the assay is then terminated after the appropriate time period by washing of the sections in buffer. From this type of assay, the observed association rate or $\mathbf{k_{obs}}$

($min^{-1}$) can be derived, and from this the more useful association rate constant $k_{+1}$ ($M^{-1}min^{-1}$). The association rate is defined by a Second Order rate equation . Therefore, the time taken to reach equilibrium depends upon the concentration of the two reactants as well as the rate constant. i.e. the lower the concentration of receptor or radioligand, the longer before equilibrium is reached.

Raw data from an illustrative association time course experiment can been seen in Fig. 5. This data can be transformed to obtain a linear representation of association, from which $k_{obs}$ can be derived. A plot of lnBe/Be-BT against time, where Be is specific binding at equilibrium and BT is specific binding at time T, yields a straight line with the observed association rate ($k_{obs}$) equal to the slope of the line. An example of association data transformed in such a manner can be seen in Fig. 6.

Experimental derivation of $k_{-1}$ (the dissociation rate constant) involves incubating receptors with a single concentration of radioligand until equilibrium (when formation and breakdown rates are equal) and then initiating dissociation of the ligand receptor complex by addition of excess unlabelled competitor to saturate the receptors and reduce the on rate to a negligible value. The competitor should preferentially have a structure chemically distinct from that of the radioligand. Dissociation of the ligand-receptor complex is then halted at increasing time intervals by washing of the sections in buffer. The level of dissociation occurring( without rebinding) increases in a manner proportional to the period of incubation with the competitor, and hence the amount of specifically bound ligand decreases. This type of assay is known as a Dissociation Time Course Experiment, raw data from an illustrative example can be seen in Fig. 5. This data can be transformed to give a linear representation of dissociation from which $k_{-1}$ can be calculated. A plot of ln Bt/Bo against time, where BT is specific binding at time T and Bo is specific binding at time zero (i.e. at equilibrium before dissociation is initiated), yields at straight line with $k_{-1}$ equal to the slope. An example of dissociation data transformed in such a manner can be seen in Fig. 6.

Association and Dissociation time course experiments yield the on and off rates for a radioligand, this data may then be used to determine $K_D$, as: $K_D = \frac{k_{-1}}{k_{+1}}$

**Equilibrium Studies: Saturation Analysis**

The equilibrium dissociation constant $K_D$, and the number of receptor sites $B_{max}$ may also be determined experimentally by Saturation analysis. This involves incubating a fixed amount of tissue in increasing concentrations of radioligand until such time as equilibrium is achieved. Ideally, a concentration of ten fold below to ten fold above the estimated $K_D$ value should be used. As the concentrations of ligand used are low "noise" produced by non-specific binding can be a problem with this type of assay. The level of non-specific binding is therefore determined in the presence of excess cold

## Raw Data From Theoretical Association And Dissociation Time Course Assays

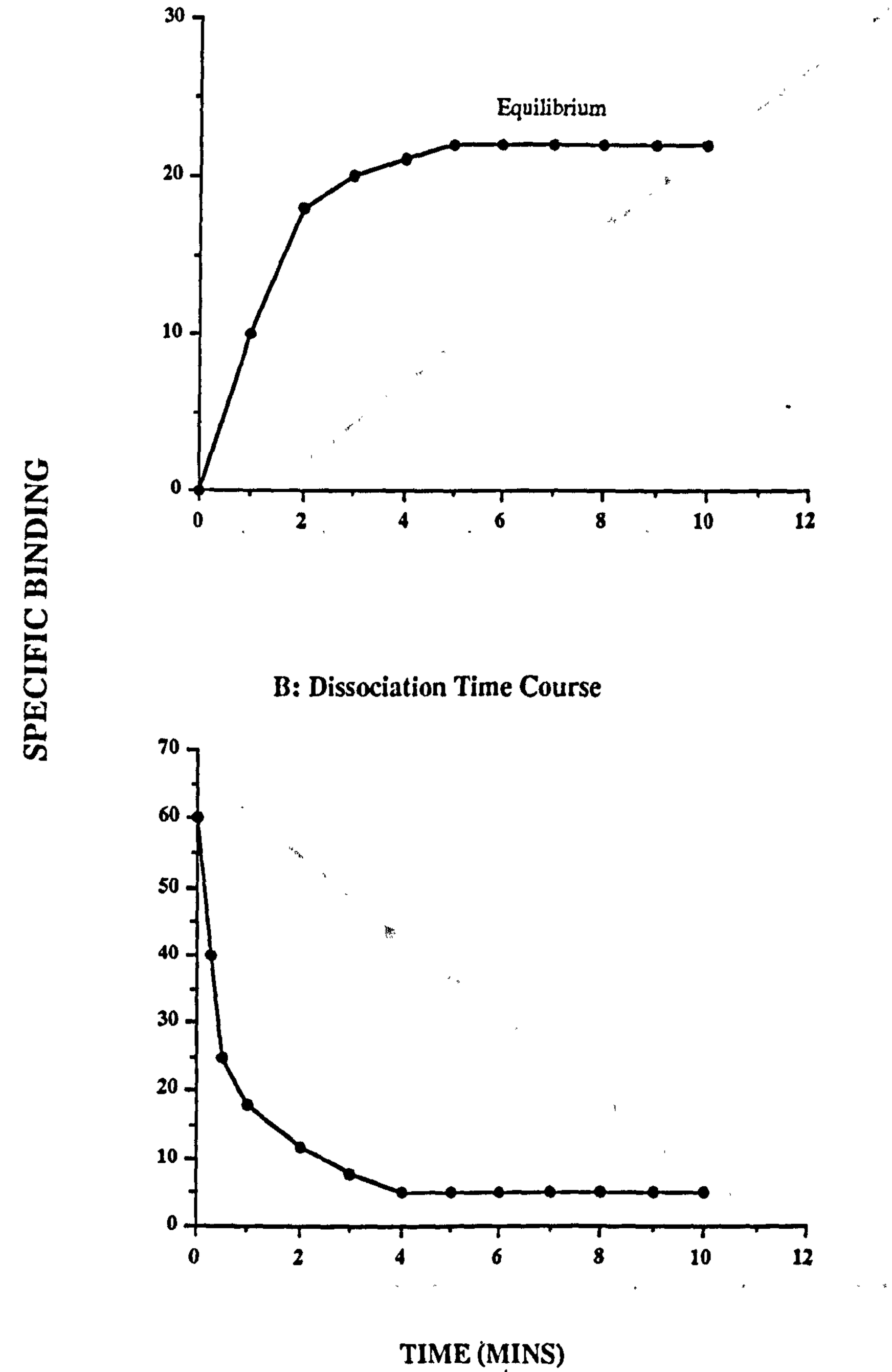


**Fig 5:** Raw data form theoretical Association (A) and Dissociation (B) assays. (A) shows saturation of specific binding sites at equilibrium. (B) shows dissociation of ligand from receptor with time in the presence of a saturating concentration o non-labelled competitor.

# Linear Transformation Of Data From Theoretical Association And Dissociation Time Course Assays

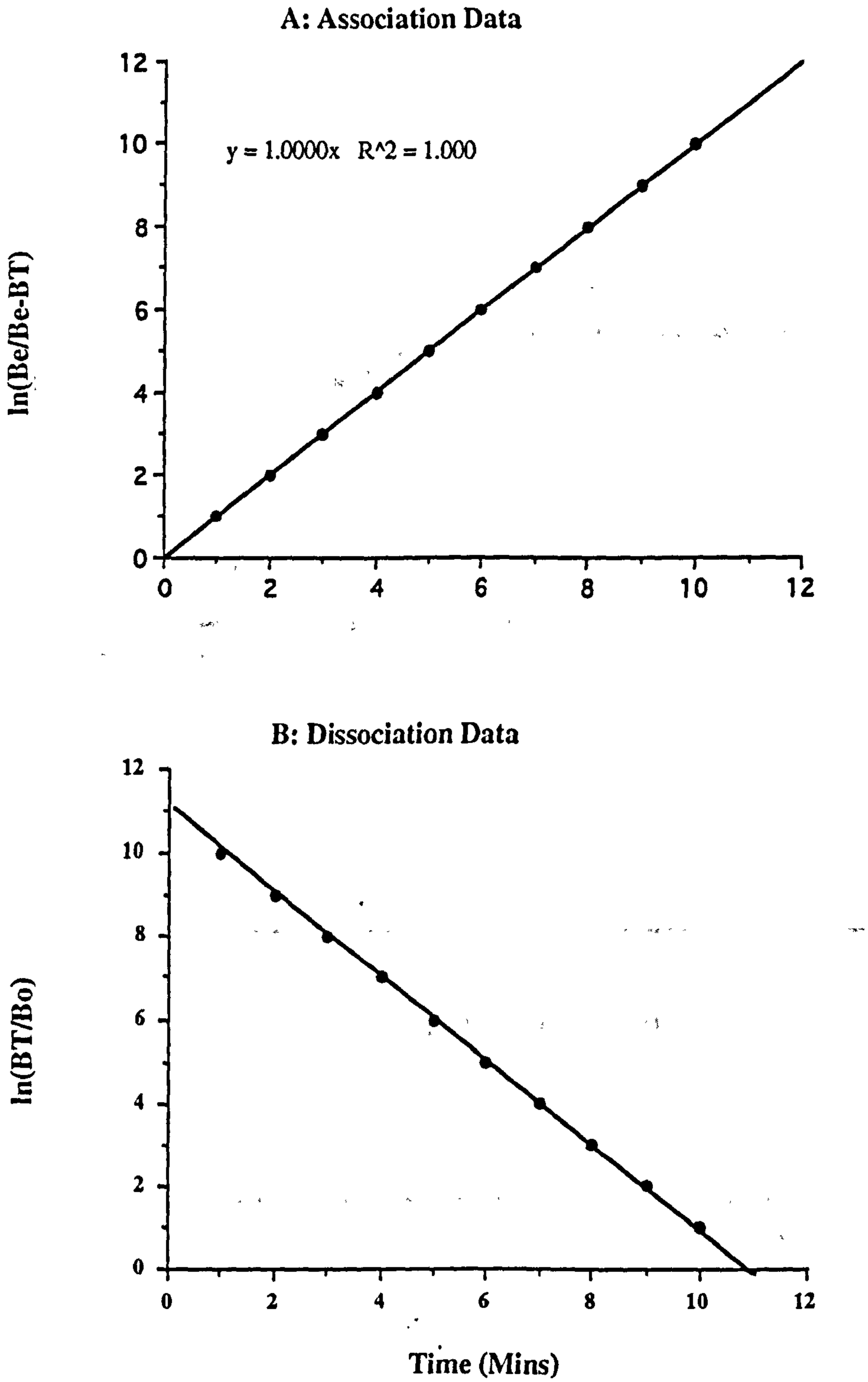


**Fig 6:** Linear transformation of raw data from theoretical Association (A) and Dissociation (B) time course assays. Where Be is equilibrium specific binding, BT is specific binding at time T, and Bo is specific binding at time zero. On and off rates are obtained from the slopes of the respective plots. The equilibrium dissociation constant KD is equal to the off rate divided by the on rate.

## Raw Data From A Theoretical Saturation Assay

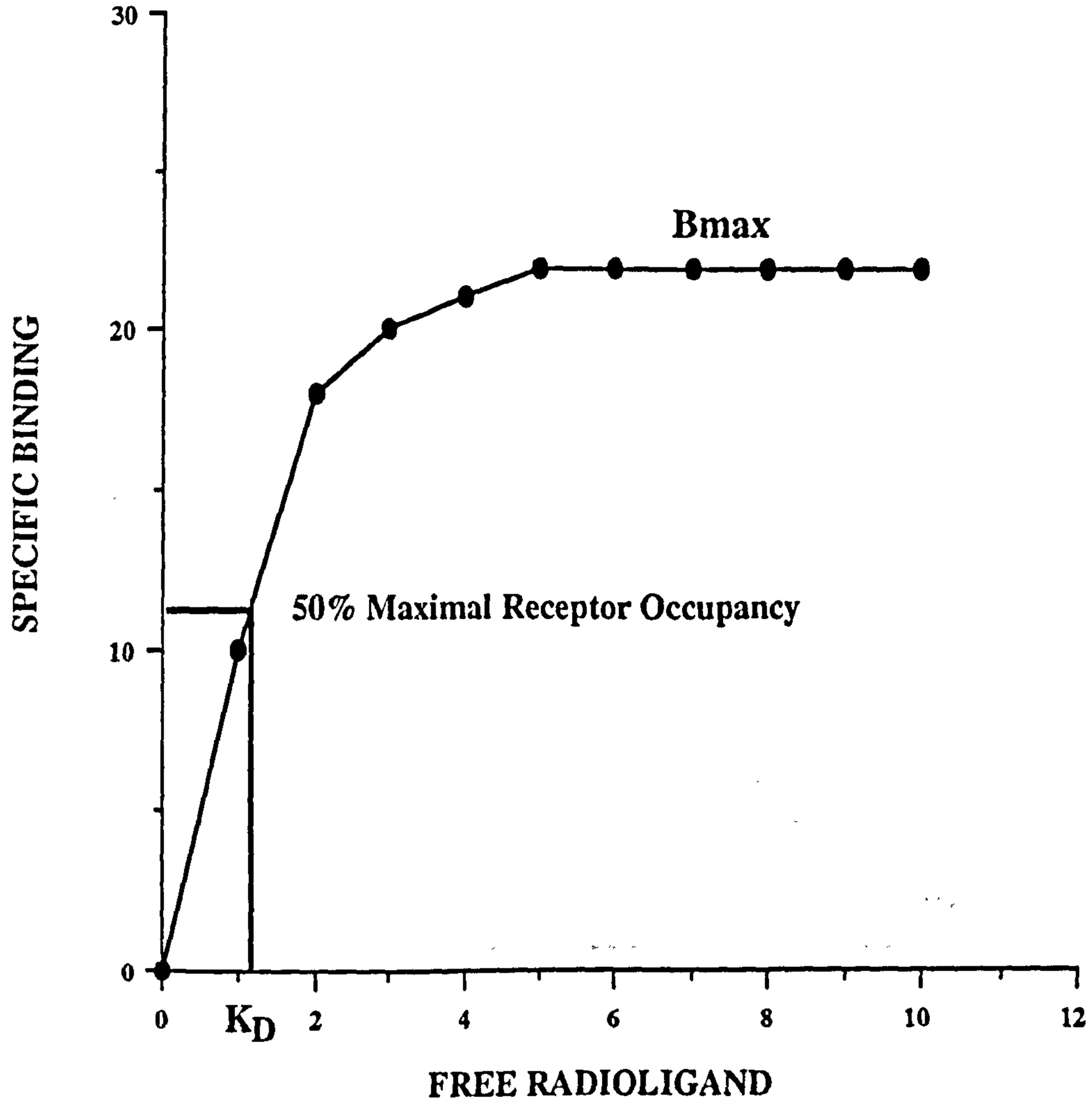


**Fig 7:** Typical rectangular hyperbola from a theoretical saturation assay. Plot shows specific binding of radioligand to receptors against free radioligand concentration. KD and Bmax may be calculated from this curve.

# Scatchard Plot

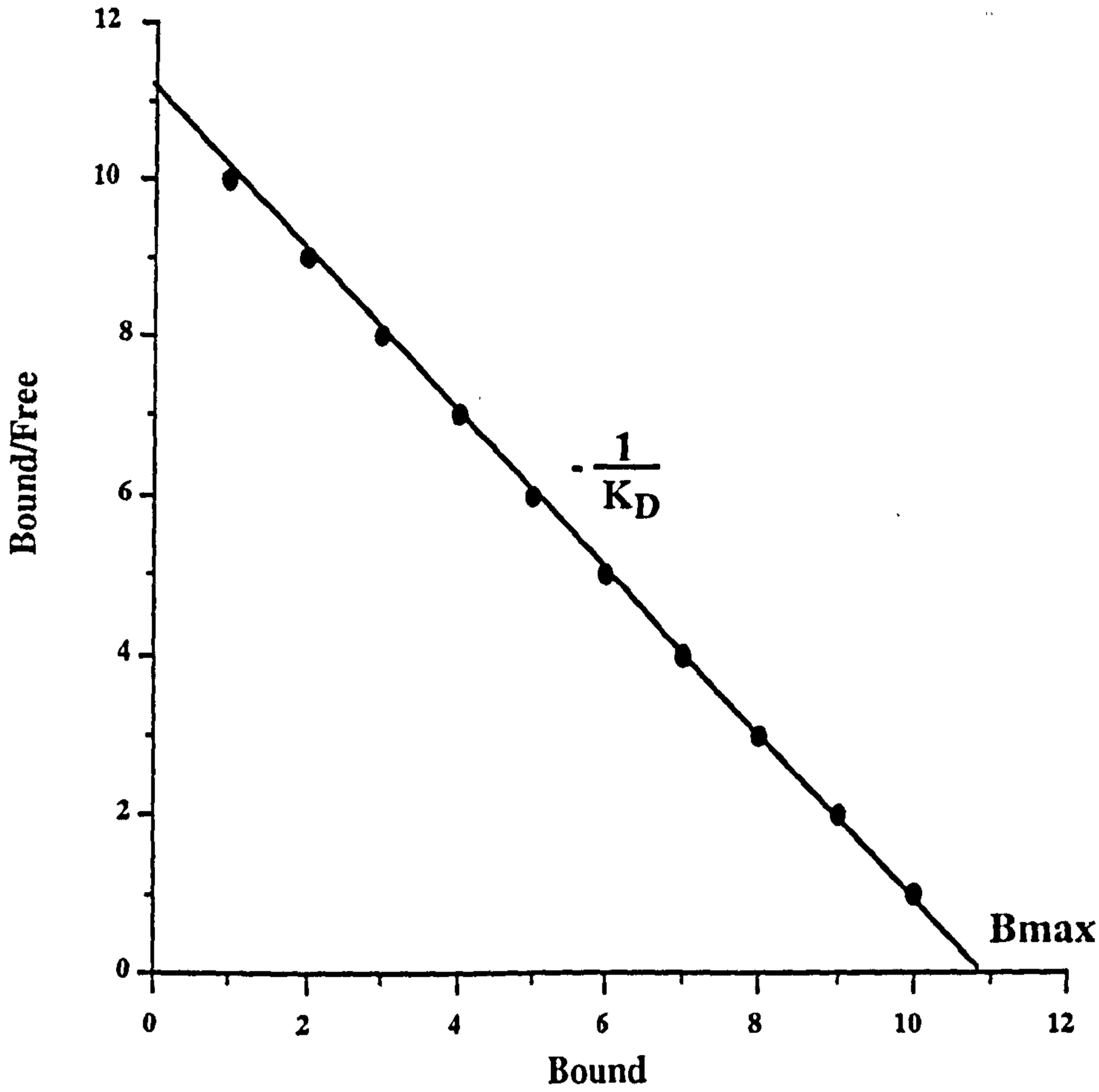


**Fig 8:** Scatchard plot of data from a theoretical saturation asssay.
Plot shows specifically bound radioligand against ratio of Bound/Free radioligand. this produces a straight line the slope of which is equal to -1/KD. The x intercept defines Bmax.

ligand. This saturates the receptors and effectively eliminates specific binding. Specific binding is then calculated by subtracting Non-specific binding from Total binding.
Fig. 7 shows as typical rectangular hyperbola from a saturation experiment, with specific binding plotted against free radioligand concentration.
The $K_D$ value can be estimated from this plot and is defined as the concentration of free radioligand at which 50% maximal binding is produced at equilibrium.
Several arithmetical transformations have been devised to derive linear plots of data from saturation assays in an effort to allow more accurate determination of binding parameters. The most commonly used of these is the Scatchard Plot, which is based upon the Scatchard equation (equation 3 above). This equation was derived by Scatchard in 1949 to describe the binding of molecules to proteins which were independent of each other with identical $K_D$ values.
Scatchard analysis involves plotting the ratio of bound to free radioligand against bound radioligand. This produces a linear plot, the slope of which is equal to $-1/K_D$, while the x intercept defines $B_{max}$.(Fig. 8).

## 2.2.1 *In Vitro* Association Time Course Assay: Determination of Observed Association Rate Constants for (R,S)- and (R,R)-[$^{125}$I]-QNB

### Surgical Preparation

Male sprague dawley rats (300-400g) were placed in a perspex box and euthanasia by an excess of halothane (5%) in a nitrous oxide and oxygen mixture (70% : 30%). Death was defined as the point at which there was complete failure of respiration and at which no heartbeat could be found. Rats were then decapitated and the whole brain carefully dissected out. Excess blood, small bone fragments and any hair adhering to the brain was then removed before the brain was rapidly frozen in isopentane at -42$^{o}$C for 10 mins. Brains were then mounted onto swivel headed microtome chucks with Gurr O.C.T. Compound (BDH) over solid $CO_2$ and coated in plastic embedding matrix (M1-Lipshaw) to reduce the effects of dehydration during cold storage. Brains were then sectioned in a cryostat microtome at -20$^{0}$C with serial 20µm coronal sections of the caudate nucleus, dorsolateral hippocampus and cerebellum identified anatomically by reference to the rat brain atlas of Paxinos and Watson (1986) collected onto subbed glass microscope slides. Two 20µm coronal sections were collected onto each slide. All sections were then placed in a slide box, which was taped shut to prevent access of air, and stored in a freezer at -20$^{0}$C overnight before use. This was done as freshly cut sections adhere poorly to slides and immediate use can result in loss of tissue during the performance of the assay. Storing overnight aids the bonding of the tissue section to the slide and improves the resolution of the assay. All sections were used within one week of harvest.

### Pre-washing

Before use in a binding assay, all sections were placed in slide racks and washed in 50mM phosphate buffered saline containing 10mM EDTA (pH 7.4) at 25$^{o}$C for 30 mins. Pre-washing in this solution dissociates endogenous ligand receptor complexes and inactivates most proteases ( Potter et al, 1984;Mash et al, 1985). After 30 mins washing the sections are removed from the slide racks and laid out in binding trays and dried in a cold air stream.

### Preparation Of Incubate Medium

All *in vitro* binding assays with either (R,S)- or (R,R)-[$^{125}$I]-QNB were performed in an incubate medium consisting of 50mM phosphate buffered saline (PBS) containing 1mM ethylene diaminetetraacetic acid (EDTA) and 1mM N-ethylmalemide (NEM). The addition of EDTA and NEM to the buffer stabilises the low affinity agonist states of muscarinic receptors and facilitates their labelling with QNB (Potter et al, 1984; Flynn and Potter, 1985). Mash and Potter (1986) also reported that pre-soaking of un-

fixed sections of rat brain in buffer containing 10mM EDTA increased the levels of specific binding and helped to preserve tissue integrity in their binding assays. For these reasons the above incubate medium was chosen for the performance of all *in vitro* binding assays.

**Determination Of Non-Specific Binding**

Non-specific binding in all *in vitro* assays with either (R,S)- or (R,R)-[$^{125}$I]-QNB was determined by addition of an excess concentration of the non-selective muscarinic receptor antagonist atropine.

**Experimental Procedure**

Rat brain sections at the level of the caudate nucleus, dorsolateral hippocampus and cerebellum sections were placed in binding trays before being incubated in 0.2 nM (R,S)- or (R,R)-[$^{125}$I]-QNB in 50mM PBS containing 1mM EDTA and 1mM NEM (pH 7.4), for 1, 2, 5, 10, 20, 40, 60, 90, and 120 mins at 25$^{o}$C, to determine Total binding. Non-specific binding for each brain region was determined as for Total, with the presence of 2μM atropine in the incubate medium.

Each section was incubated in 400μl of medium applied directly onto the section with an adjustable 1ml Gilson pipette. After initiation of the assay the binding tray cover was fitted to reduce loss of incubate medium from sections by evaporation.

Triplicate sections from each region were assayed to determine both Total and Non-specific binding.

After the appropriate time period had elapsed, incubation medium was poured off the sections before they were briefly dipped in distilled water. Sections were then placed in slide racks and washed in 50mM PBS (pH 7.4) for 30 mins at 25$^{0}$C.

Following washing, sections were removed from the slide racks and dried in a cold air stream before processing for [$^{125}$I] autoradiography as described below.

**Preparation of Autoradiograms**

Autoradiograms were prepared as described in section 2.1.1.

**Quantification Of Autoradiograms**

Autoradiograms for *in vitro* studies were analysed as described in section 2.1.1. For *in vitro* studies with [$^{125}$I]-QNB determination of Total, Non-specific and Specific binding is necessary. For all in vitro assays, to determine Total and Non-specific binding, bilateral readings were taken from the triplicate brain sections pre-designated as Total and Non-specific, for each of the three brain regions examined (frontal, parietal and cerebellar cortices). A value for specific binding was then derived by subtracting Non-specific from Total binding. Binding data expressed as μCi per g brain can then be converted to nmoles per g brain through knowledge of the specific

activity of the tracer.

**Data Analysis**

The observed association rate (kobs) was derived according to the theory detailed in section 2.2, with levels of Total, Non-specific and Specific binding expressed as nmoles per g for each region of interest.

### 2.2.2 *In Vitro* Saturation Analysis:
### Determination of the Equilibrium Dissociation Constant for (R,S)- and (R,R)-[$^{125}$I]-QNB

**Experimental Protocol**

20µm coronal sections of rat brain at the level of the caudate nucleus, dorsolateral hippocampus and cerebellum prepared as described in section 2.2.1.
were placed in binding trays before being incubated in 0.007 nM, 0.01 nM, 0.03 nM, 0.05 nM, 0.07 nM or 0.1 nM (R,S)- or (R,R)-[$^{125}$I]-QNB in 50mM PBS containing 1mM EDTA and 1mM NEM (pH 7.4) for 90 mins at 25$^0$C, to determine Total binding. Non-specific binding was determined as for Total with 1 µM atropine present in the incubation medium. Each section was incubated in 400µl of medium applied directly onto the section with an adjustable 1ml Gilson pipette. After initiation of the assay the cover of the binding tray was fitted to prevent loss of incubate medium form sections through evaporation. Triplicate sections from each region were assayed to determine both Total and Non-specific binding.
After 60 mins, the binding tray cover was removed and the incubation medium poured of the sections before they were briefly dipped in distilled water. Sections were then placed in slide racks and washed in 50mM PBS (pH 7.4) for 30 mins at 25$^0$C.
Following washing, sections were removed from slide racks and dried in a cold air stream.

**Preparation of Autoradiograms**

Autoradiograms were prepared as described in section 2.1.1.

**Quantification Of Autoradiograms**

Analysis of autoradiograms was performed as described in section 2.2.1.

**Data Analysis**

The equilibrium dissociation rate constant ($K_D$) was calculated by Scatchard Analysis according to the theory detailed in section 2.2, with levels of Total, Non-specific and Specific binding expressed as nmoles per g for each region of interest.

## 2.2.3 Effect Of Heptylphysostigmine On (R,S) and (R,R) [$^{125}$I]-QNB Binding *In Vitro*: Displacement Analysis

### Experimental Protocol

20$\mu$m coronal sections of rat brain at the level of the caudate nucleus, dorsolateral hippocampus and cerebellum were prepared as described in section 2.2.1.
Sections were placed in binding trays before 130$\mu$l $10^{-6}$M heptylphysostigmine was applied directly onto each section with a 1ml adjustable pipette. Sections were incubated in heptylphysostigmine for 30 mins to allow complete inhibition of any of the acetylcholinesterase enzyme present. For (R,S)-[$^{125}$I]-QNB experiments, a further 270 $\mu$l of incubate medium containing 0.1nM (R,S)-[$^{125}$I]-QNB and $10^{-5}$M, $10^{-4}$ M, $10^{-3}$M or $10^{-2}$M ACh was applied onto each section to determine Total binding. For (R,R)-[$^{125}$I]-QNB experiments 270 $\mu$l of incubate medium containing 0.2 nM (R,R) [$^{125}$I]-QNB and $10^{-6}$M, $10^{-4}$M or $10^{-3}$M ACh was applied onto each section to determine Total binding. Sections were therefore incubated with a final volume of 400$\mu$l of medium covering each section. Non-specific binding was determined as for Total with the presence of 1 $\mu$M and 2 $\mu$M atropine in the incubation medium respectively for (R,S) and (R,R) experiments . After initiation of the assay the cover of the binding tray was fitted to prevent loss of incubate medium from sections through evaporation. Triplicate sections from each region were assayed to determine both Total and Non-specific binding.
After 60 mins, the binding tray cover was removed and the incubation medium was poured off the sections before they were briefly dipped in distilled water. Sections were then placed in slide racks and washed in PBS (pH 7.4) for 30 mins at $25^0$C.

### Preparation of Autoradiograms

Autoradiograms were prepared as described in section 2.1.1.

### Quantification Of Autoradiograms

Analysis of autoradiograms was performed as described in section 2.2.1.

### Data Analysis

Levels of Total, Non-specific and Specific binding were expressed as nmoles per g for each region of interest.

## 2.3 ASSESSMENT OF REGIONAL CEREBRAL BLOOD FLOW (rCBF) BY [$^{14}$C]-IODOANTIPYRINE AUTORADIOGRAPHY

### 2.3.1 Theory Of Quantitative Auotradiographic Determination of rCBF

Quantitative determination of regional cerebral blood flow was first reported by Kety and associates using radioactive tracer trifluoroiodoethane ([$^{131}$I] $CF_3I$) (Landau et al., 1955) . The method is based upon the principles of inert gas exchange between blood and tissues, and the following equation developed by Kety (1951):

$$Ci(T) = \lambda K \int_0^T C_A e^{-K(T-t)} dt$$

Where

Ci($T$)= tissue concentration of the chemically inert diffusible tracer at a given time T

$\lambda$= the tissue:blood partition coefficient

$C_A$= the concentration of the tracer in the arterial blood

$t$= the variable time

$K$= a constant that incorporates within it the rate of blood flow in the tissue

$K$ is defined as follows:

$$K = mF/W\lambda$$

where

F/W= the rate of blood flow per unit mass of tissue

$m$= a constant between 0 and 1 that represents the extent to which diffusion equilibrium between blood and tissue is achieved during passage from arterial to venous end of the capillary.

In the brain , due to the absence of arteriovenous shunts, $m$= 1 and K becomes solely dependent upon the perfusion rate of the tissue.

The method developed by Kety depended upon the ability of the radioactive tracer to diffuse unrestricted across the blood brain barrier, hence the use of the radioactive gas [$^{131}$I]-$CF_3I$. However using [$^{131}$I]-$CF_3I$ had several disadvantages. The tracer has a relatively short half-life (8 days) , was difficult to obtain commercially and the assay of tracer concentration in the blood was difficult.

The use of this tracer for the determination of blood flow was superseded by the development of [$^{14}$C] labelled antipyrine, which has in turn been superseded by [$^{14}$C] iodoantipyrine (IAP). The use of IAP as a tracer for the determination of blood flow has a number of advantages. It is a freely diffusible tracer thus blood flow measurement is limited only by the level of blood flow to a region. It produces

excellent spatial resolution with autoradiography, is inert and non-metabolised and allows determination of blood flow in multiple regions. In addition IAP has a higher lipid/water partition coefficient than antipyrine and produces blood flow measurements similar to these obtained with $CF_3I$ (Sakurada et al., 1978).

One of the main disadvantages of the IAP is the complex nature of the methodology. Accurate measurement of time of blood sample collection and the duration of the experiment is necessary. Any inaccuracies in these parameters can result in marked errors in the value of cerebral blood flow obtained (Patlak et al., 1984). With the use of freely diffusible radioactive tracers such as IAP there is also the problem of back-flux from the tissue into blood (Patlak et al., 1984). This source of error can be minimised however, using a short experimental schedule (30 - 60 sec) and the use of a ramped infusion of isotope (Patlak et al., 1984).

### 2.3.2 Measurement of rCBF In The Conscious Rat Following Heptylphysostigmine Administration

There are a number of methods of assessing rCBF with [$^{14}$C]-IAP, two of which are the Indicator Fractionation technique (Goldman and Sapirstein, 1973) and the Tissue Equilibration technique (Sakurada et al., 1978). In this study the latter technique was performed.

This procedure assumes the tracer is in equilibrium between the tissue and blood after iv administration. The tracer is injected as a ramped infusion over 60 sec during which timed arterial blood samples are collected from a free flowing catheter. The technique is based upon a model of blood-tissue exchange which assumes equilibration between plasma, red blood cells and a single tissue compartment.

**Surgical Preparation**

Male sprague dawley rats (335-356g) were placed in a perspex chamber with 5% halothane in a gas mixture of nitrous oxide (70%) and oxygen(30%). Anaesthesia was subsequently maintained by administration of 0.5-1% halothane in the gas mixture via a face mask. A rectal temperature probe was inserted to allow monitoring of core temperature. Both left and right femoral vessels were exposed by blunt dissection through a small incision made in the groin of the rat. Polyethylene catheters (Portex, exterior diameter 0.96 mm, interior diameter 0.58 mm) were then inserted approximately 2 cm into the femoral artery and vein on both left and right sides and tied in place with surgical silk. The incisions were then infiltrated with antiseptic xylocaine gel (2%) and sutured closed with surgical silk (4/0). Catheterisation of femoral vessels allows continuous monitoring of arterial blood pressure, intermittent arterial blood sampling and administration of drugs and radioisotope tracer. The

animals were then lightly restrained in plaster casts fitting loosely around the abdomen and hind legs. The weight of the rat was then supported by means of taping the plaster cast to a lead brick placed under the animal.
Anaesthesia was discontinued and animals were allowed a minimum period of 1 hour recovery before any further procedures were performed.

## Administration Of Drugs

Following recovery from anaesthesia each animal received heptylphysostigmine tartrate 2 mg/kg (0.7 mls 0.9% saline) or vehicle (0.7 mls 0.9% saline) as an intravenous infusion at a constant rate over 30 mins.

## Measurement of Cerebral Blood Flow

Local cerebral blood flow was determined 120 mins after cessation of drug/vehicle infusion according to minor modification of the method of Sakurada et al., 1978 (see Nehls et al., 1990). Animals received a ramped infusion of 50μCi of [$^{14}$C]-Iodoantipyrine radioisotope in 1.5 mls of 0.9% saline over 60 seconds. During the infusion 15-18 timed samples of arterial blood were collected onto pre-weighed filter discs. Animals were killed by decapitation approximately 1 minute following the start of the isotope infusion. the brain was quickly removed and frozen in isopentane at -42$^{o}$C for later processing. The filter discs were then re-weighed and placed in scintillation vials. A 30% solution of hydrogen peroxide was then added to bleach the blood from the discs. Commercial scintillant was then added to the vials and [$^{14}$C] radioactivity was determined by liquid scintillation counting. In addition to those blood samples collected during the experimental protocol, further blood samples were taken immediately prior to initiation of drug/vehicle infusion and blood flow measurement to allow plasma glucose and blood gas status determination.

## Preparation of [$^{14}$C]-IAP Autoradiograms

The frozen brains were mounted onto swivel headed microtome chucks with plastic embedding matrix (Lipshaw) over solid $CO_2$. Three 20μm coronal sections were collected serially onto glass coverslips at 200μm intervals throughout the brain and rapidly dried on a hotplate at 60$^{o}$C. the coverslips were then glued onto thin card. Autoradiograms were generated by apposing the sections along with pre-calibrated [$^{14}$C] standards (44-2500 nCi/g, tissue equivalents) to Kodak Biomax MR film in light-tight cassettes for 3 days.

## Quantification Of Autoradiograms

The autoradiograms were analysed densitometrically for radioisotope content by grey level comparison with the pre-calibrated standards in a similar manner to that described in section 2.1.1 for $^{125}$I-autoradiograms. Twelve bilateral readings were taken from

33 pre-determined anatomical loci, where the region of interest could be identified from the rat brain atlas of Paxinos and Watson (1986).

**Calculation Of Cerebral Blood Flow**

The local cerebral blood flow was calculated for each region of interest from the equation of Sakurada et al., 1978, with the knowledge of the time course history of the [$^{14}$C]-IAP in the arterial blood, the [$^{14}$C] concentration in each region and the tissue:blood partition coefficient (0.79) for the rat (see above).

**Data Analysis**

The data from the two experimental groups, heptylphysostigmine and vehicle were analysed using a two tailed Student's unpaired t-test. The data were expressed as mean ± S.E.M. ml/100g/min for each region of interest.

## 2.4 ACETYLCHOLINESTERASE HISTOCHEMISTRY

### 2.4.1 Theory

The primary function of acetylcholinesterase in animal tissue is to catalyse the hydrolysis of acetylcholine to choline and acetic acid. To understand how the hydrolysis of ACh occurs it is necessary to have knowledge of the active centre of enzyme. The active centre of acetylcholinesterase has two subsites consisting of a negatively charged **anionic site** and an **esteratic site** (Wilson, 1951).The esteratic site contains both an acidic (electrophillic) and basic (nucleophillic) group. Hydrolysis is initiated when the positively charged quaternary nitrogen of an ACh molecule binds to the negatively charged anionic site on the enzyme. This causes the ACh molecule to orientate such that its carbonyl group is presented to the esteratic site. An enzyme -substrate complex is then formed. The acetyl group of the ACh molecule then transfers to the hydroxyl group of the esteratic site and a molecule of choline is liberated. Spontaneous and rapid hydrolysis of the acetyl group then occurs, producing acetic acid, and the esteratic site returns to its original state (See Fig. 9).

Histochemical staining procedures make use of this reaction by providing a substrate other than acetylcholine that may be hydrolysed by the enzyme. The hydrolysis product is then reacted with another component to from an insoluble precipitate at the site of enzyme activity. The precipitate may then be coloured by a further reaction to visualise distribution of enzyme activity. The first demonstration of histochemical staining of AChE in this manner used higher fatty acid esters of choline as substrates . The most common substrates in use however, are thiocholine esters as these show high specificity for acetylcholinesterase over other esterases that may be present in the tissue. Thiocholine esters were originally shown to be suitable histochemical substrates for acetylcholinesterase by Koelle and Friedenwald in 1949. Their technique involves incubation of the tissue to be stained in a medium containing acetylthiocholine as a substrate for the enzyme, copper in the form of copper sulphate ($CuSO4$) as the capture agent and glycine which chelates the copper to reduce its inhibitory action on enzyme activity. The reactions which occur in the tissue during incubation in the staining medium not entirely understood, however the following reaction has been proposed (Bergner and Bayliss, 1952).
Acetylthiocholine and copper glycinate react with the AChE producing copper thiocholine, glycine and acetic acid, as shown below.

$$2\,CH_3COCH_2CH_2(CH3)_3OH + (NH_2CH_2COO)_2Cu + H_2O \longrightarrow$$

Acetylthiocholine Copper Glycinate

## Mechanism of Hydrolysis of ACh by AChE

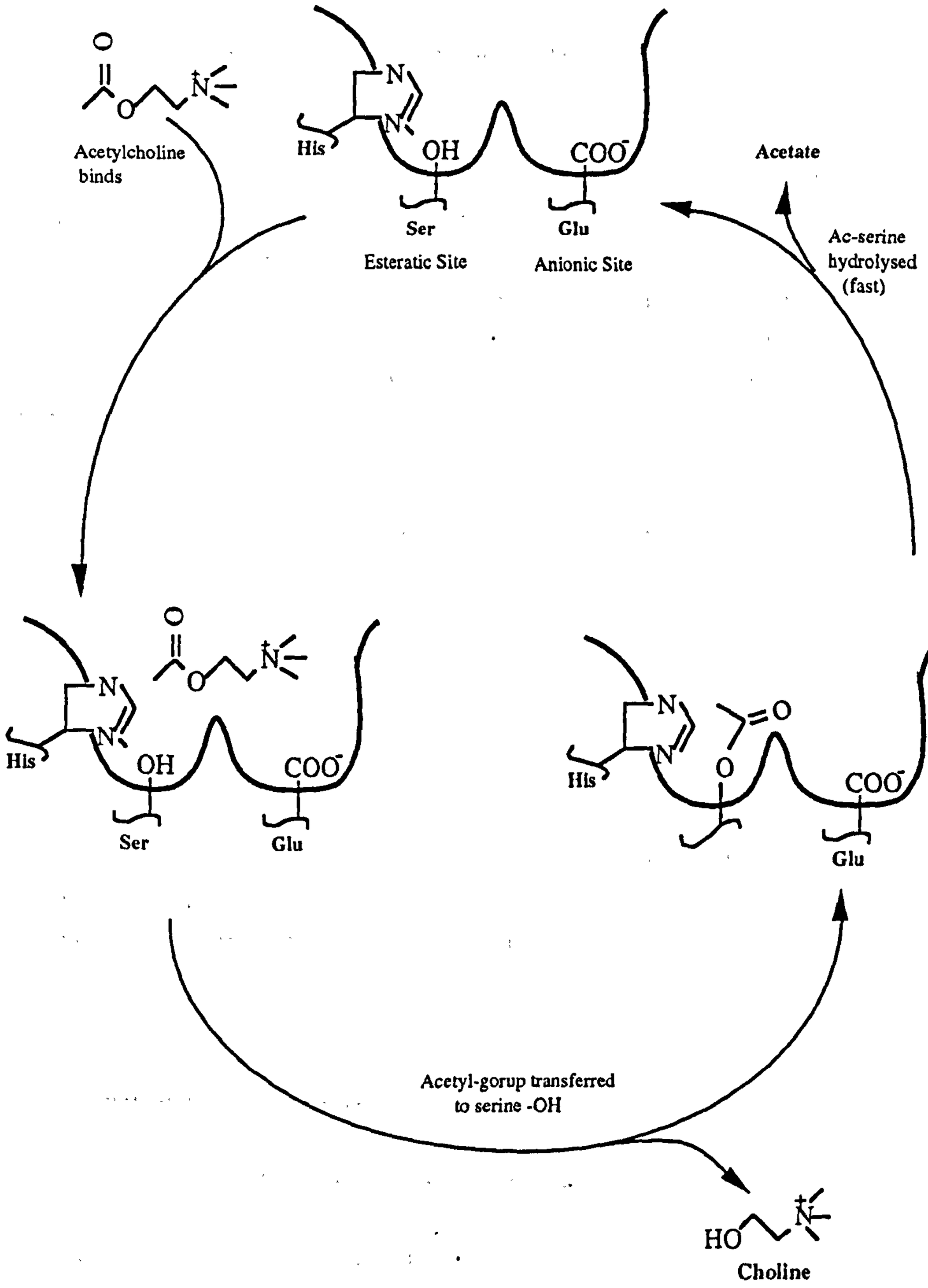


**Fig 9:** Schematic representation of ACh hydrolyisis by Acetylcholinesterase.
ACh molecule binds to anionic site on the enzyme initiating hydrolyisis, whereby the acetyl group of ACh is transferred to the serine -OH of the esteratic site producing an acetylated enzyme form and liberation of a molecule of choline. Spontaneous hydrolysis of the serine-acetyl group occurs rapidly thereafter regenerating the enzyme and producing a molecule of acetic acid.

$$Cu\,[SCH_2CHN(CH_3)_3OH]_2 + 2\,NH_2CH_2COOH + 2\,CH_3COOH$$

Copperthiocholine Glycine Acetic Acid

White copperthiocholine is then precipitated in the region of enzyme activity. The copper in the incubate immediately precipitates the newly released thiocholine produced by the enzyme reaction. This prevents it from diffusing away from the reaction site ensuring accurate identification of enzyme distribution. The white copper thiocholine can then be "developed" to produce a characteristic dark stain by incubating tissue in a sodium or ammonium sulphide solution. This replaces copperthiocholine with brown copper sulphide in the following reaction:

$$Cu\,[SCH_2CHN(CH_3)_3OH]_2 + (NH_4)_2S \downarrow$$

$$CuS + 2\,NH_4SCH_2CH_2N(CH_3)_3OH$$

The histochemical staining procedure for acetylcholinesterase used in this thesis is that described by Silver (1974) for fresh-frozen or unfixed tissue, and is based upon the technique of Lewis (1961). It is a modification of the thiocholine method of Koelle and Friedenwald (1949).

## 2.4.2 Experimental Procedure

**Preparation Of Acetylthiocholine iodide incubate**

100mg of acetylthiocholine iodide (ACThI) was dissolved in 4mls of distilled $H_2O$ in a centrifuge tube. 7mls of 0.1M copper sulphate($CuSO_4$) solution was then added to the centrifuge tube. The initial 2-3mls of $CuSO_4$ being added dropwise.

The tube was then left to stand for 10 mins before being centrifuged at 2000 rpm for 20 mins. Following centrifugation, 10 mls of supernatant was pipetted off and 62 mg of glycine dissolved in it. The pH of the resulting solution was adjusted to 5.5 by addition of 1M sodium acetate solution. The incubate solution was then made up to a final volume of 50mls with $dH_2O$ and filtered using Whatmans No. 1 filter paper. This solution may be made up to one week in advance of use if stored in a refrigerator.

For the studies performed in this thesis, the incubate medium was used no more than 24 hrs after preparation.

**Preparation Of Developer**

1g of sodium sulphide was dissolved in 45 mls of 0.2N acetic acid. The pH of the solution was then adjusted to 5.5 by addition of 1M sodium acetate, before filtering through Whatmans No.1 filter paper folded fanwise. The entire preparation of the developing solution was performed in fume hood, as the addition of acetic acid to crystals of sodium sulphide releases toxic hydrogen sulphide gas.
The shelf-life of this soultion is very short, therefore, a fresh solution was prepared daily and refrigerated until use.

**Protocol**

20μm coronal sections of rat brain mounted on subbed glass microscope slides were incubated in 0.2M sodium acetate solution containing $10^{-4}$M ethopropazine, at $25^0$C for 30mins. Sections were then removed from the sodium acetate solution and incubated in ACThI solution containing $10^{-4}$M ethopropazine for 4 hrs at $25^0$C. Ethopropazine is an inhibitor of butrylcholinesterase. The presence of this compound in the incubation medium ensures that only acetylcholinesterase enzyme activity is stained. Following incubation, sections underwent 3 x 1 min washes in $dH_2O$. Sections were then immersed in sodium sulphide developer for 2mins, before undergoing 2 x 2 min washes in $dH_2O$ and were then allowed to dry. Dehydration of sections was produced by 3 sequential incubations of 1 min in 100% alcohol. Sections were then cleared by dipping in xylene and mounted with coverslips using DPX.

Although great care was taken to standardise the staining procedure, histochemistry is intrinsically variable and small differences in incubation time, temperature or pH which affect the intensity of stain are unavoidable in the performance of the technique. To reduce the effect of such variations on staining intensity, sections were simultaneously stained in batches. In addition, control sections from an untreated animal were stained along with experimental tissue to provide an internal control for each batch.

**Semi-quantitative analysis of AChE stained sections**

In this thesis enzyme activity in histochemically stained sections was determined by a semi-quantitative densitometric technique using a computer based image analysis system. Absolute quantitative analysis of acetylcholinesterase activity in histochemically stained sections is possible when tissue standards containing known amounts of purified enzyme are prepared and incubated along with the experimental sections (Biegon and Wollf, 1986). Due to the constraints of time and unavailability of

a purified enzyme source, preparation of standards as described above was impractical. The image analyser was instead calibrated against as set of optical density standards. Enzyme activity in analysed sections was therefore converted to units of optical density, with areas of greater enzyme activity(i.e. greater stain intensity) scoring a higher optical density.

Histochemically stained sections were analysed using a computer based image analysis system (M4 MCID, Imaging Research Inc.). Sections were analysed densitometrically for enzyme activity in discrete brain regions by grey level comparison with pre-calibrated optical density standards. The image analyser was calibrated against optical density standards (Kodak Wratten gelatin filters) in the range of 0 -1.0, with the zero value taken as the background level when no filter was present in the image field. Measurements were made by placing a measuring frame over each anatomical region of interest. The size of the measuring frame was variable but was kept constant for anatomical regions of interest between individual studies. Bilateral readings were taken from individual sections for each region of interest. Background readings were taken from each slide and subtracted from the O.D. value measured for each region of interest. This was done to reduce the effect slight differences the mounting procedure produces in the density of the staining.

Structures in the rat brain were defined anatomically by reference to the stereotaxic atlas of Paxinos and Watson (1986).

**Data Analysis**

To reduce measurement variability, sections from a single batch of staining were analysed on the same day. Similarly, direct comparisons in the level of staining were made only between sections stained in the same batch. Data from heptylphysostigmine and vehicle treated sections were analysed using a two tailed Student's unpaired *t* - test. Data are expressed as mean ± S.E.M optical density, as a semi-quantitative measure of enzyme function. A higher O.D. representing greater enzyme activity.

# CHAPTER 3

# RESULTS

## 3.1 *IN VIVO* AUTORADIOGRAPHIC STUDIES

### 3.1.1 Uptake and Retention of (R,S)-[$^{125}$I]-QNB in Rat Brain

The uptake and retention of (R,S)-[$^{125}$I]-QNB in the brain of conscious rat between 2 and 24 hours following intravenous administration of tracer was determined by *in vivo* autoradiography. Quantitative densitometric analysis of autoradiograms was performed to determine (R,S)-[$^{125}$I]-QNB levels in 33 anatomically distinct brain regions with tracer level in each region expressed as a ratio relative to uptake in the caudate nucleus (Table 5).

**General Observations**

Physiologic variables were measured prior to and at various time points after administration of (R,S)-[$^{125}$I]-QNB. No significant differences were observed in any of the variables measured following administration at any of the time points. Tables of physiologic variables are presented in Appendix B.

**Regional Uptake and Retention of (R,S)-[$^{125}$I]-QNB**

(R,S)-[$^{125}$I]-QNB shows a heterogeneous pattern of distribution within the brain. Autoradiographic images of (R,S)-[$^{125}$I]-QNB distribution in the brain are shown in Fig 10. Notable differences in regional tracer retention can be seen between the 2 hour and 24 hour images. High levels of activity were observed in the cortex, caudate nucleus and hippocampus at 2 hours which persisted up to 24 hours. In the thalamus, (R,S)-[$^{125}$I]-QNB levels were initially high at 2 hours, but activity was then observed to decrease significantly over the next few hours with a 40% reduction in activity observable by 24 hours. In comparison a reduction in activity of 10% is observed in the frontal cortex over the same time period . In contrast (R,S)-[$^{125}$I]-QNB activity in the cerebellum was initially low at 2 hours (less than 10% of that in frontal cortex) and remained at this low level up to 24 hours. Regional activity-time profiles of normalised data for (R,S)-[$^{125}$I]-QNB are shown in Fig 11 for frontal cortex, CA1 of the hippocampus, mediodorsal thalamus and the cerebellum.

The regional distribution of (R,S)-[$^{125}$I]-QNB in rat brain *in vivo* generally corresponds to the rank order of mAChR concentration as determined *in vitro* . Highest levels of (R,S)-[$^{125}$I]-QNB are observed in the caudate and cortex, with low levels observed in the cerebellum and intermediate levels observed in the thalamus. Correlation of non-normalised regional activity (μCi/g) for (R,S)-[$^{125}$I]-QNB with mAChR concentration is displayed in Fig 12. An overall correlation coefficient of r=0.87 indicates a high degree of association between regional (R,S)-[$^{125}$I]-QNB distribution and mAChR concentration.

### Plasma Clearance of (R,S)-[$^{125}$I]-QNB

The concentration-time profile of (R,S)-[$^{125}$I]-QNB in plasma following intravenous injection is presented in Fig 13. Radioactivity is detectable in the plasma of rat up to 24 hours following administration, albeit at a low level. This data is uncorrected for the presence of metabolites however and therefore the proportion of radioactivity in plasma representing authentic ligand cannot be determined.

### Normalisation of Data to the Caudate Nucleus

Raw data (μCi per g brain) for regional (R,S)-[$^{125}$I]-QNB activity in rat brain were expressed as a ratio of percent of the injected dose relative the level in the caudate nucleus to reduce the impact of interanimal variability on the data. Normalisation to this region was performed as tracer levels in this region are reproducible from animal to animal and are relatively unchanged over the experimental time period. Raw data (μCi/g) for (R,S)-[$^{125}$I]-QNB in caudate nucleus between 2 and 24 hours is shown in Fig14. Complete regional tables of non-normalised time-activity data for (R,S)-[$^{125}$I]-QNB are displayed in Appendix A.

## Table 5

## (R,S)-[$^{125}$I]-QNB in the Brain of Conscious Rat

| Region | TIME FOLLOWING ADMINISTRATION OF TRACER 2 Hours | 6 Hours | 12 Hours | 24 Hours |
|---|---|---|---|---|
| ***Cerebellum*** | | | | |
| Cerebellar Cortex | 0.108 ± 0.021 | 0.147 ± 0.029 | 0.092 ± 0.043 | 0.073 ± 0.036 |
| ***Medulla/Pons*** | | | | |
| Pontine Grey | 0.907 ± 0.247 | 0.799 ±0.081 | 0.377 ± 0.093 | 0.411 ± 0.178 |
| Nucleus of the Lateral Lemniscus | 0.322 ± 0.089 | 0.302 ± 0.029 | 0.220 ± 0.031 | 0.101 ± 0.075 |
| Lateral Dorsal Tegmental nucleus | 0.451 ± 0.127 | 0.409 ±0.066 | 0.415 ±0.178 | 0.266 ± 0.137 |
| ***Mesencephalon*** | | | | |
| Inferior Colliculus | 0.471 ± 0.121 | 0.480 ±0.106 | 0.276 ± 0.060 | 0.273 ± 0.121 |
| Superior Colliculus | 0.725 ±0.068 | 0.464 ±0.021 | 0.279 ± 0.074 | 0.172 ± 0.100 |
| Substantia Nigra (pars compacta) | 0.504 ± 0.064 | 0.476 ± 0.007 | 0.328 ± 0.098 | 0.206 ± 0.079 |
| Substantia Nigra (pars reticulata) | 0.495 ± 0.074 | 0.418 ± 0.029 | 0.275 ± 0.080 | 0.179 ± 0.073 |
| ***Diencepahlon*** | | | | |
| Hippocampus CA1 | 0.659 ± 0.082 | 0.816 ± 0.040 | 0.741 ± 0.263 | 0.831 ± 0.038 |
| Hippocampus CA2 | 0.869 ± 0.061 | 0.971 ± 0.075 | 0.805 ± 0.288 | 0.837 ± 0.019 |
| Hippocampus CA3 | 0.762 ± 0.059 | 0.871 ± 0.075 | 0.747 ± 0.245 | 0.797 ± 0.023 |
| Medial Geniculate Body | 0.841 ± 0.061 | 0.763 ± 0.022 | 0.540 ± 0.193 | 0.435 ± 0.087 |
| Sub Thalamic Nucleus | 0.596 ± 0.064 | 0.410 ± 0.026 | 0.376 ± 0.103 | 0.240 ± 0.118 |
| Lateral Geniculate Nucleus | 0.713 ± 0.082 | 0.687 ± 0.070 | 0.533 ± 0.182 | 0.341 ± 0.131 |
| Hypothalamus | 0.471 ± 0.108 | 0.544 ± 0.037 | 0.383 ± 0.146 | 0.309 ± 0.097 |
| Mediodorsal Thalamic Nucleus | 0.762 ± 0.083 | 0.750 ± 0.074 | 0.584 ± 0.020 | 0.465 ± 0.011 |
| Ventrolateral Thalamic Nucleus | 0.642 ± 0.093 | 0.643 ± 0.051 | 0.464 ± 0.147 | 0.327 ± 0.109 |
| ***Telencephalon*** | | | | |
| Visual Cortex (layer IV) | 0.751 ± 0.345 | 0.971 ±0.022 | 0.910 ± 0.279 | 1.057 ± 0.165 |
| Dentate Gyrus | 0.837 ± 0.060 | 0.927± 0.062 | 0.782 ± 0.263 | 0.749 ± 0.058 |
| Auditory Cortex (layer IV) | 1.365 ± 0.081 | 1.279 ± 0.095 | 1.140 ± 0.414 | 1.204 ± 0.086 |
| Hippocampus Molecular Layer | 0.897 ± 0.046 | 0.956 ±0.071 | 0.893 ± 0.314 | 0.805 ± 0.065 |
| Amygdala | 0.698 ± 0.054 | 0.693 ± 0.055 | 0.607 ± 0.211 | 0.562 ± 0.025 |
| Globus Pallidus | 0.365 ± 0.085 | 0.368 ± 0.043 | 0.275 ± 0.097 | 0.266 ± 0.093 |
| Caudate Nucleus | 1.000 ± 0.000 | 1.000 ± 0.000 | 1.000 ± 0.000 | 1.000 ± 0.000 |
| Septal Nuclei | 0.682 ± 0.055 | 0.664 ± 0.056 | 0.576 ± 0.178 | 0.486 ± 0.086 |
| Nucleus Basalis Magnocellularis | 0.383 ± 0.083 | 0.409 ± 0.042 | 0.326 ± 0.128 | 0.292 ± 0.074 |
| Nucleus Accumbens | 1.03 ± 0.069 | 1.094 ± 0.037 | 1.016 ± 0.040 | 1.085 ± 0.055 |
| Sensory Motor Cortex (layer IV) | 1.275 ± 0.042 | 1.114 ± 0.084 | 1.112 ± 0.041 | 1.09 ± 0.044 |
| Anterior Cingulate Cortex | 1.067 ± 0.064 | 1.111 ± 0.049 | 1.004 ± 0.04 | 1.078 ± 0.054 |
| Frontal Cortex | 1.181 ± 0.050 | 1.128 ± 0.049 | 1.035 ± 0.041 | 1.072 ± 0.065 |
| Parietal Cortex | 0.926 ± 0.145 | 1.091 ± 0.093 | 1.021 ± 0.038 | 1.028 ± 0.035 |
| ***Myelinated Fibre Tracts*** | | | | |
| Internal Capsule | 0.351 ± 0.071 | 0.287 ± 0.039 | 0.222 ± 0.056 | 0.220 ± 0.075 |
| Genu | 0.338 ± 0.046 | 0.344 ± 0.035 | 0.270 ± 0.109 | 0.281 ± 0.056 |

Table shows (R,S)-[$^{125}$I]-QNB in discrete brain regions of the conscious rat 2, 6, 12 and 24 hours following iv administration of 200μCi of tracer. Data are expressed as mean ± S.E.M % dose per g brain normalised to the caudate nucleus, n= 3-5 animals for each time point.

## (R,S)-[$^{125}$I]-QNB In Brain Of Conscious Rat

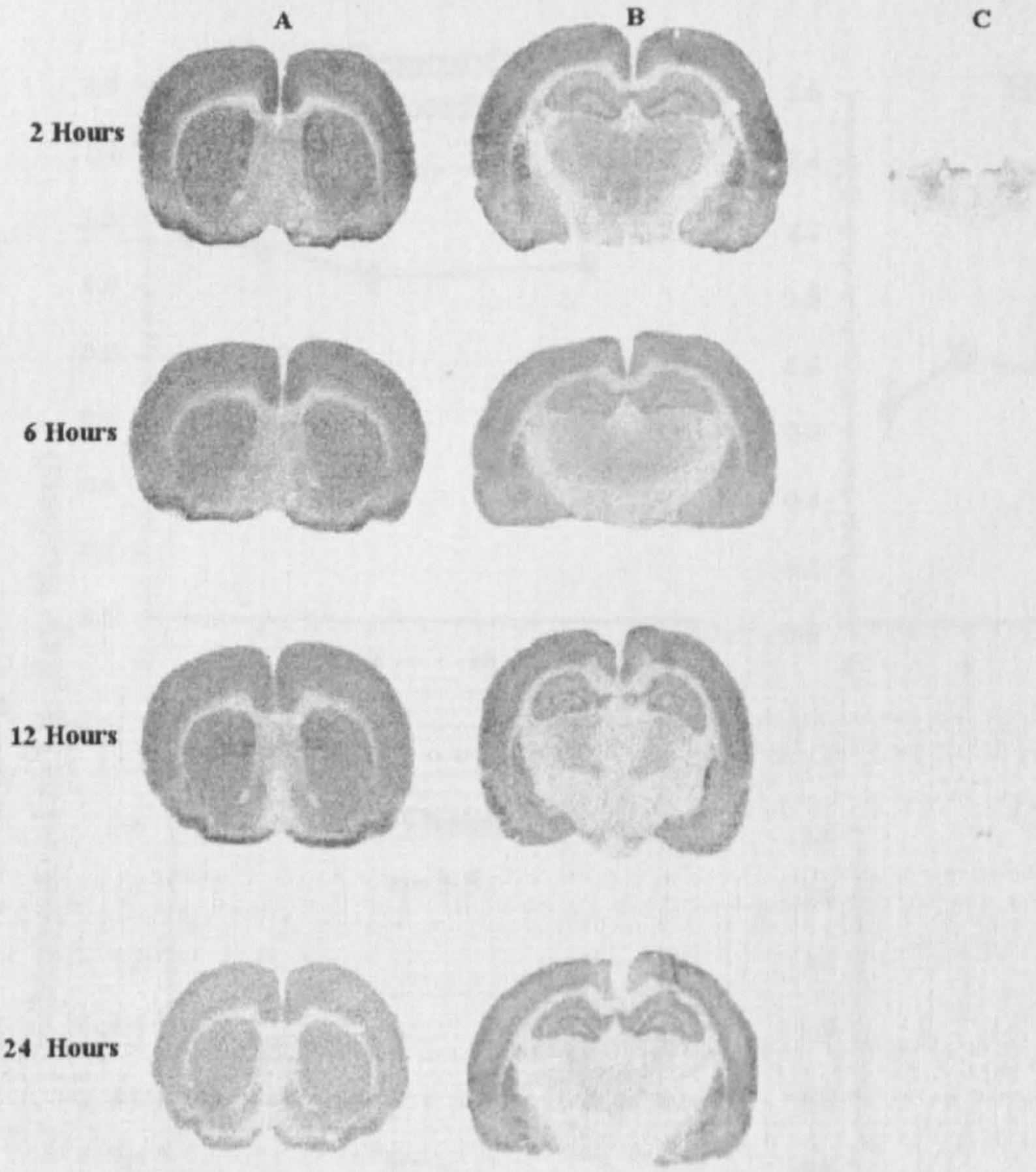


**Fig 10:** (R,S)-[$^{125}$I]-QNB in the brain of conscious rat at 2,6, 12 and 24 hours. Illustrative autoradiograms show tracer uptake at the level of the caudate nucleus (A), dorsolateral hippocampus (B) and cerebellum (C) of rat brain. Tracer uptake shows a heterogeneous distribution within the brain corresponding to regional mAChR density. High levels of activity are observed in the caudate and cortex, intermediate levels in the thalamus and low levels in the cerebellum. Washout of tracer from thalamus and cerebellum is considerably faster than in the caudate and cortex, with neglible amounts of activity observed in the cerbellum by 6 hours. Each brain section represents a digitised video image taken directly from individual autoradiograms at the relevant time point.

## Regional Distribution of (R,S)-[$^{125}$I]-QNB in Rat Brain

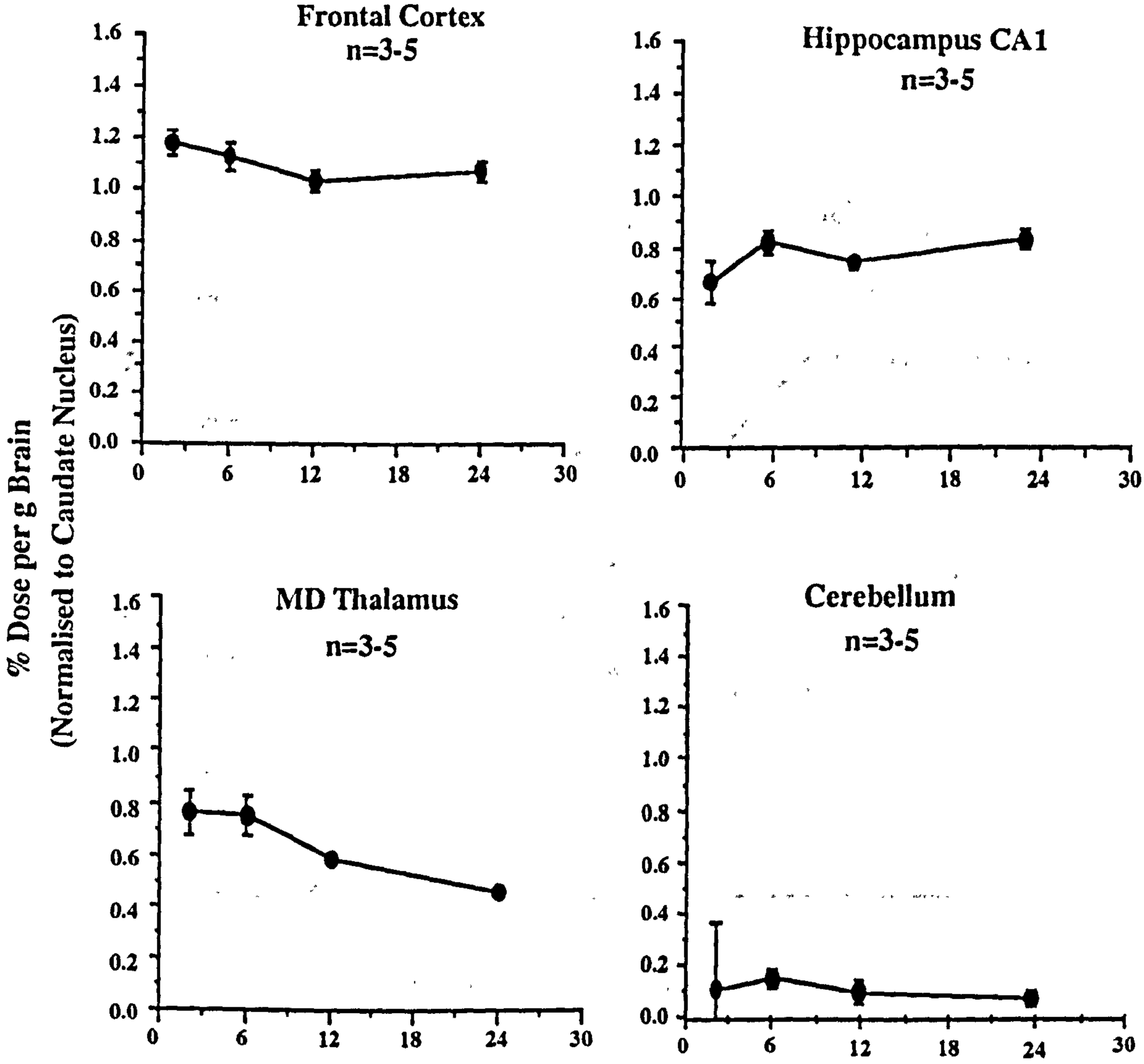


**Fig 11:** Uptake and retention of (R,S)-[$^{125}$I]-QNB in the frontal cortex, hippocampus CA1, mediodorsal thalamus and cerebellum between 2 and 24 hours following tracer administration, note loss of (R,S)-[$^{125}$I]-QNB from mediodorsal thalamus with time. Data are expressed as mean ± S.E.M. % dose per g brain normalised to caudate nucleus. n= number of animals in each group.

**Fig 12:** Figure shows a plot of raw data for (R,S)-[$^{125}$I]-QNB at 2 hours at the level of the caudate nucleus, frontal cortex, hippocampus, mediodorsal thalamus, and cerebellum against regional mAChR concentration. Correlation coefficient of $r^2$=0.87 indicates a high degree of association between regional levels of (R,S)-[$^{125}$I]-QNB and mAChR concentration. (R,S)-[$^{125}$I]-QNB for each region is expressed as mean ± S.E.M μCi per g of Brain, n= 5 animals per region. mAChR concentration is expressed as the average concentration of receptors in nmoles for each region as adapted from Boulay et al., (1996).

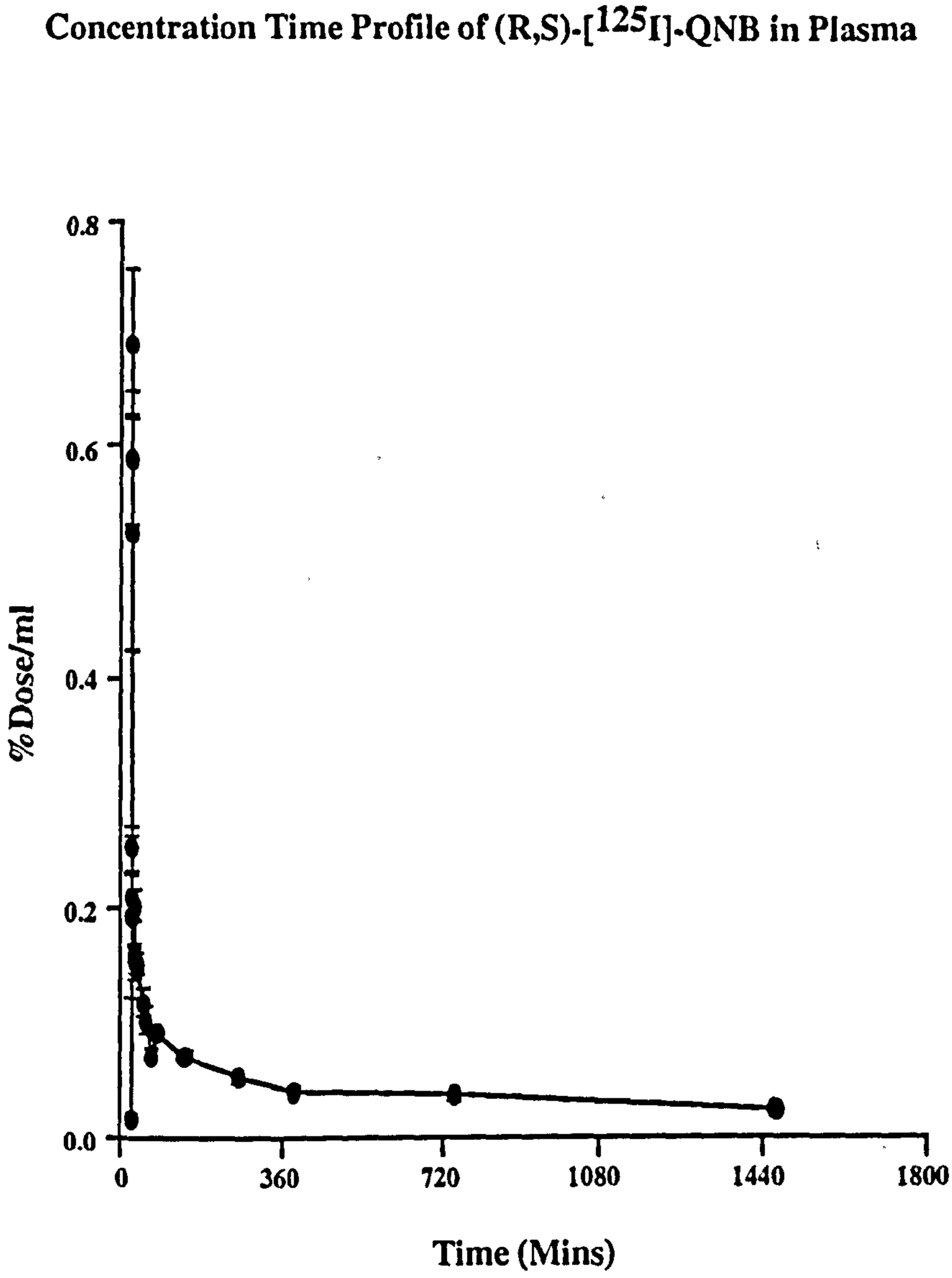


**Fig 13:** Timecourse of radioactivity in plasma up to 24 hours following intravenous administration of 200μCi (R,S)-[$^{125}$I]-QNB. Data is uncorrected for metabolites and therefore the proportion of radioactivity representing authentic tracer cannot be determined. Data is expressed as mean ± S.E.M % dose per ml plasma of 5-16 samples.

## Uptake and Retention of (R,S)-[$^{125}$I]-QNB in Caudate Nucleus: Raw Data

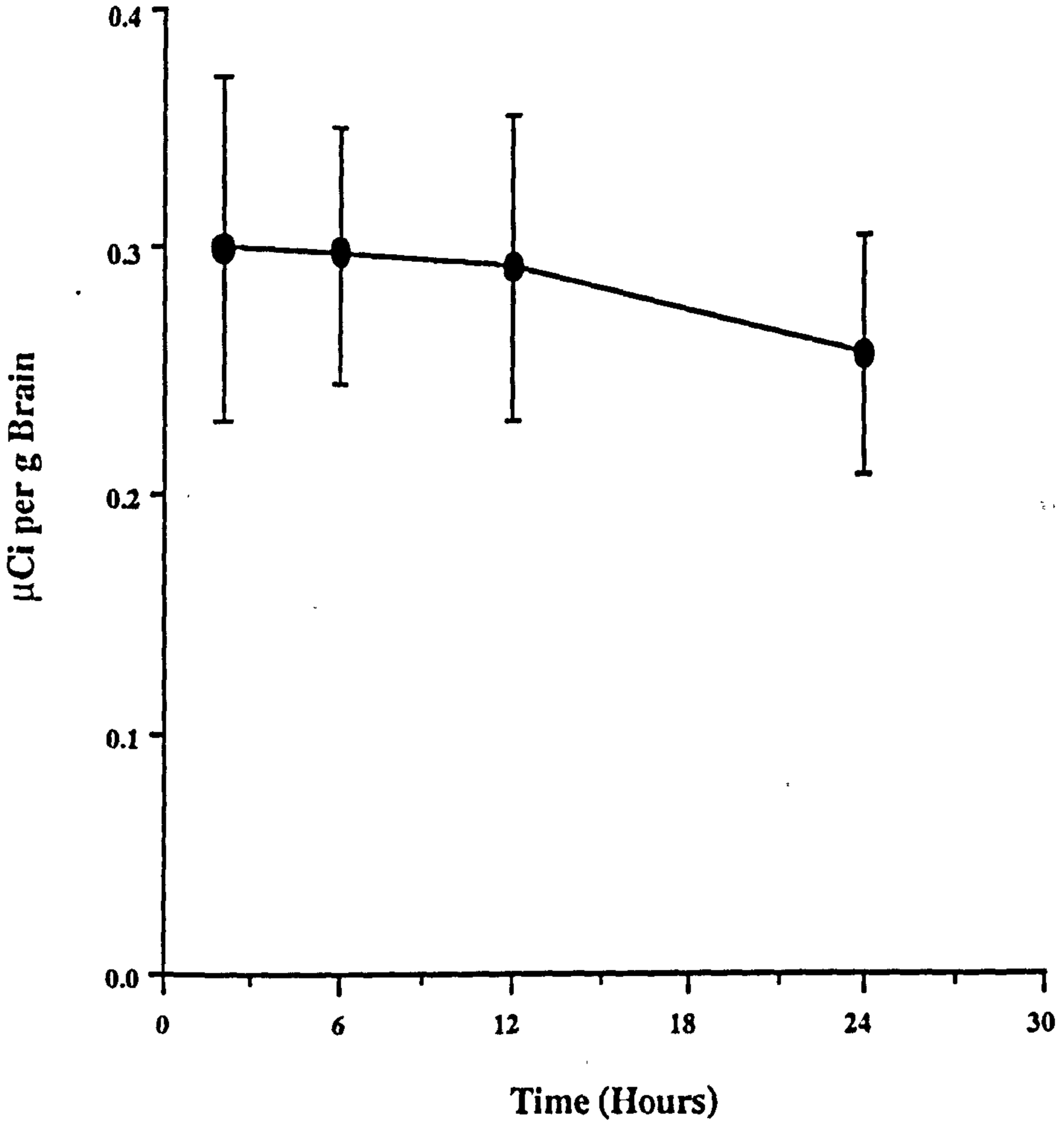


**Fig 14:** Uptake and retention of (R,S)-[$^{125}$I]-QNB in the caudate nucleus of conscious rat from 2 to 24 hours following intravenous administration of tracer. Data are expressed as mean ± S.E.M. µCi per g brain , n=3-5 animals per time point.

### 3.1.2 Uptake and Retention of (R,R)-[$^{125}$I]-QNB in Rat Brain

The uptake and retention of (R,R)-[$^{125}$I]-QNB in the brain of conscious rat between 30 mins and 6 hours following intravenous administration of tracer was determined by *in vivo* autoradiography. Quantitative densitometric analysis of autoradiograms was performed to determine (R,R)-[$^{125}$I]-QNB levels in 33 anatomically distinct brain regions with tracer level in each region expressed as a ratio relative to uptake in the caudate nucleus (Table 6). Regional uptake and retention data for (R,R)-[$^{125}$I]-QNB was compared to that determined for (R,S)-[$^{125}$I]-QNB.

#### General Observations

Physiologic variables were measured prior to and at various time points after administration of (R,R)-[$^{125}$I]-QNB. No significant differences were observed in any of the variables measured following administration at any of the time points. Tables of physiologic variables are presented in Appendix B.

#### Comparison of (R,R)-[$^{125}$I]-QNB and (R,S)-[$^{125}$I]-QNB Uptake and Retention

Autoradiographic images of (R,R)-[$^{125}$I]-QNB distribution in the brain are shown in Fig 15. (R,R)-[$^{125}$I]-QNB shows a heterogeneous pattern of distribution in the brain over 6 hours analogous to that observed for (R,S)-[$^{125}$I]-QNB over 24 hours. A comparison of regional activity-time profiles of normalised data for (R,R)-[$^{125}$I]-QNB and (R,S)-[$^{125}$I]-QNB are shown in Fig 16 for frontal cortex, CA1 of the hippocampus and the cerebellum.

In the cortex comparable levels of activity are observable with (R,S)- and (R,R)-[$^{125}$I]-QNB with little or no washout of activity observed over the time course of the experiments. In the CA1 of the hippocampus activity levels for the two tracers are also generally comparable, although (R,R)-[$^{125}$I]-QNB levels are observed to increase with time and are highest at 6 hours. In the cerebellum (R,R)-[$^{125}$I]-QNB levels are initially higher than those for (R,S)-[$^{125}$I]-QNB but washout of activity is observed with time such that levels are comparable by 2 hours.

Although the *in vivo* distribution and behaviour of (R,S)- and (R,R)-[$^{125}$I]-QNB is qualitatively similar in the above regions, an important difference between the tracers is the time course over which these observations are made. (R,S)-[$^{125}$I]-QNB essentially shows no washout from regions of high mAChR concentration such as the cortex and hippocampus over 24 hours. In contrast this is only true for (R,R)-[$^{125}$I]-QNB over 6 hours. Analysis of regional levels of (R,R)-[$^{125}$I]-QNB in a single animal at 12 hours (data not shown) indicates that a significant loss of activity is observed from all regions

with the exception of the cortex, to the extent that no activity is observable in the cerebellum at this time. (R,S)- and (R,R)-[$^{125}$I]-QNB therefore display considerable differences in kinetic behaviour *in vivo*.

This is exemplified by analysis of regions of intermediate mAChR concentration which display moderate uptake of tracer. Fig 17 shows comparison of time activity data for (R,S)- and (R,R)-[$^{125}$I]-QNB in the mediodorsal thalamus, ventrolateral thalamus and the lateral geniculate nucleus. The above regions display a significant washout of activity over time for both tracers. However, a greater loss of (R,R)-[$^{125}$I]-QNB activity is observed from these regions over a shorter period of time. In each region levels of (R,R)-[$^{125}$I]-QNB are initially higher at 30 mins than those of (R,S)-[$^{125}$I]-QNB at 2 hours, but are significantly lower than those of (R,S)-[$^{125}$I]-QNB by 6 hours. Mediodorsal thalamus, ventrolateral thalamus and lateral geniculate nucleus respectively show a 70%, 72% and 70% reduction in (R,R)-[$^{125}$I]-QNB activity from 30 mins to 6 hours. In comparison, for the same regions a 40%, 50% and 53% reduction in (R,S)-[$^{125}$I]-QNB activity was observed between 2 and 24 hours. These observations indicate that although (R,S)- and (R,R)-[$^{125}$I]-QNB display qualitatively similar distribution the time course of their uptake and retention in the brain is considerably different. Differences in their *in vivo* kinetics for association and dissociation and in their affinity for mAChRs is likely to be responsible for this.

### Plasma Clearance of (R,R)-[$^{125}$I]-QNB

The concentration-time profile of (R,R)-[$^{125}$I]-QNB in plasma following intravenous injection is presented in Fig 18. Radioactivity is detectable in the plasma of rat up to 6 hours following administration, albeit at a low level. This data is uncorrected for the presence of metabolites however and therefore the proportion of radioactivity in plasma representing authentic ligand cannot be determined.

### Normalisation of Data to the Caudate Nucleus

As with (R,S)-[$^{125}$I]-QNB raw data (μCi per g brain) for regional (R,R)-[$^{125}$I]-QNB activity in rat brain were expressed as a ratio of percent of the injected dose relative the level in the caudate nucleus to reduce the impact of interanimal variability on the data. Complete regional tables of non-normalised time-activity data for (R,R)-[$^{125}$I]-QNB are displayed in Appendix A.

## Table 6

## (R,R)-[$^{125}$I]-QNB in the Brain of Conscious Rat

| Region | TIME FOLLOWING ADMINISTRATION OF TRACER 0.5 Hours | 1 Hours | 2 Hours | 6 Hours |
|---|---|---|---|---|
| ***Cerebellum*** | | | | |
| Cerebellar Cortex | 0.388 ± 0.056 | 0.288 ± 0.012 | 0.102 ± 0.029 | 0.160 ± 0.047 |
| ***Medulla/Pons*** | | | | |
| Pontine Grey | 1.097 ± 0.053 | 0.936 ± 0.060 | 0.534 ± 0.097 | 0.487 ± 0.130 |
| Nucleus of the Lateral Lemniscus | 0.732 ± 0.096 | 0.541 ± 0.046 | 0.457 ± 0.095 | 0.363 ± 0.101 |
| Lateral Dorsal Tegmental nucleus | 0.818 ± 0.061 | 0.564 ± 0.048 | 0.328 ± 0.081 | 0.329 ± 0.099 |
| ***Mesencephalon*** | | | | |
| Inferior Colliculus | 0.744 ± 0.036 | 0.593 ± 0.034 | 0.346 ± 0.098 | 0.239 ± 0.067 |
| Superior Colliculus | 0.780 ± 0.044 | 0.650 ± 0.056 | 0.334 ± 0.096 | 0.286 ± 0.107 |
| Substantia Nigra (pars compacta) | 0.622 ± 0.035 | 0.533 ± 0.032 | 0.368 ± 0.091 | 0.305 ± 0.094 |
| Substantia Nigra (pars reticulata) | 0.525 ± 0.039 | 0.485 ± 0.029 | 0.309 ± 0.074 | 0.247 ± 0.079 |
| ***Diencepahlon*** | | | | |
| Hippocampus CA1 | 0.664 ± 0.015 | 0.817 ± 0.090 | 0.902 ± 0.067 | 1.276 ± 0.135 |
| Hippocampus CA2 | 0.896 ± 0.059 | 0.902 ± 0.044 | 0.804 ± 0.190 | 0.954 ± 0.096 |
| Hippocampus CA3 | 0.816 ± 0.016 | 0.854 ± 0.019 | 0.898 ± 0.067 | 1.131 ± 0.110 |
| Medial Geniculate Body | 0.862 ± 0.032 | 0.823 ± 0.019 | 0.549 ± 0.130 | 0.379 ± 0.080 |
| Sub Thalamic Nucleus | 0.795 ± 0.064 | 0.632 ± 0.077 | 0.428 ± 0.057 | 0.365 ± 0.067 |
| Lateral Geniculate Nucleus | 0.858 ± 0.062 | 0.752 ± 0.026 | 0.512 ± 0.052 | 0.257 ± 0.083 |
| Hypothalamus | 0.639 ± 0.030 | 0.518 ± 0.033 | 0.370 ± 0.056 | 0.189 ± 0.058 |
| Mediodorsal Thalamic Nucleus | 0.846 ± 0.079 | 0.751 ± 0.034 | 0.544 ± 0.050 | 0.254 ± 0.760 |
| Ventrolateral Thalamic Nucleus | 0.617 ± 0.026 | 0.480 ± 0.035 | 0.343 ± 0.053 | 0.175 ± 0.059 |
| ***Telencephalon*** | | | | |
| Visual Cortex (layer IV) | 1.133 ± 0.011 | 0.944 ± 0.095 | 1.052 ± 0.078 | 1.164 ± 0.280 |
| Dentate Gyrus | 0.949 ± 0.051 | 0.924 ± 0.055 | 0.969 ± 0.087 | 1.028 ± 0.227 |
| Auditory Cortex (layer IV) | 1.460 ± 0.900 | 1.341 ± 0.074 | 1.400 ± 0.094 | 1.350 ± 0.258 |
| Hippocampus Molecular Layer | 0.949 ± 0.046 | 1.004 ± 0.044 | 0.911 ± 0.097 | 1.070 ± 0.232 |
| Amygdala | 0.732 ± 0.059 | 0.721 ± 0.021 | 0.644 ± 0.064 | 0.624 ± 0.034 |
| Globus Pallidus | 0.513 ± 0.047 | 0.398 ± 0.036 | 0.394 ± 0.059 | 0.267 ± 0.052 |
| Caudate Nucleus | 1.000 ± 0.000 | 1.000 ± 0.000 | 1.000 ± 0.000 | 1.000 ± 0.000 |
| Septal Nuclei | 0.667 ± 0.047 | 0.743 ± 0.032 | 0.630 ± 0.017 | 0.461 ± 0.037 |
| Nucleus Basalis Magnocellularis | 0.551 ± 0.037 | 0.497 ± 0.029 | 0.471 ± 0.028 | 0.331 ± 0.052 |
| Nucleus Accumbens | 1.086 ± 0.012 | 1.102 ± 0.052 | 1.074 ± 0.078 | 1.189 ± 0.105 |
| Sensory Motor Cortex (layer IV) | 1.272 ± 0.064 | 1.203 ± 0.022 | 1.272 ± 0.060 | 1.106 ± 0.090 |
| Anterior Cingulate Cortex | 1.173 ± 0.079 | 1.163 ± 0.006 | 1.176 ± 0.054 | 1.219 ± 0.072 |
| Frontal Cortex | 1.144 ± 0.036 | 1.176 ± 0.027 | 1.192 ± 0.070 | 1.134 ± 0.078 |
| Parietal Cortex | 1.141 ± 0.047 | 1.100 ± 0.034 | 1.108 ± 0.066 | 1.061 ± 0.099 |
| ***Myelinated Fibre Tracts*** | | | | |
| Internal Capsule | 0.252 ± 0.039 | 0.366 ± 0.020 | 0.196 ± 0.056 | 0.069 ± 0.041 |
| Genu | 0.270 ± 0.060 | 0.324 ± 0.025 | 0.210 ± 0.053 | 0.223 ± 0.063 |

Table shows (R,R)-[$^{125}$I]-QNB in discrete brain regions of the conscious rat 0.5, 1, 2 and 6 hours following iv administration of 200μCi of tracer. Data are expressed as mean ± S.E.M % dose per g brain normalised to the caudate nucleus, n= 5 animals for each time point.

## (R,R)-[$^{125}$I]-QNB In Brain Of Conscious Rat

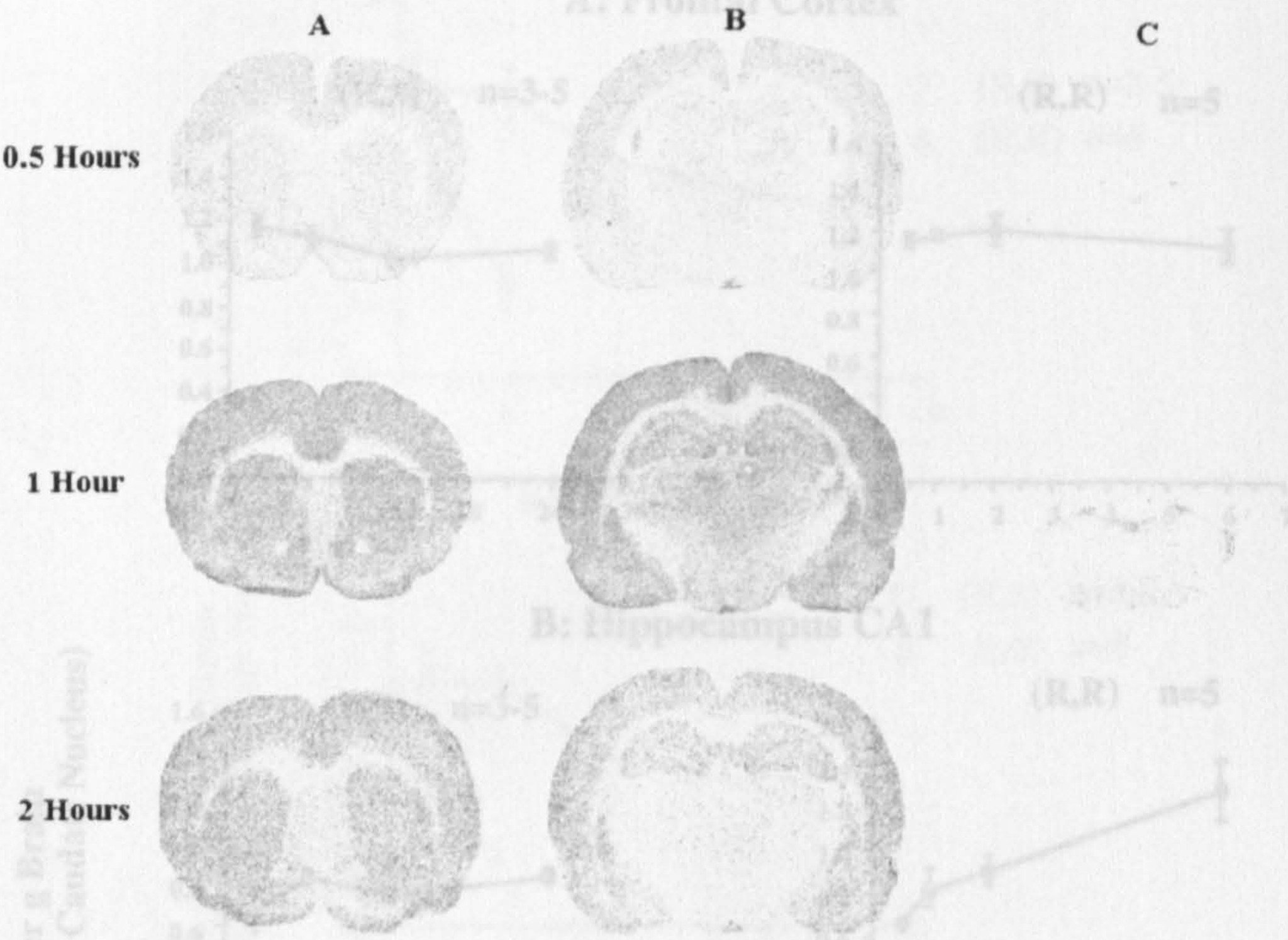


**Fig 15:** (R,R)-[$^{125}$I]-QNB in the brain of conscious rat at 30 mins, 1,2 and 6 hours. Illustrative autoradiograms show tracer uptake at the level of the caudate nucleus (A), dorsolateral hippocampus (B) and cerebellum (C) of rat brain. Tracer uptake shows a heterogeneous distribution within the brain corresponding to regional mAChR density. High levels of activity are observed in the caudate and cortex, intermediate levels in the thalamus and low levels in the cerebellum. Washout of tracer from thalamus and cerebellum is considerably faster than in the caudate and cortex, with negligible amounts of activity observed in the cerebellum by 6 hours.

## (R,S)- and (R,R)-[$^{125}$I]-QNB In the Brain of Conscious Rat

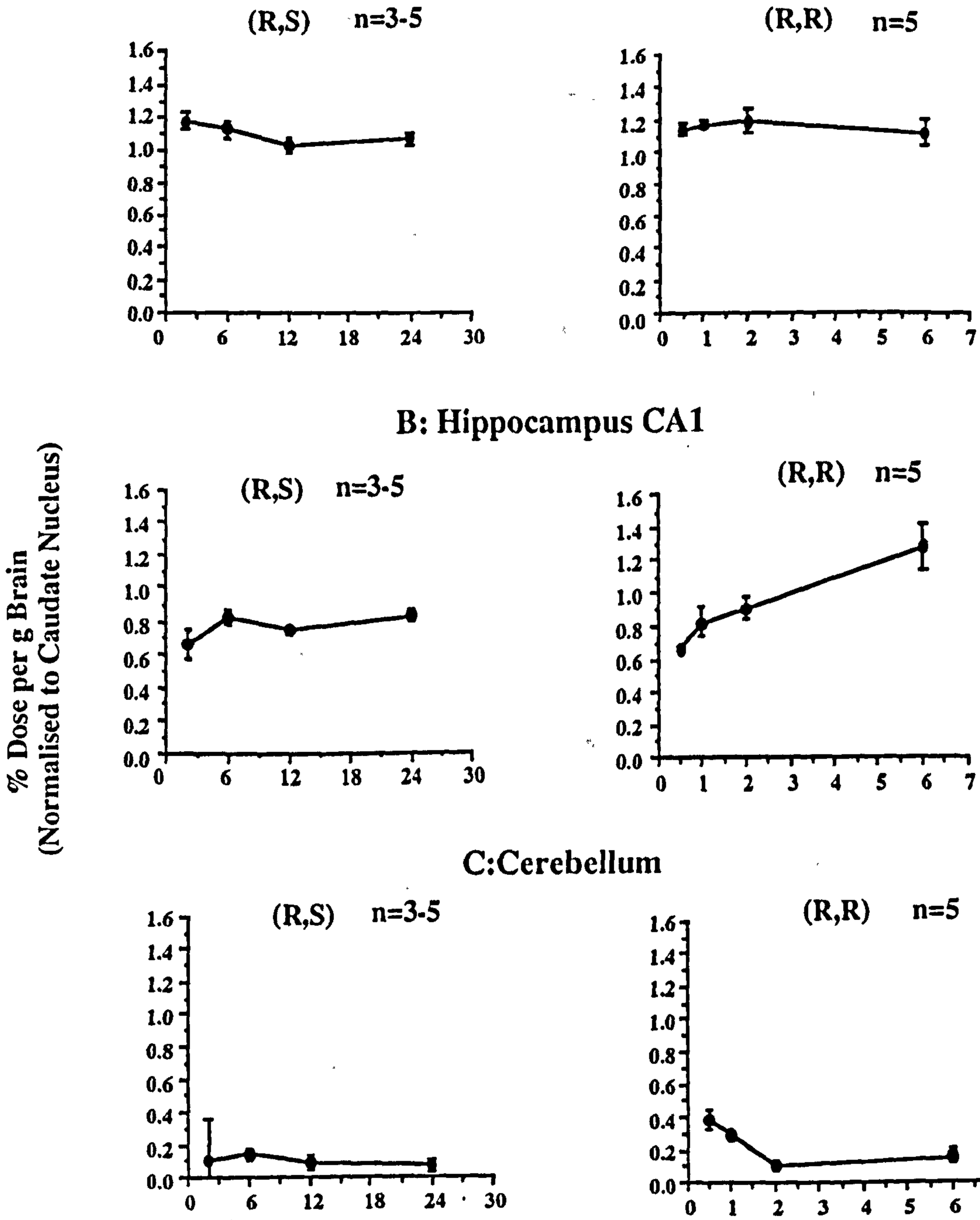


**Fig 16:** Time activity profiles of (R,S)- and (R,R)-[$^{125}$I]-QNB uptake and retention in the brain of conscious rat at the level of the frontal cortex (A), CA1 of the hippocampus (B) and cerebellum (C). Regional levels of (R,R)-[$^{125}$I]-QNB activity over 6 hours are comparable to those of (R,S)-[$^{125}$I]-QNB over 24 hours. Different time-activity profiles for (R,S)- and (R,R)-[$^{125}$I]-QNB should be noted. Data are expressed as mean ± S.E.M. % dose per g brain normalised to caudate nucleus. n= number of animals in each group.

## Uptake and Retention of (R,S)- and (R,R)-[$^{125}$I]-QNB in Thalamic Regions

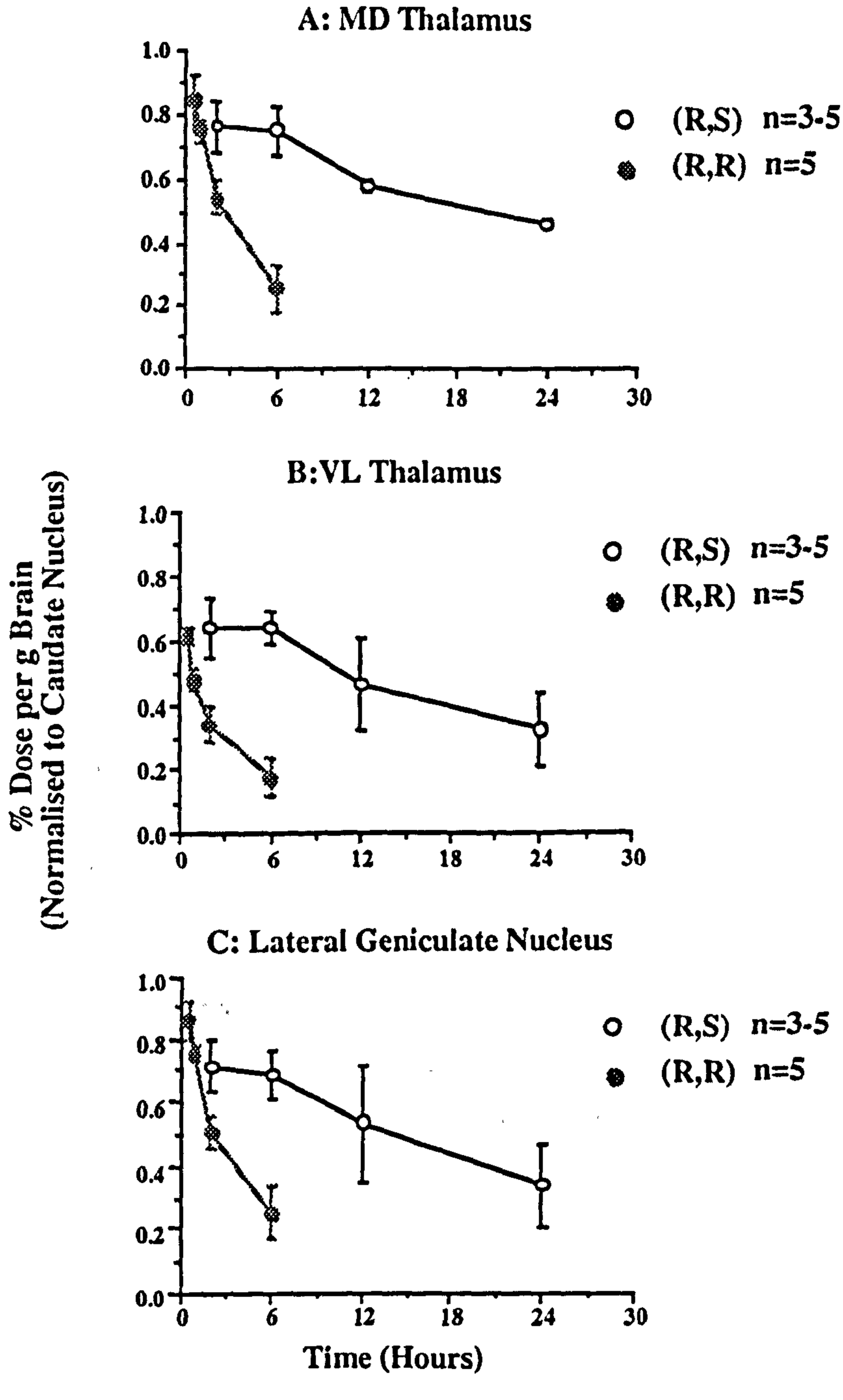


**Fig 17:** Time activity profiles of (R,S)- and (R,R)-[$^{125}$I]-QNB in rat brain at the level of the mediodorsal thalamus (A), ventrolateral thalamus (B) and the lateral geniculate nucleus (C) between 30 mins and 24 hours after tracer administration. Each region shows loss of (R,S)- and (R,R)-[$^{125}$I]-QNB activity over time. Regional loss of (R,R)-[$^{125}$I]-QNB is greater than that of (R,S)-[$^{125}$I]-QNB and occurs on a shorter timescale. Data are expressed as mean ± S.E.M. % dose per g brain normalised to the caudate nucleus. n= number of animals in each group.

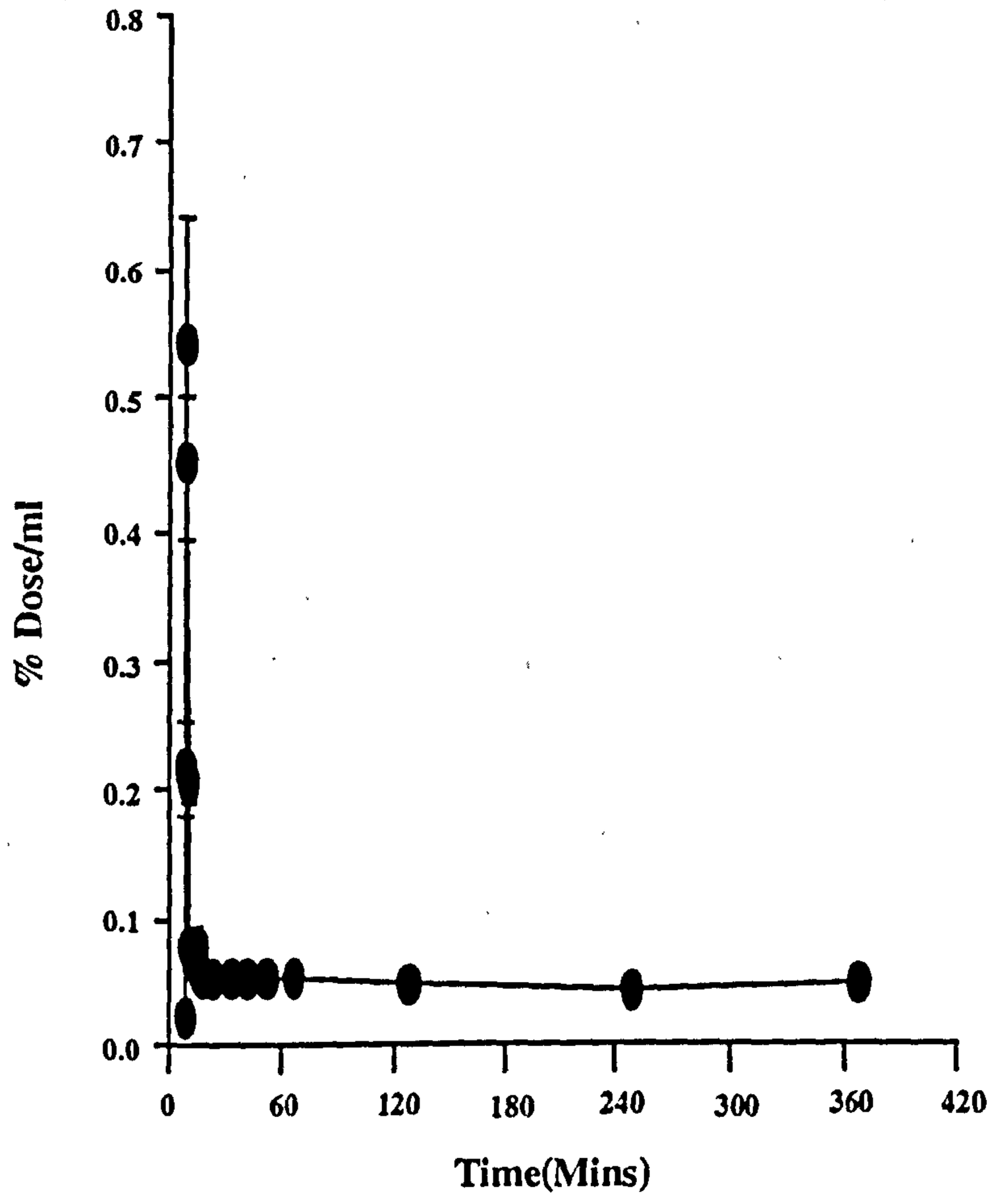


**Fig 18:** Timecourse of radioactivity in plasma up to 6 hours following intravenous administration of 200μCi (R,R)-[$^{125}$I]-QNB. Data is uncorrected for metabolites and therefore the proportion of radioactivity representing authentic tracer cannot be determined. Data is expressed as mean ± S.E.M % dose per ml plasma of 5-20 samples.

### 3.1.3 Metabolic Fate of (R,S)- and (R,R)-[$^{125}$I]-QNB in the Conscious Rat

Plasma and brain homogenate samples were taken from rats injected with (R,S)- and (R,R)-[$^{125}$I]-QNB and analysed by high performance liquid chromatography (HPLC) for the presence of authentic ligand and radioactive metabolites.

**Stability Of (R,S)- and (R,R)-[$^{125}$I]-QNB Upon Reconstitution**

Before *in vivo* investigation of the metabolism of (R,S)- and (R,R)-[$^{125}$I]-QNB samples of both ligands reconstituted in 0.9 % saline representing injectate were analysed by HPLC for authentic ligand and metabolite content.

For both (R,S)- and (R,R)-[$^{125}$I]-QNB samples of injectate were found to consist almost entirely of authentic ligand. Fig 19 shows illustrative HPLC traces from analysis of injectate samples of (R,S)- and (R,R)-[$^{125}$I]-QNB. The major peaks visible on both traces eluted with retention times of 6.6 and 8.2 mins, represent authentic (R,S)- and (R,R)-[$^{125}$I]-QNB respectively. Both traces show a minor species eluted at approximately 3 mins which represents the presence of free iodide in the sample. The HPLC trace for (R,S)-[$^{125}$I]-QNB also shows two other minor peaks at 7.7 and 12.0 mins. These peaks represent unidentified radioactive species that may be breakdown products of the parent compound that have evolved upon reconstitution.

**Metabolism of (R,S)- and (R,R)-[$^{125}$I]-QNB in the Conscious Rat**

The fraction of radioactivity representing parent (R,S)- and (R,R)-[$^{125}$I]-QNB in brain tissue and plasma at various time intervals after intravenous injection of each ligand was determined by radio-HPLC analysis. The HPLC column performs reverse phase chromatography, separating radioactive species by polarity, with the most highly charged species eluted first.

**(R,S) -[$^{125}$I]-QNB-Plasma Analysis**

Plasma samples were analysed for the presence of parent (R,S)-[$^{125}$I]-QNB and metabolites at time intervals from 1 min to 12 hours after ligand administration.

Fig 20 shows illustrative HPLC traces from plasma samples taken at 1, 5, 15, and 45 mins and 1 and 12 hours following intravenous administration of (R,S) [$^{125}$I]-QNB.

From HPLC analysis of plasma samples authentic (R,S)-[$^{125}$I]-QNB is observed to be present in plasma up to 12 hours following intravenous administration. The plasma content of ligand decreases slowly with time as free iodide concentration increases. Two unidentified metabolite species are also observable in plasma.

One minute following tracer administration a significant degree of tracer metabolism has already occurred (Fig 20:A). Parent compound remains present as a major component in

plasma represented by the peak eluted at 8.7 mins. Two major radioactive species constituting unidentified metabolites of (R,S) [$^{125}$I]-QNB are present in the sample represented by the peaks observed at 12.9 and 15.5 mins. A significant amount of free iodide is also present and is represented by the large peak observed at 3.0 mins.
By 15 mins the slower eluting metabolite with a retention time of 15.5 mins has been cleared from plasma. Authentic ligand remains present along with free iodide and a remaining metabolite species (Fig20:C). At 12 hours following administration authentic (R,S)-[$^{125}$I]-QNB remains detectable in plasma (Fig 20:F). Whether any radioactive metabolites are present in plasma at this time cannot be determined, although it is possible that peaks representative of such species are hidden by the background noise apparent on this trace. The small volume of plasma collected combined with the low level of radioactivity contained within the samples is responsible for the high level of noise observable on later traces. Under these conditions subtraction of the background noise from each trace is usually carried out to highlight the signal. This however was not possible for all samples, as the signal to noise ratio on some traces was extremely low and would result in the loss of the desired signal. This results in poor resolution of the traces and accounts for the high degree of "noise" observed.

### (R,S)-[$^{125}$I]-QNB-Brain Homogenate Analysis

HPLC analysis indicates that authentic tracer constitutes the only major radioactive species present in rat brain up to 24 hours following intravenous administration of (R,S)-[$^{125}$I]-QNB. Fig 21 shows illustrative HPLC traces from brain homogenate samples taken at 2, 6, 12 and 24 hours after (R,S)-[$^{125}$I]-QNB administration.
A single large peak representing parent ligand was observed at approximately 7.0 mins on HPLC traces from brain homogenate samples at all time points . The smaller peaks observed at approximately 8.0 and 12.0 mins on some traces represent unidentified radioactive species that may be metabolites of the parent compound. Corresponding peaks are observed at similar times on traces of injectate analysed (Fig19) and in this case may represent metabolites generated upon reconstitution of the tracer. It should be noted that these peaks are not present on traces from quality control samples of radiotracer analysed following completion of synthesis (not shown). The small single peak observed at approximately 3.0 mins on injectate and on some brain homogenate traces constitutes a highly polar compound eluted with the void volume of the column. It is highly likely that this first metabolite represents free iodide species produced by de-iodination of the tracer. The presence of these small amounts of metabolites in some brain homogenate samples may be the result of plasma metabolite contamination of brain tissue samples due to incomplete removal of blood from the brain before analysis.

## (R,R)-[$^{125}$I]-QNB-Plasma Analysis

Plasma samples were analysed for the presence of parent (R,R)-[$^{125}$I]-QNB and metabolites at time intervals from 1 min to 6 hours after ligand administration.

Fig 22A-E show illustrative HPLC traces from plasma samples taken at 1, 5, 15, and 30 mins and 1, and 6 hours following intravenous administration of (R,R)-[$^{125}$I]-QNB. From HPLC analysis of plasma samples authentic (R,R)-[$^{125}$I]-QNB is observed to be present in plasma up to 6 hours following intravenous administration. The plasma content of ligand decreases slowly with time as free iodide concentration increases. No major radioactive metabolite species are observable in plasma at any of the time points analysed.

In all samples analysed the peak observed at approximately 3.0 mins is very likely to represent a free iodide species . This indicates that the de-iodination of the tracer occurs as the major step in the metabolism of this tracer. However, a broad low level peak is observed at approximately 13.0 mins on all plasma traces from 5 mins onwards (Fig 22B). This is possibly due to the presence of one or more radioactive metabolites in plasma which are present at a very low level. It is possible that they are formed and cleared rapidly with no accumulation in the plasma. Fig 23 represents a plot of the "Free Pool" of authentic (R,R)-[$^{125}$I]-QNB (i.e. tracer available for uptake from plasma into the brain) in plasma following intravenous injection. This indicates that authentic tracer is available for uptake into the brain, albeit at a low level, up to 6 hours following administration.

## (R,R)-[$^{125}$I]-QNB-Brain Homogenate Analysis

HPLC analysis indicates that authentic tracer constitutes the only major radioactive species present in rat brain up to 6 hours following intravenous administration of (R,R)-[$^{125}$I]-QNB. Fig 24 shows illustrative HPLC traces from brain homogenate samples taken at 30 min, 1, 2, and 6 hours after (R,R)-[$^{125}$I]-QNB administration.

A single large peak representing parent ligand is observed at approximately 8.0 mins on HPLC traces from brain homogenate samples at all time points . A corresponding peak is observed at a similar time on traces of injectate analysed (Fig19) indicating that this represents authentic tracer.

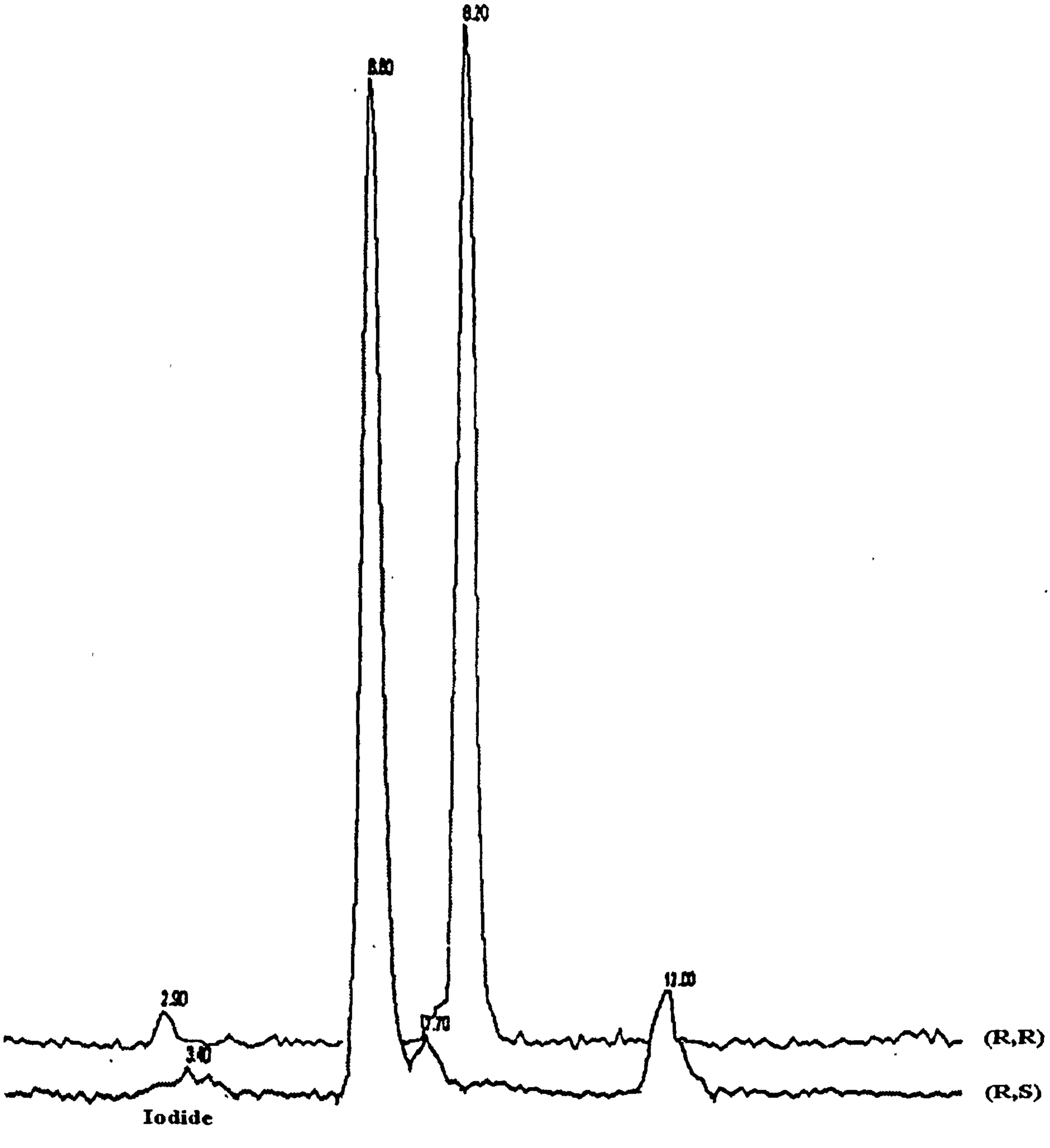


**Fig 19:** Stability of reconstituted (R,S)- and (R,R)-[$^{125}$I]-QNB.
Figure shows representative HPLC traces for injectate samples of (R,S)- and (R,R)-[$^{125}$I]-QNB reconstituted in 0.9% saline. Authentic ligand represented by the peaks at 6.6 and 8.0 mins respectively for (R,S)- and (R,R)-[$^{125}$I]-QNB constitutes the major species present in injectate. A free iodide species identified by the peak at approximately 3.0 mins is present on both traces. Two unidentified species likely to be breakdown products are present at 7.7 and 12.0 mins on the trace for (R,S)-[$^{125}$I]-QNB.

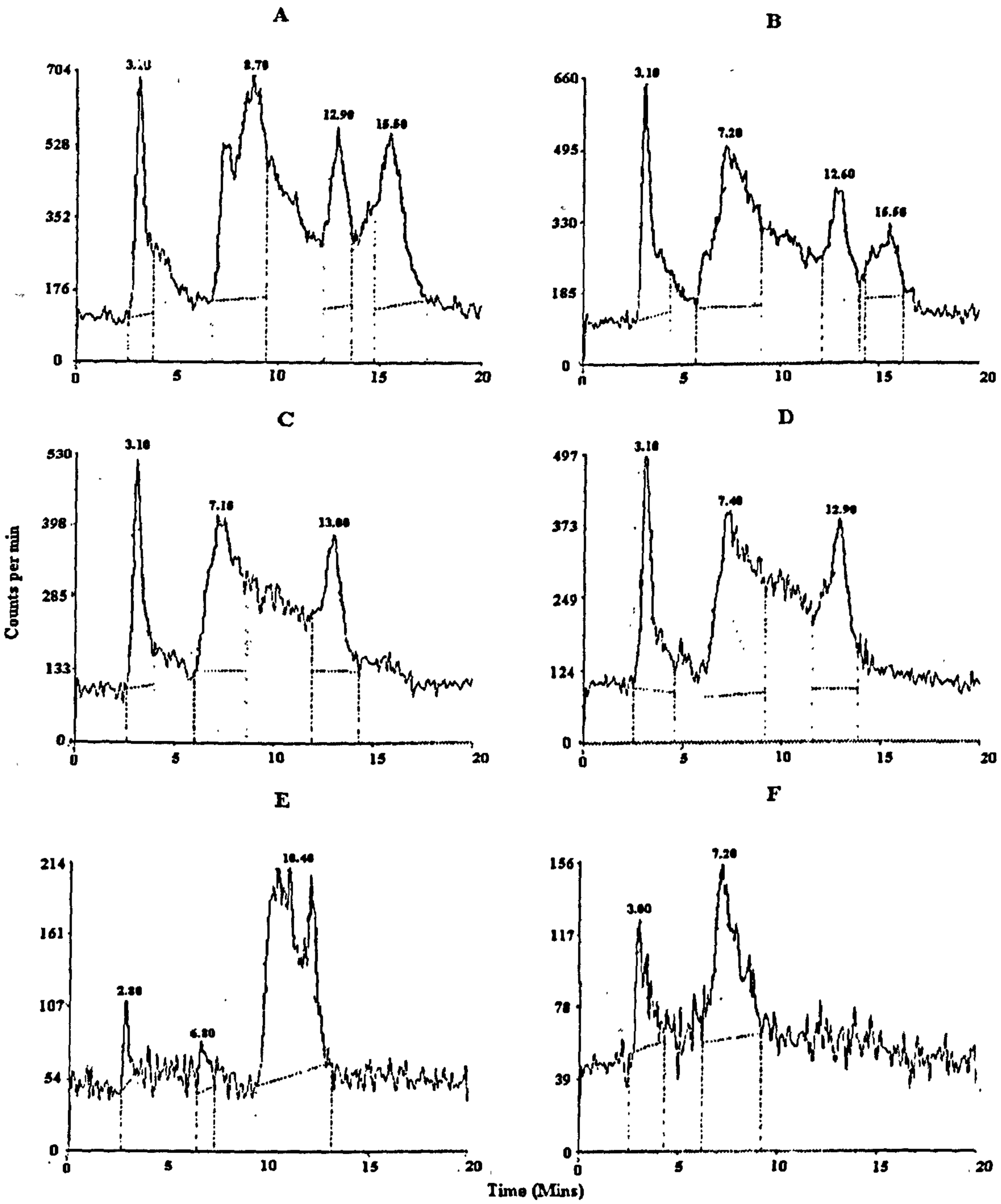


**Fig 20:** Metabolism of (R,S)-[$^{125}$I]-QNB in the rat:Plasma
Representative HPLC traces from plasma samples taken at 1, 5, 15, and 45 mins and 1 and 12 hours (traces A-F respectively) after administration of tracer. Authentic (R,S)-[$^{125}$I]-QNB (represented by peak at approximately 8.0 mins on each trace) is present in the plasma up to 12 hours. A free iodide species (earliest eluted peak) and two unidentified radioactive metabolites less polar than (R,S)-[$^{125}$I]-QNB (peaks appearing at approximately 13.0 and 15.0 mins) are also present in plasma.

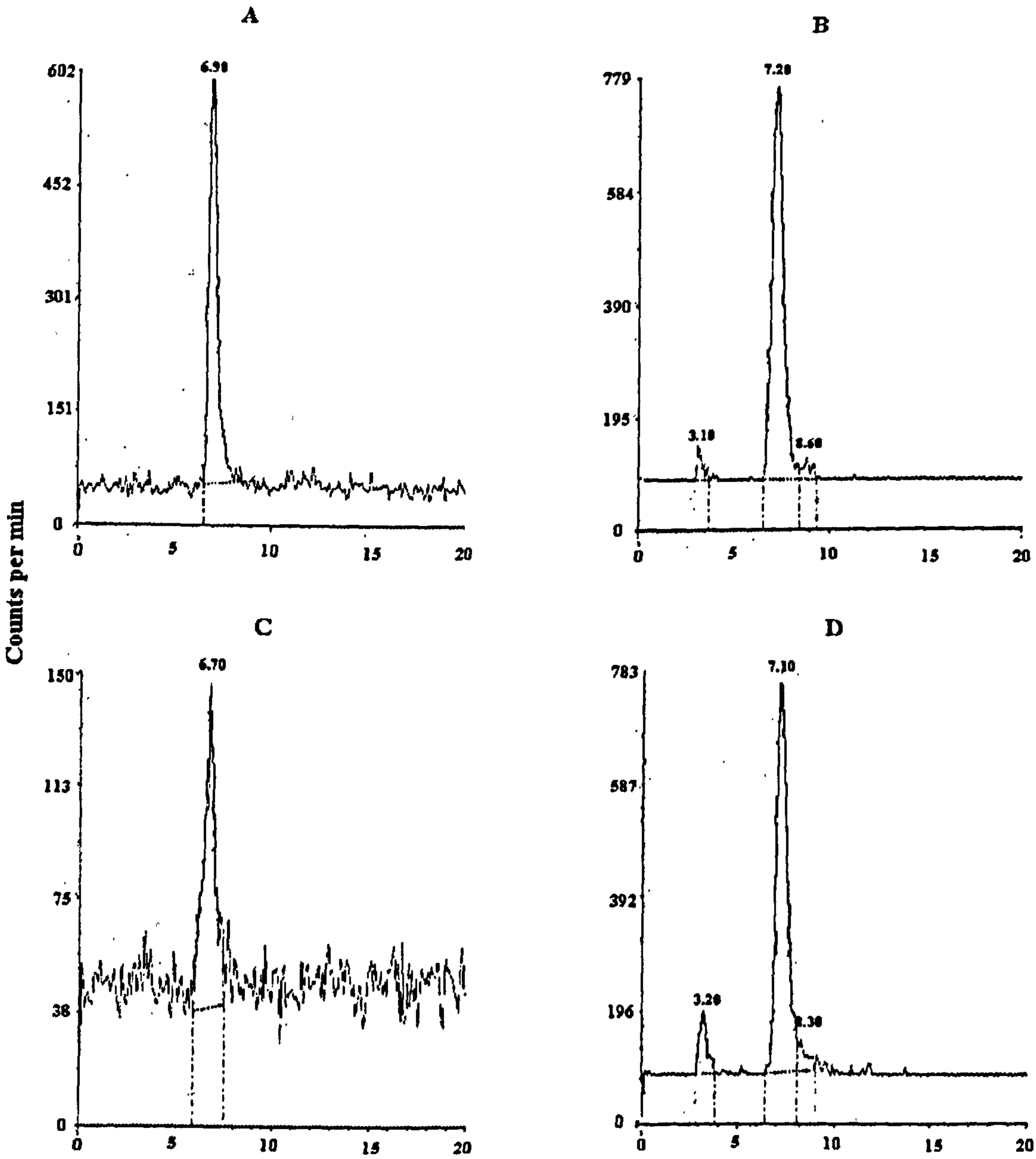


**Fig 21:** Metabolism of (R,S)-[$^{125}$I]-QNB in the rat: Brain
Representative HPLC traces of brain homogenate samples from animals sacrificed at 2, 6, 12 and 24 hours (traces A-D respectively)after administration of tracer. Authentic (R,S)-[$^{125}$I]-QNB represents the only major radioactive species present in brain. Two additional peaks present on traces for 6 and 24 hours are likely to represent contamination from blood present in the sample and do not represent a major component of brain activity.

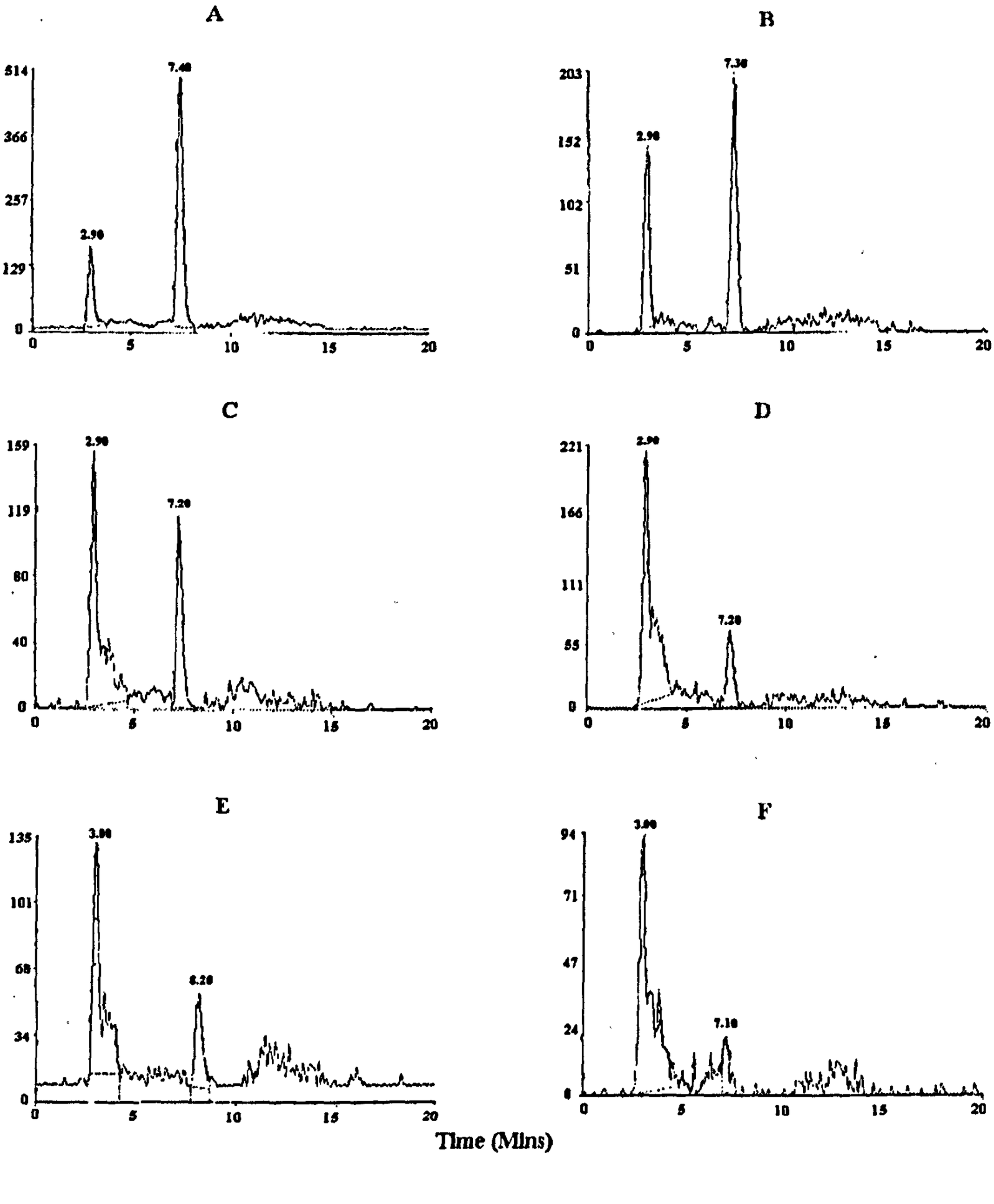


**Fig 22:** Metabolism of (R,R)-[$^{125}$I]-QNB in rat:Plasma
Representative HPLC traces from plasma samples taken at 1, 5, 15 and 45 mins and 1 and 6 hours (traces A-F respectively) after administration. Authentic (R,R)-[$^{125}$I]-QNB (represented by peak at approximately 7.0 mins on each trace) is present in the plasma up to 6 hours. In all plasma samples a free iodide species (peak at approximately 3.0 mins) represents the only metabolite detected.

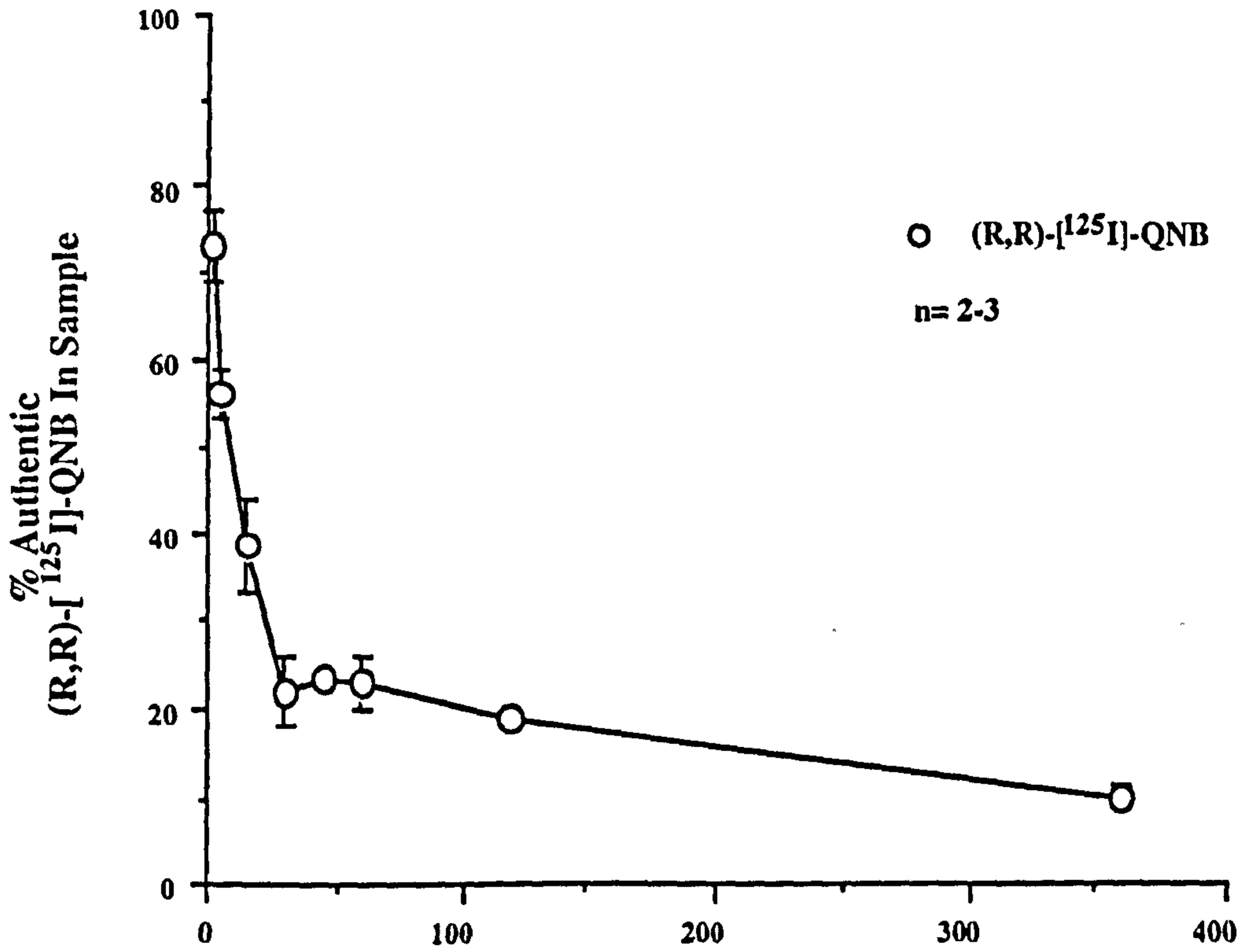


**Fig 23:** Timecourse of free (R,R)-[$^{125}$I]-QNB in plasma following intravenous injection in rat. Data points represent levels of authentic non-plasma protein bound ligand available for uptake into brain in plasma of conscious rat between 1 min and 6 hours after administration. Note that significant levels of authentic ligand are still present in plasma at 6 hours. Data are expressed as mean ± S.E.M % of injected dose (n= 2-3).

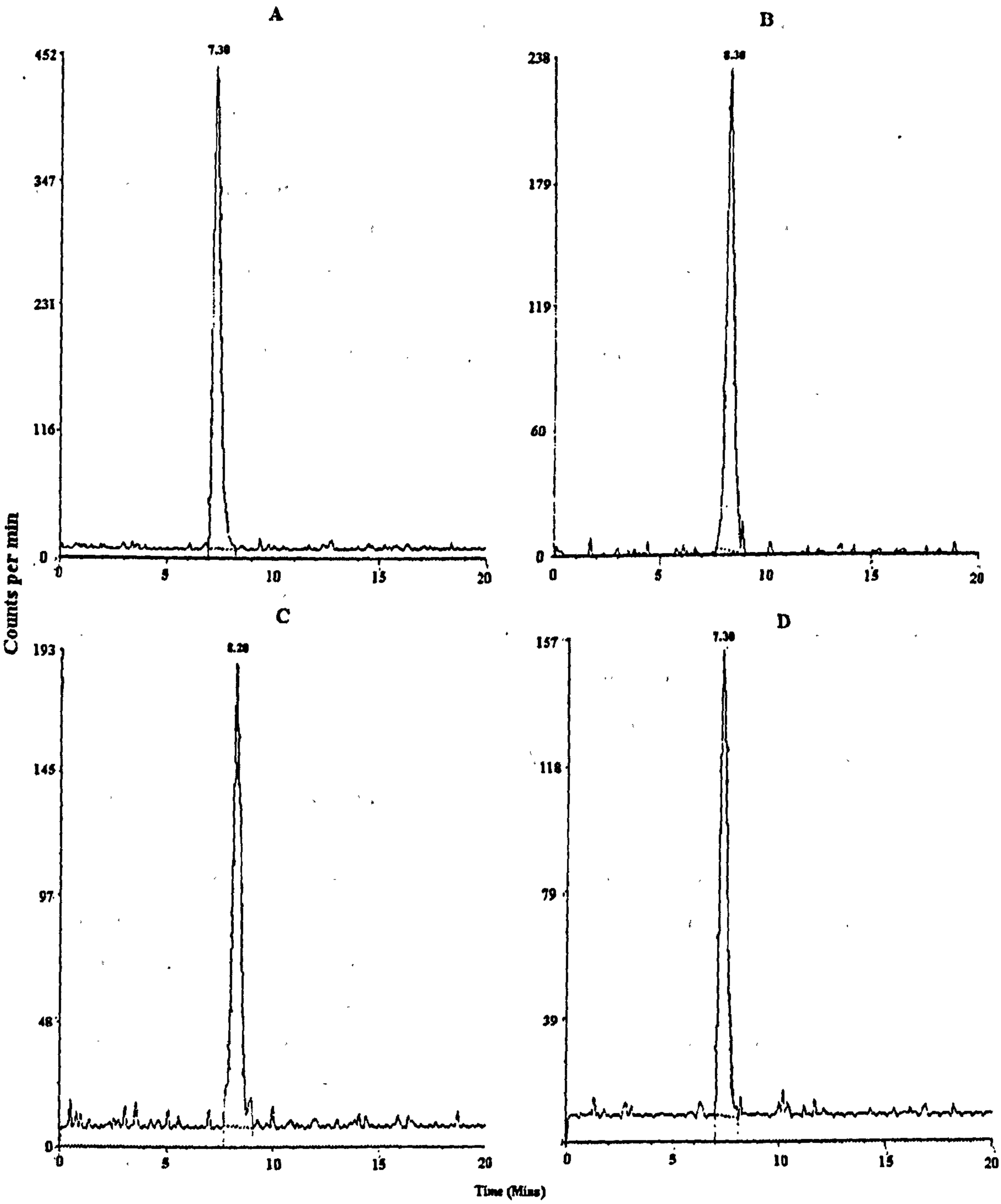


**Fig 24:** Metabolism of (R,R)-[$^{125}$I]-QNB in rat: Brain
Representative HPLC traces of brain homogenate samples from animals sacrificed at 0.5, 1, 2 and 6 hours (traces A-D respectively)after administration of tracer. Authentic (R,R)-[$^{125}$I]-QNB represents the only radioactive species present in brain.

### 3.1.4 Effect of Heptylphysostigmine on (R,S)- and (R,R)-[$^{125}$I]-QNB Levels in the Brain of Conscious Rat

Levels of (R,S)- and (R,R)-[$^{125}$I]-QNB in rat brain over 24 hours and 6 hours respectively was determined by *in vivo* autoradiography following intravenous administration of heptylphysostigmine (2mg/kg).

**General Observations**

Administration of heptylphysostigmine produced a number of overt behavioural changes in rats symptomatic of acute cholinergic toxicity which were not observed in vehicle (saline) treated animals.

Symptoms included salivation, urination, muscle tremor and fasciculation, hind limb splay and an increased sensitivity to noise. In addition, animals exhibited reduced locomotor activity and absence of the normal grooming and exploratory behaviour associated with rats. There was however no sedative effect and all animals remained conscious throughout.

These symptoms were observed in all animals receiving heptylphysostigmine, with mild effects first appearing approximately 10 mins after initiation of drug infusion. The symptoms gradually increased in severity peaking approximately 1 hour after cessation of the drug infusion. Thereafter symptoms subsided over the next few hours, with no signs of toxicity observable by 4 hours. In animals receiving a second drug infusion similar symptomology was observed. Drug effects peaked approximately 1 hour after end of infusion, with no symptoms observable 4 hours later.

Physiologic variables were measured prior to and 30 mins after heptylphysostigmine administration. Thereafter physiologic variables were measured prior to and at various time points after administration of (R,S)- or (R,R)-[$^{125}$I]-QNB. Tables of physiologic variables are presented in Appendix B.

Heptylphysostigmine administration generally had a minor effect on physiologic variables. Elevations in mean arterial blood pressure and in plasma glucose levels were measured in some experimental groups, however no consistent pattern of changes was observable (see Appendix B)

**Effect of Heptylphysostigmine on Uptake and Retention of (R,S)-[$^{125}$I]-QNB**

Quantitative densitometric analysis of autoradiograms was performed to determine (R,S)-[$^{125}$I]-QNB levels in 33 anatomically distinct brain regions at 2 and 24 hours following tracer administration in heptylphysostigmine (2mg/kg) and vehicle (0.9% saline) treated animals. Tracer level in each region was expressed as a ratio relative to uptake in the caudate nucleus (Tables 7 and 8).

## Table 7

## Effect of Heptylphysostigmine on (R,S)-[$^{125}$I]-QNB in Brain of Conscious Rat at 2 Hours

| Region | Vehicle | Heptylphysostigmine | t |
|---|---|---|---|
| ***Cerebellum*** | | | |
| Cerebellar Cortex | 0.155 ± 0.020 | 0.186 ± 0.029 | 0.894 |
| ***Medulla/ Pons*** | | | |
| Nucleus of the Lateral Lemniscus | 0.465 ± 0.014 | 0.504 ± 0.095 | 0.411 |
| Lateral Dorsal Tegmental Nucleus | 0.493 ± 0.132 | 0.691 ± 0.121 | 0.451 |
| Pontine grey matter | 1.127 ± 0.069 | 1.221 ± 0.175 | 0.503 |
| ***Mesencepahlon*** | | | |
| Inferior Colliculus | 0.738 ± 0.055 | 0.770 ± 0.128 | 0.23 |
| Superior Colliculus | 0.689 ± 0.039 | 0.943 ± 0.065* | 3.32 |
| Substantia Nigra (pars compacta) | 0.560 ± 0.029 | 0.620 ± 0.020 | 1.69 |
| Substantia Nigra (pars reticulata) | 0.512 ± 0.028 | 0.547 ± 0.026 | 0.92 |
| ***Diencephalon*** | | | |
| Medial Geniculate Body | 0.881 ± 0.057 | 1.037 ± 0.052 | 2.02 |
| Subthalamic nucleus | 0.708 ± 0.029 | 0.837 ± 0.050 | 2.21 |
| Lateral Geniculate Nucleus | 0.783 ± 0.076 | 0.888 ± 0.042 | 1.21 |
| Hippocampus CA1 | 0.768 ± 0.025 | 0.801 ± 0.012 | 0.13 |
| Hippocampus CA2 | 1.007 ± 0.024 | 1.066 ± 0.033 | 1.42 |
| Hippocampus CA3 | 0.822 ± 0.018 | 0.917 ± 0.029* | 2.77 |
| Hypothalamus | 0.637 ± 0.068 | 0.616 ± 0.025 | 0.28 |
| Mediodorsal Thalamic Nucleus | 0.860 ± 0.050 | 0.920 ± 0.032 | 1.01 |
| Ventrolateral ThalamicNucleus | 0.670 ± 0.042 | 0.705 ± 0.036 | 0.64 |
| ***Telencephalon*** | | | |
| Visual Cortex (layer IV) | 1.113 ± 0.041 | 1.104 ± 0.118 | 0.07 |
| Hippocampus (Molecular Layer) | 0.968 ± 0.051 | 1.033 ± 0.010 | 1.26 |
| Dentate gyrus | 0.948 ± 0.040 | 1.042 ± 0.032 | 1.85 |
| Auditory Cortex (Layer IV) | 1.401 ± 0.072 | 2.314 ± 0.201** | 4.47 |
| Amygdala | 0.637 ± 0.069 | 0.735 ± 0.027 | 1.32 |
| Septal nuclei | 0.746 ± 0.035 | 0.751 ± 0.035 | 0.09 |
| Nucleus Basalis Magnocellularis | 0.527 ± 0.018 | 0.565 ± 0.018 | 1.47 |
| Globus pallidus | 0.443 ± 0.022 | 0.473 ± 0.026 | 0.90 |
| Caudate Nucleus | 1.000 ± 0.000 | 1.000 ± 0.000 | |
| Sensory Motor Cortex (Layer IV) | 1.200 ± 0.072 | 1.505 ± 0.061* | 3.23 |
| Nucleus Accumbens | 1.127 ± 0.019 | 1.220 ± 0.043 | 1.97 |
| Anterior Cingulate Cortex | 1.221 ± 0.029 | 1.237 ± 0.025 | 0.42 |
| Frontal Cortex | 1.140 ± 0.089 | 1.463 ± 0.056* | 3.07 |
| Parietal Cortex | 1.150 ± 0.036 | 1.423 ± 0.101* | 2.54 |
| ***Myelinated Fibre Tracts*** | | | |
| Internal Capsule | 0.256 ± 0.017 | 0.277 ± 0.024 | 0.71 |
| Genu | 0.269 ± 0.019 | 0.316 ± 0.029 | 1.36 |

Table shows effect of heptylphysosigmine( 2mg /kg) on (R,S)-[$^{125}$I]-QNB in brain of conscious rat at 2 hours.*P <0.05 and **P <0.01 for the comparison between vehicle and heptylphysostigmine unpaired Student's t-test; critical value t= 2.306 (8 df) for P < 0.05. Data are expressed as mean ± S.E.M % dose per g brain normalised to caudate nucleus.

## Table 8

## Effect of Heptylphysostigmine on (R,S)-[$^{125}$I]-QNB in Brain of Conscious Rat at 24 Hours

| Region | Vehicle | Heptylphysostigmine | t |
|---|---|---|---|
| ***Cerebellum*** | | | |
| Cerebellar Cortex | 0.025 ± 0.013 | 0.018 ± 0.014 | 0.38 |
| ***Medulla/ Pons*** | | | |
| Nucleus of the Lateral Lemniscus | 0.068 ± 0.026 | 0.055 ± 0.019 | 0.42 |
| Lateral Dorsal Tegmental Nucleus | 0.097 ± 0.042 | 0.080 ± 0.040 | 0.28 |
| Pontine grey matter | 0.257 ± 0.030 | 0.143 ± 0.050 | 1.97 |
| ***Mesencepahlon*** | | | |
| Inferior Colliculus | 0.128 ± 0.029 | 0.111 ± 0.045 | 0.31 |
| Superior Colliculus | 0.098 ± 0.016 | 0.114 ± 0.020 | 0.65 |
| Substantia Nigra (pars compacta) | 0.091 ± 0.024 | 0.149 ± 0.013 | 2.08 |
| Substantia Nigra (pars reticulata) | 0.091 ± 0.023 | 0.118 ± 0.015 | 0.97 |
| ***Diencephalon*** | | | |
| Medial Geniculate Body | 0.444 ± 0.048 | 1.74 ± 1.313 | 0.98 |
| Subthalamic nucleus | 0.135 ± 0.038 | 0.201 ± 0.076 | 0.78 |
| Lateral Geniculate Nucleus | | | |
| Hippocampus CA1 | 0.322 ± 0.028 | 0.343 ± 0.017 | 1.18 |
| Hippocampus CA2 | 0.957 ± 0.035 | 1.004 ± 0.019 | 1.84 |
| Hippocampus CA3 | 0.926 ± 0.028 | 1.013 ± 0.038* | 2.64 |
| Hypothalamus | 0.153 ± 0.047 | 0.149 ± 0.018 | 0.07 |
| Mediodorsal Thalamic Nucleus | 0.361 ± 0.037 | 0.365 ± 0.022 | 0.09 |
| Ventrolateral ThalamicNucleus | 0.193 ± 0.038 | 0.195 ± 0.016 | 0.04 |
| ***Telencephalon*** | | | |
| Visual Cortex (layer IV) | 1.23 ± 0.078 | 0.884 ± 0.30 | 1.12 |
| Hippocampus (Molecular Layer) | 1.07 ± 0.037 | 1.023 ± 0.034 | 1.01 |
| Dentate gyrus | 1.00 ± 0.033 | 1.047 ± 0.056 | 0.75 |
| Auditory Cortex (Layer IV) | 1.44 ± 0.088 | 1.733 ± 0.070* | 2.61 |
| Amygdala | 0.543 ± 0.030 | 0.525 ± 0.017 | 0.05 |
| Septal nuclei | 0.422 ± 0.040 | 0.479 ± 0.028 | 1.16 |
| Nucleus Basalis Magnocellularis | 0.217 ± 0.028 | 0.200 ± 0.012 | 0.55 |
| Globus pallidus | 0.153 ± 0.047 | 0.147 ± 0.012 | 0.11 |
| Caudate Nucleus | 1.000 ± 0.000 | 1.000 ± 0.000 | NA |
| Sensory Motor Cortex (Layer IV) | 1.26 ± 0.058 | 1.261 ± 0.040 | 0.05 |
| Nucleus Accumbens | 1.221 ± 0.034 | 1.227 ± 0.032 | 0.12 |
| Anterior Cingulate Cortex | 1.209 ± 0.020 | 1.271 ± 0.064 | 0.48 |
| Frontal Cortex | 1.225 ± 0.060 | 1.266 ± 0.030 | 0.44 |
| Parietal Cortex | 1.283 ± 0.041 | 1.316 ± 0.053 | 0.50 |
| ***Myelinated Fibre Tracts*** | | | |
| Internal Capsule | 0.073 ± 0.011 | 0.093 ± 0.009 | 1.47 |
| Genu | 0.182 ± 0.130 | 0.139 ± 0.041 | 0.99 |

Table shows effect of heptylphysosigmine (2mg /kg) on (R,S)-[$^{125}$I]-QNB in brain of conscious rat at 24 hours. *P <0.05 for the comparison between vehicle and heptylphysostigmine unpaired Student's t-test; critical value t= 2.306 (8 df) for P < 0.05. Data are expressed as mean ± S.E.M % dose per g brain normalised to caudate nucleus.

Statistically significant increases in (R,S)-[$^{125}$I]-QNB levels were observed in 6 out of 33 regions analysed at 2 hours following heptylphysostigmine administration (Fig 25). Regions showing increased levels of (R,S)-[$^{125}$I]-QNB at 2 hours were frontal cortex (28%), sensory motor cortex (25%), auditory cortex (6%), parietal cortex (24%), superior colliculus (37%) and CA3 region of the hippocampus (24%) .

At 24 hours heptylphysostigmine administration produced significant increase in (R,S)-[$^{125}$I]-QNB levels in the auditory cortex (20%) and in the CA3 region of the hippocampus (9%). Illustrative autoradiograms showing regions of increased activity at 2 and 24 hours are displayed in Fig 26 and 27 respectively.

**Effect of Heptylphysostigmine on Uptake and Retention of (R,R)-[$^{125}$I]-QNB**

Quantitative densitometric analysis of autoradiograms was performed to determine (R,R)-[$^{125}$I]-QNB levels in 33 anatomically distinct brain regions at 05 hours, 1hour, 2 hours and 6 hours following tracer administration in heptylphysostigmine (2m/kg) and vehicle (0.9% saline) treated animals. Tracer level in each region was expressed as a ratio relative to uptake in the caudate nucleus (Tables 9 and 10).

Statistically significant increases in brain levels of (R,R)-[$^{125}$I]-QNB were observed in 20 out of 33 regions analysed between 30 mins and 20 hours following heptylphysostigmine administration. At 6 hours following heptylphysostigmine administration no significant increases in (R,R)-[$^{125}$I]-QNB were observed in any of the regions analysed.

Heptylphysostigmine administration produced significant increases in (R,R)-[$^{125}$I]-QNB levels in the parietal cortex (29%), sensory motor cortex (33%), auditory cortex (76%) and in the superior colliculus (38%) at 30 mins after tracer administration. At 1 hour 15 out of the 33 regions analysed showed significant increases in (R,R)-[$^{125}$I]-QNB levels Regions include CA3 of hippocampus (16%), auditory cortex (46%), sensory motor cortex (19%), parietal cortex (20%), globus pallidus (40%), ventrolateral thalamic nucleus (34%), amygdala (12%), lateral geniculate nucleus (17%), nucleus basalis magnocellularis (27%), CA2 of hippocampus (19%), substantia nigra pars compacta (35%), mediodorsal thalamic nucleus (15%), substantia nigra pars reticulata (31%), hypothalamus (21%) and inferior colliculus (17%).
Significant increases in (R,R)-[$^{125}$I]-QNB levels were also observed at 2 hours following heptylphysostigmine in the auditory cortex (53%), pontine grey matter (62%), septal nuclei (10%), superior colliculus (88%), molecular layer of the hippocampus (28%) and in the visual cortex (28%). Illustrative autoradiograms of regions displaying increased activity at 30 mins, 1 hour and 2 hours are presented in Figs 28-30.

**Heptylphysostigmine Increases (R,S)-[$^{125}$I]-QNB Brain Levels at 2 Hours**

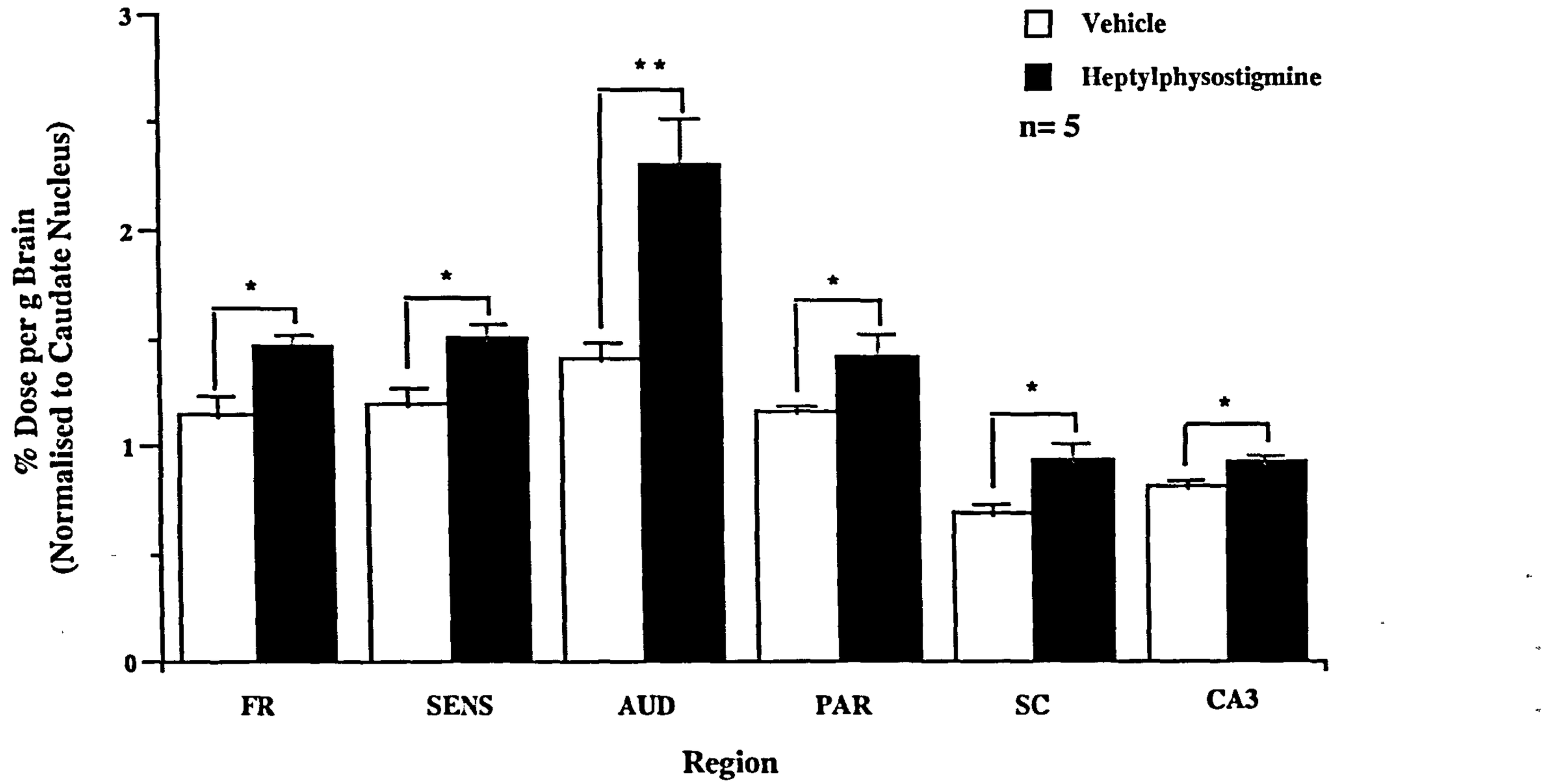


**Fig 25:** Level of (R,S)-[$^{125}$I]-QNB in discrete brain regions in vehicle and heptylphysostigmine treated animals at 2 hours. Heptylphysostigmine produced significant increases in frontal cortex (FR), sensory motor cortex (SENS), auditory cortex (AUD), parietal cortex (PAR), superior colliculus (SC) and CA3 region of the hippocampus (CA3). *P< 0.05, *P< 0.01 for statistical comparision between heptylphysostigmine and vehicle treated animals (Student's unpaired t-test). Data are expressed as mean ± S.E.M. % dose per g brain normalised to caudate nucleus. n= number of animals in each group.

# (R,S)-[$^{125}$I]-QNB In Rat Brain at 2Hours Following Heptylphysostigmine Administration

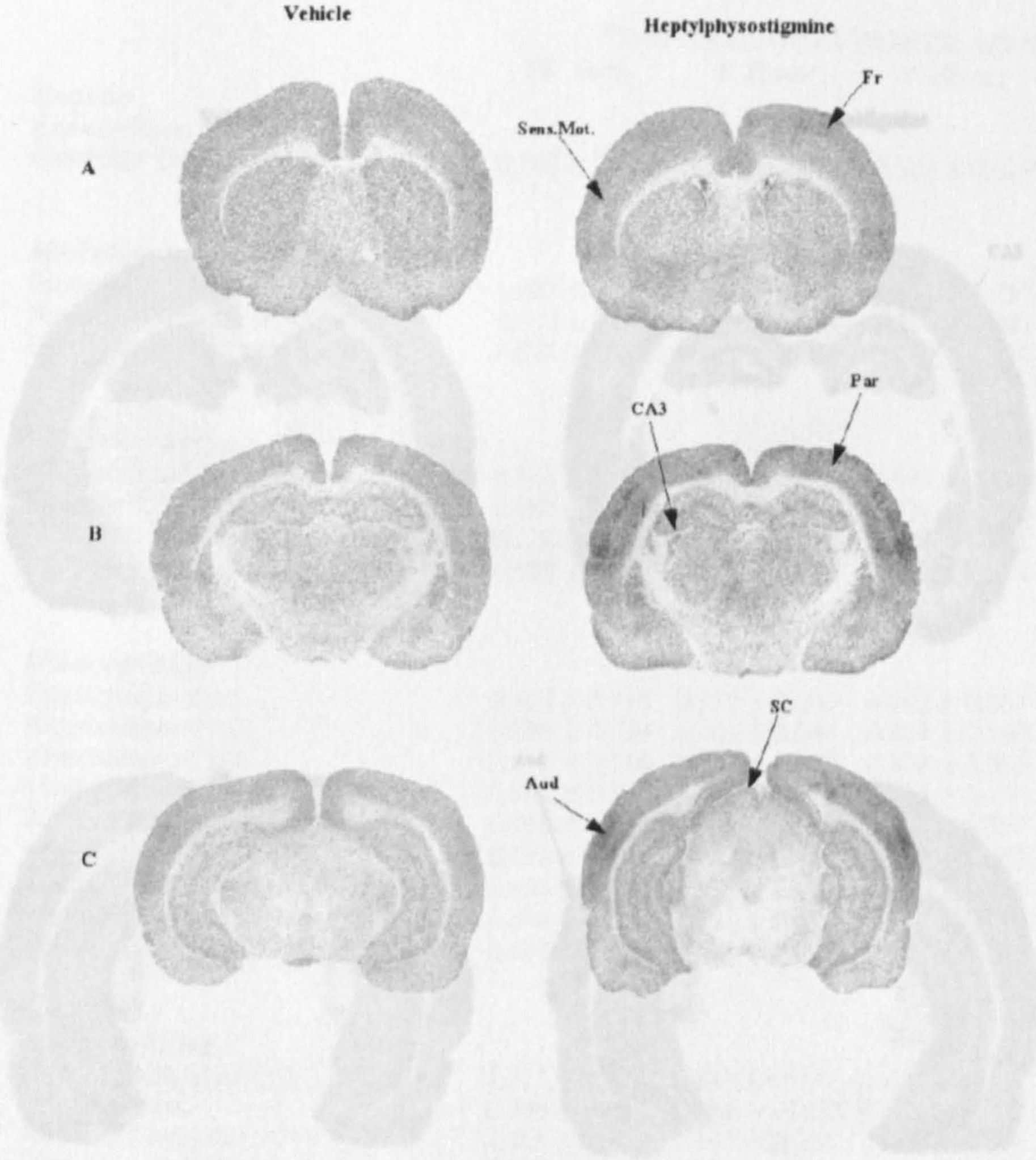


**Fig 26:**(R,S)-[$^{125}$I]-QNB levels in brain of vehicle and heptylphysostigmine treated animals at 2 hours. Autoradiograms show (R,S)-[$^{125}$I]-QNB in brain at the level of the frontal cortex (A), dorsolateral hippocampus (B) and auditory cortex (C). Heptylphysostigmine significantly increases (R,S)-[$^{125}$I]-QNB in the frontal cortex (Fr), parietal cortex (Par), sensory motor cortex (Sens.Mot.), auditory cortex (Aud), the CA3 region of the hippocampus (CA3) and the superior colliculus (SC). The auditory cortex is notably darker in the heptylphysostigmine image.

## (R,S)-[$^{125}$I]-QNB In Rat Brain at 24 Hours Following Heptyphysostigmine Administration

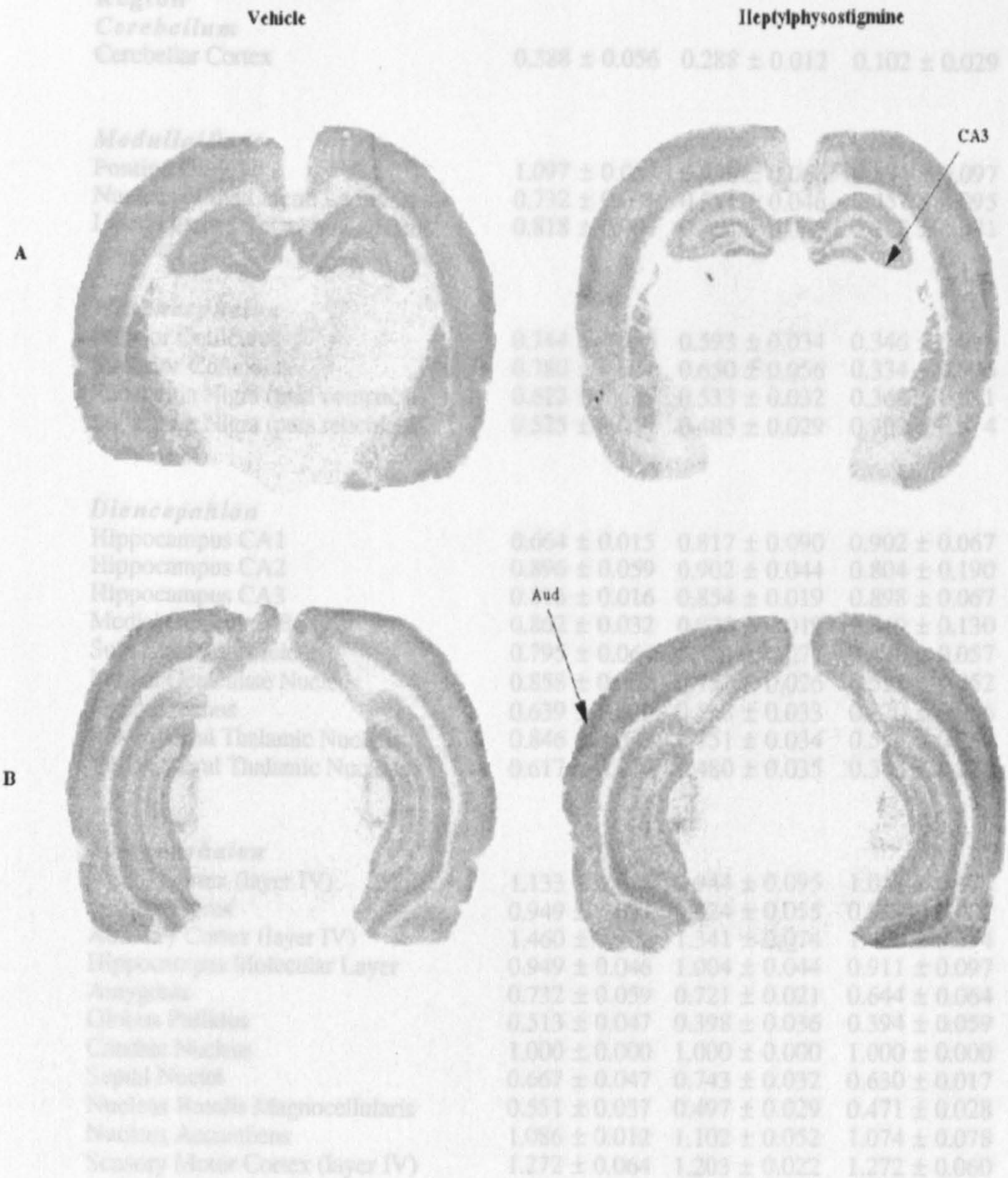


**Fig 27:** (R,S)-[$^{125}$I]-QNB in rat brain at 24 hours following heptylphysostigmine administration. Autoradiograms show (R,S)-[$^{125}$I]-QNB at the level of the dorsolateral hippocampus (A) and auditory cortex (B). Heptylphysostigmine significantly increases (R,S)-[$^{125}$I]-QNB in the CA3 region of the hippocampus (CA3) and auditory cortex (Aud).

## Table 9

## Effect of Heptylphysostigmine on (R,R)-[$^{125}$I]-QNB *in the Brain of Conscious Rat:*

## VEHICLE TREATED ANIMALS

| | TIME FOLLOWING TRACER ADMINISTRATION | | | |
|---|---|---|---|---|
| **Region** | **30 mins** | **1 Hour** | **2 Hours** | **6 Hours** |
| ***Cerebellum*** | | | | |
| Cerebellar Cortex | 0.388 ± 0.056 | 0.288 ± 0.012 | 0.102 ± 0.029 | 0.160 ± 0.047 |
| ***Medulla/Pons*** | | | | |
| Pontine Grey | 1.097 ± 0.053 | 0.936 ± 0.060 | 0.534 ± 0.097 | 0.487 ± 0.130 |
| Nucleus of the Lateral Lemniscus | 0.732 ± 0.096 | 0.541 ± 0.046 | 0.457 ± 0.095 | 0.363 ± 0.101 |
| Lateral Dorsal Tegmental nucleus | 0.818 ± 0.061 | 0.564 ± 0.048 | 0.328 ± 0.081 | 0.329 ± 0.099 |
| ***Mesencephalon*** | | | | |
| Inferior Colliculus | 0.744 ± 0.036 | 0.593 ± 0.034 | 0.346 ± 0.098 | 0.239 ± 0.067 |
| Superior Colliculus | 0.780 ± 0.044 | 0.650 ± 0.056 | 0.334 ± 0.096 | 0.286 ± 0.107 |
| Substantia Nigra (pars compacta) | 0.622 ± 0.035 | 0.533 ± 0.032 | 0.368 ± 0.091 | 0.305 ± 0.094 |
| Substantia Nigra (pars reticulata) | 0.525 ± 0.039 | 0.485 ± 0.029 | 0.309 ± 0.074 | 0.247 ± 0.079 |
| ***Diencepahlon*** | | | | |
| Hippocampus CA1 | 0.664 ± 0.015 | 0.817 ± 0.090 | 0.902 ± 0.067 | 1.276 ± 0.135 |
| Hippocampus CA2 | 0.896 ± 0.059 | 0.902 ± 0.044 | 0.804 ± 0.190 | 0.954 ± 0.096 |
| Hippocampus CA3 | 0.816 ± 0.016 | 0.854 ± 0.019 | 0.898 ± 0.067 | 1.131 ± 0.110 |
| Medial Geniculate Body | 0.862 ± 0.032 | 0.823 ± 0.019 | 0.549 ± 0.130 | 0.379 ± 0.080 |
| Sub Thalamic Nucleus | 0.795 ± 0.064 | 0.632 ± 0.077 | 0.428 ± 0.057 | 0.365 ± 0.067 |
| Lateral Geniculate Nucleus | 0.858 ± 0.062 | 0.752 ± 0.026 | 0.512 ± 0.052 | 0.257 ± 0.083 |
| Hypothalamus | 0.639 ± 0.030 | 0.518 ± 0.033 | 0.370 ± 0.056 | 0.189 ± 0.058 |
| Mediodorsal Thalamic Nucleus | 0.846 ± 0.079 | 0.751 ± 0.034 | 0.544 ± 0.050 | 0.254 ± 0.760 |
| Ventrolateral Thalamic Nucleus | 0.617 ± 0.026 | 0.480 ± 0.035 | 0.343 ± 0.053 | 0.175 ± 0.059 |
| ***Telencephalon*** | | | | |
| Visual Cortex (layer IV) | 1.133 ± 0.011 | 0.944 ± 0.095 | 1.052 ± 0.078 | 1.164 ± 0.280 |
| Dentate Gyrus | 0.949 ± 0.051 | 0.924 ± 0.055 | 0.969 ± 0.087 | 1.028 ± 0.227 |
| Auditory Cortex (layer IV) | 1.460 ± 0.900 | 1.341 ± 0.074 | 1.400 ± 0.094 | 1.350 ± 0.258 |
| Hippocampus Molecular Layer | 0.949 ± 0.046 | 1.004 ± 0.044 | 0.911 ± 0.097 | 1.070 ± 0.232 |
| Amygdala | 0.732 ± 0.059 | 0.721 ± 0.021 | 0.644 ± 0.064 | 0.624 ± 0.034 |
| Globus Pallidus | 0.513 ± 0.047 | 0.398 ± 0.036 | 0.394 ± 0.059 | 0.267 ± 0.052 |
| Caudate Nucleus | 1.000 ± 0.000 | 1.000 ± 0.000 | 1.000 ± 0.000 | 1.000 ± 0.000 |
| Septal Nuclei | 0.667 ± 0.047 | 0.743 ± 0.032 | 0.630 ± 0.017 | 0.461 ± 0.037 |
| Nucleus Basalis Magnocellularis | 0.551 ± 0.037 | 0.497 ± 0.029 | 0.471 ± 0.028 | 0.331 ± 0.052 |
| Nucleus Accumbens | 1.086 ± 0.012 | 1.102 ± 0.052 | 1.074 ± 0.078 | 1.189 ± 0.105 |
| Sensory Motor Cortex (layer IV) | 1.272 ± 0.064 | 1.203 ± 0.022 | 1.272 ± 0.060 | 1.106 ± 0.090 |
| Anterior Cingulate Cortex | 1.173 ± 0.079 | 1.163 ± 0.006 | 1.176 ± 0.054 | 1.219 ± 0.072 |
| Frontal Cortex | 1.144 ± 0.036 | 1.176 ± 0.027 | 1.192 ± 0.070 | 1.134 ± 0.078 |
| Parietal Cortex | 1.141 ± 0.047 | 1.100 ± 0.034 | 1.108 ± 0.066 | 1.061 ± 0.099 |
| ***Myelinated Fibre Tracts*** | | | | |
| Internal Capsule | 0.252 ± 0.039 | 0.366 ± 0.020 | 0.196 ± 0.056 | 0.069 ± 0.041 |
| Genu | 0.270 ± 0.060 | 0.324 ± 0.025 | 0.210 ± 0.053 | 0.223 ± 0.063 |

Table shows (R,R)-[$^{125}$I]-QNB in discrete brain regions of the conscious rat in vehicle (0.7 mls 0.9% saline) treated animals 0.5 hours, 1, 2 and 6 hours following iv administration of 200µCi of tracer. Data are expressed as mean ± S.E.M % Dose per g brain normalised to the caudate nucleus, n= 5 animals for each time point.

## Table 10

## Effect of Heptylphysostigmine on (R,R)-[$^{125}$I]-QNB in the Brain of Conscious Rat:

## HEPTYLPHYSOSTIGMINE TREATED ANIMALS

| | TIME FOLLOWING TRACER ADMINISTRATION | | | |
|---|---|---|---|---|
| **Region** | **30 mins** | **1 Hour** | **2 Hours** | **6 Hours** |
| ***Cerebellum*** | | | | |
| Cerebellar Cortex | 0.488 ± 0.098 | 0.392 ± 0.086 | 0.194 ± 0.056 | 0.253 ± 0.117 |
| ***Medulla/Pons*** | | | | |
| Pontine Grey | 1.270 ± 0.134 | 1.030 ± 0.093 | 0.863 ± 0.053 | 0.458 ± 0.137 |
| Nucleus of the Lateral Lemniscus | 0.792 ± 0.103 | 0.737 ± 0.105 | 0.603 ± 0.083 | 0.507 ± 0.248 |
| Lateral Dorsal Tegmental nucleus | 0.921 ± 0.150 | 0.607 ± 0.046 | 0.491 ± 0.049 | 0.359 ± 0.134 |
| ***Mesencephalon*** | | | | |
| Inferior Colliculus | 0.864 ± 0.100 | 0.696 ± 0.028 | 0.529 ± 0.069 | 0.357 ± 0.122 |
| Superior Colliculus | 1.082 ± 0.087 | 0.872 ± 0.079 | 0.628 ± 0.044 | 0.351 ± 0.080 |
| Substantia Nigra (pars compacta) | 0.661 ± 0.045 | 0.720 ± 0.059 | 0.580 ± 0.039 | 0.373 ± 0.077 |
| Substantia Nigra (pars reticulata) | 0.565 ± 0.045 | 0.637 ± 0.050 | 0.501 ± 0.053 | 0.326 ± 0.058 |
| ***Diencepahlon*** | | | | |
| Hippocampus CA1 | 0.717 ± 0.070 | 0.915 ± 0.046 | 0.858 ± 0.058 | 0.939 ± 0.276 |
| Hippocampus CA2 | 0.996 ± 0.068 | 1.072 ± 0.041 | 1.010 ± 0.054 | 0.832 ± 0.117 |
| Hippocampus CA3 | 0.878 ± 0.052 | 0.990 ± 0.008 | 0.871 ± 0.038 | 0.919 ± 0.122 |
| Medial Geniculate Body | 1.119 ± 0.116 | 0.956 ± 0.052 | 0.808 ± 0.024 | 0.482 ± 0.065 |
| Sub Thalamic Nucleus | 0.920 ± 0.085 | 0.782 ± 0.028 | 0.549 ± 0.066 | 0.222 ± 0.067 |
| Lateral Geniculate Nucleus | 0.874 ± 0.065 | 0.878 ± 0.031 | 0.576 ± 0.026 | 0.223 ± 0.072 |
| Hypothalamus | 0.661 ± 0.055 | 0.626 ± 0.032 | 0.405 ± 0.040 | 0.365 ± 0.156 |
| Mediodorsal Thalamic Nucleus | 0.865 ± 0.053 | 0.865 ± 0.024 | 0.625 ± 0.027 | 0.252 ± 0.076 |
| Ventrolateral Thalamic Nucleus | 0.651 ± 0.086 | 0.645 ± 0.031 | 0.432 ± 0.040 | 0.186 ± 0.050 |
| ***Telencephalon*** | | | | |
| Visual Cortex (layer IV) | 1.374 ± 0.124 | 1.183 ± 0.084 | 1.351 ± 0.087 | 1.307 ± 0.196 |
| Dentate Gyrus | 1.146 ± 0.133 | 1.007 ± 0.089 | 1.177 ± 0.043 | 1.084 ± 0.116 |
| Auditory Cortex (layer IV) | 2.565 ± 0.336 | 1.955 ± 0.063 | 2.139 ± 0.104 | 2.005 ± 0.225 |
| Hippocampus Molecular Layer | 1.065 ± 0.102 | 0.983 ± 0.092 | 1.171 ± 0.024 | 1.098 ± 0.099 |
| Amygdala | 0.790 ± 0.074 | 0.811 ± 0.019 | 0.684 ± 0.046 | 0.387 ± 0.134 |
| Globus Pallidus | 0.526 ± 0.051 | 0.562 ± 0.025 | 0.408 ± 0.015 | 0.191 ± 0.050 |
| Caudate Nucleus | 1.000 ± 0.000 | 1.000 ± 0.000 | 1.000 ± 0.000 | 1.000 ± 0.000 |
| Septal Nuclei | 0.744 ± 0.080 | 0.795 ± 0.041 | 0.692 ± 0.014 | 0.427 ± 0.095 |
| Nucleus Basalis Magnocellularis | 0.601 ± 0.047 | 0.630 ± 0.034 | 0.497 ± 0.026 | 0.258 ± 0.079 |
| Nucleus Accumbens | 1.113 + 0.100 | 1.184 ± 0.063 | 1.195 ± 0.031 | 1.025 ± 0.188 |
| Sensory Motor Cortex (layer IV) | 1.689 ± 0.063 | 1.434 ± 0.044 | 1.399 ± 0.080 | 0.988 ± 0.185 |
| Anterior Cingulate Cortex | 1.332 ± 0.055 | 1.253 ± 0.055 | 1.329 ± 0.095 | 1.037 ± 0.101 |
| Frontal Cortex | 1.625 ± 0.074 | 1.277 ± 0.117 | 1.446 ± 0.103 | 1.202 ± 0.056 |
| Parietal Cortex | 1.475 ± 0.030 | 1.317 ± 0.045 | 1.444 ± 0.152 | 1.153 ± 0.172 |
| ***Myelinated Fibre Tracts*** | | | | |
| Internal Capsule | 0.295 ± 0.043 | 0.359 ± 0.024 | 0.253 ± 0.063 | 0.163 ± 0.066 |
| Genu | 0.258 ± 0.067 | 0.363 ± 0.031 | 0.321 ± 0.045 | 0.282 ± 0.076 |

Table shows (R,R)-[$^{125}$I]-QNB in discrete brain regions of the conscious rat in heptylphysostigmine (2 mg/kg) treated animals 30 mins, 1, 2 and 6 hours following iv administration of 200μCi of tracer. Data are expressed as mean ± S.E.M % dose per g brain normalised to the caudate nucleus, n= 5 animals for each time point.

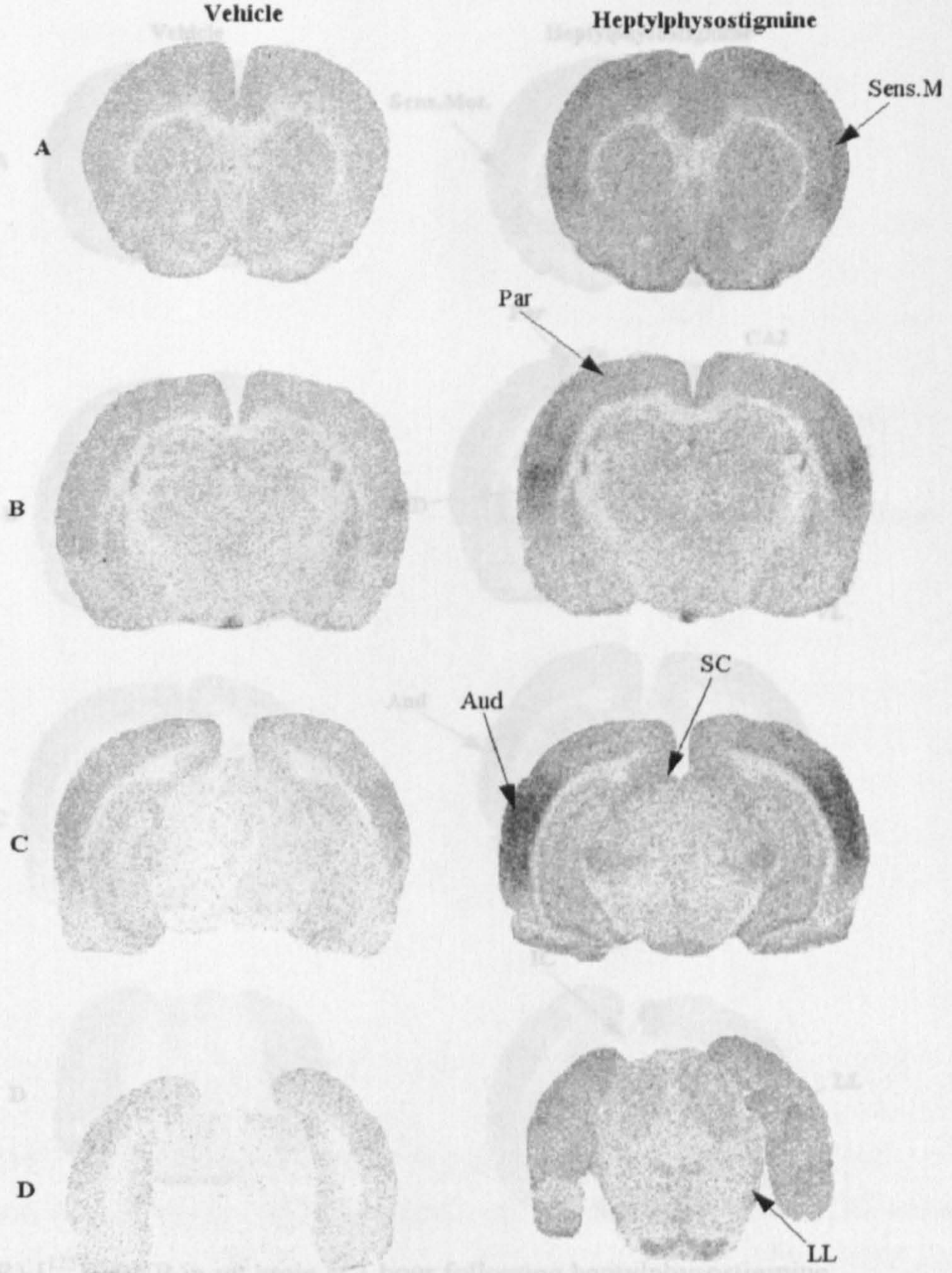


**Fig 28:** (R,R)-[$^{125}$I]-QNB in rat brain at 30 mins following heptylphysostigmine administration. Autoradiograms show activity at the level of the caudate nucleus (A), dorsolateral hippocampus (B), auditory cortex (C) and inferior colliculus (D). Heptylphysostigmine (2mg/kg) increased (R,R)-[$^{125}$I]-QNB in a number of regions including the superior colliculus (SC), auditory cortex (Aud) and lateral lemniscus (LL). Profound increases in tracer levels were observed in the parietal cortex (Par) and sensory motor cortex (Sens. Mot.)

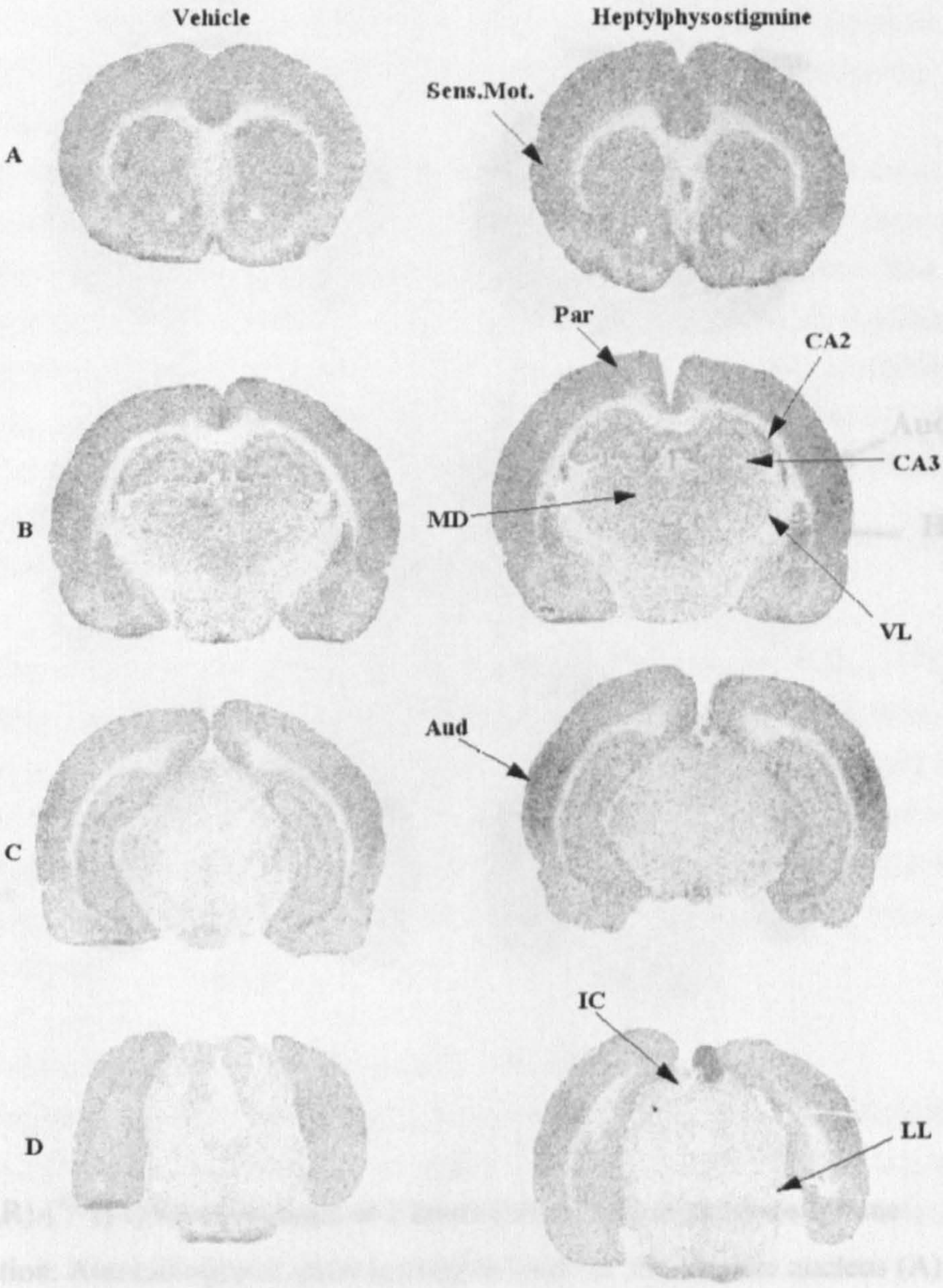


**Fig 29:** (R,R)-[$^{125}$I]-QNB in rat brain at 1 hour following heptylphysostigmine administration. Autoradiograms show activity at the level of the caudate nucleus (A), dorsolateral hippocampus (B), auditory cortex (C) and inferior colliculus (D). Heptylphysostigmine increased in (R,R)-[$^{125}$I]-QNB in a number of regions including inferior colliculus (IC), lateral lemniscus (LL), CA2 region of hippocampus (CA2), parietal cortex (Par), mediodorsal thalamus (MD), ventrolateral thalamus (VL) and sensory motor cortex (Sens.Mot.) Profound increases in tracer levels were observed in the auditory cortex (Aud) and CA3 region of the hippocampus (CA3).

## (R,R)-[$^{125}$I]-QNB In Rat Brain at 2 Hours Following Heptylphysostigmine Administration

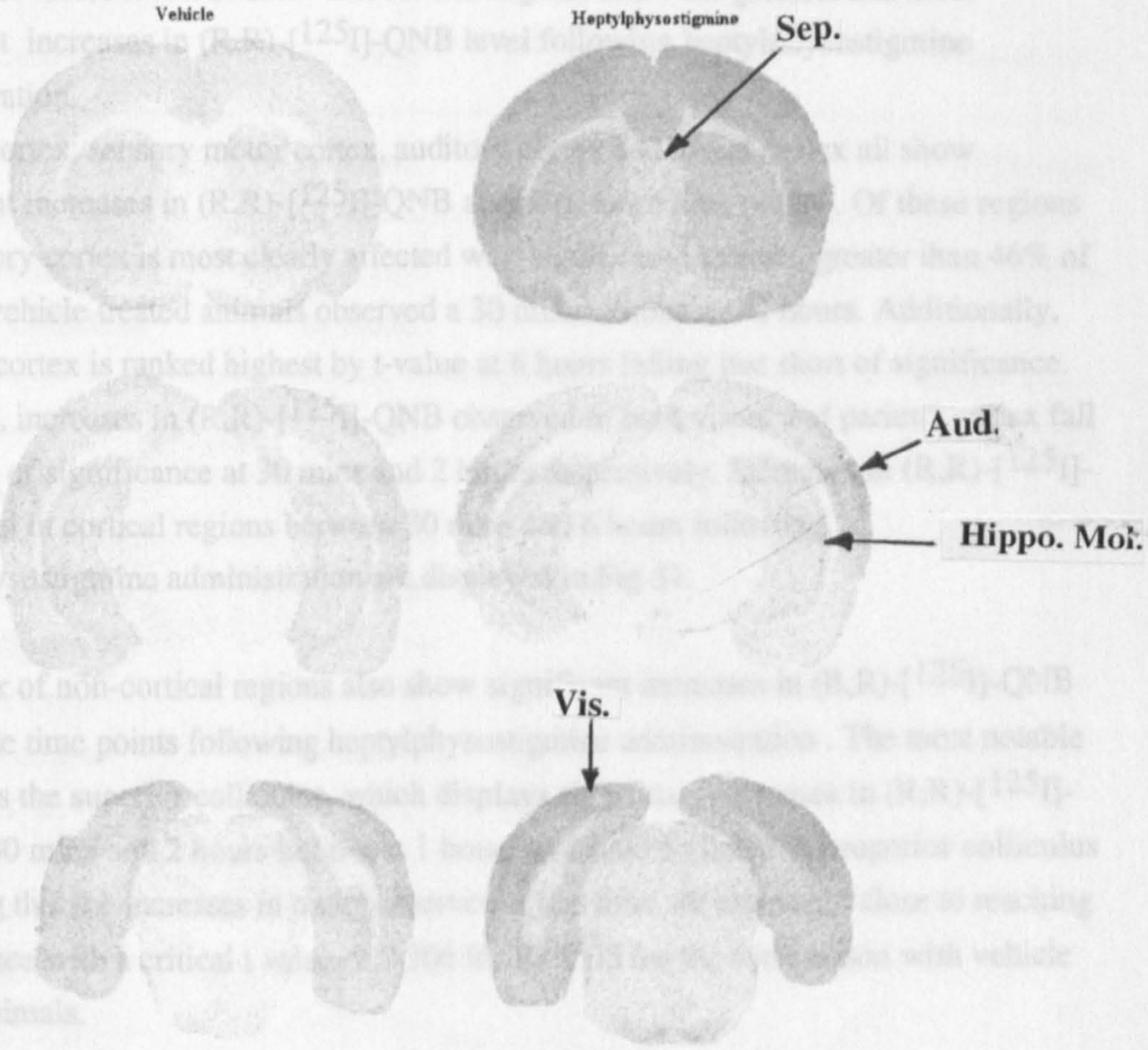


**Fig 30:**(R,R)-[$^{125}$I]-QNB in rat brain at 2 hours following heptylphysostigmine administration. Autoradiograms show activity at level of the caudate nucleus (A), auditory cortex (B) and visual cortex (C). Heptylphysostigmine increased (R,R)-[$^{125}$I]-QNB levels in a number of regions including the septal nucleus (Sep), auditory cortex (Aud), molecular layer of the hippocampus (Hipp.Mol.) and in the visual cortex (Vis).

Tables 11-14 display regions of increased (R,R)-[$^{125}$I]-QNB in heptylphysostigmine treated animals rank ordered by t-value for Student's unpaired t-test for the comparison with vehicle treated animals at 0.5 hours, 1hour, 2 hours and 6 hours.
From these tables it can be seen that cortical regions show the greatest and most consistent increases in (R,R)-[$^{125}$I]-QNB level following heptylphysostigmine administration.
Parietal cortex, sensory motor cortex, auditory cortex and visual cortex all show significant increases in (R,R)-[$^{125}$I]-QNB at one or more time points . Of these regions the auditory cortex is most clearly affected with significant increases greater than 46% of those in vehicle treated animals observed a 30 mins, 1 hour and 2 hours. Additionally, auditory cortex is ranked highest by t-value at 6 hours falling just short of significance. Similarly, increases in (R,R)-[$^{125}$I]-QNB observed in both visual and parietal cortex fall just short of significance at 30 mins and 2 hours respectively. Increases in (R,R)-[$^{125}$I]-QNB level in cortical regions between 30 mins and 6 hours following heptylphysostigmine administration are displayed in Fig 31.

A number of non-cortical regions also show significant increases in (R,R)-[$^{125}$I]-QNB at multiple time points following heptylphysostigmine administration . The most notable of these is the superior colliculus, which displays significant increases in (R,R)-[$^{125}$I]-QNB at 30 mins and 2 hours but not at 1 hour. At 1 hour t= 2.293 for superior colliculus indicating that the increases in tracer observed at this time are extremely close to reaching significance with a critical t value of 2.306 for $P< 0.05$ for the comparison with vehicle treated animals.

**Normalisation of Data to the Caudate Nucleus**

As previously described raw data (μCi per g brain) for regional (R,S)- and (R,R)-[$^{125}$I]-QNB activity in rat brain were expressed as a ratio of percent of the injected dose relative the level in the caudate nucleus to reduce the impact of interanimal variability on the data. Normalisation to this region was performed as tracer levels in this region are reproducible from animal to animal and are relatively unchanged over the experimental time period.

Fig 32 shows raw data (μCi/g) for (R,S)- and (R,R)-[$^{125}$I]-QNB in caudate nucleus of vehicle and heptylphysostigmine treated animals. Heptylphysostigmine administration had no significant effect on tracer levels in the caudate nucleus indicating that normalisation of data to this region therefore remains valid for experiments utilising heptylphysostigmine.
Complete regional tables of un-normalised time-activity data for (R,S)- and (R,R)-[$^{125}$I]-QNB for heptylphysostigmine experiments are displayed in Appendix A.

**Hierarchy of Regional Increases in (R,R)-[$^{125}$I]-QNB at 0.5 hours: Rank Order By t-value**

| | | |
|---|---|---|
| Parietal Cortex | t= 5.990 | ***P<0.001 |
| Sensory Motor Cortex | t= 4.643 | **P< 0.01 |
| Auditory Cortex | t= 3.177 | *P< 0.05 |
| Superior Colliculus | t= 3.098 | |
| Visual Cortex | t= 1.936 | P> 0.05 |
| Pontine Grey | t= 1.201 | |
| Hippocampus CA3 | t=1.14 | |
| Inferior Colliculus | t= 1.129 | |
| Hippocampus CA1 | t= 1.111 | |
| Molecular Layer of Hippocampus | t= 1.037 | |
| Septal Nuclei | t= 0.822 | |
| SNc | t= 0.684 | |
| SNr | t=0.672 | |
| Amygdala | t= 0.613 | |
| NBM | t= 0.427 | |
| Nucleus of the Lateral Lemniscus | t= 0.426 | |
| VL Thalamus | t= 0.378 | |
| Hypothalamus | t=0.351 | |
| MD Thalamus | t=0.199 | |
| Globus Pallidus | t=0.187 | |
| Lateral Genculate Nucleus | t= 0.178 | |

**Table 11:** Rank order by t-value of regions showing increases in (R,R)-[$^{125}$I]-QNB levels in heptylphysostigmine treated animals at 30 mins ***P< 0.001, **P< 0.01 and *P< 0.05 indicate a statistcally significant increase in (R,R)-[$^{125}$I]-QNB level (Student'ts unpaired t-test) for comparison with vehicle treated animals.
SNc= substantia nigra pars compacta, SNr= substantia nigra pars reticulata, NBM= nucleus basalis magnocellularis, VL= ventrolateral, MD= mediodorsal.

**Hierarchy of Regional Increases in (R,R)-[$^{125}$I]-QNB at 1 Hour: Rank Order By t-value**

| | | |
|---|---|---|
| Hippocampus CA3 | t= 6.597 | ***P<0.001 |
| Auditory Cortex | t=6.318 | |
| Sensory Motor Cortex | t= 4.696 | **P< 0.01 |
| Parietal Cortex | t= 3.847 | |
| Globus Pallidus | t= 3.742 | |
| VL Thalamus | t= 3.529 | |
| Amygdala | t= 3.178 | *P< 0.05 |
| Lateral Geniculate Nucleus | t= 3.114 | |
| NBM | t= 2.976 | |
| Hippocampus CA2 | t= 2.827 | |
| SNc | t= 2.786 | |
| MD Thalamus | t= 2.739 | |
| SNr | t= 2.630 | |
| Hypothalamus | t= 2.349 | |
| Inferior Colliculus | t= 2.338 | |
| Superior Colliculus | t= 2.293 | P>0.05 |
| Nucleus of the Lateral Lemniscus | t= 1.710 | |
| Visual Cortex | t= 1.490 | |
| Pontine Grey | t= 0.849 | |
| Molecular Layer of Hippocampus | t= 0.206 | |
| Septal Nuclei | t= 0.100 | |

**Table 12:** Rank order by t-value of regions showing increases in (R,R)-[$^{125}$I]-QNB levels in heptylphysostigmine treated animals at 1 hour ***P< 0.001, **P< 0.01 and *P< 0.05 indicate a statistcally significant increase in (R,R)-[$^{125}$I]-QNB level (Student'ts unpaired t-test) for comparison with vehicle treated animals.
See Table 11 for a list of abbreviations.

**Hierarchy of Regional Increases in (R,R)-[$^{125}$I]-QNB at 2 Hours: Rank Order By t-value**

| | | |
|---|---|---|
| Auditory Cortex | t= 5.285 | **P< 0.01 |
| Pontine Grey | t= 2.990 | **P< 0.05 |
| Septal Nuclei | t= 2.851 | |
| Superior Colliculus | t= 2.755 | |
| Molecular Layer of Hippocampus | t= 2.594 | |
| Visual Cortex | t= 2.565 | |
| SNc | t= 2.138 | P>0.05 |
| SNr | t= 2.105 | |
| Parietal Cortex | t= 2.025 | |
| Inferior Colliculus | t= 1.525 | |
| MD Thalamus | t= 1.427 | |
| VL Thalamus | t= 1.343 | |
| Sensory Motor Cortex | t= 1.277 | |
| Nucleus of the Lateral Lemniscus | t= 1.159 | |
| Lateral Geniculate Nucleus | t= 1.103 | |
| Hippocampus CA2 | t= 1.040 | |
| NBM | t= 0.684 | |
| Hypothalamus | t= 0.514 | |
| Amygdala | t= 0.509 | |
| Hippocampus CA3 | t= 0.343 | |
| Globus Pallidus | t= 0.228 | |

**Table 13:** Rank order by t-value of regions showing increases in (R,R)-[$^{125}$I]-QNB levels in heptylphysostigmine treated animals at 2 hours ***P< 0.001, **P< 0.01 and *P< 0.05 indicate a statistcally significant increase in (R,R)-[$^{125}$I]-QNB level (Student'ts unpaired t-test) for comparison with vehicle treated animals.
See Table 11 for a list of abbreviations.

## Hierarchy of Regional Increases in (R,R)-[$^{125}$I]-QNB at 6 Hours: Rank Order By t-value

| | | |
|---|---|---|
| Auditory Cortex | t= 1.917 | P>0.05 |
| Amygdala | t= 1.767 | |
| Hippocampus CA2 | t= 1.290 | |
| Hypothalamus | t= 1.058 | |
| Globus Pallidus | t= 1.054 | |
| Inferior Colliculus | t= 0.850 | |
| Hippocampus CA2 | t= 0.805 | |
| SNr | t= 0.805 | |
| NBM | t= 0.770 | |
| Septal Nuclei | t= 0.747 | |
| Sensory Motor Cortex | t= 0.572 | |
| SNc | t= 0.559 | |
| Nucleus of the Lateral Lemniscus | t= 0.538 | |
| Superior Colliculus | t= 0.486 | |
| Parietal Cortex | t= 0.463 | |
| Visual Cortex | t= 0.419 | |
| Lateral Geniculate Nucleus | t= 0.308 | |
| VL Thalamus | t= 0.142 | |
| Molecular Layer of Hippocampus | t= 0.111 | |
| Pontine Grey | t= 0.106 | |
| MD Thalamus | t= 0.018 | |

**Table 14:** Rank order by t-value of regions showing increases in (R,R)-[$^{125}$I]-QNB levels in heptylphysostigmine treated animals at 6 hours t-values calculated for Student's unpaired t-test for comparison with vehicle treated animals.
See Table 11 for a list of abbreviations.

## Heptylphysostigmine Increases (R,R)-[$^{125}$I]-QNB In Cortex of Conscious Rat

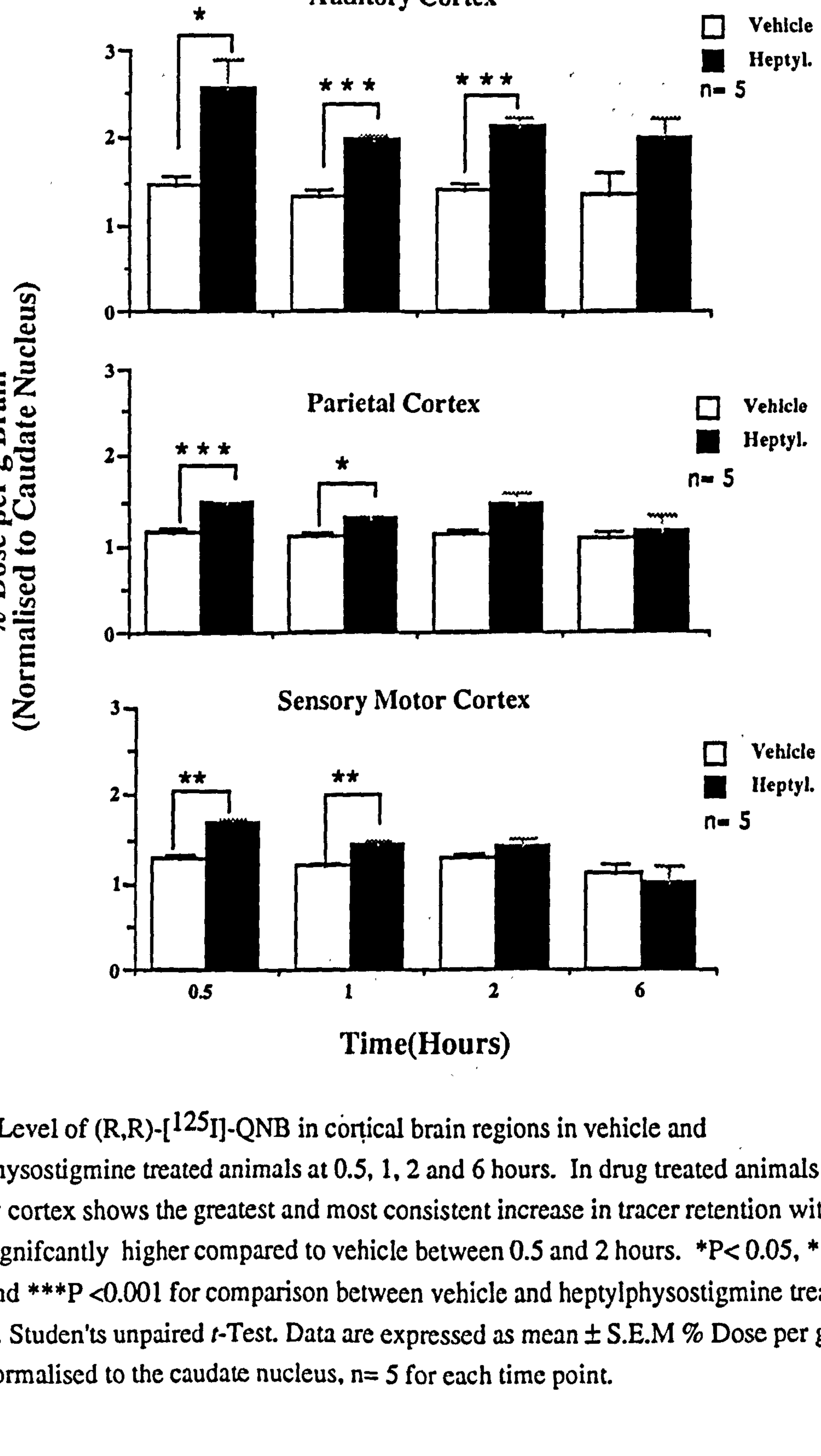


**Fig 31** Level of (R,R)-[$^{125}$I]-QNB in cortical brain regions in vehicle and heptylphysostigmine treated animals at 0.5, 1, 2 and 6 hours. In drug treated animals auditory cortex shows the greatest and most consistent increase in tracer retention with levels signifcantly higher compared to vehicle between 0.5 and 2 hours. *P< 0.05, **P <0.01 and ***P <0.001 for comparison between vehicle and heptylphysostigmine treated animals. Studen'ts unpaired *t*-Test. Data are expressed as mean ± S.E.M % Dose per g Brain normalised to the caudate nucleus, n= 5 for each time point.

## Heptylphysostigmine has no effect on (R,S)- and (R,R)-[$^{125}$I]-QNB in the Caudate Nucleus

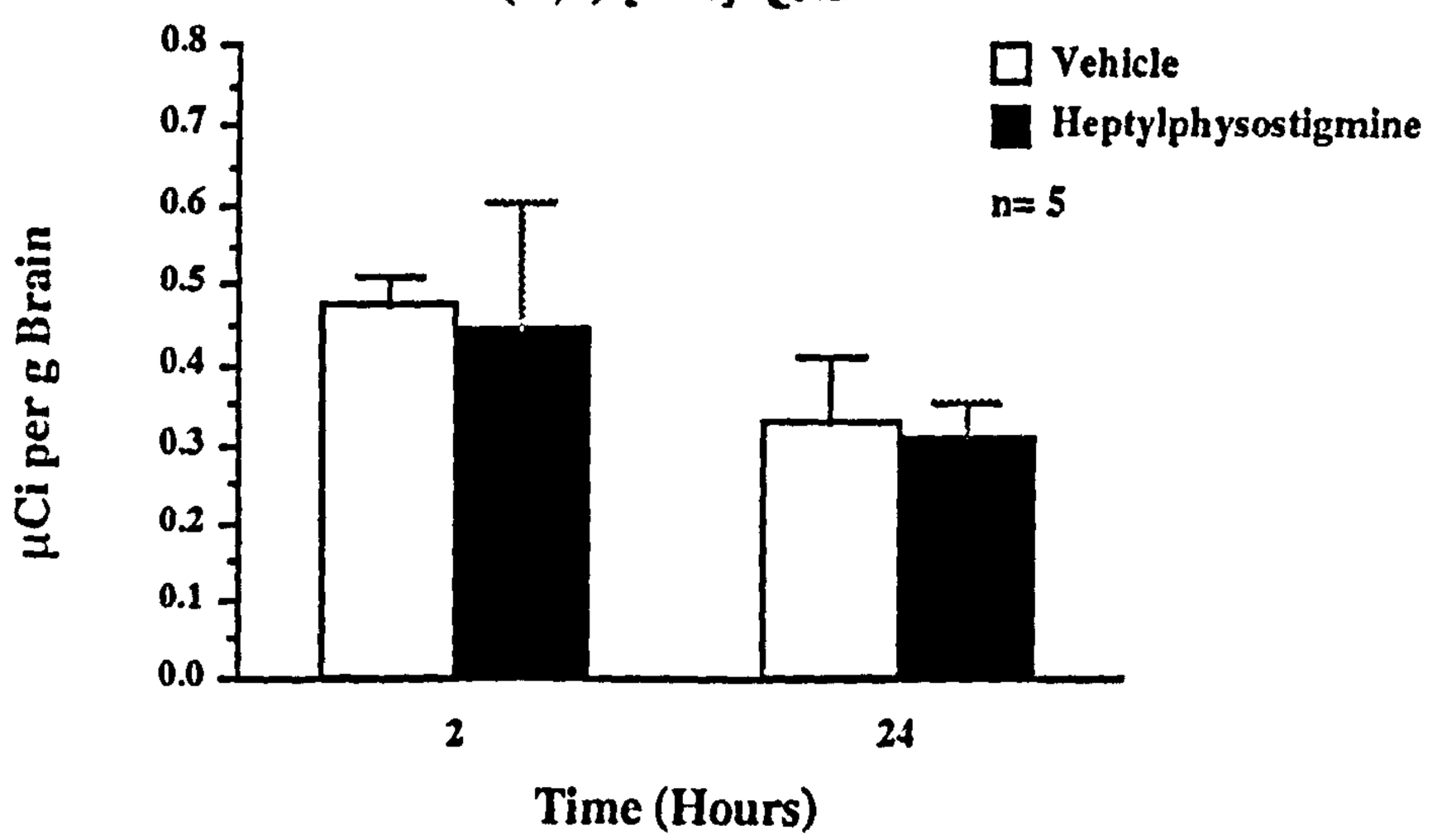


**Fig 32:** Uptake and retention of (R,S)-[$^{125}$I]-QNB (top) and (R,R)-[$^{125}$I]-QNB (bottom) in the caudate nucleus of conscious rat in vehicle and heptylphysostigmine (2mg/kg) treated animals. Heptylphysostigmine administration had no significant effect on levels of either ligand in caudate nucleus. Expression of data as a ratio of the level in the caudate nucleus is therefore a valid means of normalisation in experiments with heptylphysostigmine. Data are expressed as mean ± S.E.M μCi per g Brain, n= 5.

### 3.1.5 Acetylcholinesterase Activity in Rat brain Sections Following Heptylphysostigmine Administration

**Effect of Heptylphysostigmine on AChE Activity *in Vivo***

AChE activity in sections of rat brain taken from heptylphysostigmine and vehicle treated animals was determined by semi-quantitative histochemistry. Figure 33 shows illustrative sections stained for AChE activity taken from drug and vehicle treated animals from (R,S)- and (R,R)-[$^{125}$I]-QNB studies. Heptylphysostigmine (2mg/kg) produced a prolonged inhibition of AChE activity in the brain.

**AChE Activity in Sections from Studies with (R,S)-[$^{125}$I]-QNB**

Statistically significant reductions in enzyme activity were measured in the parietal cortex and CA1 of the hippocampus at 2 hours and in the parietal cortex at 24 hours. Heptylphysostigmine administration (2mg/kg) reduced AChE activity in all regions at both 2 and 24 hours with the exception of the cerebellum. Enzyme activity in this region was not reduced following heptylphysostigmine administration and was apparently greater at 24 hours (Fig 34). The intrinsically low levels of enzyme present in the cerebellum and the limited sensitivity of the assay to accurately determine low levels of staining are likely to account for this apparent anomaly. Complete tables of measured AChE activity in sections from vehicle and heptylphysostigmine treated animals are displayed in Appendix C.

**AChE Activity in Sections from Studies with (R,R)-[$^{125}$I]-QNB**

At 30 mins heptylphysostigmine (2mg/kg) significantly inhibits AChE activity in all regions analysed. At 1 hour AChE activity is significantly inhibited in frontal cortex, parietal cortex and CA1 of hippocampus. At 2 hours AChE activity is significantly inhibited in the parietal cortex and CA1 of hippocampus and at 6 hours AChE activity is significantly inhibited in the CA1 of hippocampus. AChE activity in the cerebellum appeared to be least sensitive to inhibition, again this may be due to the limited sensitivity of the assay combined with the intrinsically low level of enzyme present in this region. Fig 35 shows AChE activity in the parietal cortex, CA1 of hippocampus and cerebellum between 30 mins and 6 hours. As in studies with (R,S)-[$^{125}$I]-QNB heptylphysostigmine (2mg/kg) produced a prolonged inhibition of AChE activity in the majority of brain regions analysed. Complete tables of measured AChE activity in sections from vehicle and heptylphysostigmine treated animals are displayed in Appendix C.

These observations indicate that heptylphysostigmine is effective in producing a significant inhibition of AChE activity *in vivo* for a prolonged period of time particularly in cortex and hippocampus.

# Effect Of Heptylphysostigmine On AChE Activity *In Vivo*

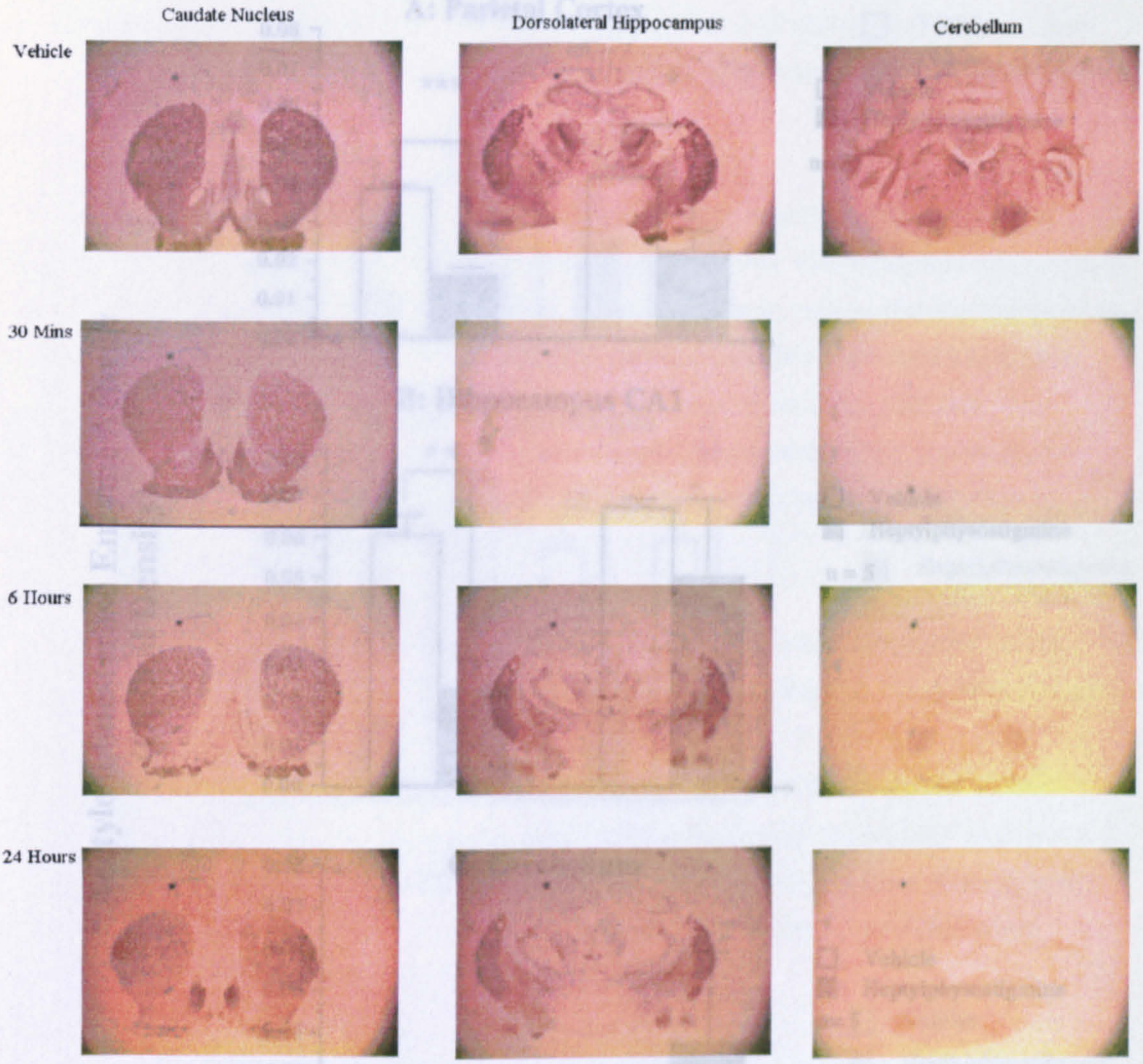


**Fig 33:** Figure shows AChE histochemical staining in rat brain sections at the level of the caudate nucleus, dorsolateral hippocampus and cerebellum taken from vehicle treated animals and from heptylphysostigmine treated animals at 30 mins, 6 hours and 24 hours following drug administration. Heptylphysostigmine (2 mg/kg) produced a prolonged inhibition of AChE activity. It should be noted that animals in the 24 hour group received a second infusion of heptylphysostigmine 8 hours after the first.

# Heptylphysostigmine Produces a Prolonged Inhibition of Brain AChE Activity

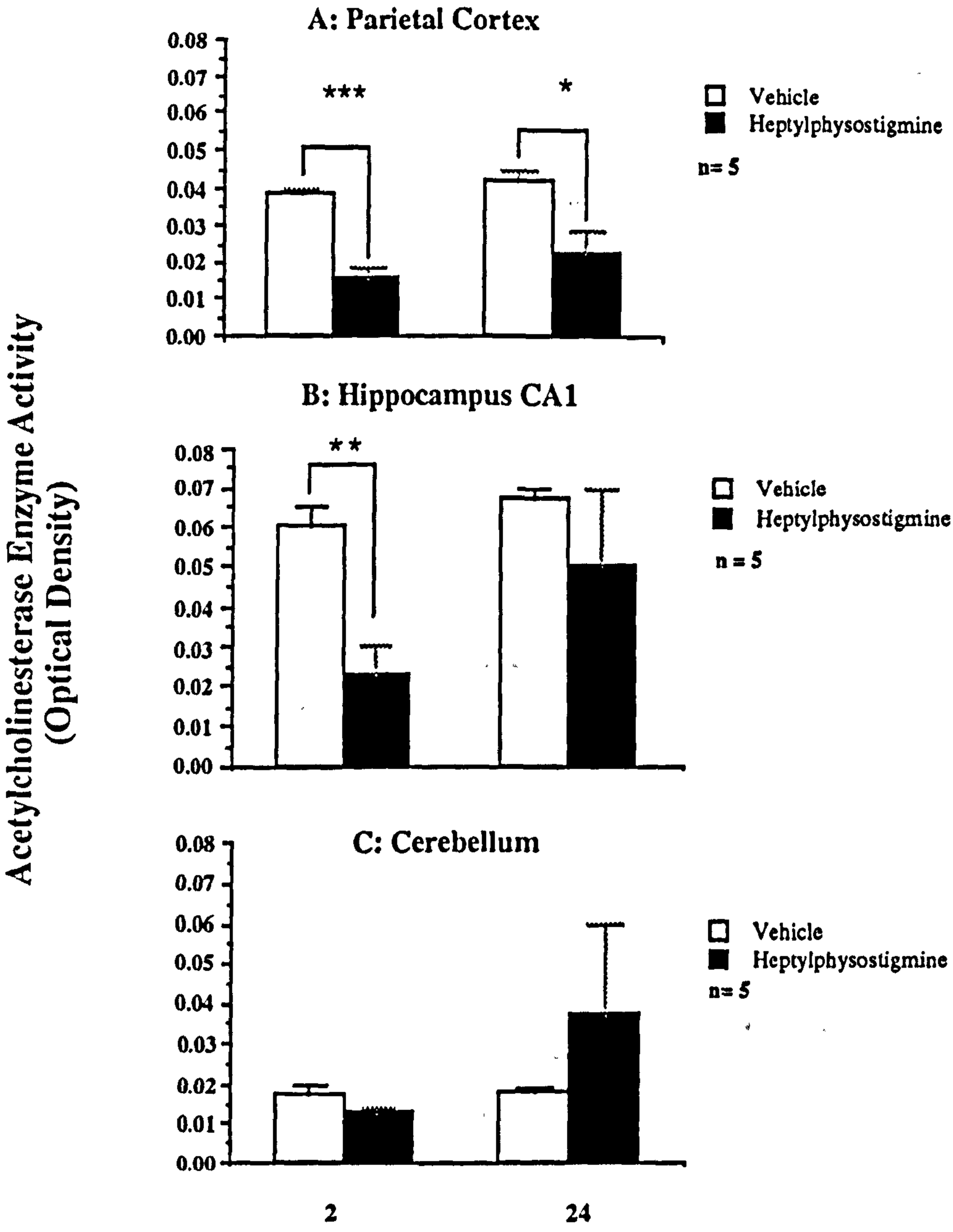


**Fig 34:** AChE activity measured by semi-quantitative histochemistry in rat brain sections at the level of parietal cortex (A), CA1 of hippocampus (B) and cerebellum(C) from vehicle and heptylphysostigmine treated animals in studies with (R,S)-[$^{125}$I]-QNB at 2 and 24 hours. Heptylphysotigmine produced significant reductions in AChE activity in parietal cortex and CA1 of hippocampus at 2 hours and in parietal cortex at 24 hours. Data are expressed as mean ± S.E.M Optical Density as a measure of staining intensity. *P <0.05, **P <0.01 and ***P <0.001 Student's unpaired *t*-Test (n= 5).

# Heptylphysostigmine Produces a Prolonged Inhibition of Brain AChE Activity

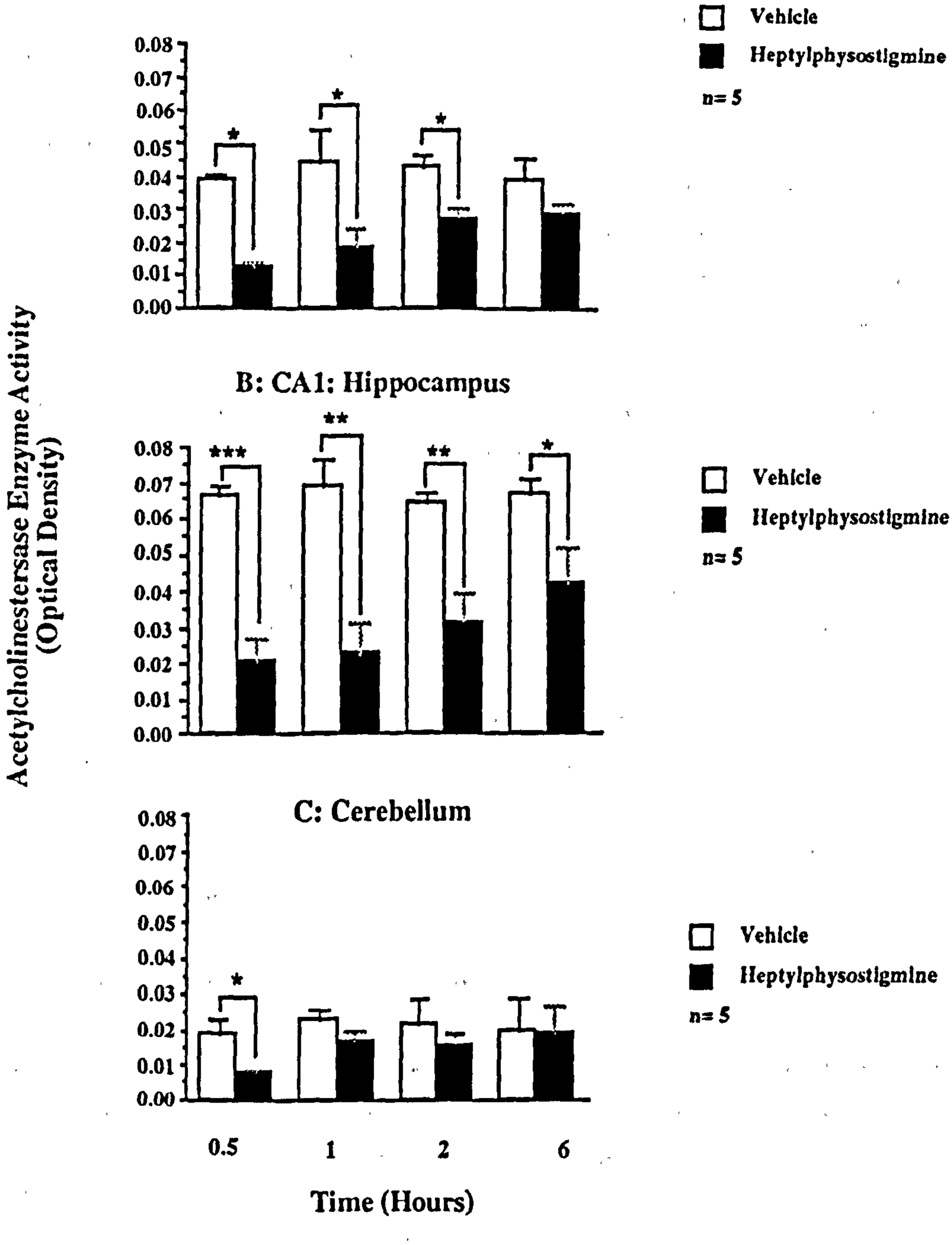


**Fig 35:** AChE activity measured by semi-quantitative histochemistry in rat brain sections at the level of parietal cortex (A), CA1 of hippocampus (B) and cerebellum(C) from vehicle and heptylphysostigmine treated animals in studies with (R,R)-[$^{125}$I]-QNB at 0.5, 1, 2 and 6hours. Heptylphysotigmine produced significant reductions in AChE activity in parietal cortex and CA1 of hippocampus at 2 hours and in parietal cortex at 6 hours. *P <0.05, **P <0.01 and ***P <0.001 Student's unpaired two-tailed *t*-Test. Data are expressed as mean ± S.E.M optical density as a measure of staining intensity [n= 5].

## 3.2 REGIONAL CEREBRAL BLOOD FLOW IN THE CONSCIOUS RAT FOLLOWING HEPTYLPHYSOSTIGMINE ADMINISTRATION

Regional cerebral blood flow was measured by [$^{14}$C]-IAP autoradiography 2 hours following vehicle or heptylphysostigmine (2mg/kg) administration in the conscious rat.

### General Observations

Animals receiving heptylphysostigmine (2mg/kg) were observed to display overt behavioural changes identical to those previously observed following administration of this drug. Symptoms included salivation, urination, muscle tremor and fasciculation and an increased sensitivity to noise. In addition, animals exhibited reduced locomotor activity and absence of the normal grooming behaviour associated with rats. The majority of animals displayed mild symptoms by 2 hours when CBF was measured. Animals receiving saline displayed none of these symptoms and exhibited normal behaviour.

Physiologic variables were measured prior to vehicle / heptylphysostigmine infusion and before measurement of CBF (i.e. 2 hours after initiation of vehicle / heptylphysostigmine infusion).

Heptylphysostigmine was observed to significantly increase mean arterial blood pressure and plasma glucose and to significantly reduce body temperature compared to vehicle treated animals when measured pre-CBF. Additionally, plasma glucose levels were significantly higher in heptylphysostigmine treated animals pre-CBF when compared levels measured pre-infusion (Appendix B).

### Effect of Heptylphysostigmine on Cerebral Blood Flow in the Conscious Rat

Quantitative densitometric analysis was performed to determine regional cerebral blood flow in 33 anatomically distinct brain regions at 2 hours following a cholinergic challenge produced by the administration of the cholinesterase inhibitor heptylphysostigmine(2mg/kg).

Heptylphysostigmine produced highly circumscribed alterations in regional cerebral blood flow at 2 hours after administration. Table 15 shows rCBF in vehicle and heptylphysostigmine treated animals. Significant increases in CBF were measured in parietal cortex, visual cortex, sensory motor cortex, auditory cortex and frontal cortex in heptylphysostigmine treated animals (Fig 36). Illustrative autoradiograms of [$^{14}$C]-IAP levels in vehicle and heptylphysostigmine treated animals are presented in Fig 37. Cortical regions in heptylphysostigmine treated animals are notably darker than those in vehicle treated animals. It should be noted that the cortical regions displaying increased

**Table 15.**

**Effect Of Heptylphysostigmine On Local Cerebral Blood Flow In The Conscious Rat**

| Region | Vehicle | Heptylphysostigmine | t |
|---|---|---|---|
| ***Cerebellum*** | | | |
| Cerebellar Cortex | 101 ± 10 | 87 ± 9 | 1.041 |
| ***Medulla/ Pons*** | | | |
| Nucleus of the Lateral Lemniscus | 154 ± 8 | 138 ± 11 | 1.176 |
| Lateral Dorsal Tegmental Nucleus | 122 ± 14 | 135 ± 11 | 0.730 |
| Pontine grey matter | 130 ± 7 | 149 ± 10 | 1.557 |
| ***Mesencepahlon*** | | | |
| Inferior Colliculus | 177 ± 17 | 181 ± 16 | 0.171 |
| Superior Colliculus | 116 ± 12 | 147 ± 94 | 0.327 |
| Substantia Nigra (pars compacta) | 110 ± 17 | 94 ± 6 | 0.887 |
| Substantia Nigra (pars reticulata) | 78 ± 17 | 73 ± 4 | 0.286 |
| ***Diencephalon*** | | | |
| Medial Geniculate Body | 155 ± 12 | 183 ± 16 | 1.4 |
| Subthalamic nucleus | 149 ± 23 | 127 ± 9 | 0.891 |
| Lateral Geniculate Nucleus | 128 ± 16 | 135 ± 17 | 0.299 |
| Hippocampus CA1 | 67 ± 7 | 65 ± 7 | 0.202 |
| Hippocampus CA2 | 77 ± 5 | 77 ± 9 | 0 |
| Hippocampus CA3 | 84 ± 14 | 91 ± 11 | 0.393 |
| Hypothalamus | 81 ± 10 | 76 ± 4 | 0.464 |
| Mediodorsal Thalamic Nucleus | 135 ± 13 | 131 ± 15 | 0.201 |
| Ventrolateral ThalamicNucleus | 97 ± 8 | 100 ± 11 | 0.220 |
| ***Telencephalon*** | | | |
| Visual Cortex (layer IV) | 119 ± 15 | 172 ± 14* | 2.583 |
| Hippocampus (Molecular Layer) | 98 ± 11 | 102 ± 10 | 0.269 |
| Dentate gyrus | 105 ± 32 | 119 ± 9 | 0.421 |
| Auditory Cortex (Layer IV) | 215 ± 24 | 291 ± 22* | 2.334 |
| Amygdala | 86 ± 6 | 82 ± 5 | 0.512 |
| Septal nuclei | 79 ± 10 | 74 ± 8 | 0.390 |
| Nucleus Basalis Magnocellularis | 79 ± 5 | 74 ± 5 | 0.707 |
| Globus pallidus | 77 ± 15 | 66 ± 5 | 0.696 |
| Caudate nucleus | 113 ± 14 | 95 ± 9 | 1.082 |
| Sensory Motor Cortex (Layer IV) | 143 ± 11 | 211 ± 26* | 2.409 |
| Nucleus Accumbens | 131 ± 11 | 138 ± 19 | 0.318 |
| Anterior Cingulate Cortex | 140 ± 24 | 161 ± 23 | 0.631 |
| Frontal Cortex | 122 ± 18 | 190 ± 23* | 2.328 |
| Parietal Cortex | 151 ± 20 | 244 ± 28* | 2.703 |
| ***Myelinated Fibre Tracts*** | | | |
| Internal Capsule | 53 ± 15 | 53 ± 2 | 0 |
| Genu | 35 ± 3 | 41 ± 4 | 1.2 |

Local cerebral blood flow was measured in the conscious rat at 2 hours following vehicle/heptylphysostigmine infusion. Significant increases in blood flow are observed in cortical regions in heptylphysostigmine treated animals. * $P < 0.05$ for the comparison between vehicle and heptylphysostigmine unpaired Student's t-test; critical value t= 2.306 (8 df) . Data are expressed as mean ± S.E.M. ml/100g/min (n = 5 in each group).

## Heptylphysostigmine Increases Blood Flow In the Cortex of The Conscious Rat

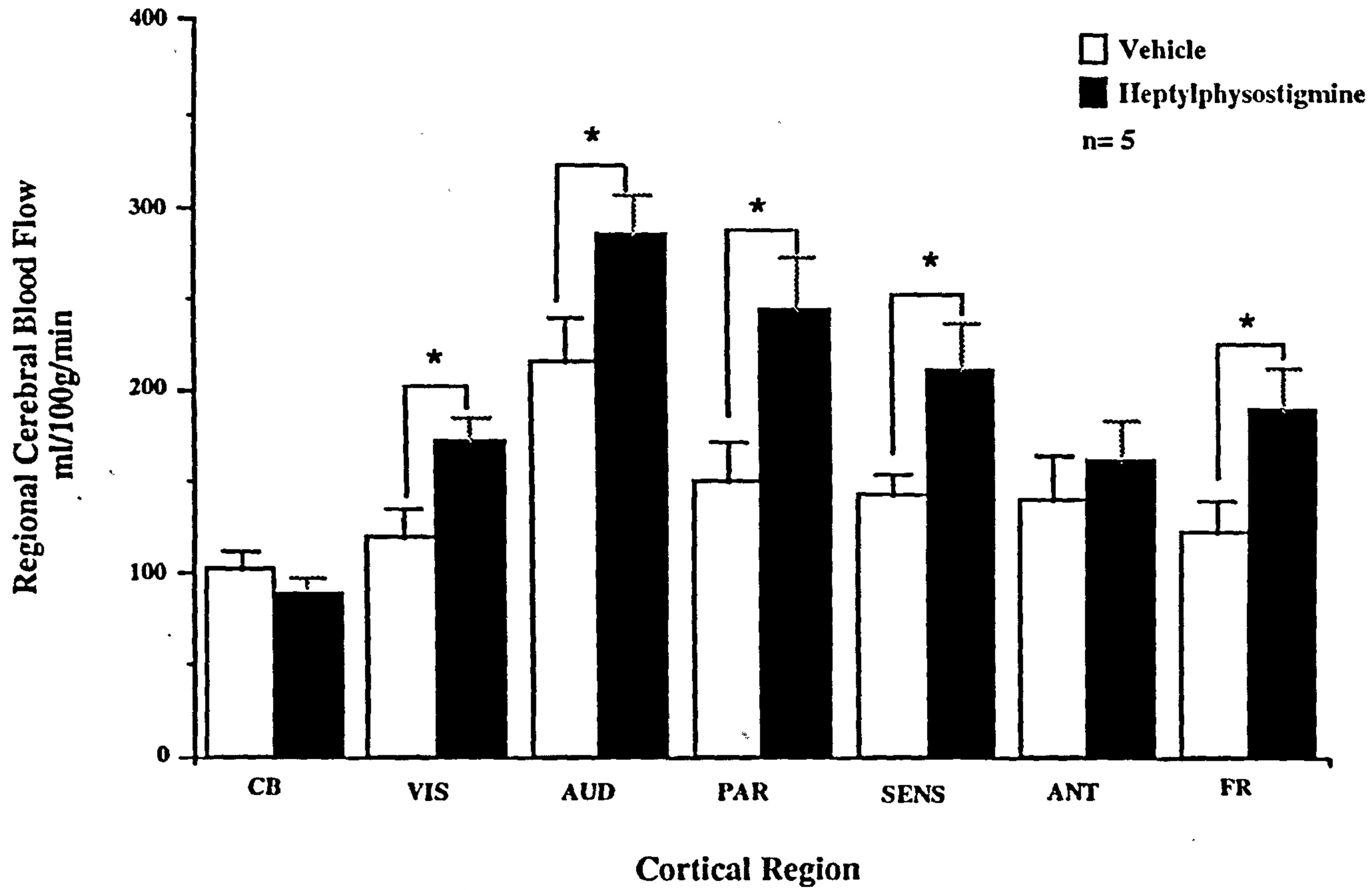


**Fig 36:** Regional cerebral blood flow in cortical regions of the conscious rat 2 hours after vehicle or heptylphysostigmine administration. Heptylphysostigmine increases blood flow in 5 out of 7 cortical regions analysed with significant increases observed in the visual cortex (VIS), auditory cortex (AUD), parietal cortex (PAR), sensory motor cortex (SENS) and frontal cortex (FR). *P <0.05 Student's unpaired t-test. Data are expressed as mean ± S.E.M. ml per 100g brain per minute n= number of animals in each group[. CB= cerebellar cortex, ANT= anterior cingulate cortex.

## Heptylphysostigmine Increases Cerebral Blood Flow In The Conscious Rat

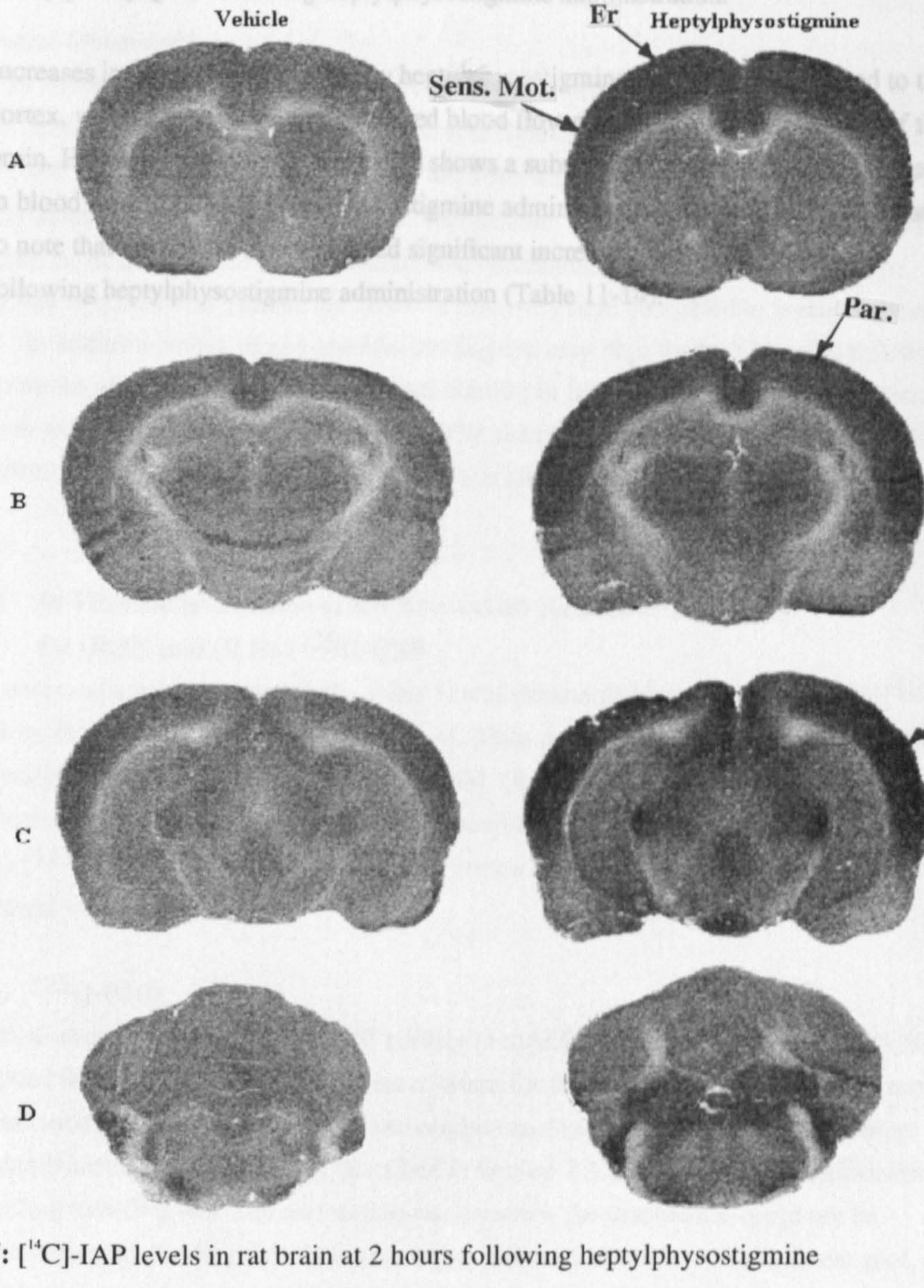


**Fig 37:** [$^{14}$C]-IAP levels in rat brain at 2 hours following heptylphysostigmine administration. Autoradiograms show [$^{14}$C]-IAP at the level of the caudate nucleus (A), dorsolateral hippocampus (B), auditory cortex (C) and cerebellum (D). Heptylphysostigmine significantly increased in cerebral blood flow in a number of cortical regions including the frontal cortex (Fr), sensory motor cortex (Sens.Mot.), auditory cortex (Aud) and parietal cortex (Par). [$^{14}$C]-IAP levels in cortical regions of heptylphysostigmine treated animals are notably higher.

blood flow correspond to those regions observed to have increased levels of (R,S)- and (R,R)-[$^{125}$I]-QNB following heptylphysostigmine administration.

Increases in blood flow produced by heptylphysostigmine appear to be restricted to the cortex, with no general pattern of altered blood flow obvious throughout the rest of the brain. However, the superior colliculus shows a substantial but non-significant increase in blood flow following heptylphysostigmine administration (Table 15). It is interesting to note that this region also displayed significant increases in (R,R)-[$^{125}$I]-QNB following heptylphysostigmine administration (Table 11-14).

## 3.3 *IN VITRO* AUTORADIOGRAPHIC RESULTS

### General Observations

Fig 38 shows illustrative autoradiograms of (R,S)- and (R,R)-[$^{125}$I]-QNB binding to rat brain sections *in vitro*. Regional distribution of ligand *in vitro* is generally similar to that observed *in vivo* . High levels of activity are observed in the caudate, with uniformly high levels observed in the cortex and high to intermediate levels observed in the hippocampal formation. Activity levels in the thalamus and cerebellum although lower than those observed in cortex and caudate are however relatively high compared to levels observed *in vivo*. In addition levels of non-specific binding are very high for both ligands, constituting a minimum of approximately 50 % of total binding in the majority of studies performed despite extensive post incubation washing. The calculated *in vitro* association rate and equilibrium dissociation constants for (R,S)- and (R,R)-[$^{125}$I]-QNB are presented in Table 16.

### 3.3.1 *In Vitro* Determination of the Association Rate Constant for (R,S)- and (R,R)-[$^{125}$I]-QNB

The observed association rate (kobs, mins$^{-1}$) was determined for (R,S)- and (R,R)-[$^{125}$I]-QNB by *in vitro* autoradiographic analysis of 20µm coronal rat brain sections following incubation for 2 hours with 0.1 nM and 0.2 nM (R,S)- and (R,R)-[$^{125}$I]-QNB respectively. Complete tables for total, non-specific and specific binding of (R,S)- and (R,R)-[$^{125}$I]-QNB to frontal cortex, parietal cortex, caudate nucleus and cerebellum are displayed in Appendix D.

#### (R,S)-[$^{125}$I]-QNB

The time course of (R,S)-[$^{125}$I]-QNB binding to mAChRs *in vitro* from 1-120 mins is presented in Fig 39. The association rate constant for frontal cortex (kobs= 0.0156 min$^{-1}$), parietal cortex (kobs= 0.0303 min$^{-1}$) and caudate nucleus (kobs= 0.0105 min$^{-1}$) were calculated according to the theory described in section 2.3.2 from a linear transformation of binding data (Fig 40). The association rate constant for cerebellum could not be determined as the binding data from this region did not transform well to a linear plot, possibly due to the high levels of non-specific binding observed in this region. Comparison of regional association rates indicates that (R,S)-[$^{125}$I]-QNB displays more rapid binding to cortex than caudate, with the rate of association approximately 3 fold faster in the parietal cortex than in the caudate nucleus

#### (R,R)-[$^{125}$I]-QNB

Association rate constants for (R,R)-[$^{125}$I]-QNB in frontal cortex (kobs= 0.0185 min-1), parietal cortex (kobs= 0.0203 min-1) and caudate nucleus (kobs= 0.0462 min -1) were

determined in an identical manner to those for (R,S)-[$^{125}$I]-QNB. Time course of (R,R)-[$^{125}$I]-QNB binding to mAChRs and linear transformation of this data to yield association rate constants are displayed in Figs 41 and 42. As with (R,S)-[$^{125}$I]-QNB the association rate constant for cerebellum could not be determined due to the non-linearity of transformed data. Comparison of regional association rates indicates that (R,R)-[$^{125}$I]-QNB displays most rapid association kinetics in the caudate nucleus , with the rate of association 2.5 fold faster than in the frontal cortex

**Comparison of association rates for (R,S)- and (R,R)-[$^{125}$I]-QNB**

The *in vitro* association kinetics for (R,S)- and (R,R)-[$^{125}$I]-QNB display some subtle differences. In cortical regions kobs is broadly similar between the two ligands, with the rate of association of (R,R)-[$^{125}$I]-QNB less than twofold faster i.e. (R,S) kobs= 0.0156 $min^{-1}$ and 0.0303 $min^{-1}$ and (R,R) kobs= 0.0185 $min^{-1}$ and 0.0203 $min^{-1}$ for frontal and parietal cortices respectively.

In the caudate nucleus however, kobs of (R,R)-[$^{125}$I]-QNB is more than four fold faster than that of (R,S)-[$^{125}$I]-QNB i.e. kobs= 0.0105 $mins^{-1}$ and 0.0462 $mins^{-1}$ for (R,S)- and (R,R) respectively.

## Table 16

### Association Rate Constants and Equilibrium Dissociation Constants for (R,S)- and (R,R)-[$^{125}$I]-QNB Determined by *In Vitro* Autoradiography

| Region | | (R,S)-[$^{125}$I]-QNB | (R,R)-[$^{125}$I]-QNB |
|---|---|---|---|
| Frontal Cortex | kobs (mins$^{-1}$) | 0.0156 | 0.0185 |
| | KD (nM) | 0.036 | 0.226 |
| | | | |
| Parietal Cortex | kobs | 0.0303 | 0.0203 |
| | KD | 0.050 | 0.115 |
| | | | |
| Caudate Nucleus | kobs | 0.0105 | 0.0462 |
| | KD | 0.028 | 0.206 |

Tables show association rate constant ($k_{obs}$) and equilibrium dissociation rate constant (KD) for (R,S)- and (R,R)-[$^{125}$I]-QNB binding to mAChRs in rat brain sections as determined by *in vitro* autoradiography in this thesis .Rate constant values determined by *in vitro* autoradiography in this thesis are consistent with literature values determined by binding to transfected cell membranes.

## (R,S)- and (R,R)-[$^{125}$I]-QNB In Rat Brain Sections *In Vitro*

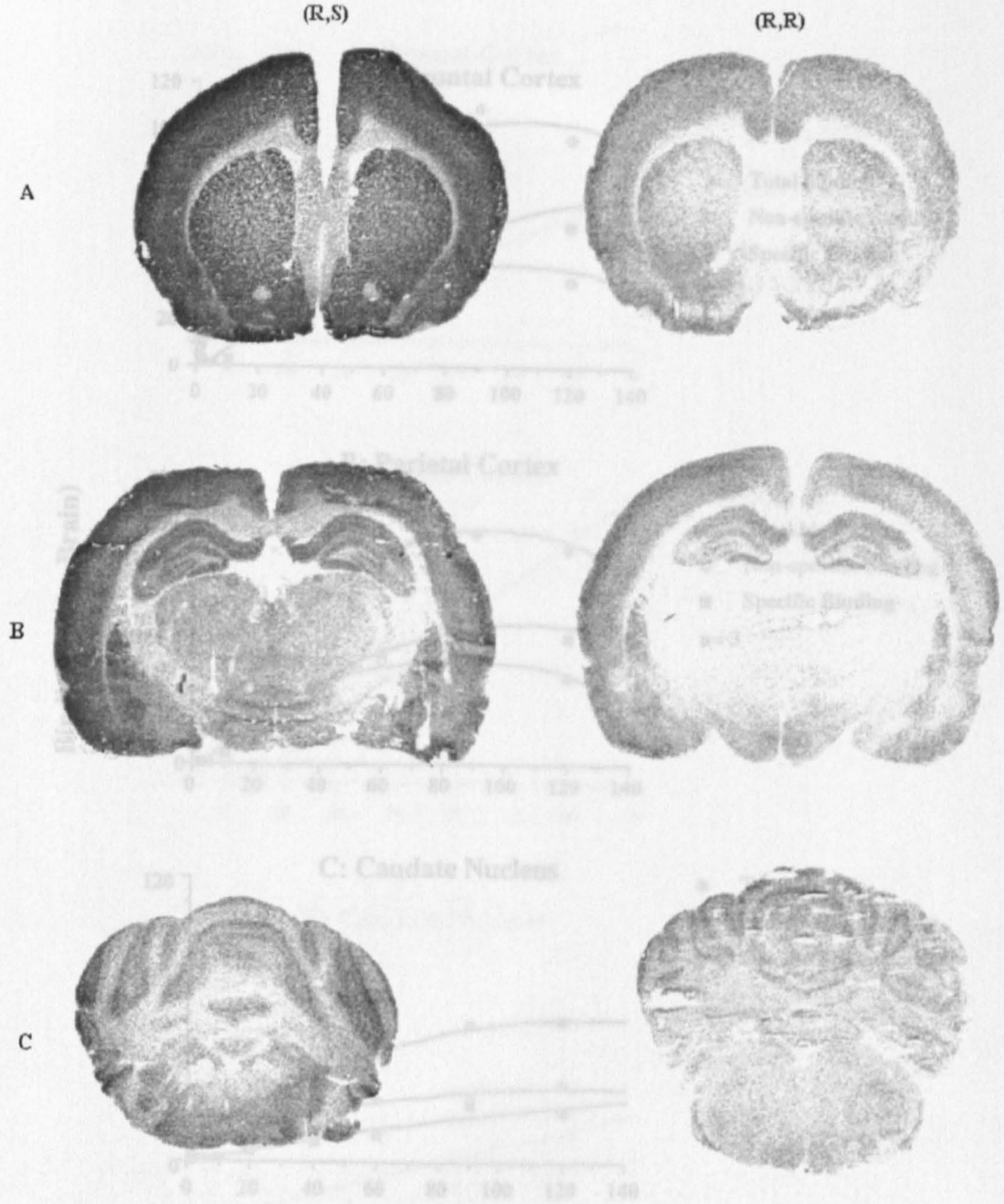


**Fig 38:** (R,S)- and (R,R)-[$^{125}$I]-QNB in rat brain sections *in vitro*.

Autoradiograms show (R,S)- and (R,R)-[$^{125}$I]-QNB at the level of the caudate nucleus (A), dorsolateral hippocampus (B) and cerebellum (C). Regional distribution of ligand *in vitro* corresponds to that observed *in vivo* and to regional mAChR distribution. High levels of activity are observed in the cortex and caudate and intermediate levels are observed in the thalamus. Activity levels in the cerebellum although lower than in cortex are higher than would be expected considering the relatively low mAChR density of this region.

## *In Vitro* Association of (R,S)-[$^{125}$I]-QNB to Muscarinic Receptors

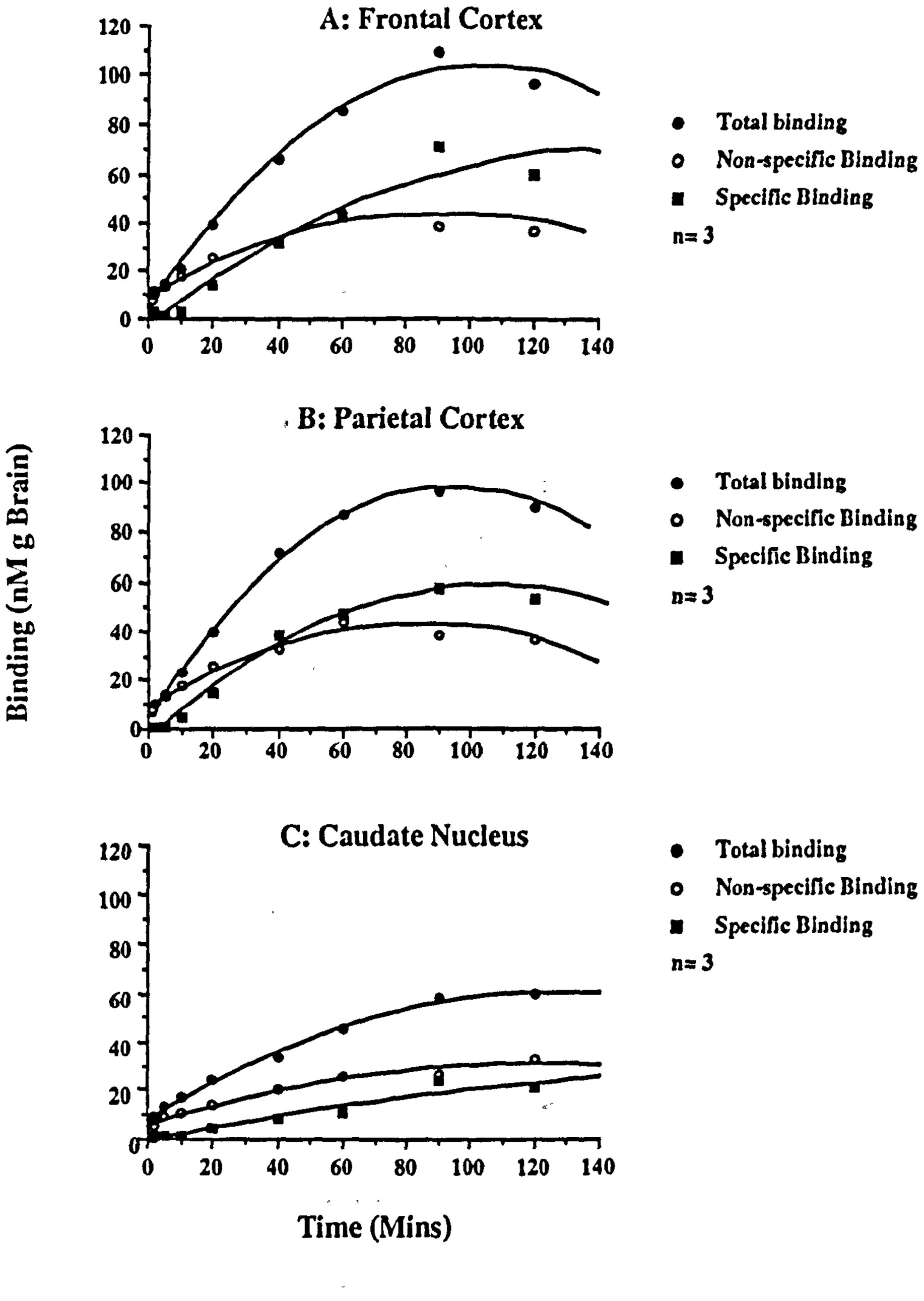


**Fig 39:** Time course of of (R,S)-[$^{125}$I]-QNB(0.1 nM) binding to mAChRS showing total (●), non-specific (o) and specific (■) binding in frontal cortex (A), parietal cortex (B) and caudate nucleus (C) of 20 µm coronal rat brain sections as determined by *in vitro* autoradiography. Binding is expressed as mean nmols per g of Brain from 3 individual experiments. Values for S.E.M are not shown as they would obscure the data points.

## Graphical Determination of Observed Association Rate Constant for (R,S)-[$^{125}$I]-QNB *in vitro*

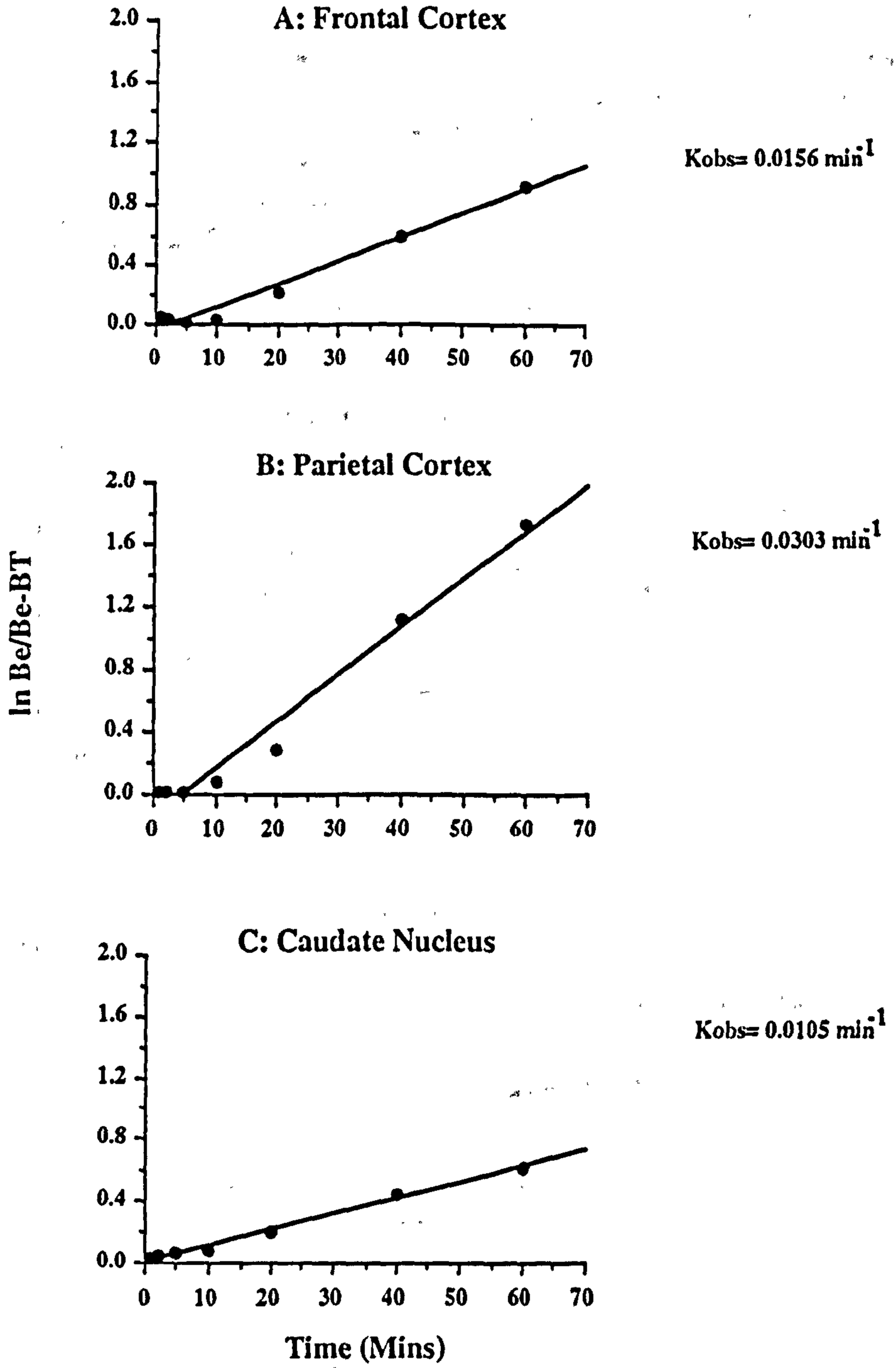


**Fig 40:** Linear transformation of association specific binding of (R.S)-[$^{125}$I]-QNB to frontal cortex (A), parietal cortex (B) and cauate nucleus (C) mAChRs in 20 µm coromal rat brain sections *in vitro*. Association assays were performed with 0.1 nM (R,S)-[$^{25}$ I]-QNB over 120 mins, with kobs calculated for each region from the mean of 3 individual assays as described in section 2.3.2. kobs= 0.0156 mins$^{-1}$, 0.0303 mins$^{-1}$ and 0.0105 mins$^{-1}$ for frontal cortex, parietal cortex and caudate nucleus respectively.

## *In Vitro* Association of (R,R)-[$^{125}$I]-QNB to Muscarinic Receptors

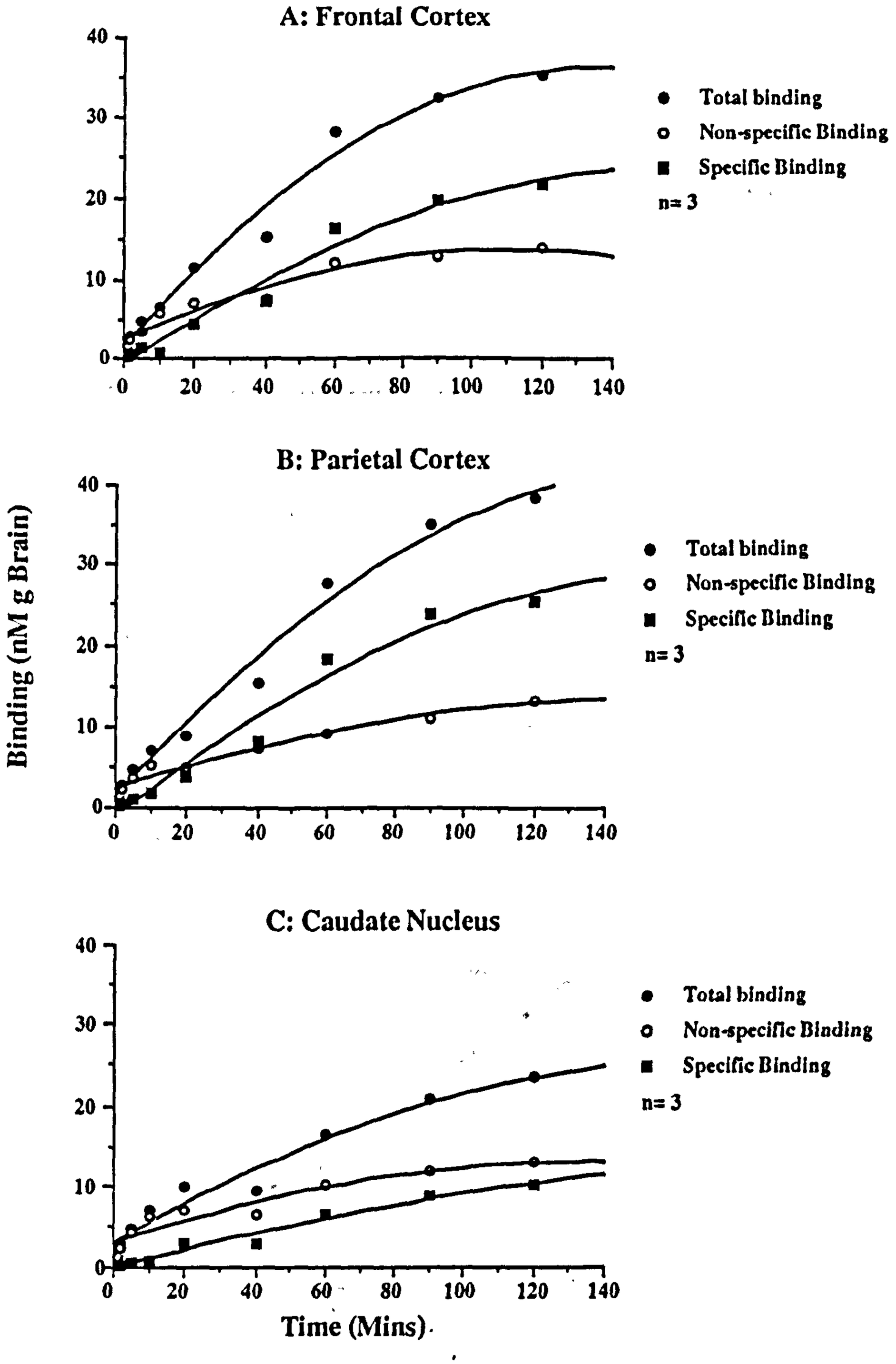


**Fig 41:** Time course of of (R,R)-[$^{125}$I]-QNB(0.2 nM)binding to mAChRS showing total (•), non-specific (○) and specific (■) binding in frontal cortex (A), parietal cortex (B) and caudate nucleus (C) of 20 µm coronal rat brain sections as determined by *in vitro* autoradiography. Binding is expressed as mean nmols per g of Brain from 3 individual experiments. Values for S.E.M are not shown as they would obscure the data points.

## Graphical Determination of Observed Association Rate Constant for (R,R)-[$^{125}$I]-QNB *in vitro*

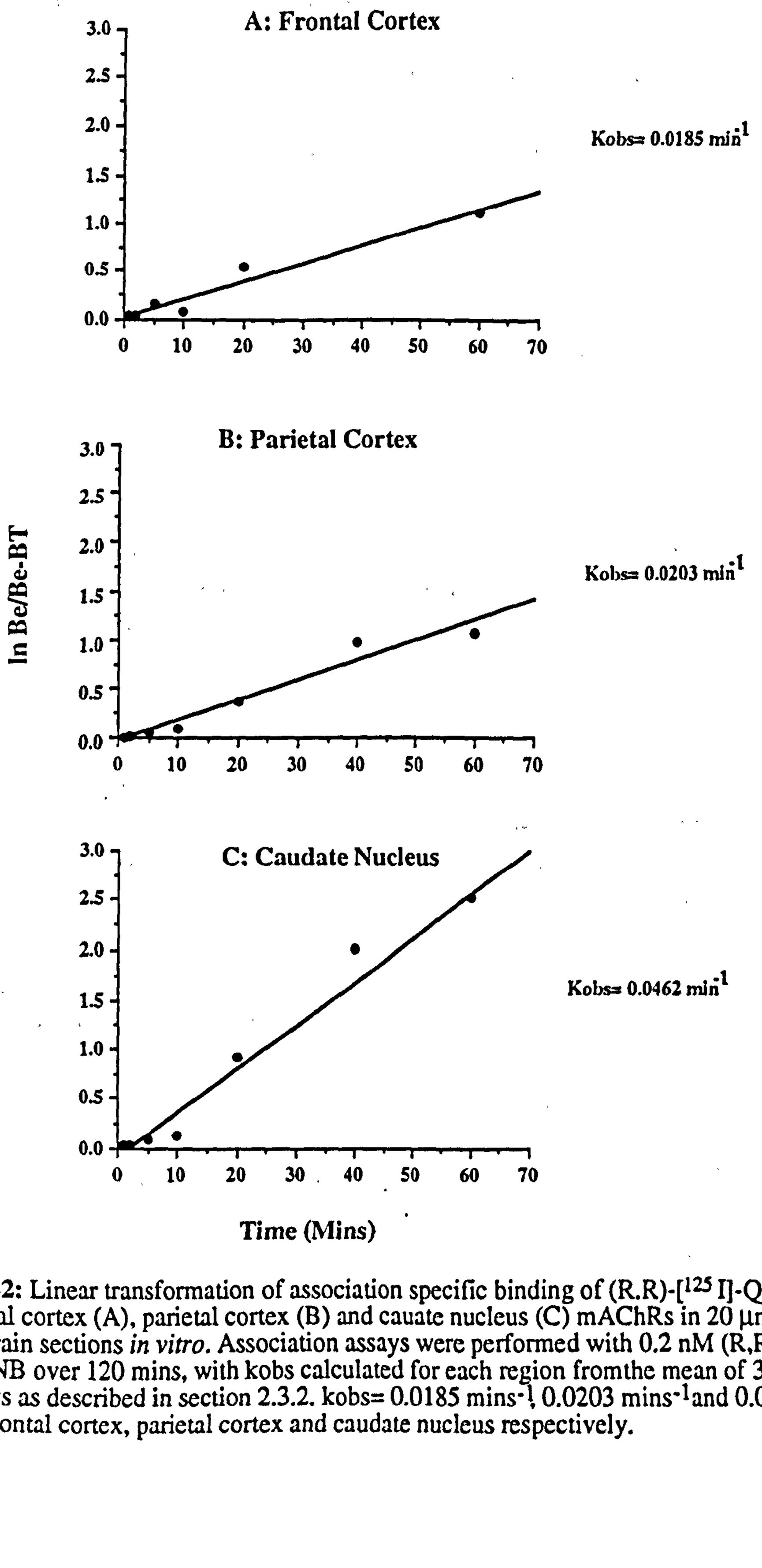


**Fig 42:** Linear transformation of association specific binding of (R.R)-[$^{125}$I]-QNB to frontal cortex (A), parietal cortex (B) and cauate nucleus (C) mAChRs in 20 µm coronal rat brain sections *in vitro*. Association assays were performed with 0.2 nM (R,R)-[$^{125}$I]-QNB over 120 mins, with kobs calculated for each region fromthe mean of 3 individual assays as described in section 2.3.2. kobs= 0.0185 mins$^{-1}$, 0.0203 mins$^{-1}$and 0.0462 mins$^{-1}$ for frontal cortex, parietal cortex and caudate nucleus respectively.

### 3.3.2 *In Vitro* Determination of the Equilibrium Dissociation Constant for (R,S)- and (R,R)-[$^{125}$I]-QNB.

The equilibrium dissociation constant ($K_D$ nM) was determined for (R,S)- and (R,R)-[$^{125}$I]-QNB by *in vitro* autoradiographic analysis of 20µm coronal rat brain sections following incubation for 1 hour with 0.007nM-0.1 nM (R,S)- and (R,R)-[$^{125}$I]-QNB . Tables of total, non-specific and specific binding for (R,S)- and (R,R)-[$^{125}$I]-QNB are presented in Appendix D.

**(R,S)-[$^{125}$I]-QNB**

Saturation analysis of (R,S)- [$^{125}$I]-QNB binding to frontal cortex, parietal cortex and caudate nucleus of rat brain sections is shown in Fig 43.

The equilibrium dissociation constant (KD) was calculated as a single line according to Scatchard analysis for each region (Fig 44). Scatchard analysis indicates that (R,S)-[$^{125}$I]-QNB binds with high affinity ($K_D$ in the sub-nanomolar range) to mAChRs in frontal cortex ($K_D$= 0.036 nM), parietal cortex ($K_D$= 0.050 nM) and caudate nucleus ($K_D$= 0.028 nM). $K_D$ determination for cerebellum was not possible as binding data from this region was unsuitable for Scatchard analysis. $K_D$ values indicate that (R,S)-[$^{125}$I]-QNB displays similar affinity for receptors in each region with less than a 2 fold difference in affinity observed between frontal cortex , parietal cortex and caudate nucleus

**(R,R)-[$^{125}$I]-QNB**

Equilibrium dissociation rate constants for frontal cortex ($K_D$= 0.266 nM), parietal cortex ($K_D$=0.115nM) and caudate nucleus ($K_D$=0.206 nM) were determined for (R,R)-[$^{125}$I]-QNB in an identical manner to those for (R,S)-[$^{125}$I]-QNB. $K_D$ values for (R,R)-[$^{125}$I]-QNB indicate that this ligand also binds to mAChRs with high affinity and displays less than 2 fold difference in affinity for receptors between regions .As with (R,S)-[$^{125}$I]-QNB $K_D$ for cerebellum could not be determined. Saturation binding of (R,R)-[$^{125}$I]-QNB to frontal cortex, parietal cortex and caudate nucleus and Scatchard transformation of this data to allow calculation of $K_D$ is displayed in Fig 45 and 46 respectively.

**Comparison of equilibrium dissociation rates for (R,S)- and (R,R)-[$^{125}$I]-QNB**

Scatchard analysis indicates that both ligands display high affinity for mAChRs in frontal cortex , parietal cortex and caudate nucleus. However, (R,S)-[$^{125}$I]-QNB displays a 2.3 to 7.4 fold greater affinity for mAChRs than (R,R)-[$^{125}$I]-QNB across the regions , with greatest difference in affinity observed in the caudate nucleus i.e. $K_D$=0.028 nM and 0.206 nM for (R,S) and (R,R) respectively.

## *In Vitro* Saturation Binding of (R,S)-[$^{125}$I]-QNB

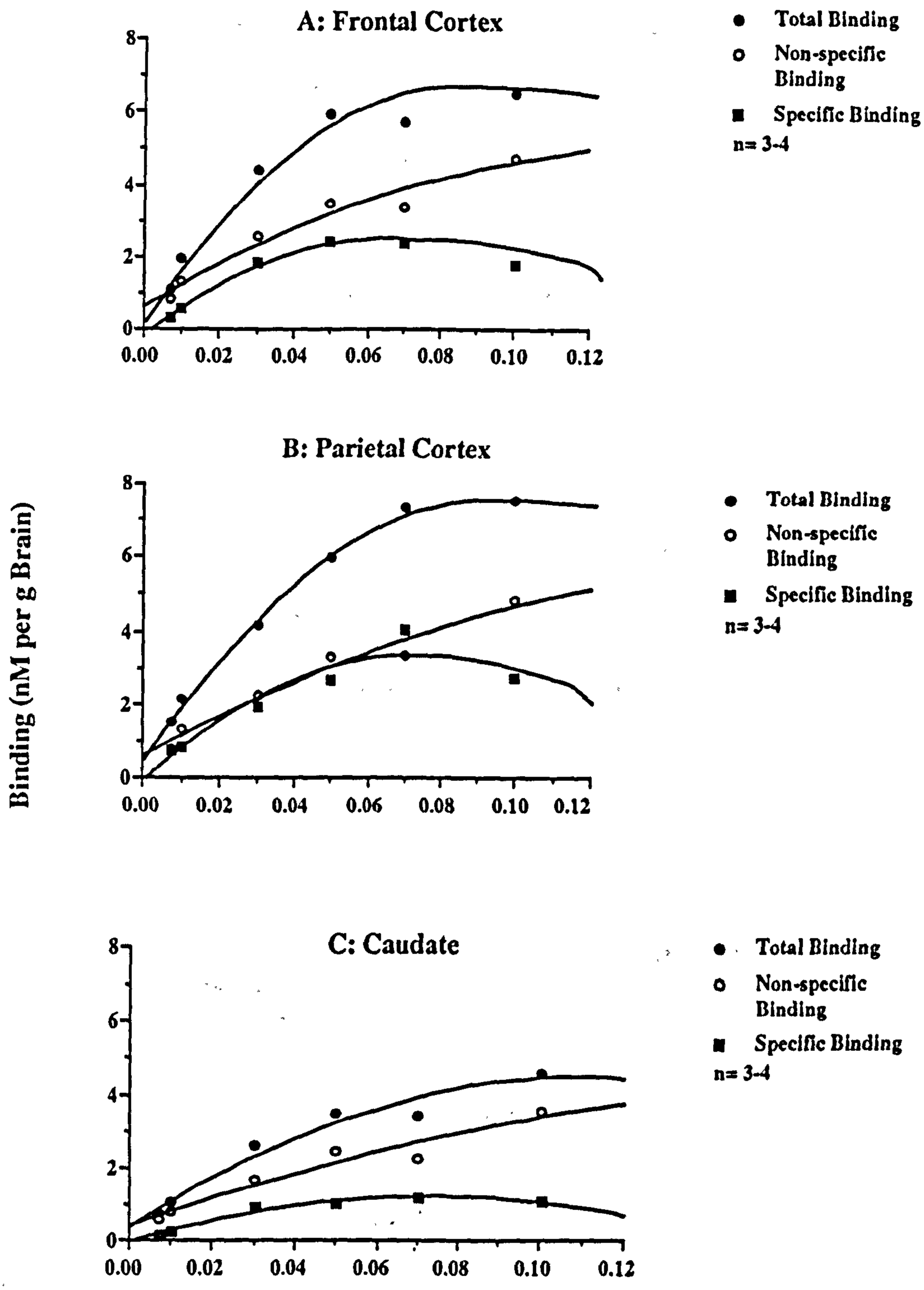


**Fig43:** Saturation curves showing total (●), non-specific (o) and specific (■) binding of (R,S)-[$^{125}$I]-QNB to mAChRs in frontal cortex (A), parietal cortex (B) and caudate nucleus (C) of 20 µm coronal rat brain sections as determined by *in vitro* autoradiography. Binding is expressed as mean nmols per g of Brain from 3-4 individual experiments. Values for S.E.M are not shown as they would obscure the data points.

## Graphical Determination of Equilibrium Dissociation Constant ($K_D$) for (R,S)-[$^{125}$I]-QNB *in vitro*

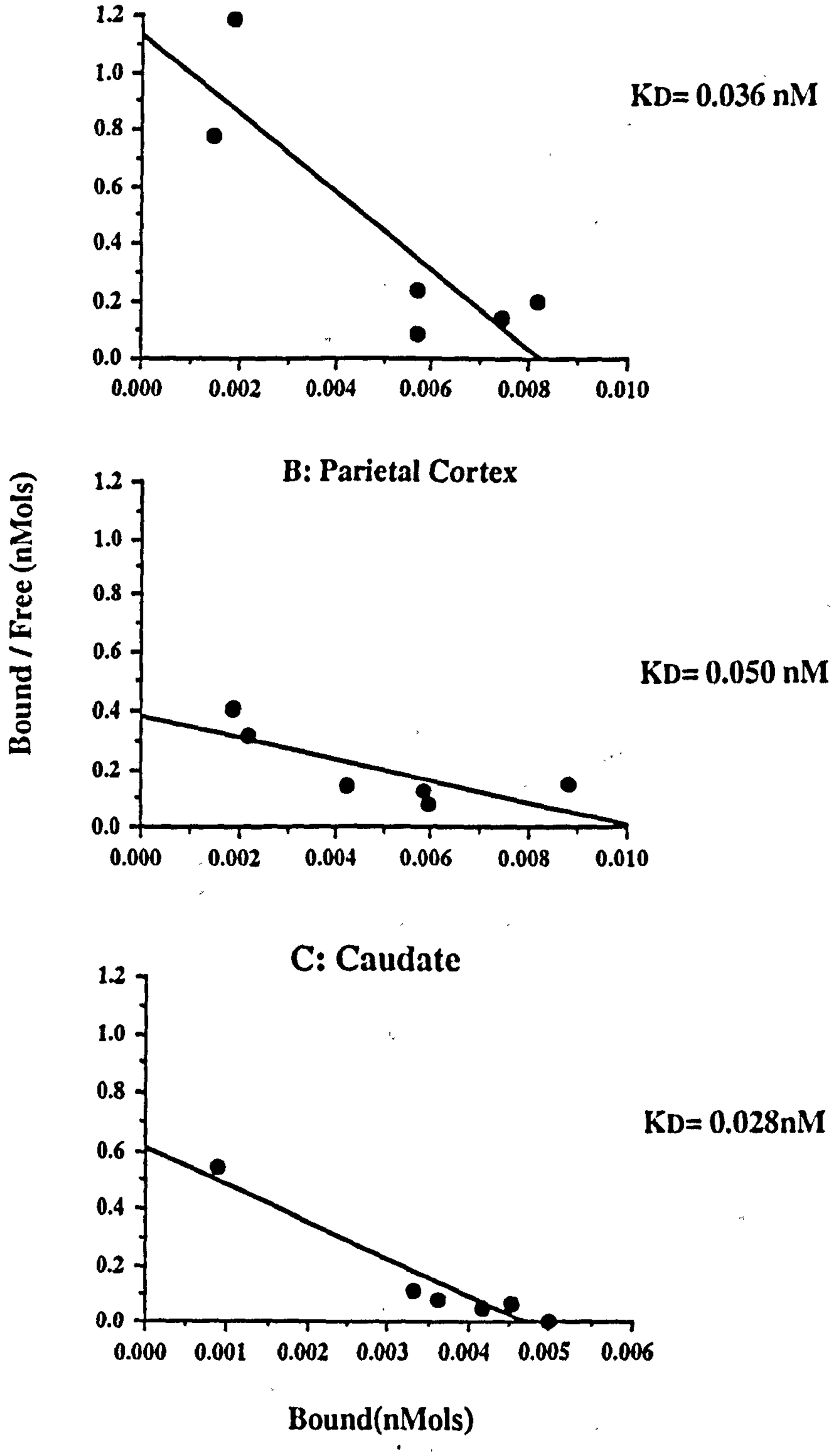


**Fig 44:** Representitative Scatchard plots of (R,S)-[$^{125}$I]-QNB binding to frontal cortex (A) , parietal cortex (B) and caudate nucleus (C) from a single experiment. The saturation binding experiments were carried out with (R,S)-[$^{125}$I]-QNB concentrations ranging from 0.007 to 0.1 nM with a 1 hour incubation period followed by Scatchard analysis. KD= 0.036nM, 0.050 nM and 0.028 nM for frontal cortex, pariteal cortex and caudate nucleus respectivley. KD values for each region were calculated from the mean data of 3-4 individual experiments.

## *In Vitro* Saturation Binding of (R,R)-[$^{125}$I]-QNB

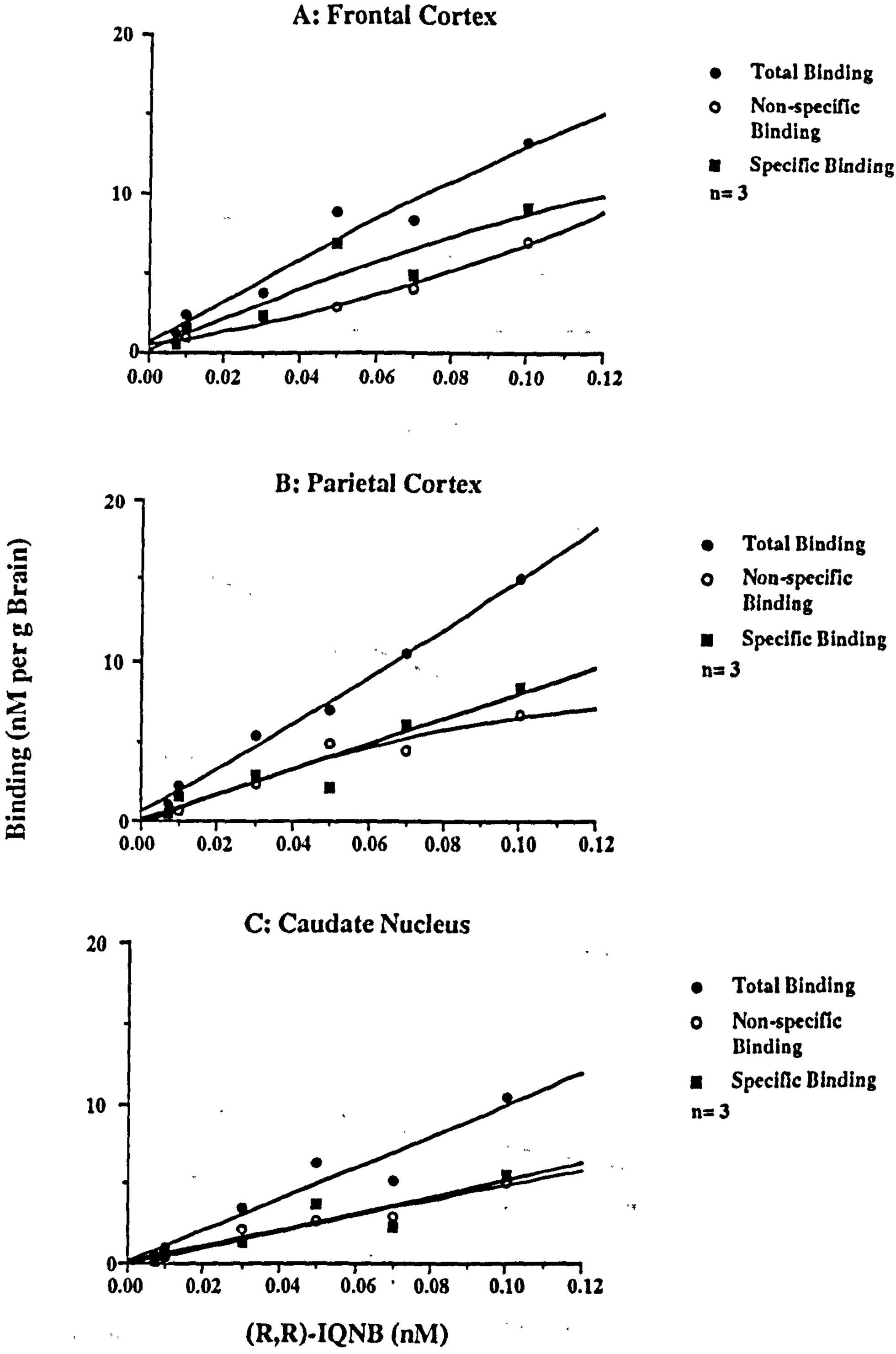


**Fig 45:** Saturation curves showing total (●), non-specific (○) and specific (■) binding of (R,R)-[$^{125}$I]-QNB to mAChRs in frontal cortex (A), parietal cortex (B) and caudate nucleus (C) of 20 µm coronal rat brain sections as determined by *in vitro* autoradiography. Binding is expressed as mean nmols per g of Brain from 3 individual experiments. Values for S.E.M are not shown as they would obscure the data points.

## Graphical Determination of Equilibrium Dissociation Constant ($K_D$) for (R,R)-[$^{125}$I]-QNB *in vitro*

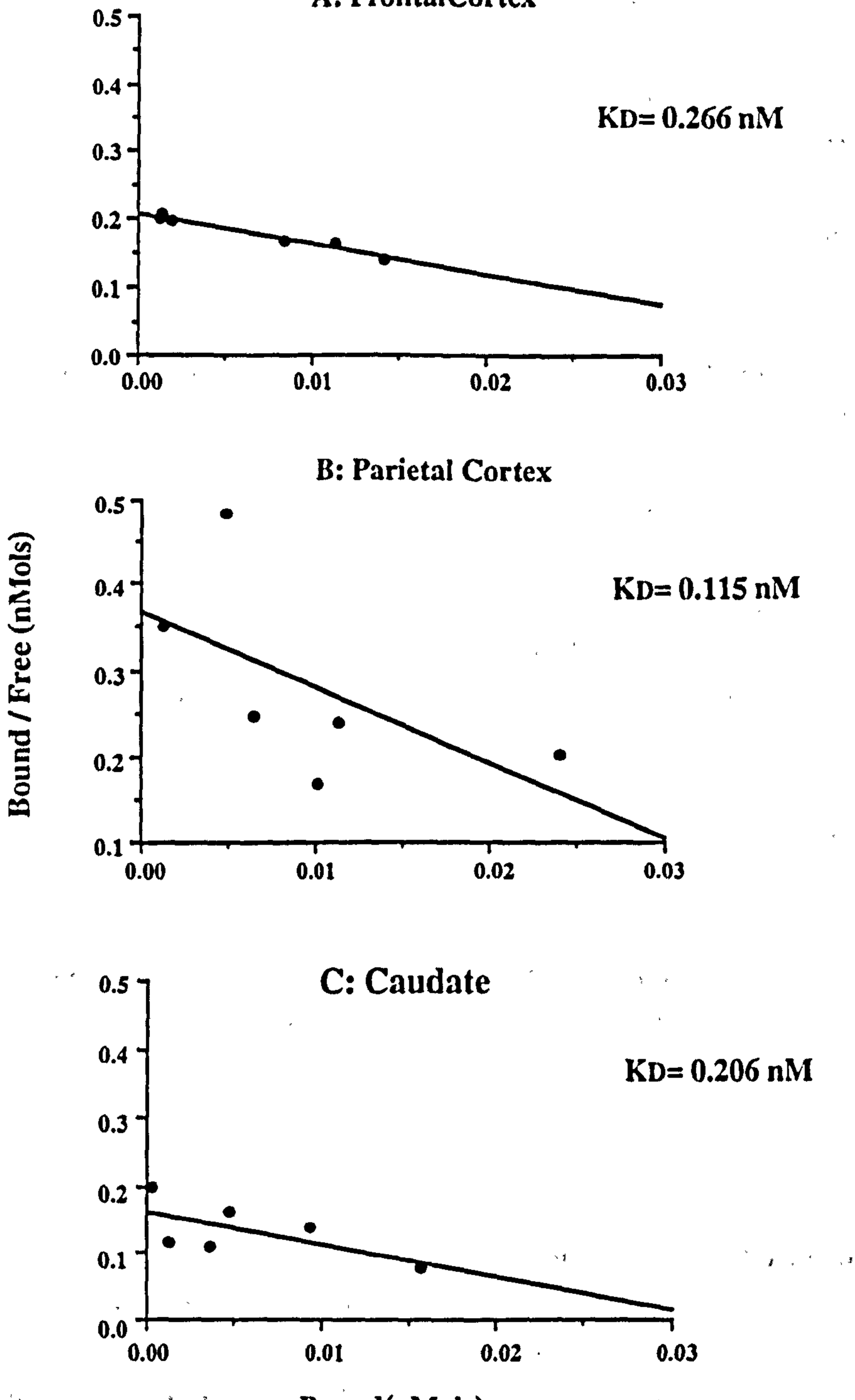


**Fig 46:** Representitative Scatchard plots of (R,R)-[$^{125}$I]-QNB binding to frontal cortex (A) , parietal cortex (B) and caudate nucleus (C) from a single experiment. The saturation binding experiments were carried out with (R,R)-[$^{125}$I]-QNB concentrations ranging from 0.007 to 0.1 nM with a 1 hour incubation period followed by Scatchard analysis. KD= 0.226nM, 0.115 nM and 0.206 nM for frontal cortex, parietal cortex and caudate nucleus respectivley. KD values for each region were calculated from the mean data of 3 individual experiments.

### 3.3.3 Effect Of Acetylcholine on Binding of (R,S)- and (R,R)-[$^{125}$I]-QNB to Rat Brain Sections *In Vitro* in the Presence of Heptylphysostigmine

The effect of ACh ($10^{-6}$ to $10^{-2}$M) on the binding of (R,S)- and (R,R)-[$^{125}$I]-QNB (0.1nM and 0.2 nM respectively) to 20µm coronal rat brain sections was determined by *in vitro* autoradiography in the presence of heptylphysostigmine ($10^{-6}$M). Tables of total. non-specific and specific binding for (R,S)- and (R,R)-[$^{125}$I]-QNB displacement studies are presented in Appendix D.

**Effect of Heptylphysostigmine on (R,R)-[$^{125}$I]-QNB binding *In Vitro***

Before investigation of the ability of ACh to displace (R,S)- and (R,R)-[$^{125}$I]-QNB binding *in vitro*, the effects of a range of concentrations of heptylphysostigmine ($10^{-3}$M, $10^{-4}$M and $10^{-6}$M) on the binding of (R,R)-[$^{125}$I]-QNB to rat brain sections *in vitro* was determined by autoradiography (Fig 47).

$10^{-3}$M heptylphysostigmine significantly reduced specific binding of (R,R)-[$^{125}$I]-QNB in rat brain sections at the level of the frontal cortex, parietal cortex and cerebellum. Reductions in specific binding of (R,R)-[$^{125}$I]-QNB were also observed with $10^{-4}$ M heptylphysostigmine but did not reach statistically significant levels. $10^{-6}$ M heptylphysostigmine had no effect on (R,R)-[$^{125}$I]-QNB binding , this concentration was therefore used in all subsequent *in vitro* displacement studies with (R,S)- and (R,R)-[$^{125}$I]-QNB.

**Effect of Acetylcholine on (R,S)- and (R,R)-[$^{125}$I]-QNB Binding *in vitro***

ACh ($10^{-5}$M to $10^{-2}$M) had no effect on (R,S)-[$^{125}$I]-QNB binding to rat rain sections at the level of the frontal cortex, parietal cortex and cerebellum (Fig 48). Similarly, ACh ($10^{-6}$M to $10^{-3}$M) had no effect on (R,R)-[$^{125}$I]-QNB binding to rat brain sections at the level of the frontal cortex, parietal cortex and cerebellum (Fig 49).

### 3.3.4 Acetylcholinesterase Activity in Rat Brain Sections *In Vitro* Following Heptylphysostigmine Administration

**Effect of Heptylphysostigmine ($10^{-6}$M) on AChE activity *in Vitro***

AChE activity in heptylphysostigmine treated sections and control sections taken from *in vitro* displacement studies with (R,S)- and (R,R)-[$^{125}$I]-QNB was determined by semi-quantitative histochemistry. Sections were processed for acetylcholinesterase activity to determine that inhibition of the enzyme was maintained throughout the duration of the assay.

$10^{-6}$ M heptylphysostigmine significantly inhibited AChE activity in frontal cortex,

parietal cortex and cerebellum in sections taken from displacement studies with (R,S)-[$^{125}$I]-QNB and in frontal and parietal cortex in sections taken from displacement studies with (R,R)-[$^{125}$I]-QNB (Fig 50). Illustrative sections stained for AChE are displayed in Fig 51. Inhibition of AChE activity is apparent by the residual level of staining observable in heptylphysostigmine treated sections compared to that in control sections.
Tables of regional AChE activity for (R,S)- and (R,R)-[$^{125}$I]-QNB displacement studies are presented in Appendix C.

## Heptylphysostigmine Displaces (R,R)-[$^{125}$I]-QNB from Rat Brain Sections *In Vitro* at High Concentrations

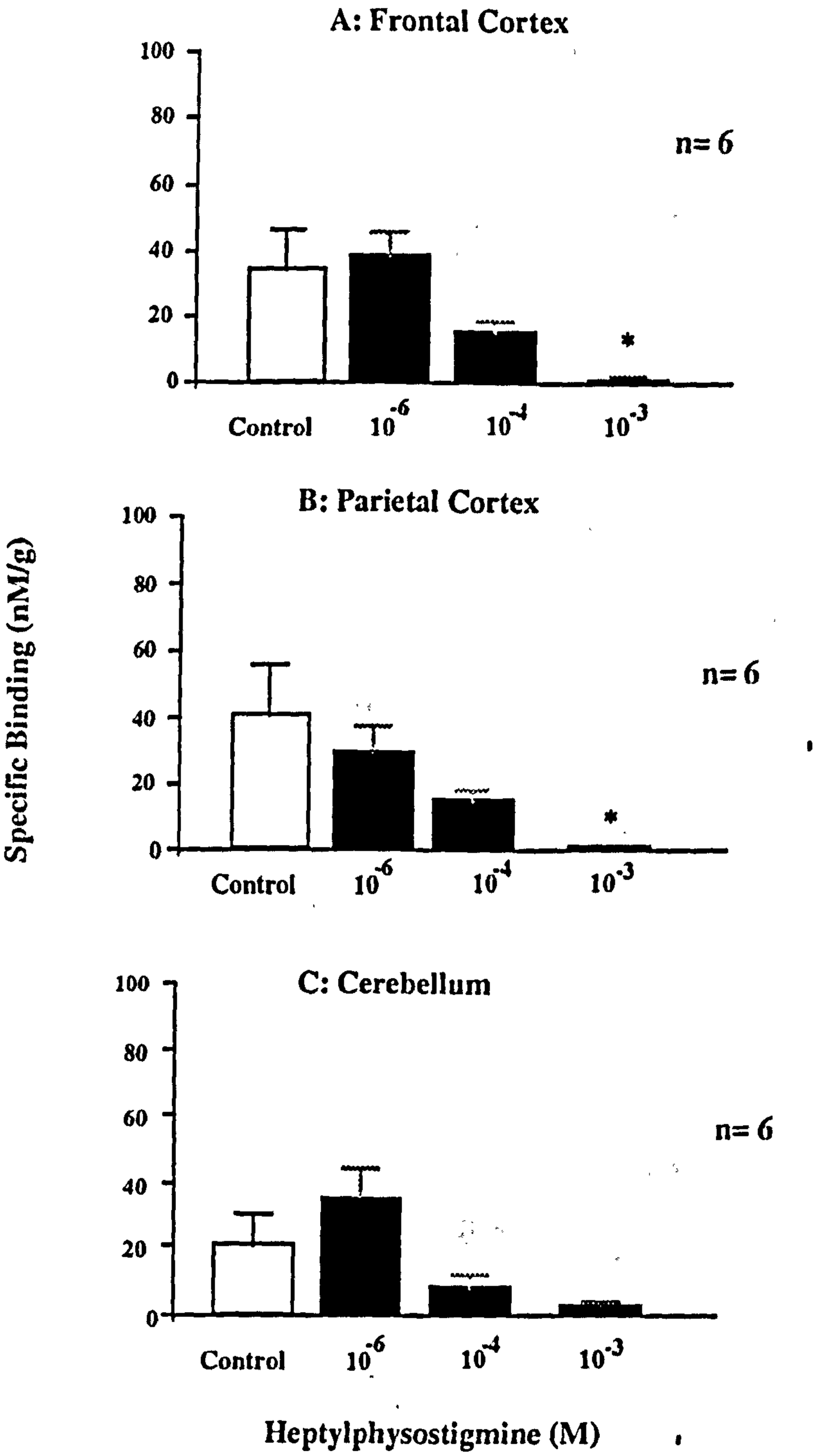


**Fig 47:** Specific binding of (R,R)-[$^{125}$I]-QNB (0.2 nM) to 20 µm coronal rat brain sections *in vitro*. Heptylphysostigmine ($10^{-3}$ M) reduces (R,R)-[$^{125}$I]-QNB in frontal cortex (A), parietal cortex (B) and cerebellum (C) of rat brain sections . *P <0.05 for statistical comparison between control and each concentration of heptylphysostigmine (ANOVA, Student's t-Test with Bonferroni Correction). Data are expressed as mean ± S.E.M nM per g brain of specifically bound ligand of 3 individual experiments.

## ACh Does not Displace (R,S)-[$^{125}$I]-QNB from Rat Brain Sections *In Vitro* in the Presence of Heptylphysostigmine

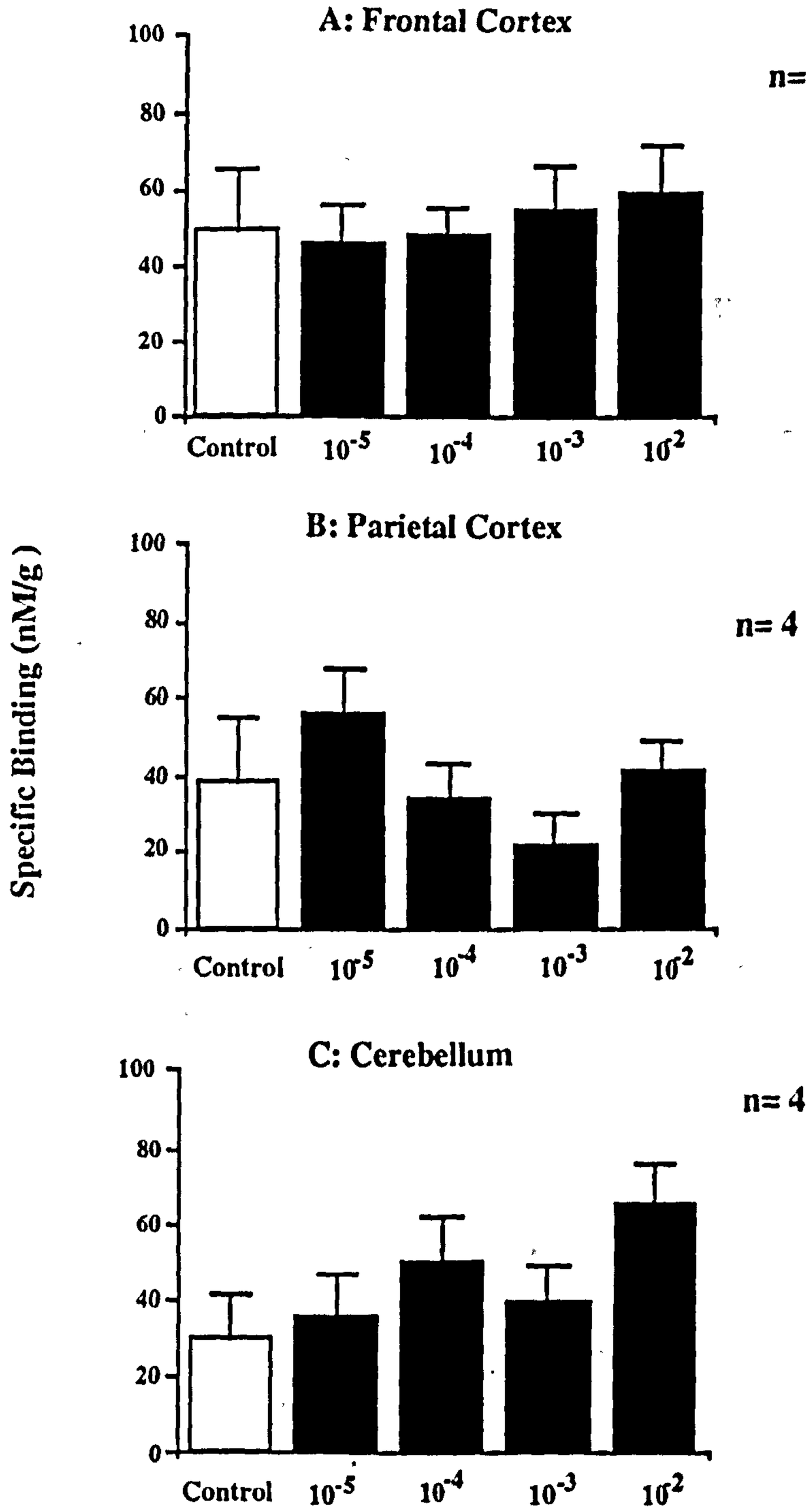


**Fig 48:** Specific binding of (R,S)-[$^{125}$I]-QNB(0.1 nM) to 20 µm coronal rat brain sections *in vitro*. ACh ($10^{-5}$ to $10^{-2}$ M) fails to displace (R,S)-[$^{125}$I]-QNB from frontal cortex (A), parietal cortex (B) and cerebellar cortex (C) of rat brain sections in the presence of heptylphysostigmine ($10^{-6}$M). Data are expressed as mean ± S.E.M nM per g brain of specifically bound ligand of 4 individual experiments.

## ACh Does not Displace (R,R)-[$^{125}$I]-QNB from Rat Brain Sections *In Vitro* in the Presence of Heptylphysostigmine

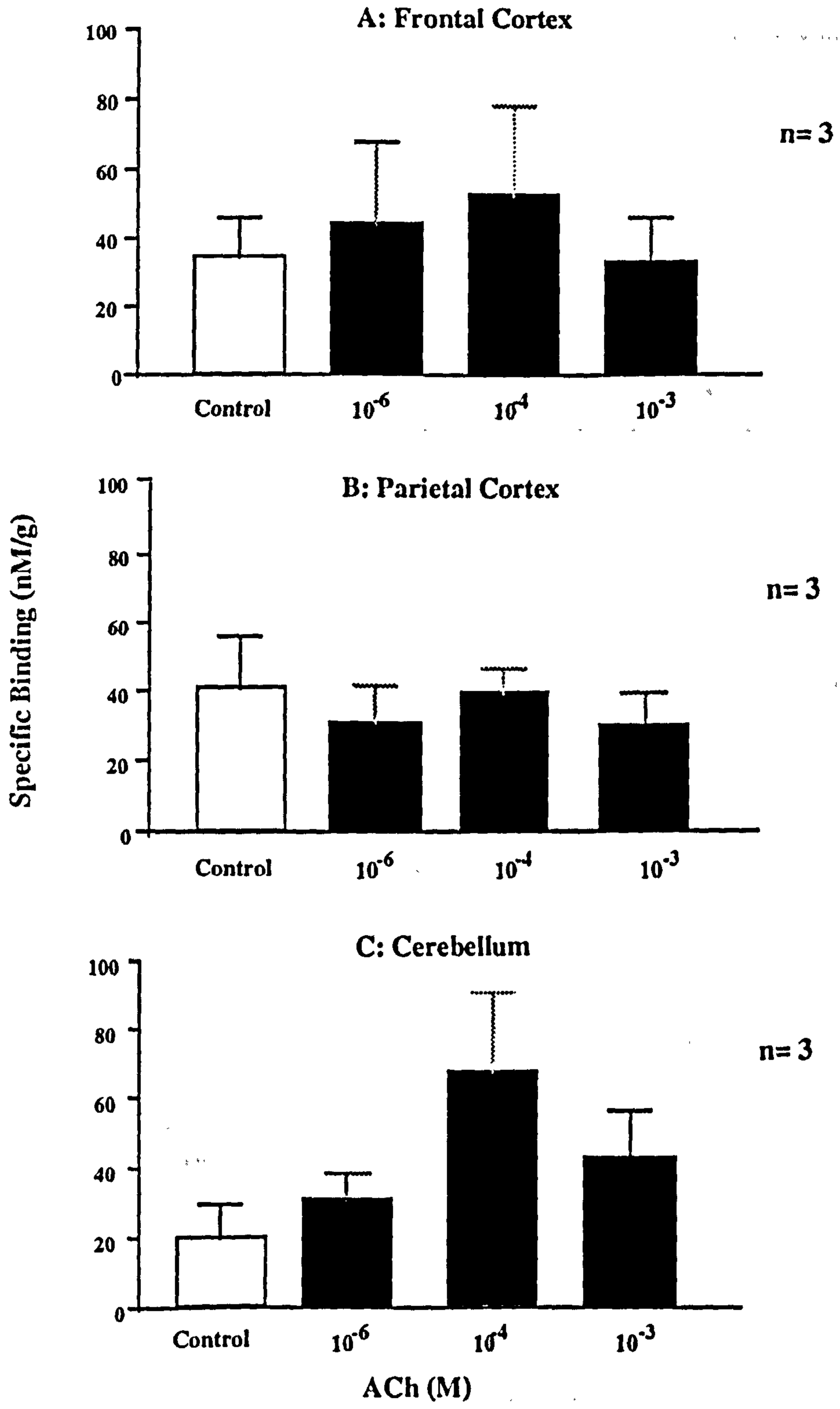


**Fig 49:** Specific binding of (R,R)-[$^{125}$I]-QNB(0.2 nM) to 20 µm coronal rat brain sections *in vitro*. ACh ($10^{-6}$ to $10^{-3}$ M) fails to displace (R,R)-[$^{125}$I]-QNB from frontal cortex (A), parietal cortex (B) and cerebellum (C) of rat brain sections in the presence of heptylphysostigmine ($10^{-6}$M). Data are expressed as mean ± S.E.M nM per g brain of specifically bound ligand of 3 individual experiments.

## Heptylphysostigmine Inhibits AChE Activity *In Vitro*

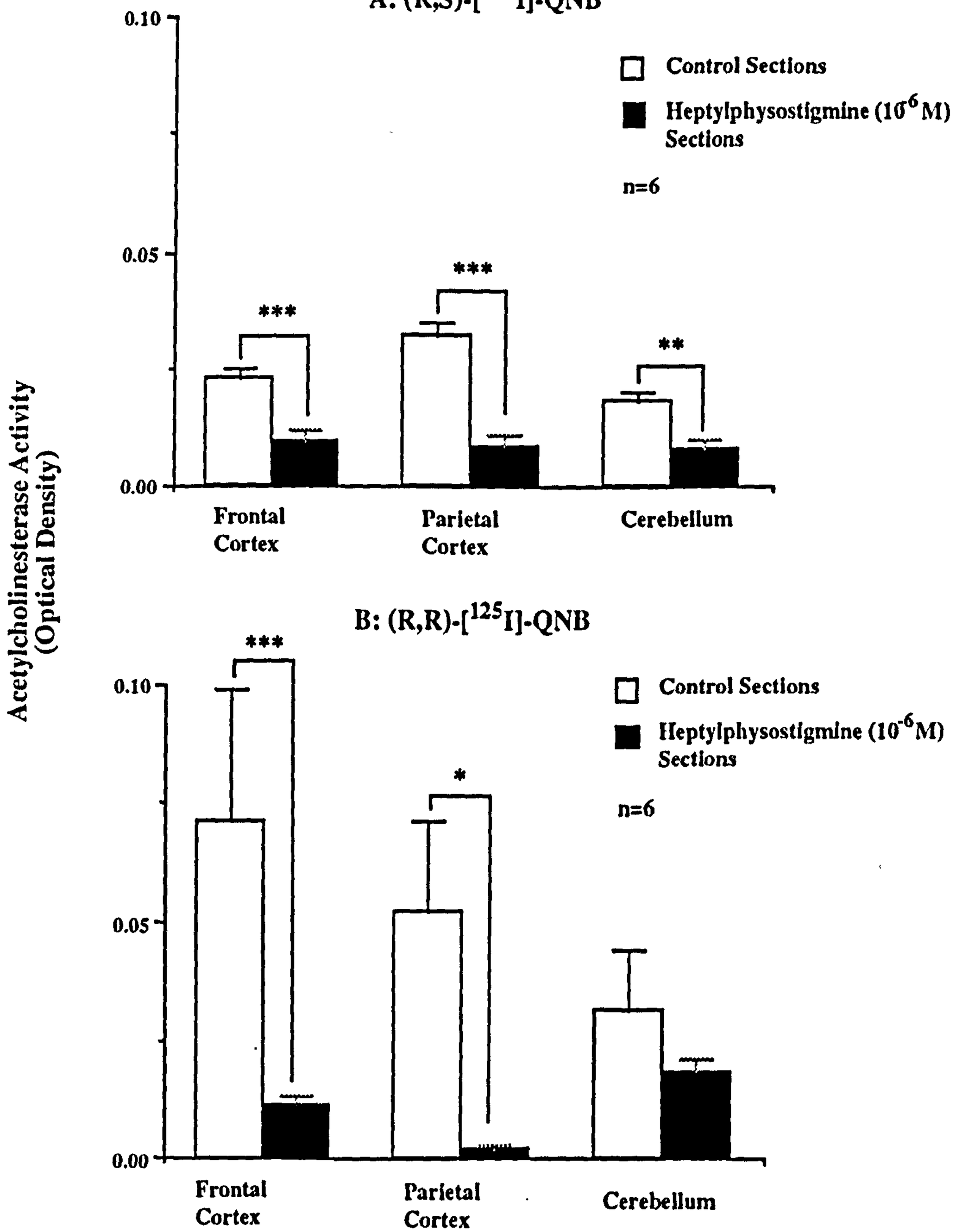


**Fig 50:** AChE enzyme activity measured by semi-quantitative histochemistry in untreated (control) and heptylphysostigmine ($10^{-6}$M) treated sections of rat brain taken from *in vitro* displacement studies with (R,S)- and (R,R)-[$^{125}$I]-QNB (Figs A and B respectively). Heptylphysostigmine inhibits enzyme activity in all regions analysed, with profound reductions observed in all regions in sections from (R,S)-[$^{125}$I]-QNB studies and in the frontal and parietal cortices in sections from (R,R)-[$^{125}$I]-QNB studies. *P <0.05, **P <0.01 and ***P <0.001 for the statistical comparison between control and heptylphysostigmine treated sections (Student's unpaired t-test). Data are expressed as mean ± S.E.M. optical density as a measure of staining intensity, n= number of sections analysed per region.

# Effect Of Heptylphysostigmine On AChE Activity *In Vitro*

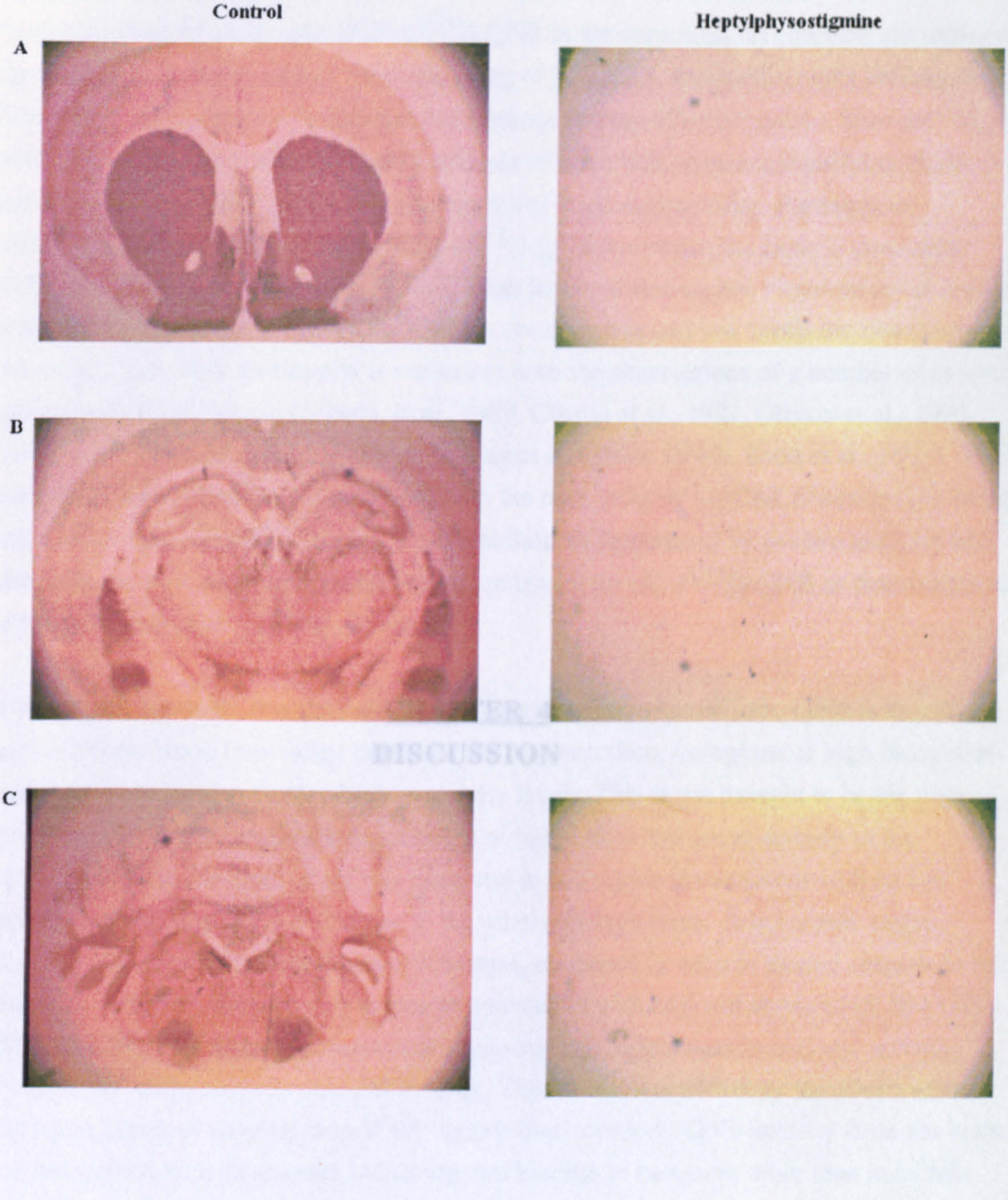


**Fig 51:** Figure shows AChE histochemical staining in rat brain sections at the level of the caudate nucleus (A), dorsolateral hippocampus (B) and cerebellum (C) taken from *in vitro* displacement experiments with (R,S)- and (R,R)-[$^{125}$I]-QNB. Heptylphysostigmine ($10^{-6}$ M) significantly inhibits AChE activity.

# CHAPTER 4
# DISCUSSION

## 4.1 (R,S)- AND (R,R)-[$^{125}$I]-QNB ARE SUITABLE LIGANDS FOR MAPPING MUSCARINIC CNS RECEPTORS *IN VIVO*

### Ligand Distribution *in vivo*

*In vivo* analysis of (R,S)- and (R,R)-[$^{125}$I]-QNB in the conscious rat confirms the utility of these ligands as *in vivo* agents for the imaging of mAChRs. Autoradiographs indicate that following intravenous administration both ligands display effective uptake from the plasma into the brain; with metabolite analysis of brain homogenates identifying (R,S)- and (R,R)-[$^{125}$I]-QNB as the sole constituents of brain radioactivity. Furthermore, regional localisation of (R,S)- and (R,R)-[$^{125}$I]-QNB activity in the brain is consistent with the known distribution of mAChRS. High levels of activity are observed in the cortex and caudate, moderate levels are observed in the thalamus and low levels are observed in the cerebellum. This distribution is consistent with the observations of a number of *in vivo* studies with these ligands (Gibson, et al., 1989, Gibson et al., 1991, Gibson et al., 1992, Gitler et al., 1995, McRee et al., 1995, Boulay et al, 1996a, 1996b, Sood et al., 1997). This pattern of *in vivo* distribution correlates with the rank order of mAChR concentration in the brain of caudate > cortex > thalamus > cerebellum as determined by *in vitro* analysis and also with the rank order of regional binding potential for (R)-[$^{125}$I]-QNB as determined *in vivo* by Sawada et al., (1990b).(Table 17).

It is possible however, that the regional uptake and distribution of iodo-QNB is dependent upon cerebral blood flow rather than mAChR concentration, as regions of high blood flow such as the cortex also display highest activity levels. This is not thought to be the case however, as there is significant dissociation of blood flow and tracer activity in the cerebellum. The low level of activity observed in this region is consistent with its low density of mAChRs but is in contrast to the relatively high blood flow for this region. Furthermore, regional cerebral blood flow rates, measured in vehicle treated animals in this thesis (section 3.2), show a poor degree of correlation with regional levels of (R,S)-[$^{125}$I]-QNB (Fig 52). It is therefore reasonable to assume that differences in regional activity levels reflect differences in mAChR binding. This view is supported by the observation that co-injection of unlabelled mAChR ligands displaces iodo-QNB activity from the brain in a non-region specific manner indicating that binding to receptors other than mAChRs does not contribute to the signal observed (Gitler et al., 1995, McRee et al., 1995, Lee et al., 1995).

### *In Vitro* Distribution and Binding Kinetics

Examination of the *in vitro* autoradiographs of (R,S)- and (R,R)-[$^{125}$I]-QNB binding to rat brain sections reveals that both ligands display regional distribution appropriate for CNS

## *In Vivo* Distribution of (R,S)- and (R,R)-[$^{125}$I]-QNB is Consistent with Regional mAChR Concentration

| Region | mAChR Concentration (nM) | Binding Potential (k3/k4) | (R,S)-QNB ROI/Caudate | (R,R)-QNB ROI/Caudate |
|---|---|---|---|---|
| | | | | |
| Caudate Nucleus | 57 | 1116 | 1.0 | 1.0 |
| Frontal Cortex | 45 | 1171 | 1.181 | 1.108 |
| Hippocampus | 37 | NA | 0.763 | 0.868 |
| Thalamus | 18 | 247 | 0.762 | 0.544 |
| Cerebellum | 5 | 51 | 0.108 | 0.102 |

**Table 17:** Comparison of mAChR concentration , binding potential for R-IQNB and (R,S)- and (R,R)-[$^{125}$I]-QNB level in caudate nucleus, frontal cortex, hippocampus, thalamus and cerebellum in rat brain. Regional distribution of (R,S)- and (R,R)-[$^{125}$I]-QNB as measured *in vivo* is generally consistent with mAChR concentration as determined *in vitro* and with the regional binding potential of R-IQNB as determined *in vivo* by Sawada et al., 1990b). *In vitro* mAChR concentration is expressed as the average concentration of m1,m2,m3 and m4 receptors in nM adapted from Table 2 in Boulay et al., (1996).

Regional binding potential for R-IQNB is equal to the ratio of the *in vivo* association rate constant (k3) and dissociation rate (k4) constant as determined by Sawada et al., (1990b) for R-IQNB in rat. Regional concentrations of (R,S)- and (R,R)-[$^{125}$I]-QNB are expressed as mean % Dose per g Brain normalised to the caudate nucleus (n= 5) measured at 2 hours after intravenous administration as measured in this thesis.

## Correlation Of Regional (R,S)-[$^{125}$I]-QNB Activity And Regional Cerebral Blood Flow

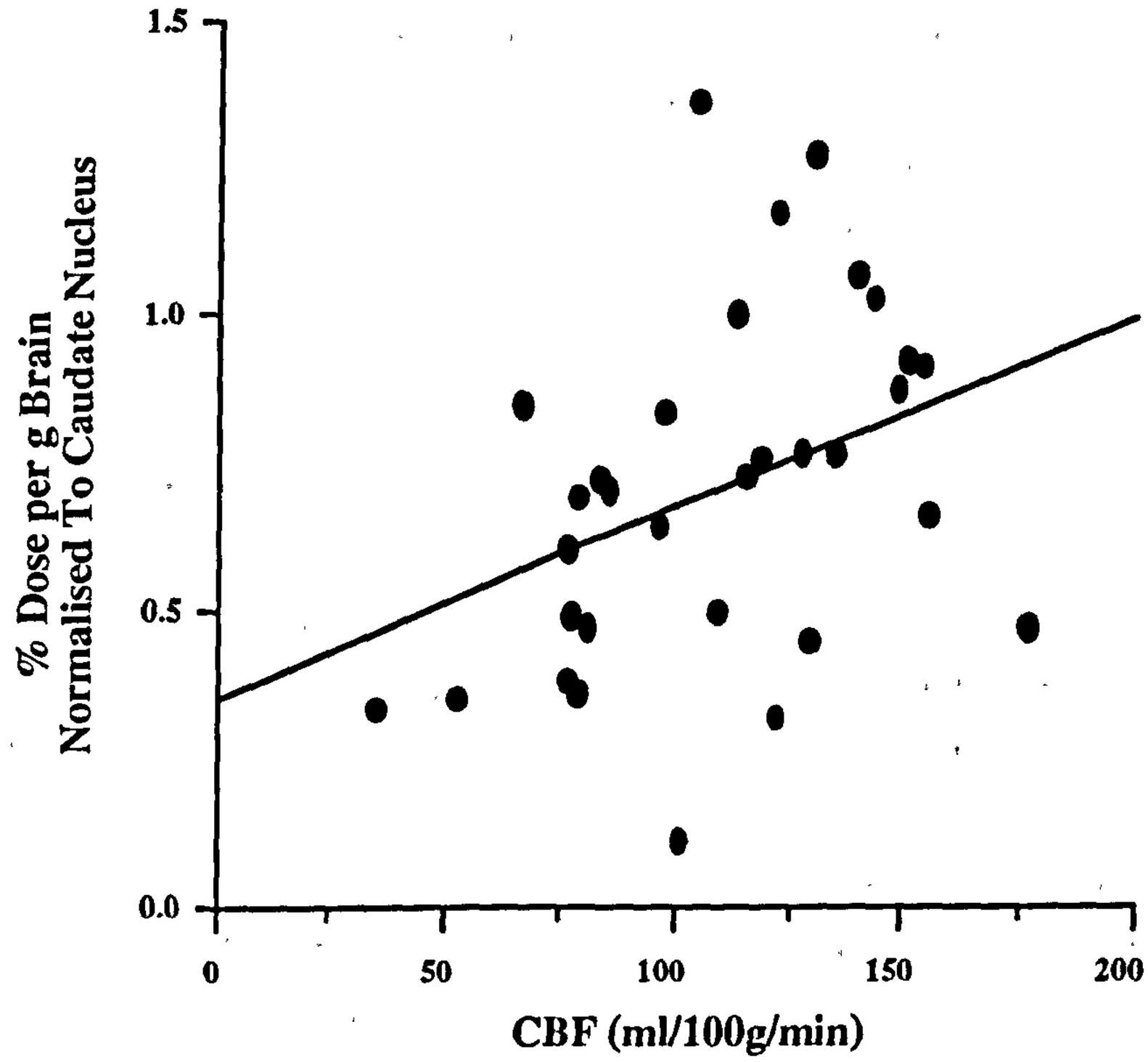


**Fig 52:** Figure shows a plot of (R,S)-[$^{125}$I]-QNB levels in 33 discrete rat brain regions at 2 hours against local cerebral blood flow rates for the same regions. A correlation coefficient of $r^2$=0.162 indicates that there is a low degree of association between regional cerebral blood flow and regional levels of (R,S)-[$^{125}$I]-QNB in the brain of the conscious rat. Data are expressed as mean % dose per g Brain, n= 5 for (R,S)-[$^{125}$I]-QNB and mean ml/100g/min n= 5 for CBF. Regional cerebral blood flow data was measured by [$^{14}$C]-IAP autoradiography in saline treated animals as described in section 3.2 in this thesis.

mAChRs, similar to that observed *in vivo* . Ligand distribution is heterogeneous, with high levels of binding observed in the cortex, caudate and the hippocampal formation with lower levels observed in the thalamus and cerebellum. The binding pattern is consistent with that of with [$^{3}$H]-QNB described by Nonaka and Moroji (1984) and with the distribution of the putative "M$_1$ sites" described by Mash and Potter (1986). These observations support the view that the pattern of (R,S)- and (R,R-[$^{125}$I]-QNB distribution observed *in vivo* reflects mAChR binding. However, the level of binding observed *in vitro* in the cerebellum in studies performed in this thesis is relatively high for the low mAChR concentration in this region. A high degree of non-specific binding is observed in all assays [see Appendix D] and is likely to be due to the high lipophilicity afforded to the ligand by iodination of the molecule. Post-incubation washing of sections is usually employed to reduce non-specific binding to increase signal to noise ratio. However, despite extended periods of post-incubation washing (30 mins) levels of non-specific binding remain high in assays with both (R,S)- and (R,R)-[$^{125}$I]-QNB. It is likely that this accounts in part for the unexpectedly high level of activity observed in the cerebellum.

Estimated equilibrium dissociation constants (KD) for both ligands are in the sub-nanomolar range in all regions analysed (0.036nM - 0.226 nM) indicating that both ligands display high affinity for mAChRs. Additionally, the association kinetics of the ligands are rapid enough to support their use *in vivo*, with kobs ranging from 0.0105 mins$^{-1}$ to 0.0462 mins$^{-1}$ between regions. The values for KD and kobs determined by *in vitro* autoradiography for (R,S)- and (R,R)-[$^{125}$I]-QNB are intended only as an approximation and it is recognised that the autoradiographic methodology employed in this thesis suffers from a number of disadvantages compared to homogenate binding which is accepted to produce more accurate data when characterising ligand binding *in vitro* .
Nevertheless, the *in vitro* binding kinetics of (R,S)- and (R,R)-[ $^{125}$I]-QNB presented in this thesis are in general agreement with the data from homogenate binding assays performed in a number of tissue preparations [Table 18 and 19] (Gibson, et al., 1984a, Gibson et al., 1989, Zeeberg et al., 1991, Gibson et al., 1992). The binding parameters calculated indicate high affinity and specificity of (R,S)- and (R,R)-[$^{125}$I]-QNB for mAChRs.

***In Vivo* Selectivity for mAChR Subtypes**

Investigation of (R,S)- and (R,R)-[$^{125}$I]-QNB binding to transfected cell membranes expressing a single cloned mAChR subtype indicates m$_1$ selectivity for these ligands *in vitro* (Zeeberg et al., 1991). This is supported by the observation that the dissociation rate

**Table 18**

**Association Rate Constants and Equilibrium Dissociation Constants for (R,S)- and (R,R)-[$^{125}$I]-QNB Determined by *In Vitro* Autoradiography**

| Region | | (R,S)-[$^{125}$I]-QNB | (R,R)-[$^{125}$I]-QNB |
|---|---|---|---|
| Frontal Cortex | kobs (mins$^{-1}$) | 0.0156 | 0.0185 |
| | KD (nM) | 0.036 | 0.226 |
| | | | |
| Parietal Cortex | kobs | 0.0303 | 0.0203 |
| | KD | 0.050 | 0.115 |
| | | | |
| Caudate Nucleus | kobs | 0.0105 | 0.0462 |
| | KD | 0.028 | 0.206 |

**Table 19**

**Association and Dissociation Rate Constants and Equilibrium Dissociation Constants for (R,S)- and (R,R)-[$^{125}$I]-QNB Determined by *In Vitro* Binding to Transfected Cell Membranes Expressing Muscarinic Receptors**

| Radioligand | Subtype | kass (mins$^{-1}$) | kdis (mins$^{-1}$) | KD (nM) |
|---|---|---|---|---|
| (R,S) | m1 | 0.0158 | 0.00276 | 0.0116 |
| | m2 | 0.1787 | 0.10362 | 0.0482 |
| | m3 | 0.0144 | 0.00431 | 0.0470 |
| | | | | |
| (R,R) | m1 | 0.0681 | 008134 | 0.490 |
| | m3 | 0.0724 | 0.05564 | 1.268 |

Tables show association rate constant (kobs) and equilibrium dissociation rate constant (KD) for (R,S)- and (R,R)-[$^{125}$I]-QNB binding to mAChRs in rat brain sections as determined by *in vitro* autoradiography in this thesis [Table 18] and the association rate constant ($k_{ass}$), dissociation rate constant ($k_{dis}$) and equilibrium dissociation rate constant (KD) for (R,S)- and (R,R)-[$^{125}$I]-QNB binding to transfected cell membranes expressing $m_1$, $m_2$ and $m_3$ mAChRs as determined by Zeeberg et al., (1991)[Table 19].Rate constant values determined by *in vitro* autoradiography in this thesis are consistent with literature values determined by binding to transfected cell membranes.

of (R,S)-[$^{125}$I]-QNB from $M_2$ receptors *in vitro* was 20 fold faster than from $M_1$, $M_3$ or $M_4$ receptors and was reflected by *in vivo* washout of ligand which was predominantly faster in regions of high $M_2$ density (Sawada et al., 1990b, Gibson et al., 1992).
In contrast, [$^3$H]-QNB displays $M_2$ selectivity *in vitro* (Boulay et al., 1996b). A relatively low homogeneous distribution of [$^3$H]-QNB is observed *in vivo* in accordance with $m_2$ distribution and suggests a significant population of $m_2$ receptors is present in the cerebellum. In contrast the *in vivo* distribution of (R,S)- and (R,R)-[$^{125}$I]-QNB is more highly circumscribed with (R,S)-[$^{125}$I]-QNB distributed in accordance with total mAChR concentration and (R,R)-[$^{125}$I]-QNB distributed in accordance with $m_1/m_4$ concentration (Boulay et al., 1996b). That is, levels of (R,S)- and (R,R)-[$^{125}$I]-QNB were high in the cortex, caudate and hippocampus but were extremely low in the cerebellum, consisting almost entirely of non-specific binding.
The *in vivo* distribution of (R,S)- and (R,R)-[$^{125}$I]-QNB observed in this thesis is in general agreement with observations from the above studies. High levels of activity observed in the cortex, caudate and hippocampus compared with very low levels in the cerebellum indicate that (R,S)- and (R,R)-[$^{125}$I]-QNB display predominantly m1 or "m1 like" selectivity *in vivo*.

### 4.1.1 Uptake and Retention of (R,S)- and (R,R)-[$^{125}$I]-QNB

Although regional uptake and distribution of (R,S)- and (R,R)-[$^{125}$I]-QNB are qualitatively similar (corresponding to mAChR concentration) the ligands display considerable differences in regional retention and washout *in vivo*.
Comparison of regional time-activity profiles of (R,S)- and (R,R)-[$^{125}$I]-QNB in rat brain highlight these differences. (R,S)-[$^{125}$I]-QNB displays essentially no washout from cortex between 2 and 24 hours after administration. In thalamus however, a considerable loss of activity is observed over this time. These observations are in general agreement with those of Sawada et al., (1990b) for R-IQNB in rat brain. Graphical analysis (Patlak Plot) indicated that uptake of R-IQNB into cortex and caudate was essentially irreversible over the first 6 hours following intravenous administration, with a slow loss of activity observable when the plot was extended to 26 hours. Similar analysis of time-activity data for the thalamus indicated that uptake in this region was irreversible only for the first 2 hours following administration and that loss of activity could be observed after this time. These observations are qualitatively similar to regional time-activity profiles for (R,S)-[$^{125}$I]-QNB presented in this thesis and provides a degree of validation of the methodology employed here.
In contrast, regional time activity data for (R,R)-[$^{125}$I]-QNB is considerably different from that of (R,S)-[$^{125}$I]-QNB and R-IQNB, although some comparisons can be made.

Washout of (R,R)-[$^{125}$I]-QNB from brain follows a similar regional pattern to that of (R,S)-[$^{125}$I]-QNB, with little loss of activity observed in cortex and considerable loss of activity observed in thalamic regions. However this occurs over a much shorter time-scale i.e. 6 hours as opposed to 24 hours. Washout of (R,S)- and (R,R)-[$^{125}$I]-QNB from regions such as mediodorsal thalamus, ventrolateral thalamus and lateral geniculate nucleus best demonstrate the differences in *vivo* kinetic behaviour of these ligands. Although washout of activity from each of these regions is observed with time, a much greater loss of (R,R)-[$^{125}$I]-QNB activity occurs over a shorter time i.e.. 70%, 72% and 70% for (R,R) over 6 hours compared to 39%, 49% and 53% over 24 hours for (R,S), respectively for each region.

Initially, for studies with (R,R)-[$^{125}$I]-QNB the same temporal profile as that for (R,S)-[$^{125}$I]-QNB was to be used to allow direct comparison of tracers over 24 hours. However preliminary analysis of (R,R)-[$^{125}$I]-QNB indicated that by 12 hours although tracer levels in cortex were comparable with those of (R,S)-[$^{125}$I]-QNB at this time, activity in the thalamus was significantly lower and was undetectable in the cerebellum. and by 24 hours after administration radioactivity was undetectable in the brain. Fig 53 shows a comparison of time-activity profiles of (R,S)- and (R,R)-[$^{125}$I]-QNB in frontal cortex, mediodorsal thalamus and cerebellum over 24 hours.

From these observations it is reasonable to assume that (R,S)- and (R,R)-[$^{125}$I]-QNB display considerable differences in their *in vivo* binding kinetics with mAChRS.

The differences in the regional washout rates of (R,S)- and (R,R)-[$^{125}$I]-QNB described above are consistent with their *in vitro* binding kinetics. The dissociation rate for (R,R)-[$^{125}$I]-QNB from mAChRS is 13-20 fold faster than that for (R,S)-[$^{125}$I]-QNB (Gibson et al., 1989, Gibson et al., 1992). The increased washout of (R,R)-[$^{125}$I]-QNB observed in this thesis is also consistent with previous reports indicating that this ligand clears more rapidly from all brain regions than (R,S)-[$^{125}$I]-QNB *in vivo* (Gibson, et al., 1989, Zeeberg et al., 1996). The more rapid clearance of (R,R)-IQNB activity from brain promotes its greater suitability over (R,S)-IQNB as an *in vivo* agent for use in man. (R,S)-[$^{123}$I]-QNB has been successfully used in man to image mAChRS but suffers from slow washout kinetics in that it takes longer than 20 hours to reach optimal specific to non-specific binding ratios (Fig 54) (Wyper et al., 1993). The *in vivo* rat data presented here suggests that (R,R)-[$^{123}$I]-QNB would reach optimal binding conditions more rapidly than (R,S)-[$^{123}$I]-QNB indicating its greater utility as an *in vivo* imaging agent in man. Similarly, these observations suggest that (R,R)-[$^{125}$I]-QNB would be more sensitive to changes in ACh function than (R,S)-[$^{125}$I]-QNB.

## (R,S)- and (R,R)-[$^{125}$I]-QNB in Rat Brain over 24 hours

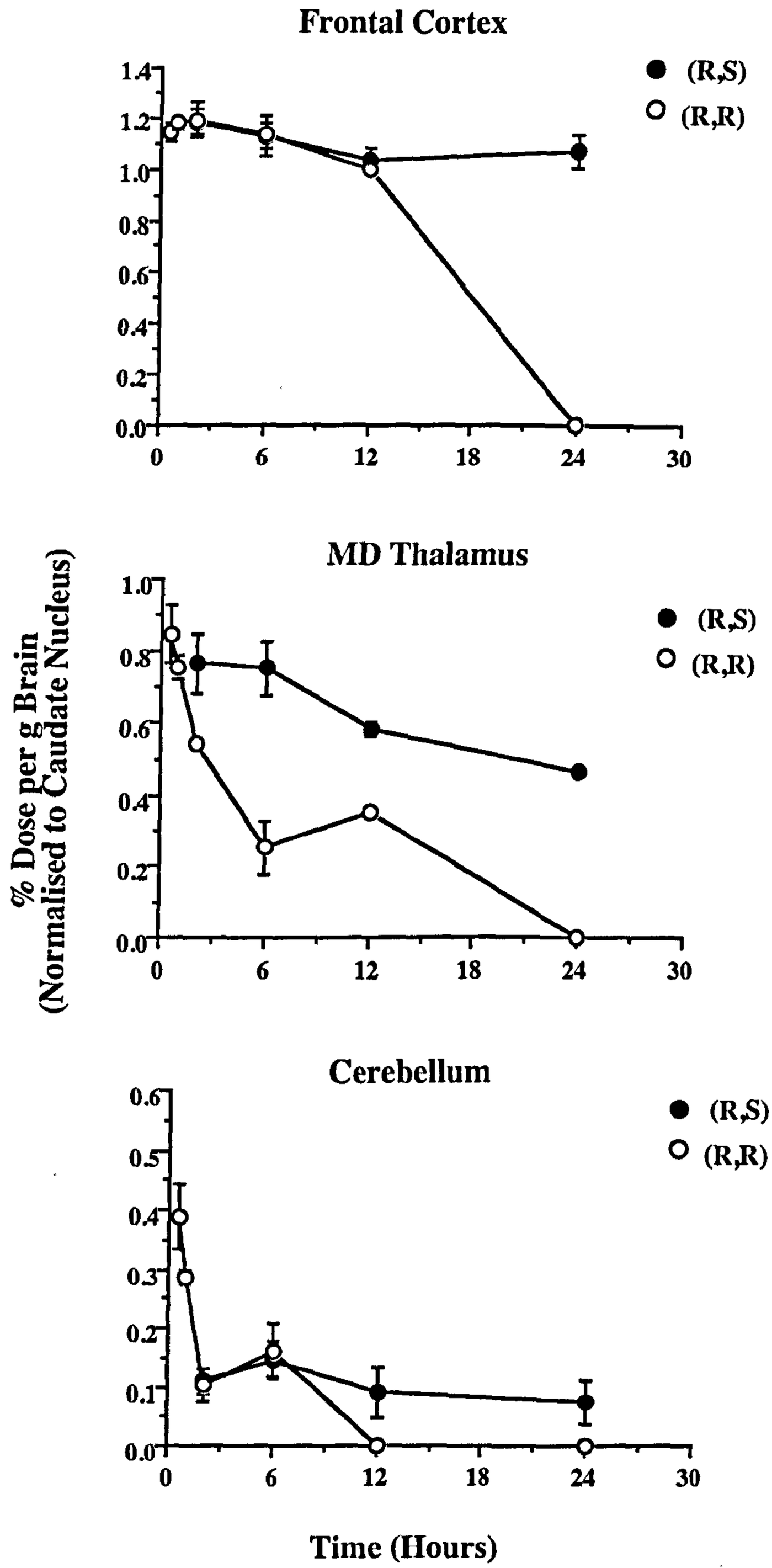


**Fig 53:** Figure shows (R,S)- and (R,R)-[$^{125}$I]-QNB in rat brain at the level of the frontal cortex, mediodorsal thalamus (MD) and cerebellum at 30 mins to 24 hours after intravenous administration. (R,R)-[125I]-QNB is washed out of brain more quickly than (R,S)-[$^{125}$I]-QNB. Data are expressed as mean ± S.E.M % Dose per g Brain normalised to caudate nucleus. n=3-5 for (R,S)-[125I]-QNB and n= 5 for (R,R)-[125I]-QNB, with the exception of data points at 12 and 24 hours where n= 1.

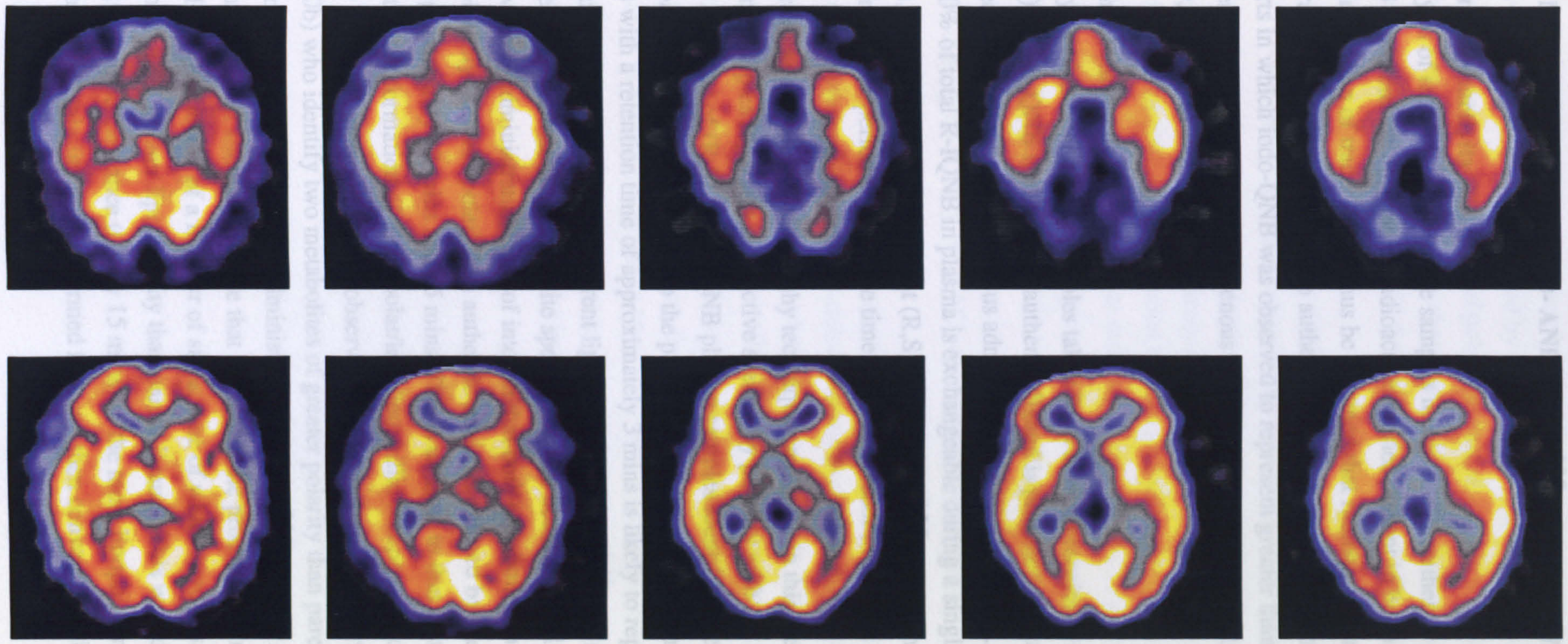


**Fig 54:** (R,S)-[$^{123}$I]-QNB uptake and retention in normal human brain.

Axial SPECT images show distribution of radioactivity in the brain of a normal human subject at the level of the cerebellum (top) and basal ganglia (bottom) for [$^{99m}$Tc]-HMPAO and for (R,S)-[$^{123}$I]-QNB at 1-44 hours following administration. "Hot" colours represent areas with high tracer uptake and "cold" colours represent areas with low uptake. Early images (1 hour-21 hours) indicate that distribution of (R,S)-[$^{123}$I]-QNB is blood flow dominated. Washout of non-specific activity is slow with optimal specific to non-specifc ratios achieved at times post 21 hours.

## 4.2 METABOLISM OF (R,S)- AND (R,R)-[$^{125}$I]-QNB *IN VIVO*

### Brain Radioactivity

Analysis of rat brain homogenate samples indicates that authentic (R,S)- and (R,R)-[$^{125}$I]-QNB represent the only major radioactive species present in brain following intravenous administration of tracer. It can thus be assumed that radioactivity measured in autoradiograms is entirely due to authentic ligand. This observation is consistent with other reports in which iodo-QNB was observed to represent greater than 90% of the radioactivity present in brain following intravenous administration (Blasberg et al., 1986, Gibson et al., 1989, Sawada et al., 1990b).

### Plasma Radioactivity

Analysis of arterial plasma samples taken from animals receiving (R,S)-[$^{125}$I]-QNB and (R,R)-[$^{125}$I]-QNB indicate that authentic ligand is present in plasma up to 12 and 6 hours respectively following intravenous administration . Blasberg et al., (1986) estimated that 15-30% of total R-IQNB in plasma is exchangeable during a single capillary pass in the brain, thus it can be assumed that (R,S)- and (R,R)-[$^{125}$I]-QNB may be transported into the brain for a period equal to the time they are present in plasma.

The reverse phase chromatography technique employed in this thesis in the analysis of plasma samples separates radioactive species by polarity with the most polar species eluted first. Analysis of (R,S)-[$^{125}$I]-QNB plasma samples identified the presence of 3 radioactive species in addition to the parent ligand. The fastest eluting (i.e. most polar) of these with a retention time of approximately 3 mins is likely to represent free iodide, produced by de-iodination of parent ligand and /or its radioactive metabolites. Two unidentified radioactive metabolite species are also observed in plasma following intravenous administration. It is of interest that both metabolite species are of higher lipophilicity (i.e. less polar) than authentic tracer as evinced by their longer retention times of approximately 13 mins and 15 mins. This is unusual in that metabolic processes usually result in the formation of more polar/less lipophillic compounds to aid clearance from the body and is in opposition to the observations of Blasberg et al., (1986) and Sawada et al., (1990b) who identify two metabolites of greater polarity than parent compound in the plasma following intravenous administration of (R)-[$^{125}$I]-QNB. A possible explanation for this apparent anomaly may be that the metabolic process leading to clearance of (R,S)-[$^{125}$I]-QNB consists of a number of steps, one of which involves the formation of compounds of greater lipophilicity than parent ligand. This would correlate with the relatively rapid clearance (i.e. by 15 mins) of the more lipophilic metabolite from plasma, in that this metabolite may be formed first and then converted to the second less lipophilic

metabolite species. The second metabolite may then undergo further processing probably involving de-iodination as evinced by the increase in free iodide observed with time. This would also account for the lack of polar radioactive metabolite species on HPLC traces. Neither of the metabolite species observed in plasma were identified, but their lack of presence in the brain indicates that they possess no affinity for mAChR or other brain receptors.

In contrast to (R,S)-[$^{125}$I]-QNB, analysis of plasma samples following administration of (R,R)-[$^{125}$I]-QNB indicates that free iodide constitutes the major radioactive metabolite species present in plasma .This observation suggests that de-iodination represents the major metabolic event in the clearance of (R,R)-[$^{125}$I]-QNB from the body. However, the broad low level peak with a retention time of 13.0 mins on a number of traces is possibly due to the presence of one or more radioactive metabolites in plasma which are present at a very low level. It is possible that metabolites are formed and cleared with sufficient rapidity that no significant accumulation in the plasma occurs. As (R,R)-[$^{125}$I]-QNB represents the sole radioactive species in brain it is likely that any radioactive metabolites formed display no affinity for mACh or other brain receptors.

Fig 55 shows the percentage of authentic (R,R)-[$^{125}$I]-QNB bound to plasma protein up to 6 hours following tracer administration. Plasma protein bound activity peaks at approximately 22% 2 hours after administration. This is in contrast to previous observations which estimate greater than 90% of authentic ligand in plasma is bound to plasma proteins at any one time following intravenous administration (Blasberg et al., 1986). These observations indicate that a significant proportion of the authentic ligand detectable in plasma constitutes a "free pool" which is available for uptake into the brain. This theory is supported by the increases in brain (R,R)-[$^{125}$I]-QNB activity observed between 30 mins to 2 hours after administration of tracer.

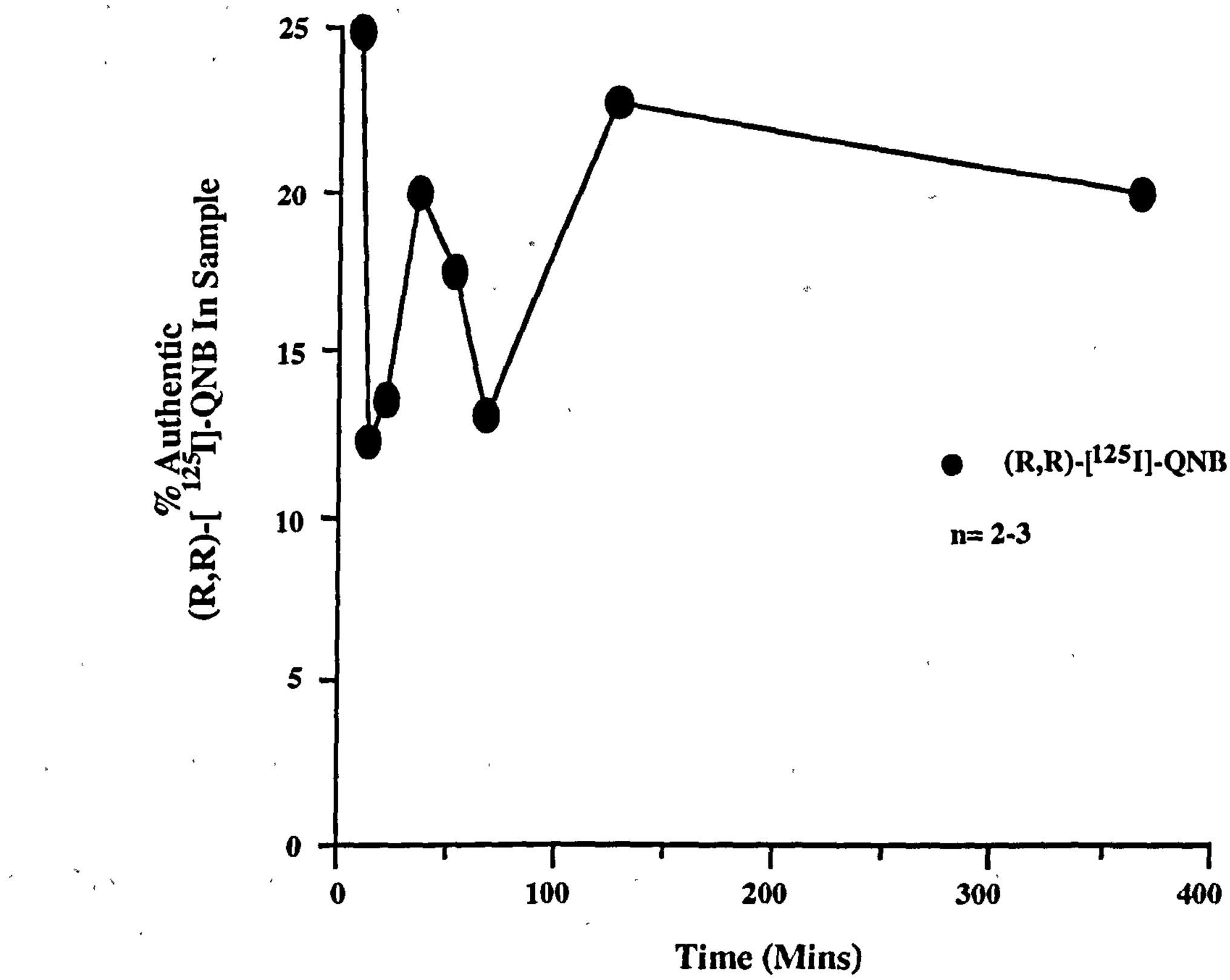


**Fig 55:** Timecourse of protein bound (R,R)-[$^{125}$I]-QNB in plasma following intravenous injection in rat. Data points represent levels of authentic ligand bound to protein in plasma of conscious rat between 1 min and 6 hours after administration. Protein bound ligand constitutes no more than 25 % of authentic ligand present in plasma at any one time. Data are expressed as mean ± S.E.M % of injected dose (n= 2-3).

## 4.3 KINETIC MODELLING

A 3 compartment model [Fig 56] was used to examine the hypothetical brain concentrations arising from intravenous administration of tracer with an input function like that of (R,S)- [$^{125}$I]-QNB where tracer is cleared slowly from plasma.
A number of specifications of this model require discussion. The model is set up to reflect the situation where a tracer moves from the plasma into a second compartment within the brain which describes free and non-specifically bound tracer.

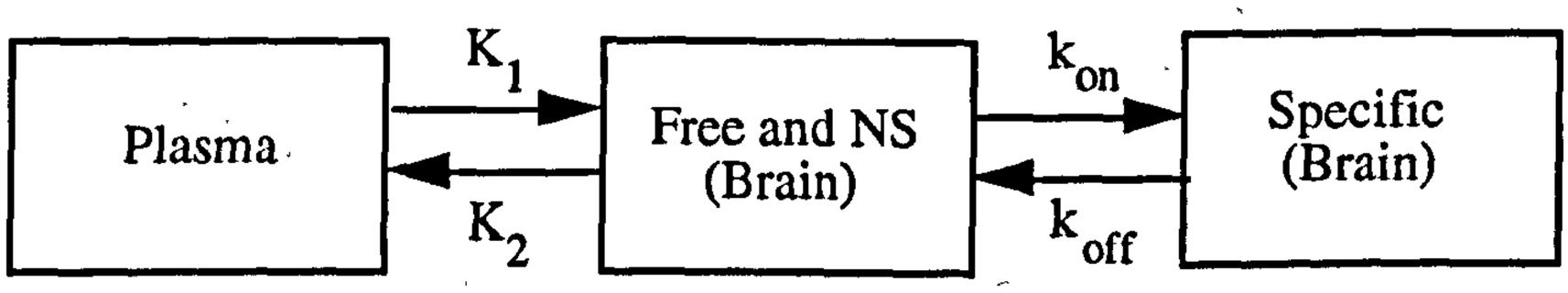


A third compartment describes tracer bound specifically to receptors within the brain. The factors influencing the movement of tracer between these three compartments are described below.

1) $K_1$ is an input constant describing the amount of tracer delivered to the brain which is determined by the plasma concentration of tracer, the free fraction of tracer within the plasma, cerebral blood flow, and the extraction fraction.

- Plasma concentration is described by a plasma time-activity graph based upon the plasma clearance of (R,S)-[$^{125}$I]QNB as observed in *in vivo* studies (Fig 12).
- The free fraction of tracer in plasma was set 0.086, as estimated by Sawada et al., (1990b) for R-IQNB.
- Cerebral blood flow (ml/g/min) was variable with values of 0.8 ml/g/min set for cortex and cerebellum and 0.4 ml/g/min set for caudate nucleus and thalamus to represent the differences in blood flow between these regions.
- The extraction fraction is dependent on the capillary surface area S, the capillary permeability P and perfusion (flow) F. The dependence on blood flow reflects the fact that at higher flows, the tracer spends less time within the capillary. The extraction fraction itself may vary with time as the concentration of tracer in plasma changes, but is set at 0.431 as determined by Sawada et al., (1990a) for R-IQNB.

2) $K_2$ is the elimination rate constant describing the amount of tracer flowing out of the brain into plasma. $K_2$ can be expressed as K1/(V2*f1) where $K_1$ is the association rate constant, $V_2$ is the volume of distribution of the free and non-specifically bound compartment and $f_1$ is the free fraction of tracer within the blood. $K_2$ is dependent

## A 3 Compartment Model of tracer Uptake Into The Brain

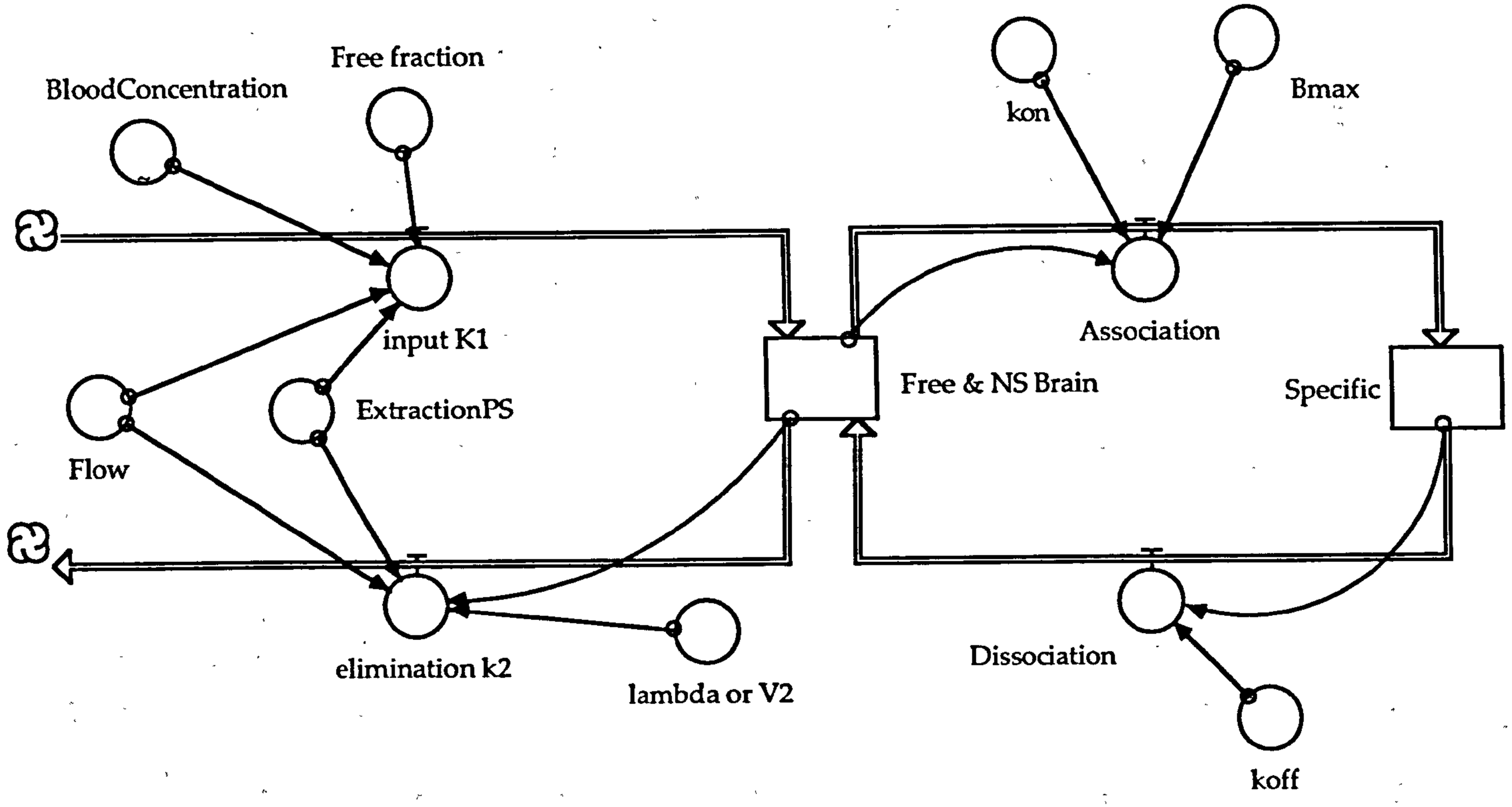


**Fig 56**: A 3 compartment model of tracer uptake into the brain was devised using the Stella II modelling program. The model is set up to reflect the situation where a tracer moves from the plasma into a second compartment within the brain which describes free and non-specifically bound tracer. An equilibrium exists between the 'free" brain pool and a third compartment describing tracer bound specifically to receptors within the brain. The factors influencing movement of tracer between these three compartments are shown above. An explanation of terms is contained within the text.

upon the concentration of tracer within the brain, the partition coefficient or volume of distribution of the tracer, the extraction fraction and cerebral blood flow.
The volume of distribution of specifically bound tracer varies between brain regions and was therefore set at 24,16,6 and 0.6 for cortex, caudate nucleus, thalamus and cerebellum based upon the values estimated Sawada et al., (1990b) for R-IQNB.

3) Unbound ligand reversibly binds to receptors at a rate dependent upon the concentration of the 2 reactants. The rate constant for this reaction is known as the association rate constant $k_{on}$. The value of $k_{on}$ is variable for the uptake of tracer into different brain regions and was set at 2.04, 2.10, 0.78 and 1.10 for cortex, caudate nucleus, thalamus and cerebellum respectively based on parameters estimated by Sawada et al., (1990b) for R-IQNB. $B_{max}$ equals the concentration of receptors available for binding which is also variable from region to region and was set at 0.19, 0.24, 0.08 and 0.02 based upon the relative concentrations of mAChRs in cortex, caudate nucleus, thalamus and cerebellum respectively.

4) The rate of dissociation of the tracer from the receptor is determined by the dissociation rate constant $k_{off}$ and the concentration of tracer within the specifically bound compartment. As with $k_{on}$ and $B_{max}$ the value of $k_{off}$ varies between regions and was set at 0.0017, 0.0018, 0.0032 and 0.045 for cortex, caudate nucleus , thalamus and cerebellum respectively based on parameters estimated by Sawada et al., (1990b) for R-IQNB.

Comparison of hypothetical concentrations of radioactivity arising from the input curve for (R,S)-[$^{125}$I]-QNB and actual tracer uptake (μCi/g) in the frontal cortex, caudate nucleus, thalamus and cerebellum is displayed in Fig 57. In general, simulated regional uptake of tracer is consistent with actual uptake. Highest levels of activity are observed in the cortex and caudate with no washout of tracer observed to occur from these regions over 24 hours. A lower level of uptake is observed in the thalamus with washout of activity observed from this region with time. Uptake and retention of tracer in the cerebellum is negligible. A number of inconsistencies are evident however. The time course of modelled uptake is slower than that of actual uptake. Activity in the thalamus takes in excess of 5 hours to reach peak levels with washout of activity observed thereafter. In contrast, actual radioactivity in the thalamus *in vivo* is at its highest measured level at 2 hours, with washout of activity observed thereafter. Similarly, modelled levels of activity in the cortex and caudate are estimated to increase steadily over 24 hours in contrast to the steady state levels measured *in vivo*.

**Fig 57:** Comparison of Actual and Hypothetical uptake and retention of (R,S)-[$^{125}$I]-QNB in rat brain-raw and normalised data.

A 3 compartment model was used to model the hypothetical uptake and retention of (R,S)-[$^{125}$I]-QNB in frontal cortex, caudate nucleus, thalamus and cerebellum of conscious rat using the plasma input curve for (R,S)-[$^{125}$I]-QNB. All model parameters were identical to those described in section 4.3.
Hypothetical concentrations of un-normalised tracer (top right graph) in brain are generally consistent with actual un-normalised concentrations (top left graph) of tracer measured *in vivo*, although differences in the time course of uptake and retention of radioactivity are evident. Comparison of hypothetical and actual concentrations of tracer in the brain normalised to the concentration in the caudate nucleus (bottom right and bottom left graphs respectively) show greater consistency than un-normalised data sets. The time course of uptake and retention is comparable as are levels of tracer in each brain region.
The 3 compartment model described in section 4.2 therefore adequately describes the uptake and retention of (R,S)-[$^{125}$I]-QNB in brain and provides validation of the normalisation procedure employed.
Data are expressed as mean ± S.E.M μCi per g Brain for Actual data: Un-normalised (n= 5), μCi per g Brain for Modelled Data: Un-normalised , mean ± S.E.M % Dose per g Brain normalised to the caudate nucleus (n= 5) for Actual Data: Normalised , and % Dose per g Brain normalised to the caudate nucleus for Modelled Data: Normalised .

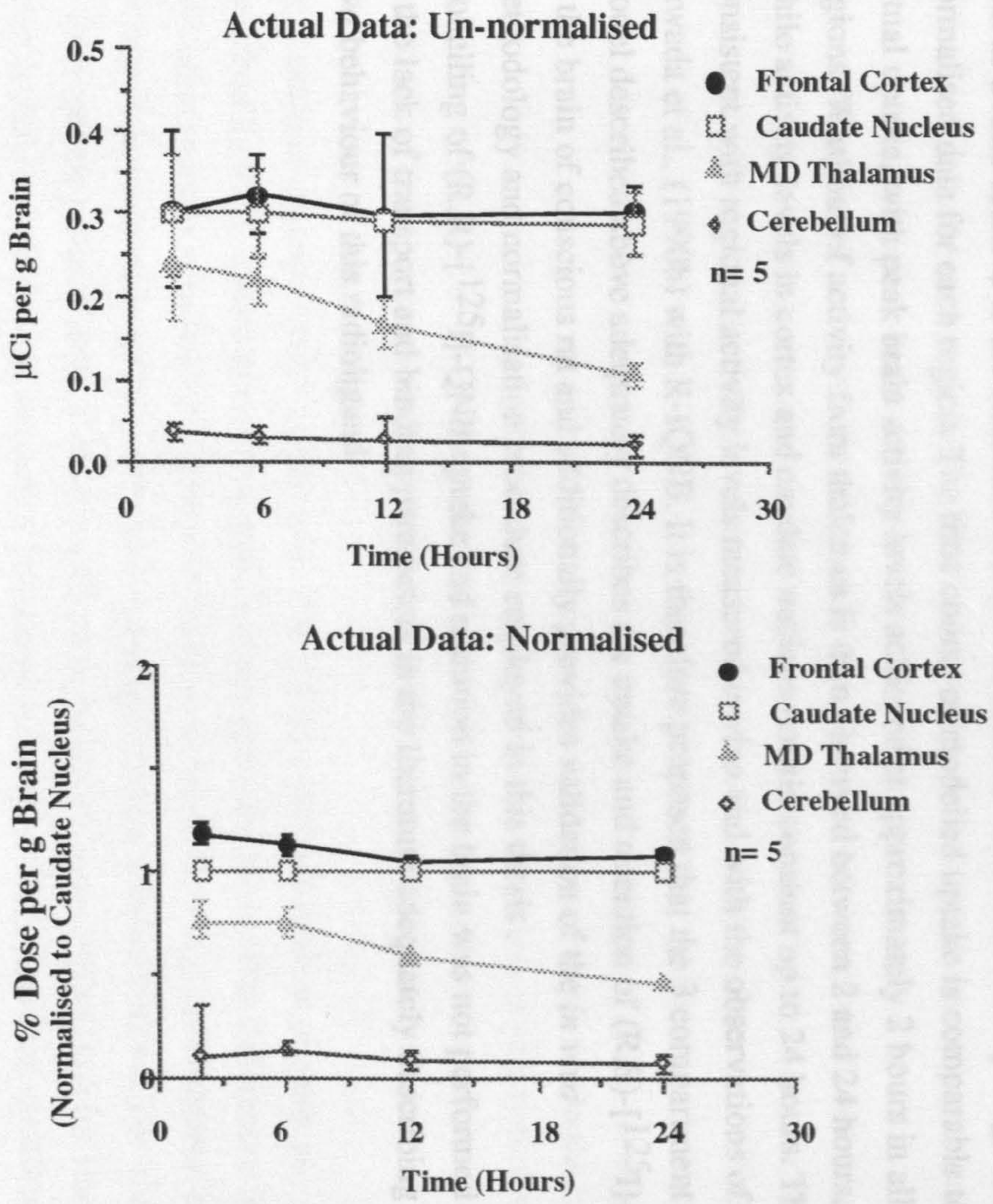


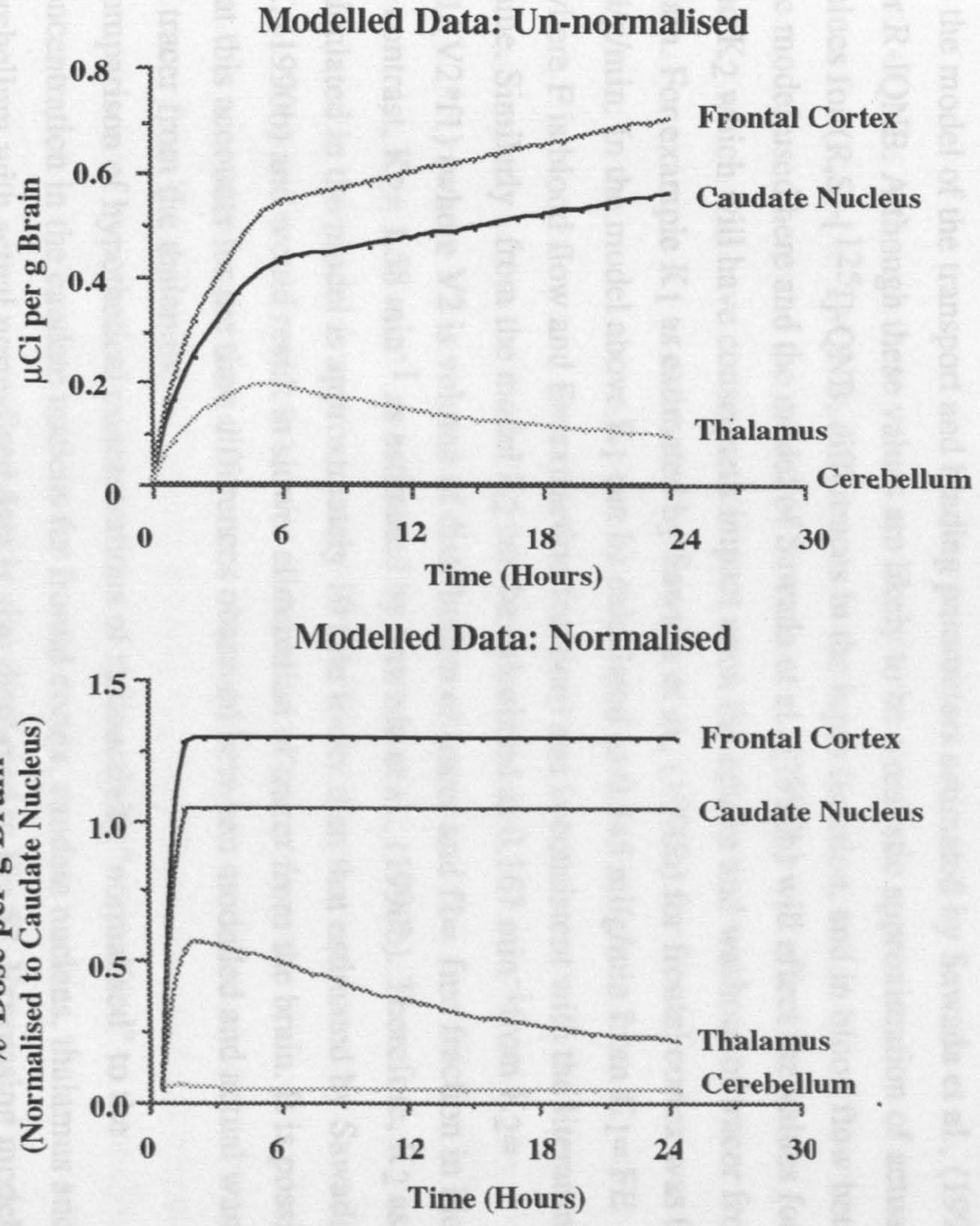








**Fig 57:** Comparison of Actual and Hypothetical uptake and retention of (R,S)-[$^{125}$I]-QNB in rate brain.-raw and normalised data.

The inconsistencies observed between modelled data and actual data may be due to the use in the model of the transport and binding parameters estimated by Sawada et al., (1990b) for R-IQNB. Although these values are likely to be a realistic approximation of actual values for (R,S)-[$^{125}$I]-QNB, differences in the input function, and in blood flow between the model used here and the model of Sawada et al., (1990b) will effect the values for $K_1$ and $K_2$ which will have consequent impact upon the uptake and washout of tracer from the brain. For example $K_1$ as estimated by Sawada et al., (1990b) for frontal cortex was 0.320 ml/g/min. In the model above $K_1$ can be calculated as 0.345 ml/g/min from $K_1$= FE (where F is blood flow and E= extraction fraction) and is consistent with the literature value. Similarly , from the model $K_2$ can be calculated as 0.167 $min^{-1}$from $K_2$= K1/(V2*f1) (where V2 is volume of distribution of tracer and f1= free fraction in blood). In contrast, $K_2$= 1.58 $min^{-1}$ as estimated by Sawada et al., (1990b). Therefore, $K_2$ as calculated in the model is approximately 10 fold lower than that estimated by Sawada et al., (1990b) and would result in slower elimination of tracer from the brain. It is possible that this accounts for the time differences observed between modelled and actual washout of tracer from the thalamus.

Comparison of hypothetical concentrations of radioactivity "normalised" to the concentration in the caudate nucleus for frontal cortex, caudate nucleus, thalamus and cerebellum with actual normalised data is also displayed in Fig 57. Expressing modelled data as a ratio relative to the caudate nucleus is consistent with actual raw (µCi/g) and normalised data for each region. The time course of modelled uptake is comparable to actual uptake, with peak brain activity levels achieved at approximately 2 hours in all brain regions. Washout of activity from thalamus is then observed between 2 and 24 hours, while activity levels in cortex and caudate nucleus remain constant up to 24 hours. This is consistent with regional activity levels measured *in vivo* and with the observations of Sawada et al., (1990b) with R-IQNB. It is therefore proposed that the 3 compartment model described above adequately describes the uptake and retention of (R,S)-[$^{125}$I]-QNB in the brain of conscious rat and additionally provides validation of the *in vivo* methodology and normalisation procedure employed in this thesis .

Modelling of (R,R)-[$^{125}$I]-QNB uptake and retention in the brain was not performed due to the lack of transport and binding parameters in the literature adequately describing the *in vivo* behaviour of this radioligand.

## 4.4. NORMALISATION OF DATA

Data from *in vivo* experiments with iodo-QNB is routinely normalised to a control region (caudate nucleus) in which activity levels have been shown to be highly reproducible from animal to animal (Gitler et al., 1995, Boulay et al., 1996, Sood et al., 1997, Zeeberg et al., 1997). In accordance with this, all *in vivo* data in this thesis has been expressed as a ratio of % injected dose per g brain to caudate nucleus. Normalisation of data in this manner is particularly important where the data set is inherently variable as in this thesis where time-activity data for the uptake and retention of tracer is obtained from multiple animals for each time point analysed. The benefit of data normalisation can be appreciated by comparing raw and normalised data sets for the uptake and retention of (R,S)-[$^{125}$I]-QNB activity in the frontal cortex between 2 and 24 hours . The average standard deviation of binding was 10% of the mean for normalised data (% dose per g brain /caudate) and 47 % of the mean for un-normalised data (% dose per g brain) respectively. This observation is roughly consistent with those of previous investigations where the standard deviations of binding were 8% and 30% of the mean for data normalised to the caudate nucleus and un-normalised data respectively (Gitler et al., 1995) and confirms the utility of normalisation of data by this means.

Although normalisation of data to the caudate nucleus is well accepted, alternative means of data normalisation were considered in this thesis. These included normalisation of data to the cerebellum and to the concentration of tracer in plasma.

Comparison of regional activity levels with those observed in the cerebellum has been proposed as a means of accounting for the degree of non-specific binding apparent with a number of tracers including those specific for glutamate and dopamine receptors (Farde et al., 1990, McCulloch et al., 1992). The validity of this comparison is based upon the theory that cerebellar uptake and retention of tracer acts as a measure of non-specific binding due to the relative paucity of receptors in this region compared to target regions. On the basis that mAChR density in the cerebellum is similarly low, activity levels in this region should be relatively reproducible from animal to animal and expression of data as cerebellar ratio should thus provide a means to normalise data and account for inter-animal variation in activity levels.

Expression of regional brain activity as a ratio of tracer concentration in plasma, as described by the 5 minute plasma integral, is based upon the theory that differences in individual animals uptake of tracer into the brain or in its metabolism and clearance of tracer will be accurately reflected by the level of tracer present in the plasma. The choice of the 5 minute plasma integral for normalisation should allow sufficient time for tracer levels to fall from their peak immediately following injection (thus avoiding variations in activity resulting from differences in injected dose), while also allowing time for tissue

uptake and metabolism of tracer. Additionally, activity levels in plasma at 5 mins are high enough to allow accurate determination by liquid scintillation analysis.

However, normalisation of the same data from frontal cortex for (R,S)-[$^{125}$I]-QNB to cerebellum and to 5 min plasma integral indicates that they offer no improvement over normalisation to the caudate nucleus. Fig 58 shows (R,S)-[$^{125}$I]-QNB activity levels in the frontal cortex of conscious rat between 2 and 24 hours as raw data (% dose per g brain), and data normalised to caudate nucleus, cerebellum and to the 5 minute plasma integral. The average standard deviation of the binding was 93 % and 45% of the mean for normalisation to cerebellum and to plasma respectively. These normalisation procedures therefore produce either a significant increase or little improvement in data variation over un-normalised data and profound increases in data variation compared to normalisation to caudate . The unworthiness of normalisation either to the cerebellum or to plasma is likely to reside in some inherent flaws in the respective data sets used. The extremely low levels of tracer observed in the cerebellum at all time points make accurate quantification of autoradiograms difficult. The image analysis system used in this thesis is most accurate when working in the middle of its calibrated range, therefore the low levels of isotope combined with the limitations of the detection system can produce both overestimation and underestimation of activity in the cerebellum. Therefore any small change in the level cerebellar activity measured can have enormous impact on the ratio calculated, particularly when the numerator is from a region of high activity such as the frontal cortex.
This "instability" in the ratios formed when normalising to the cerebellum is likely to be responsible for the significant increase in the data variability observed. In addition, the identification of a small but significant population of mAChRs in the cerebellum suggests that this region is less suitable as a reference region for cholinergic ligands than it is for other neurotransmitter ligands.

Normalisation of data to the 5 minute plasma integral is no improvement in data variation on raw data. Plasma activity is assumed to consist entirely of authentic ligand with no correction for radioactive metabolites or for the proportion of tracer that is plasma protein bound. Therefore whole plasma radioactivity does not accurately reflect the level of authentic tracer in plasma or the relative uptake of tracer for each animal. These inaccuracies may therefore account for the poor efficacy of this normalisation technique. The viability of normalisation of data to the caudate nucleus is confirmed by the reproducibility of tracer uptake and retention observed between animals, the lack of effect of heptylphysostigmine on tracer level in this region and the significant reduction in standard deviation produced by normalisation of data to this region. Therefore normalisation of data to the caudate nucleus is an effective means of correcting for data variability.

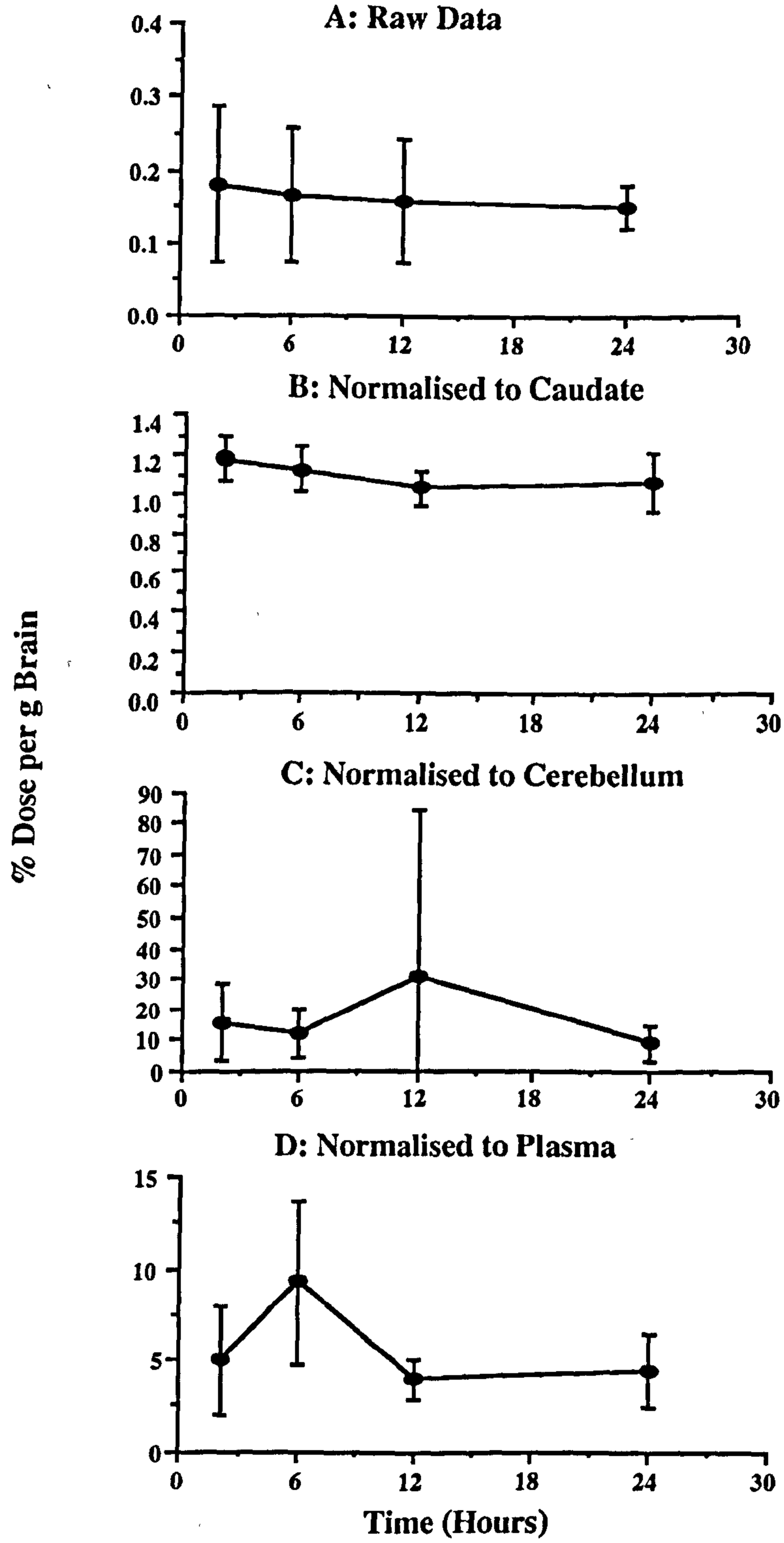


**Fig 58:** Figure shows (R,S)-[$^{125}$I]-QNB activity at the level of the frontal cortex as un-normalised data (A), data normalised to caudate nucleus (B), to cerebellum (C) and to 5 minute plasma integral (D) between 2 and 24 hours. Expression data as a ratio of ROI/caudate provides the best means of correction for inter-animal variation. Data are expressed a mean ± S.D. % Dose per g Brain, n= 3-5 for each time point.

## 4.5 EFFECT OF HEPTYLPHYSOSTIGMINE ON UPTAKE AND RETENTION OF (R,S)- AND (R,R)-[$^{125}$I]-QNB

It has been established that the localisation of (R,S)- and (R,R)-[$^{125}$I]-QNB in the brain following intravenous administration generally reflect mAChR distribution. It was therefore postulated that these stereoisomers may be suited to detect changes in cholinergic function *in vivo*. Quantification of postsynaptic receptor occupancy of either radioligand following a pharmacologically induced release of ACh would provide an indirect measure of synaptic ACh concentration and thus the ability to assess cholinergic function *in vivo* in a given brain region. To this end the sensitivity of (R,S)- and (R,R)-[$^{125}$I]-QNB to detect increases in endogenous ACh produced by administration of the AChE inhibitor heptylphysostigmine was assessed. In theory, inhibition of AChE the catabolic enzyme for ACh, will increase synaptic ACh concentration . ACh will then compete with radioligand for mAChR sites producing a reduction in measured radioligand concentration in the brain. Of the two ligands it was postulated that (R,R)-[$^{125}$I]-QNB was more likely to be displaced from mAChRs by ACh. The more rapid washout from brain *in vivo* and the lower affinity and faster dissociation rate for mAChRs of this ligand *in vitro* and *in vivo* compared to (R,S)-[$^{125}$I]-QNB, suggest its greater sensitivity to displacement by ACh *in vivo*.

Analysis of (R,S)- and (R,R)-[$^{125}$I]-QNB levels in brain following heptylphysostigmine administration indicate that no significant reduction in radioactivity was observed in any of the regions analysed. Similarly, a range of concentrations of ACh ($10^{-6}$M to $10^{-2}$M) failed to displace (R,S)- and (R,R)-[$^{125}$I]-QNB from rat brain sections *in vitro* in the presence of heptylphysostigmine. On the contrary, administration of heptylphysostigmine was observed to produce significant increases in (R,S)- and (R,R)-[$^{125}$I]-QNB levels *in vivo* , most notably in cortical regions. Average increases in activity of 30 % and 39% respectively for (R,S)- and (R,R)-[$^{125}$I]-QNB were observed in cortical regions of heptylphysostigmine treated animals over vehicle treated animals. Of the cortical regions showing increases in activity the auditory cortex displayed the greatest and most consistent increases at all time points analysed. At 2 hours increases in (R,S)- and (R,R)-[$^{125}$I]-QNB activity are almost identical in this region with levels measured at 52% and 53% greater than vehicle respectively.

### 4.5.1 Heptylphysostigmine increases cortical cerebral blood flow

It is possible that the increases in regional brain activity of (R,S)- and (R,R)-[$^{125}$I]-QNB observed following heptylphysostigmine administration are the result of dynamic changes in cerebral blood flow. The initial uptake of a lipophilic molecule into the brain with no diffusion restriction is determined by its rate of delivery to the tissue (Rapoport, 1976).

Therefore, an increase in cerebral blood flow, particularly during the period immediately following (R,S)- or (R,R)-[$^{125}$I]-QNB administration would result in increased tracer delivery to the brain and increased tracer uptake into specific regions. The distribution of capillaries within the brain is heterogeneous with capillary density greatest in grey matter regions such as the cortex (Zeman and Innes, 1963). Brain regions of high capillary density also have greater rates of glucose use and higher blood flow with capillary density in sensory and correlative regions of the cortex greater than that of motor regions (Edvinsson et al., 1993). It is therefore reasonable to hypothesise that an increase in cerebral blood flow produced by heptylphysostigmine administration could account for the increases in (R,S)- and (R,R)-[$^{125}$I]-QNB observed in cortical regions and in particular the striking increases observed in the auditory cortex.

To this end regional cerebral blood flow was measured in the conscious rat after heptylphysostigmine administration. Significant increases in blood flow were measured in a number of cortical regions in the conscious rat, including those regions displaying increased levels of iodo-QNB following heptylphysostigmine administration. Previous investigations into the effect of heptylphysostigmine on cerebral blood flow confirm the observations made in this thesis, with increases in blood flow observed in the cortex (Linville at al., 1992, Scremin et al., 1993). A peak increase in cortical blood flow of 80% was observed at 40 mins after drug administration, with increased levels of blood flow observed up to 360 mins after administration (Scremin et al., 1993). The increases in cortical blood flow of between 20% and 53% measured at 2 hours after heptylphysostigmine administration in this thesis are therefore consistent with the above results. As measured blood flow is increased 2 hours following drug administration it is reasonable to assume that it is also elevated at earlier time points. If this is the case then it is extremely likely that tracer delivery to the brain will be enhanced for a crucial period immediately following administration when plasma levels of ligand are high. It is therefore likely that increased cerebral blood flow is responsible for the increased levels of (R,S)- and (R,R)-[$^{125}$I]-QNB observed in brain following heptylphysostigmine administration.

The increases in blood flow produced by heptylphysostigmine are characteristic of AChE inhibitor administration. The vasodilatory effects of AChE inhibitors are well known., with physostigmine inducing a significant increase in cerebral blood flow without concomitant metabolic activation (Scremin et al, 1982). Increases in cerebral blood flow produced by AChE inhibitors result from the action of excess ACh on mAChRs in the cerebrovasculature (Taylor, 1990). It is therefore assumed that the effects of heptylphysostigmine on cerebral blood flow observed in this thesis are produced by increased levels of endogenous ACh. It is possible however, that the blood flow effects

observed are at least in part the result of direct action of heptylphysostigmine on mAChRs in the cerebrovasculature. Heptylphysostigmine is known to bind to both mAChRs and nAChRs *in vitro*, showing greater affinity for mAChRs (De Sarno et al., 1989). It displaces [$^{3}$H]-QNB binding *in vitro* with an $IC_{50}$= 1.9 x $10^{-5}$ M and has greater affinity for mAChRs than physostigmine (Ki= 4.4 x $10^{-6}$ M and 3.8 x $10^{-5}$M respectively). The ability of $10^{-3}$M heptylphysostigmine to displace (R,R)-[$^{125}$I]-QNB binding to rat brain sections observed in this thesis is consistent with the data presented above.

Regional differences in the degree of AChE inhibition may account for the pattern of altered blood flow observed following heptylphysostigmine administration. Heptylphysostigmine (5mg/kg im) produced an 80% inhibition of AChE activity in the cortex while only inhibiting cerebellar AChE activity by 40% (De Sarno et al., 1989). A similar reduction in AChE inhibition in the cerebellum of heptylphysostigmine treated animals was identified by AChE histochemical analysis of rat brain sections in this thesis. This may account for the unaltered blood flow measured and the lack of change in QNB levels observed in the cerebellum following heptylphysostigmine administration. A lower level of enzyme inhibition will result in a smaller increase in ACh concentration and reduced effects on cerebral blood flow with consequent effects on tracer delivery and uptake in this region.. In support of this theory is the observation that increases in ACh following heptylphysostigmine vary from region to region (De Sarno et al., 1989). Additionally, the cholinergic input to the cerebrovasculature in this region is low compared to that in the cortex, thus raised levels of ACh are likely to have a comparatively smaller vasodilatory effect with subsequent effects on the rate of blood flow and level of QNB accumulation (Arneric et al., 1988).

**Kinetic Modelling**

The effects of increased cortical blood flow on uptake and retention of (R,S)-[$^{125}$I]-QNB in the frontal cortex of conscious rat were modelled using the 3 compartment model described in section 4.3. All model parameters effecting tracer uptake and elimination from brain were unchanged with the exception of blood flow which was set at 0.8, 1.0 and 1.2 ml/g/min to represent "normal" blood flow, a 25% increase in blood flow and a 50% increase in blood flow, respectively. Fig 59 shows hypothetical levels of (R,S)-[$^{125}$I]-QNB in the frontal cortex for the 3 blood flow rates. According to this model higher blood flow rates increase tracer uptake and retention with no concomitant increase in washout. Modelled increases in tracer concentration in the frontal cortex resulting from increased blood flow are consistent with measured increases in tracer level in the frontal cortex of conscious rats following heptylphysostigmine administration (Fig 60). These observations confirm the hypothesis that the increases in tracer concentration observed in cortex of rats are the result of heptylphysostigmine induced increases in cerebral blood flow.

## Increasing Cerebral Blood Flow Increases Hypothetical Tracer Uptake and Retention

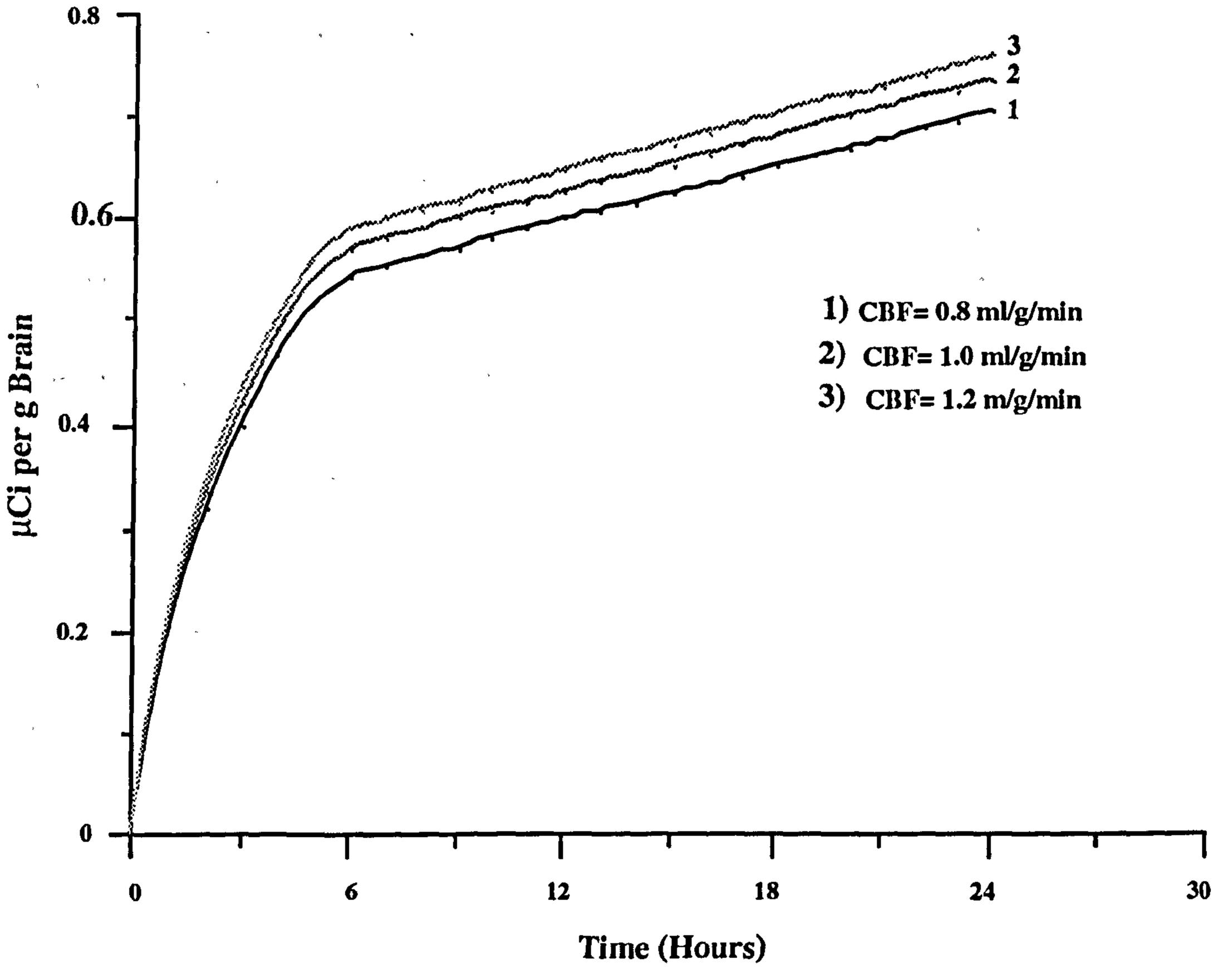


**Fig 59** Hypothetical concentrations of (R,S)-[$^{125}$I]-QNB in frontal cortex as determined by a 3 compartment model with blood flow of 0.8. 1.0 and 1.2 ml/g/min. Increasing blood flow increases uptake and retention of tracer in brain. Data is expressed as µCi per g brain as calculated by the 3 comparment model described in section 4.3. With the exception of blood flow all parameters effecting tracer uptake and elimination from the brain were identical.

**Fig 60:** Comparison of actual concentration of (R,S)-[$^{125}$I]-QNB in frontal cortex in vehicle and heptylphysostigmine treated animals (left hand graph) as measured *in vivo*, with hypothetical brain concentrations in frontal cortex for "normal" blood flow (0.8 ml/g/min) and for blood flow increases of 50% (1.2 ml/g/min) (right hand graph).

A 3 compartment model was used to simulate the effect of increased cerebral blood flow on the hypothetical uptake and retention of (R,S)-[$^{125}$I]-QNB in frontal cortex of conscious rat using the plasma input curve for (R,S)-[$^{125}$I]-QNB. All model parameters were identical to those described in section 4.3 with the exception of blood flow which was set at 0.8 ml/g/min representing normal blood flow or 1.2 ml/g/min to simulate a 50% increase in cortical blood flow.
Increasing blood flow to 1.2 ml/g/min produces approximately a 7% increase in hypothetical (R,S)-[$^{125}$I]-QNB concentration in the frontal cortex (right hand graph). This is consistent with the increase in (R,S)-[$^{125}$I]-QNB measured in frontal cortex of conscious rats following heptylphysostigmine administration (left hand graph). According to this model the increases in tracer levels observed in the cortex of heptylphysostigmine treated animals can be explained as a result of increased cerebral blood flow.

Data are expressed as mean ± S.E.M % Dose per g Brain normalised to the caudate nucleus (n= 5) for Actual Data, and % Dose per g Brain normalised to the caudate nucleus for Modelled Data. *P <0.05 Student's unpaired t-test for the comparison between vehicle and heptylphysostigmine treated animals.

## Effect of Increased Blood Flow on Hypothetical Uptake of (R,S)-[$^{125}$I]-QNB in Frontal Cortex

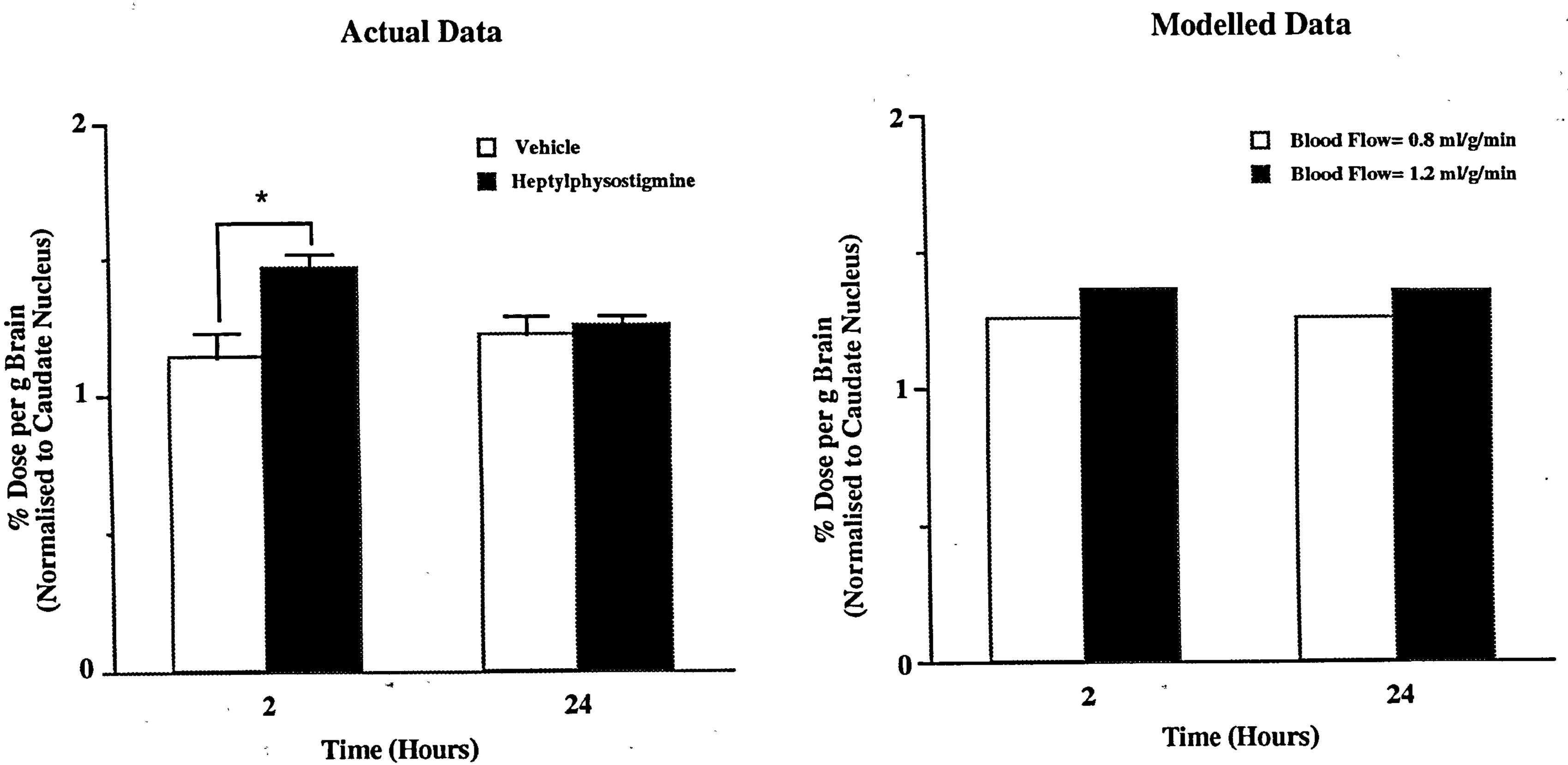


**Fig 60:** Comparision of actual concentration of (R,S)-[$^{125}$I]-QNB in frontal cortex in vehicle and heptylphysostigmine treated animals (left hand graph) as measured *in vivo* with hypothetical brain concentrations in frontal cortex for "normal" blood flow (0.8 ml/g/min) and for blood flow increases of 50% (1.2 ml/g/min) (right hand grpah).

### 4.5.2 AChE inhibition and synaptic ACh concentration

Data from *in vivo* experiments indicates that heptylphysostigmine administration does not displace (R,S)- or (R,R)-[$^{125}$I]-QNB from rat brain *in vivo* by increasing synaptic levels of endogenous ACh. It is possible that heptylphysostigmine (2mg/kg) did not inhibit AChE activity effectively or for a long enough period to raise synaptic ACh concentration to a level where it could displace iodo-QNB from mAChRs. However, a number of lines of evidence suggest that this is not the case. Histochemical analysis of brain AChE performed in this thesis indicates that enzyme activity is significantly reduced for a prolonged period. Secondly, the elevated cerebral blood flow rates measured *in vivo* and the overt behaviour displayed by the animals following heptylphysostigmine administration are indicative of raised levels of ACh. Finally, the efficacy of the dosing regime utilised in this thesis to inhibit AChE activity for extended periods and to increase synaptic ACh concentration is vindicated by the literature (De Sarno et al., 1989, Messamore et al., 1993, Cuadra et al., 1994).

Semi-quantitative analysis of AChE histochemical staining of rat brain sections taken from *in vivo* studies appears to validate the dosing regime used in this thesis. Significant reductions in AChE enzyme activity were observed in a number of brain regions including frontal cortex, parietal cortex, hippocampus CA1 and cerebellum between 30 mins and 24 hours after heptylphysostigmine administration. Furthermore, a number of *in vivo* microdialysis studies support these results indicating that heptylphysostigmine significantly inhibits brain AChE activity for prolonged periods. Following intramuscular administration heptylphysostigmine (5mg/kg) was observed to produce greater than 80% inhibition of AChE activity in the frontal cortex of rat for up to 6 hours (De Sarno et al., 1989, Cuadra et al., 1994). Additionally, heptylphysostigmine (5mg/kg ip) was observed to produce a significant level of inhibition (approximately 20%) of cortical AChE activity up to 24 hours after administration (Messamore et al., 1993).

In most studies maximal inhibition of AChE activity is observed approximately 1-1.5 hours after administration a time co-inciding with the administration of radiotracers in this thesis (De Sarno et al., 1989, Messamore et al., 1993, Cuadra et al., 1994).

Pharmacokinetic analysis of heptylphysostigmine in rat provides further evidence for the use of this compound. After a single administration (2mg/kg iv -the same dose and route of administration used in this thesis) heptylphysostigmine displays a prolonged plasma half-life of approximately 12 hours and preferential accumulation in the brain with levels as high as 22 times those found in plasma (Segre et al., 1992).

These observations all support the utility of heptylphysostigmine in the dosing regime used in this thesis to produce a sustained and effective inhibition of brain AChE.

However, magnitude of AChE inhibition is not a predictive determinant of extracellular ACh levels. Heptylphysostigmine and physostigmine have both been observed to produce increases of 1000% in extracellular ACh concentration while inhibiting AChE activity by 90% and 54 % respectively (Messamore at al., 1993). Inconsistencies between duration of AChE inhibition and the time course of increases in extracellular ACh are also apparent. Heptylphysostigmine (5mg/k ip)produces a peak increase in ACh of 1000% of baseline 1.5 hours following administration, with significant increases in ACh levels observed up to 9.5 hours after administration. However, in the period between 2 and 6 hours following drug administration however there is a drop in ACh levels of 700% during which time AChE inhibition falls by only 10% (Messamore et al., 1993). Indeed AChE activity is significantly inhibited long after (up to 24 hours) ACh levels have returned to normal. Therefore, although AChE activity appears to have been significantly inhibited for prolonged periods during the studies performed in this thesis, as evinced by AChE histochemistry, there is no evidence to indicate the magnitude or duration of increase in ACh concentration, or indeed whether ACh levels were raised at all.

A number of factors however suggest that extracellular levels of ACh were increased for a significant period following heptylphysostigmine administration.

The behaviour of animals receiving heptylphysostigmine was characteristic of cholinergic toxicity and lasted up to 4 hours after drug administration, indicating that extracellular concentration of ACh was raised for a prolonged period in the periphery at least. The increases in cerebral blood flow measured following heptylphysostigmine administration are characteristic of AChE inhibitor administration and are acknowledged to result from the action of excess ACh on mAChRs in the cerebrovasculature (Taylor, 1990). This observation indicates raised ACh concentration in the brain. Further evidence for increased ACh concentration in the brain comes from the observation that blood pressure was increased in a number of animals following hetylphysostigmine administration. Centrally administered physostigmine has been observed to produce dose dependent increases in heart rate and blood pressure in rats through the
action of ACh on central $M_2$ receptors (Ally et al., 1995). The central basis of this action is likely as it is in opposition to the characteristic inhibitory effects of peripherally administered cholinomimetics on heart rate.

Additionally, microdialysis studies of brain extracellular ACh concentration following heptylphysostigmine administration indicate significant increases in extracellular ACh are measurable for more than 6 hours after administration (De Sarno et al., 1989, Messamore et al., 1993, Cuadra et al., 1994). Furthermore, maximal levels of extracellular ACh are reached approximately 1 to 1.5 hours following administration. This correlates well with the increases in cerebral blood flow measured at 2 hours . These observations suggest that the dosing regime used in this thesis was successful in raising extracellular ACh levels to a significant degree for a period greater than 3 hours although no measurement of ACh was

made. Continuous infusion of heptylphysostigmine or physostigmine was considered as an alternative to the bolus administration employed in this thesis, but was decided to be impractical due to the prolonged experimental period necessary with some animals. Therefore administration of heptylphysostigmine a AChE inhibitor with prolonged duration of action was preferred.

### 4.5.3 Displacement of (R,S)- and (R,R)-[$^{125}$I]-QNB by endogenous ACh

Assuming that levels of extracellular ACh were raised for a significant period following heptylphysostigmine administration there may be several reasons why no displacement of (R,S)- or (R,R)-[$^{125}$I]-QNB from brain is observed. One possibility is that (R,S)- and (R,R)-[$^{125}$I]-QNB accumulation in brain does not reflect binding to mAChRs. Increasing ACh would therefore have little effect on brain levels of radioactivity. Previously described evidence suggests that brain accumulation of both tracers is receptor mediated. However, an *in vivo* displacement study with co-administration of either cold tracer or another mAChR antagonist would need to be performed to confirm mAChR occupancy by (R,S)- and (R,R)-[$^{125}$I]-QNB. Displacement of iodo-QNB in such a manner has been described in a number of studies with (R,S)-[$^{125}$I]-QNB (Gitler et al., 1995, McRee et al., 1995, Lee et al., 1995).

Additionally, it is possible that a small amount of radioligand is displaced from receptors by ACh but that this is masked by the effects of elevated blood flow increasing tracer delivery and uptake into the brain. Increased blood flow is also likely to increase washout of the tracer from the brain once it is dissociated from receptors. However, metabolism and clearance of both (R,S)- and (R,R)-[$^{125}$I]-QNB from plasma is slow with measurable levels of authentic ligand present in plasma for significant periods after administration (> 6 hours), albeit at a low concentration. Ligand washed out of brain which is not immediately metabolised and cleared may feasibly contribute to the pool of authentic ligand in plasma and may thus be available for re-uptake into brain. Furthermore, authentic ligand is present in plasma for a period exceeding that in which there will be significant competition from raised levels of endogenous ACh.

It is perhaps more likely therefore that extracellular ACh levels do not reach a concentration great enough to effect displacement of ligand from receptors. This theory is supported by evidence from displacement of $D_2$ receptor ligands *in vivo* by pharmacologically induced increases in endogenous dopamine. The magnitude of dopamine increase produced is usually several fold greater than the ligand displacement observed (Brier et al., 1997, Laruelle et al., 1997). Amphetamine induced displacement of [$^{11}$C]-raclopride combined with *in vivo* microdialysis in monkeys reported a mean dopamine increase to [$^{11}$C]-raclopride binding reduction ratio of 44 to 1, indicating that relatively small changes in ligand binding reflect large changes in transmitter outflow

raclopride(Endres et al., 1990). Therefore, significant increases in synaptic concentration of endogenous neurotransmitter are no indication of magnitude of ligand displacement occurring.

If a similar linear relationship exists between cortical ACh levels and iodo-QNB and assuming that heptylphysostigmine (2 mg/kg) produces an increase of 1000% in extracellular ACh concentration (based on the data of Messamore et al., 1993) a reduction of approximately 20% in cortical radioactivity would be observed following heptylphysostigmine administration. This however is obviously a gross oversimplification of the situation as evinced by the complete absence of QNB displacement observed in the studies presented in this thesis. Even if the relationship between ACh concentration and radioligand displacement is linear the kinetics of binding and affinity of raclopride and dopamine for $D_2$ receptors are considerably different to those of (R,S)- and (R,R)-[$^{125}$I]-QNB and ACh for mAChRs.

Differences in the relative affinity of ligands are an extremely important factor in their ability to reflect changes in endogenous ligand concentration, e.g. binding of [$^{11}$C]-raclopride is affected to a much greater extent than [$^{18}$F]-N-methylspiroperidol following amphetamine induced increases in dopamine due its larger $K_D$ value (i.e. 10nM and 0.25nM respectively) for $D_2$ receptors (Logan et al., 1991).

Raclopride is a highly selective but a relatively low affinity ligand for $D_2$ receptors, with a $K_D$ value of approximately 10nM (Farde et al., 1989). In contrast, (R,S)- and (R,R)-[$^{125}$I]-QNB are high affinity mAChR antagonists and assuming relative $m_1$ selectivity $K_D$ values equal 0.0116 nM and 0.490 nM respectively (Zeeberg et al., 1991). Therefore the affinity of iodo-QNB for mAChRs is approximately 20 to 1000 fold greater than that of raclopride for $D_2$ receptors. Furthermore, the affinity of the endogenous neurotransmitters for their target receptors must be taken into account when considering their ability to displace radioligand binding. The $K_D$ of dopamine for $D_2$ receptors has been estimated at 5 nM to 50 nM (Seeman et al., 1990, Ross et al., 1991). In contrast the $K_D$ of ACh for high affinity mAChR sites has be estimated at 3.3$\mu$M (Berstein et al., 1988). Therefore, at best dopamine displays 66 fold higher affinity for $D_2$ receptors than ACh for mAChRs. These observations suggest that displacement of iodo-QNB by endogenous ACh is likely to be very modest even when synaptic concentrations of ACh are significantly increased. Therefore, the synaptic concentration of ACh in cortex under normal conditions has a significant impact on the likelihood of radioligand displacement occurring under conditions where synaptic ACh concentrations are increased. The synaptic concentration of ACh in the cortex of the conscious rat as determined by *in vivo* microdialysis is estimated at 3-6 nM under normal conditions (Messamore et al., 1993, Cuadra et al., 1994 , Cuadra et al., 1995). An increase of ACh levels of 1000% following heptylphysostigmine

Cuadra et al., 1995). An increase of ACh levels of 1000% following heptylphysostigmine administration would give a synaptic concentration of 60nM, a value significantly lower than the $K_D$ of ACh for mAChRs.

The observations above suggest that although heptylphysostigmine can be predicted to produce a significant increase in cortical ACh concentration this may not be sufficient to displace (R,S)- or (R,R)-[$^{125}$I]-QNB binding from mAChRs due to the relative affinity of the radioligands and ACh for receptors and the basal synaptic concentration of ACh in the cortex. Furthermore, the dissociation evident between synaptic increases in dopamine and the observed displacement of [$^{11}$C]-raclopride binding-where the *in vivo* conditions are considerably more conducive to producing radioligand displacement -indicates that it may be impossible to raise synaptic ACh levels to a sufficient concentration to displace iodo-QNB binding with the use of heptylphysostigmine.

### 4.5.4 Sensitivity of radiotracers to dynamic neurotransmitter changes

A recent study has modelled radiotracer characteristics that confer maximum sensitivity to neurotransmitter release *in vivo* (Endres and Carson, 1998).

Using an extended compartmental model, the effect of a pharmacologically induced increase in endogenous neurotransmitter was modelled to calculate the percent reduction in distribution volume ($\Delta V$) of tracer in the brain. The magnitude of $\Delta V$ detected was found to be dependent upon a number of factors including the integral of the neurotransmitter pulse, clearance rate ($k_2$) of tracer from brain and binding potential of the tracer as well as on the free tracer concentration in the brain. In general the value of $\Delta V$ increases with the integral of neurotransmitter pulse i.e. the reduction in volume of distribution of ligand is dependent upon the overall increase in transmitter concentration and not just upon the peak level of neurotransmitter produced. Furthermore, the time at which the increase in neurotransmitter is induced has significant impact upon the magnitude of $\Delta V$.

Simultaneous release of neurotransmitter with tracer delivery was found to maximise $\Delta V$, with stimulation of neurotransmitter release before or after tracer administration producing suboptimal values of $\Delta V$. This has significant relevance to the studies performed in this thesis where increased levels of neurotransmitter were produced before administration of tracer. Therefore, optimal conditions for tracer displacement may not have been achieved in the studies presented in this thesis.

The clearance rate ($k_2$) of tracer from brain is also important in defining $\Delta V$-with a higher $k_2$ producing a larger $\Delta V$.

However, the binding potential of a tracer for receptors was identified as being the most useful parameter to describe the sensitivity of a tracer to neurotransmitter changes. Simulations revealed that tracers with smaller binding potentials generally produced the

biggest values of ΔV, with a binding potential of 3-10 optimal for tracer sensitivity to neurotransmitter changes (Endres and Carson, 1998). Use of the binding parameters k3 (association rate of specific binding), k4 (dissociation rate of specific binding) as determined by Sawada et al., (1990b) for R-IQNB allows estimation of the binding potential for iodo-QNB which is defined by these rate constants as k3/k4. The smallest binding potential values for frontal cortex, parietal cortex, caudate nucleus, thalamus and cerebellum were estimated as 1171, 977, 1116, 247 and 51 for each region respectively . Each value is significantly outwith the optimum range proposed by Endres and Carsson (1998), indicating that iodo-QNB is likely to be insensitive to changes in neurotransmitter levels due to its high binding potential.

### 4.5.5 Competition studies with AChE inhibitors and muscarinic radioligands

It has been established that (R,S)- and (R,R)-[$^{125}$I]-QNB are unsuitable ligands for the detection of dynamic changes in ACh levels *in vivo*. The viability of using AChE inhibitors such as heptylphysostigmine to increase ACh concentrations to levels sufficient to produce ligand displacement is also in question. Several factors are likely to restrict the extracellular ACh concentration following AChE administration. Accumulation of ACh at cholinergic synapses may have inhibitory actions on pre-synaptic autoreceptors resulting in reduced release of ACh from neurons. Recent evidence suggests that auto-inhibition such as this is an important factor governing extracellular ACh concentration at higher levels of AChE inhibition (Moor et al., 1998). In addition to increasing synaptic ACh concentration administration of AChE inhibitors elicit simultaneous increases in noradrenaline and dopamine in the cortex of rat (Cuadra et al., 1994). Interactions between noradrenergic and cholinergic systems are known to exist with noradrenaline inhibiting the release of cortical ACh through direct action on pre-synaptic α-adrenoceptors present on ACh terminals and indirectly through modulation of GABA release (Moroni et al., 1993 , Beani et al., 1986).Increases in noradrenaline may therefore also have an impact upon extracellular levels of ACh. The preferential inhibition of cytosolic (intracellular) AChE over molecular (extracellular) AChE by heptylphysostigmine may also play a role in the dissociation between synaptic ACh levels and the degree of inhibition of AChE observed and serve to limit synaptic ACh concentration (Ogane et al., 1992).

These observations suggest that AChE inhibitors may not be suitable for use in displacement studies with mAChR ligands. However, continuous infusion of physostigmine was observed to produce a 35% reduction in specific binding of the novel $M_2$ selective (i.e. Ki= 2.2 nM for $M_2$ and 7.4 nM for M1 receptors) PET ligand [$^{18}$F]FP-TZTP in monkeys (Carson et al., 1998). A significantly smaller reduction in binding of 12% was observed in the basal ganglia, consistent with the markedly higher AChE activity in this region. These results confirm the viability of using AChE inhibitors to displace

radioligands and indicate that ACh function can be measured *in vivo* with the use of mAChR ligands.

## REFERENCES


Abreo MA, Lin NH, Garvey DS, et al. Novel 3-Pyridyl Ethers With Subnanomolar Affinity For Central Neuronal Nicotinic Acetylcholine Receptors. Journal Of Medicinal Chemistry 1996; 39:817-825.

Akaike A, Sasa M, Takaori S. Muscarinic Inhibition As A Dominant Role In Cholinergic Regulation Of Transmission In The Caudate Nucleus. Journal Of Pharmacology And Experimental Therapeutics 1988; 246:1129-1136.

Alkondon M, Alberquerque E. Diversity Of Nicotinic Acetylcholine Receptors In Rat Hippocampal Neurons.1 Pharmacological And Functional Evidence For Distinct Structural Subtypes. Journal Of Pharmacology And Experimental Therapeutics 1993; 265:1455-1473.

Ally A, Wilson LB, Nobrega ACL, Mitchell JH. Cardiovascular Effects Elicited By Central Administraation Of Physostigmine Via $M_2$ Muscarinic Receptors In Conscious Cats. Brain Research 1995; 677:268-276.

Anderson R, Higgins GA. Absence Of Central Cholinergic Deficits In ApoE Knockout Mice. Psychopharmacology 1997; 132:135-144.

Andrews JS, Jansen JHM, Linders S, Princen A. Effects Of Disrupting The Cholinergic System On Short Term Spatial Memory In Rats. Psychopharmacology 1994; 115:485-494.

Appel NM, Contrera JF, DeSouza EB. Fenfluramine Selectively And Differentially Decreases The Density Of Serotonergic Nerve Terminals In Rat Brain. Evidence From Immunocytochemical Studies. Journal Of Pharmacology And Experimental Therapeutics 1989; 249:928-943.

Araujo DM, Lapchak PA, Collier B, Quirion R. Characterization Of N-[$^3$H] Methylcarbamylcholine Binding Sites And Effect Of N-Methylcarbamylcholine on ACetylcholine Release In Rat Brain. Journal Of Neurochemistry 1988; 51:292-299.

Arneric SP, Honig MA, Milner TA, Greco S, Iadecola C, Reis DJ. Neuronal And Endothelial Sites Of Acetylcholine Synthesis And Release Associated With Microvessels In Rat Cerebral Cortex: Ultrastructural And Neurochemical Studies. Brain Research 1988; 454:11-30.

Arneric SP, Iadecola C, Underwood MD, Reis DJ. Local Cholinergic Mechanisms Participate In The Increase In Cortical Cerebral Blood Flow Elicited By Electrical Stimulation Of The Fastigial Nucleus In Rat. Brain Research 1987; 411:212-225.

Ashkenazi A, Peralta EG, Winslow JW, Ramachandran J, Capon DJ. Functionally Distinct G-Proteins Selectively Couple Different Receptors To PL Hydrolysis in The Same Cell. Cell 1989; 56:487-493.

Ashkenazi A, Winslow JW, Peralta EG, et al. An $M_2$ Muscarinic Receptor Subtype Coupled To Both Adenylyl Cyclase And Phosphoinositide Turnover. Science 1987; 238:672-675.

Aubert I, Cecyre D, Gauthier S, Quirion R. Characterization And Autoradiographic Distribution Of [$^3$H] AF-DX 384 Binding To Putative Muscarinic $M_2$ Receptors In The Rat Brain. European Journal Of Pharmacology 1992; 217:173-184.

Aubineau P, Sercombe R. Evidence For A Double Cholinergic Mechamism Capable Of Reducing The Tone Of Cerebral Arteries. Acta Neurologica Scandinavica Supplement 1977; 64:296-297.

Bahr BA, Parsons SM. Acetylcholine Transport And Drug Inhibition Kinetics In Torpedo Synaptic Vesicles. Journal Of Neurochemistry 1986; 46:1214-1218.

Barlow RB, Berry KJ, Glenton PAM, Nikolaou NM, Soh KS. A Comparison Of Affinty Constants For Muscarine-sensitive Acetylcholine recepotrs In Guinea-pig Atrial pacemaker Cells At 29$^o$C And in ileum At 29$^o$C. British Journal Of Pharmacology 1976; 58:613-620.

Baron JC, Samson Y, Comar D, Crouzel C, Deniker P, Agid Y. An In Vivo Study Of Central Serotonin Receptors In Humans Using C11-Labelled Ketanserin And Positron Emmission Tomography. Revue Neurologique 1985; 141:537-545.

Bartus RT, Dean RL, Beer B, Lippa AS. The Cholinergic Hypothesis Of Geriatric Memory Dysfunction. Science 1982; 217:408-417.

Battaglia G, Sharkey J, Kuhar MJ, DeSouza EB. Neuroanatomical Specificity And Time Course Of Alterations In Rat Brain Serotonergic Pathways Induced By MDMA. Synapse 1991; 8249:260.

Baumgold J, Cohen VI, Paek R, Reba RC. Muscarinic Receptor Subtype Selectivity Of Novel Heterocyclic QNB Analogs. Life Sciences 1991; 48:2325-2329.

Baumgold J, Fishman PH. Muscarinic Receptor Mediated Increase In cAMP Levels In SK-N-SH Human Neuroblastoma Cells. Biochemical And Biophysical Research Communications 1988; 154:1137-1143.

Baumgold J, Paek R, Yasumoto T. Agents That Stimulate Phosphoinositide Turnover Also Elevate cAMP In SK-N-SH Human Neuroblastoma Cells. Life Sciences 1992; 50:1755-1759.

Beach TG, Walker DG, Cynader MS, Hughes LH. Increased Beta Amyloid Precursor Protein Messenger RNA In The Rat Cerebral Cortex And Hippocampus After Chronic Systemic Atropine Treatment. Neuroscience Letters 1996; 210:13-16.

Beani L, Tanganelli S, Antonelli T, Biachi C. Noradrenergic Modulation Of Cortical Acetylcholine Release Is Both Direct And Gamma Aminobutyric Acid Mediated. Journal Of Pharmacology And Experimental Therapeutics 1986; 236:230-236.

Bergner AD, Bayliss MW. Histochemical Detection Of Fatal Anticholinestersase Poisoning. US Armed Forces Medical Journal 1952; 3:1637-1649.

Berridge MJ. Rapid Accumulation Of Inositol Trisphosphate Reveals That Agonists Hydrolyze Polyphosphoinositides Instead Of Phosphatidylinositol. Biochemical Journal 1983; 212:849-858.

Berridge MS, Adler LP, Nelson AD, et al. Measurement Of Human Cerebral Blood Flow With [$0^{15}$] Butanol And Positron Emmission Tomography. Journal Of Cerebral Blood Flow And Metabolism 1991; 11:707-715.

Berstein G, Blank JL, Smrcka AV, et al. Reconstitution Of Agonist Stimulated Phosphatidylinositol 4,5-bisphosphate Hydrolysis Using Purified $M_1$ Muscarinic Receptor Gq/11 And Phospholipase $Cb_1$. Journal Of Biological Chemistry 1992; 267:8081-8088.

Berstein G, Haga K, Haga T, Ichiyama A. Agonist And Antagonist Binding Of Muscarinic Acetylcholine Receptors Purified From Porcine Brain: Interconversion Of High And Low Affinity Sites By Sulfhydryl Reagents. Journal Of Neurochemistry 1988; 50:1687-1694.

Biegon A, Woolf M. Quantitative Histochemistry Of Acetylcholinesterase In Rat And Human Brain Postmortem. Journal Of Neuroscience 1986; 16:39-45.

Biesold D, Inanami O, Sato A, Sato Y. Stimulation Of The Nucleus Basalis Of Meynert Increases Cerebral Cortical Blood Flow In Rats. Neuroscience Letters 1989; 98:39-44.

Bizzarri C, Digirolamo M, Dorazio MC, Corda D. Evidence That A guanine Nucleotide Binding Protein Linked To A Musarinic Recptor Inhibits Directly Phospholipase C. Proceedings Of The National Academy Of Sciences Of The United States OF America 1990; 87:4889-4893.

Blasberg R, Patlak C, Hiraga S, et al. IQNB And The Muscarinic ACh Receptor System In Rat Brain. Protein Binding, Metabolism And Kinetics. Journal Of Nuclear Medicine 1986; 27:937.

Blokland A, Honig W, Raaijmakers WGM. The Effect Of Intrahippocampal Scopolamine Injections In A Repeated Spatial Acquisition Task In The Rat. Psychopharmacology 1992; 109:373-376.

Blozovski D, Hennocq N. Effects Of Antimuscarinic Cholinergic Drugs Injected Systemically Or Into The Hippocampo-Entorhinal Area Upon Passive Avoidance Learning In Young Rats. Psychopharmacology 1982; 76:351-358.

Blusztajn JK, Lopez Gonzalez-Coviella I, Logue M, Growdon JH, Wurtman RJ. Levels Of Phospholipid Catabolic Intermediates, Glycerolphosphocoline and Glycerolphosphoethanolamine Are Elevated In Brains Of Alzheimer's Disease But Not Of Down's Syndrome Patients. Brain Research 1990; 536:240-244.

Bonner TI, Buckley NJ, Young AC, Brann MR. Identification Of A Family Of Muscarinic Acetylcholine Receptor Genes. Science 1987; 237:527-5332.

Boulay SF, Gitler MS, Sood VK, Cohen VI, Zeeberg BR, Reba RC. Comparison Of The In Vivo Rat Brain Regional Pharmacokinetics Of [$^3$H]-QNB, (R,S)-[$^{125}$I]-QNB and (R,R)-[$^{125}$I]-QNB Binding To The Muscarinic Acetylcholine Receptor In Relationship To The Regional Subtype Composition. Receptor 1996; 5:207-218.

Boulay SF, Sood VK, Rayeq MR, Cohen VI, Zeeberg BR, Reba RC. Autoradiographic Evidence That 3-Quinuclidinyl-4-fluorobenzilate (FQNB) Displays In Vivo Selectivity For The $m_2$ Subtype. Neuroimage 1996; 3:35-39.

Brandi ML, Rotella CM, Tanini A, Toccafondi R, Aloj SM. Cholinergic Control Of Cyclic Nucleotide Metabolism in Human Thyroid Cells. Journal Of Endocrinological Investigation 1987; 10:451-458.

Breese CR, Adams C, Logel J, et al. Comparison Of The Regional Expression Of Nicotinic Acetylcholine Receptor a7 mRNA and [$^{125}$I] Alphabungarotoxin Binding In Human Postmortem Brain. Journal Of Comparative Neurology 1997; 387:385-398.

Breier A, Su TP, Saunders R, et al. Schizophrenia Is Associated With Elevated Amphetamine Induced Synaptic Dopamine Concentrations: Evidence From A Novel Positron Emission Tomography Method. Proceedings Of The National Academy Of Science Of The United States Of America 1997; 94:2569-2574.

Brito GNO, Davis BJ, Stopp LC, Stanton ME. Memory And The Septo-Hippocampal Cholinergic System In The Rat. Psychopharmacology 1983; 76:315-320.

Brouselle EP, Wong DF, Fanelli RJ, London ED. In Vivo Specific Binding Of [$^{3}$H] 1-Nicotine In The Mouse Brain. Life Sciences 1989; 44:1123-1132.

Browne SE, Muir JL, Robbins TW, Page KJ, Everitt BJ, McCulloch J. The Effects Of Manipulating Excitatory Amino Acid Receptors In The Basal Forbrain On Central Glucose Metabolism. European Journal Of Neuroscience 1998; 10:649-663.

Browning ET, Schulman MP. [$^{14}$C] Acetylcholine Synthesis By Cortex Slices Of Rat Brain. Journal Of Neurochemistry 1968; 15:1391-1405.

Brucke T, Podreka I, Angelberger P, et al. Dopamine $D_2$ Receptor Imaging With SPECT-Studies In Different Neuropsychiatric Disorders. Journal Of Cerebral Blood Flow And Metabolism 1991; 11:220-228.

Buccafusco JJ, Jackson WJ. Beneficial Effects Of Nicotine Administered Prior To A Delayed Matching To Sample Task in Young And Aged Monkeys. Neurobiology Of Aging 1991; 12:233-238.

Buckley NJ, Burnstock G. Autoradiographic Localization Of Peripheral $M_1$ Muscarinic Recptors Using [H-3] Pirenzepine. Brain Research 1986; 375:83-91.

Butcher LL, Oh JD, Woolf NJ. Cholinergic Neurons Identified By In Situ Hybridization. Progress In Brain Research 1993; 98:1-8.

Butcher LL, Oh JD, Woolf NJ, Edwards RH, Roghani A. Organization Of Central Cholinergic Neurons Revealed by Combined In Situ Hybridization Histochemistry And Choline-o-Acetyltransferase Immunocytochemistry. Neurochemistry International 1992; 21:429-445.

Butcher LL, Woolf NJ. Histochemical Distribution Of Acetlycholinesterase In The Central Nervous System: Clues To The Localization Of Cholinergic Neurons. In: Bjorkland A, Hokflet Y, Kuhar MJ, eds. Handbook Of Chemical Neuroanatomy. Vol3: Classical Transmitter Receptors In The Central Nervous System, PartII. Amsterdam: Elsevier, 1984:1-50.

Buzsaki G, Bickford RG, Armstrong DM, et al. Electric Activity In The Neocortex Of Freely Moving Young And Aged Rats. Neuroscience 1988; 26:735-744.

Buzsaki G, Bickford RG, Ponomareff G, Thal LJ, Mandel R, Gage FH. Nucleus Basalis And Thalamic Control Of Neocortical Activity. Journal Of Neuroscience 1988; 8:4007-4026.

Callahan MJ, Kinsora JJ, Harbaugh RE, Reeder TM, Davis RE. Continuous ICV Infusion Of Scopolamine Impairs Sustained Attention Of Rhesus Monkeys. Neurobiology Of Aging 1993; 14:147-151.

Camps M, Carozzi A, Schnabel P, Scheer A, Parker PJ, Gierschik P. Isoenzyme Selective Stimulation Of Phospholipase C-Beta2 by G-Protein Beta-Gamma Subunits. Nature 1992; 360:684-686.

Carson RE, Breier A, deBartolomeis A, et al. Quantification Of Amphetamine Induced Changes in [$^{11}$C]Raclopride Binding With Continuous Infusion. Journal Of Cerebral Blood Flow And Metabolism 1997; 17:437-447.

Carson RE, Kiesewetter DO, Jagoda E, Der MG, Herscovitch P, Eckelman WC. Muscarinic Cholinergic Receptor Measurements With [$^{18}$F] FP-TZTP: Control And Competition Studies. Journal Of Cerebral Blood Flow And Metabolism 1998; In Press:

Cartaud J, Benedetti EL, Cohen JB, Meunier JC, Changeux JP. Presence Of A Lattice Structure In Membrane Fragments Rich In Nicotinic Receptor Protein From The Electric Organ Of Torpedo Marmorata. FEBS Letters 1973; 33:109-113.

Celsis P, Goldman T, Henriksen L, Lassen NA. A Method For Calculating Regional Cerebral Blood Flow From Emission Computed Tomography Of Inert Gas Concentrations. Journal Of Computer Assisted Tomography 1981; 5:641-645.

Chakeres DW, Schmalbrock P. Fundamentals Of Magnetic Resonance Imaging. Baltimore, Maryland: Williams and Wilkins, 1992:

Chalifour RJ, Kanfer JN. Microsomal Phospholipase D Of Rat Brain And Lung Tissues. Biochem biophys Res Commun 1980; 96:742-747.

Clark AL, Mitchelson F. The Inhibitory Effect Of Gallamine On Muscarinic Receptors. British Journal Of Pharmacology 1976; 58:323-331.

Clarke PBS, Schwartz RD, Paul SM, Pert CB, Pert A. Nicotinic Binding In Rat Brain Autoradiographic Comparsion Of [$^{3}$H] Acetylcholine, [$^{3}$H] Nicotine and [$^{125}$I] Alphabungarotoxin. Journal Of Neuroscience 1985; 5:1307-1315.

Collier B, Katz HS. Acetylcholine Synthesis From Recaptured Choline By A Sympathetic Ganglion. Journal Of Physiology 1974; 238:639-655.

Conklin BR, Brann MR, Buckley NJ, Ma AL, Bonnner TI, Axelrod J. Stimulation Of Arachidonic Acid Release And Inhibition Of Mitogenesis by Cloned Genes For Muscarinic Receptor Subtypes Stably Expressed In A9 L-Cells. Proceedings Of The National Academy Of Sciences Of The United States OF America 1988; 85:8698-8702.

Cortes R, Palacios JM. Muscarinic Cholinergic Receptor Subtypes In The Rat Brain I. Quantitative Autoradiographic Studies. Brain Research 1996; 362:227-238.

Court JA, Perry EK. CNS Nicotinic Receptors Possible Therapeutic Targets In Neurodegenerative Disorders. CNS Drugs 1994; 2:216-233.

Coyle JT, Price DL, Delong MR. Alzheimer's Disease-A Disorder Of Cortical Cholinergic Innervation. Science 1983; 219:1184-1190.

Crawford GD, Correa L, Salvaterra PM. Interaction Of Monoclonal Anitbodies With Mammalian Choline Acetyltransferase. Proceedings Of The National Academy Of Sciences Of The United States OF America 1982; 79:7031-7035.

Cuadra G, Giacobini E. Effects Of Cholinesterase Inhibitors And Clonidine Coadministraation On Rat Cortex Neurotransmitters In Vivo. Journal Of Pharmacology And Experimental Therapeutics 1995; 275:228-236.

Cuadra G, Summers K, Giacobini E. Cholinesterase Inhibitor Effects On Neurotransmitter In Rat Cortex In Vivo. Journal Of Pharmacology And Experimanetal Therapeutics 1994; 270:277-284.

Dacey RG, Bassett JE. Cholinergic Vasodilatation Of Intracerebral Arterioles In Rats. American Journal Of Physiology 1987; 253:H1253-H1260.

Dale HH. The Action Of Certain Esters And Ethers Of Choline, And Their Relation To Muscarine. Journal Of Pharmacology And Experimanetal Therapeutics 1914; 6:147-190.

Dannals RF, Ravert HT, Wilson AA. Synthesis Of High Specific Activity $^{11}C$ Labelled Tracers For Neuroreceptor Studies. Applied Radiation And Isotopes-International Journal Of Radiation Applications And Instrumentation Part A 1988; 39:559.

De Sarno P, Pomponi M, Giacobini E, Tang XC, Williams E. The Effect Of Heptylphysostigmine, A New Cholinesterase Inhibitor, On The Central Cholinergic System Of the Rat. Neurochemical Research 1989; 14:971-977.

Delacourte A, Defossez A. Alzheimer's Disease-Tau Proteins, The Promoting Factors Of Microtubule Assembly, Are Major Components Of Paired Helical Filaments. Journal Of Neurological Sciences 1986; 76:173-186.

DeSouza EB, Battaglia G, Insel TR. Neurotoxic Effects Of MDMA On Brain Serotonin Neurons. Evidence From Neurochemical And Radioligand Binding Studies. Annals Of The New York Academy Of Sciences 1990; 600:682-698.

Dewey SL, Brodie JD, Fowler JS, et al. Positron Emission Tomography (PET) Studies Of Dopaminergic Cholinergic Interactions In The Baboon Brain. Synapse 1990; 6:321-327.

Dinely-Miller K, Patrick J. Gene Transcripts For The Nicotinic Acetylcholine Receptor Subunit b4 Are Distributed In Multiple Areas Of The Rat Central Nervous System. Molecular Brain Research 1992; 16:339-344.

Doods HN, Quirion R, Mihm G, et al. Therapeutic Potential Of CNS Active $M_2$ Antagonist. Novel Structures And Pharmacology. Life Sciences 1993; 52:497-503.

Dorje F, Wess J, Lambrecht G, Tacke R, Mutschler E, Brann MR. Antagonist Binding Profiles Of Five Cloned Human Muscarinic Receptor Subtypes. Journal Of Pharmacology And Experimental Therapeutics 1991; 256:727-733.

Dow Edwards D, Dam M, Peterson JM, Rappaport SI, London ED. Effect Of Oxotremorine On Local Cerebral Glucose Utilization In Motor System Regions Of Rat Brain. Brain Research 1981; 226:281-289.

Drachman DA, Leavitt J. Human Memory And The Cholinergic System. A Relationship To Aging?. Archives In Neurology 1974; 30:113-121.

Dubner R, Bennett GJ. Spinal And Trigeminal Mechanisms Of Nociception. Annual Review Of Neuroscience 1983; 6:381-418.

Dunnett SB, Everitt BJ, Robbins TW. The Basal Forebrain Cortical Cholinergic System. Interpreting The Functional Consequences Of Excitoxic Lesions. Trends In Neuroscience 1991; 14:494-501.

Dunnett SB, Whishaw IQ, Jones GH, Bunch ST. Behavioural Biochemical And Histochemical Effects Of Different Neurotoxic Amino Acids Injected Into Nucleus Basalis Magnocellularis Of Rats. Neuroscience 1987; 20:653-669.

Eckelman WC, Grissom M, Conklin J, Rzeszotarski WJ, Gibson RE. In Vivo Competition Studies With Analogs Of 3-Quinuclidinyl Benzilate. Journal Of Pharmaceutical Sciences 1984; 73:529-534.

Eckelman WC, Reba RC, Rzeszotarski WJ, et al. External Imaging Of Muscarinic Acetylcholine Receptors. Science 1984; 223:291-293.

Edvinsson L, Falck B, Owman C. Possibilities For A Cholinergic Action On Smooth Musculature And On Sympathetic Axons In Brain Vessels Mediated By Muscarinic And Nicotinc Receptors. Journal Of Pharmacology And Experimental Therapeutics 1977; 200:117-126.

Edvinsson L, MacKenzie ET, McCulloch J. General And Comparative Anatomy Of The Cerebral Circulation. In: Cerebral Blood Flow And Metabolism. New York: Raven Press, 1993:15-21.

Efange SMN, Mach RH, Lhare AB, Michelson RH, Nowak PA, Evora PH. N-P-[F-18] Fluorobenzyltrozamicol ([F-18] FBT) Molecular Decomposition Reconstitution Approach To Novel Vesamicol Receptor Radioligands. Journal Of Nuclear Medicine 1993; 34:SSP8.

Efange SMN, Michelson RH, Khare AB, Thomas JR. Synthesis And Tissue Distribution Of (M-[$^{125}$I] Iodobenzyl)trozamicol ([$^{125}$I] MIBT). Potential Radioligand For Mapping Central Cholinergic Innervation. Journal Of Medicinal Chemistry 1993; 36:1754-1760.

Efange SMN, Michelson RH, Knusel B, et al. Synthesis And Biological Evaluation Of Radioiodinated N-2-(4-Piperidyl)ethyl Benzamides. Nuclear Medicine And Biology 1993; 20:527-538.

Ehlert FJ, Roeske WR, Yamamura HI. Regulation Of Muscarinic Receptor Binding By Guanine Nucleotides And N-Ethylmalemide. Journal Of Supramolecular Structure 1980; 1:149-162.

Ehlert FJ, Tran LLP. Regional Distribution Of $M_1$, $M_2$ And Non-$M_1$, Non-$M_2$ Subtypes Of Muscarinic Binding Sites In Rat Brain. Journal Of Pharmacology And Experimental Therapeutics 1990; 255:1148-1157.

Ellis J, Huyler J, Brann MR. Allosteric Regulation Of Cloned $M_1$-$M_5$ Muscarinic Receptor Subtypes. Biochem Pharmacol 1991; 42:1927-1932.

Endres CJ, Carson RE. Assessment Of Dynamic Neurotransmitter Changes With Bolus Or Infusion Delivery Of Neuroreceptor Ligands. Journal Of Cerebral Blood Flow And Metabolism 1998; In Press:

Endres CJ, Carson RE, Kolachana B, et al. Simultaneous Modelling Of [$^{11}$C] Raclopride PET And Dopamine Microdialysis Data. Journal Of Nuclear Medicine 1990; 37:77p.

Evans DA, Funkenstein H, Albert MS, et al. Prevalance Of Alzheimer's Disease In A Community Population Of Older Persons-Higher Than Previously Reported. Journal Of The American Medical Association 1989; 18:2551-2556.

Exton JH. Signalling Through Phosphatidylcholine Breakdown. Journal Of Biological Chemistry 1990; 265:1-4.

Fairclough RH, Miakelye RC, Stroud RM, Hodgson KO, Doniach S. Location Of Terbium Binding Sites On ACetylcholine Receptor Enriched Membranes. Journal Of Molecular Biology 1986; 189:673-680.

Farde L, Eriksson L, Blomqvist G, Hallidin C. Kinetic Analysis Of Central [$^{11}$C]-Raclopride Binding To $D_2$ Receptors in The Living Human Brain. Science 1989; 231:258-261.

Farde L, Hall H, Ehrin E, Sedvall G. Quantitative Analysis Of $D_2$ Dopamine Receptor Binding In The Living Human Brain By PET. Science 1986; 231:258-261.

Farde L, Suhara T, Halldin C, et al. PET Study Of The $M_1$ Agonists[$^{11}$C] Xanomeline And [$^{11}$C] Butylthio-TZTP In Monkey And Man. Dementia 1996; 7:187-195.

Farde L, Vonbahr C. Distribution Of Remoxipride To The Human Brain And Central $D_2$ Dopamine Receptor Binding Examined In Vivo By PET. Acta Psychiatrica Scandinavica 1990; 82 S358:67.

Farde L, Wiesel FA, Stoneelander S, et al. $D_2$ Dopamine Receptors In Neuroleptic Naive Schizophrenic Patients: A Positron Emission Tomography Study With [C11]-Raclopride. Archives Of General Psychiatry 1990; 47:213-219.

Fibiger HC. The Organization And Some Projections Of Cholinergic Neurons Of The Mammalian Brain. Brain Research Reviews 1982; 4:327-388.

Fischer A, Mantione CR, Abraham DJ, Hanin I. Long Term Central Cholinergic Hypofunction Induced In Mice By Ethylcholine Aziridinium (AF64A) In Vivo. Journal Of Pharmacology And Experimanetal Therapeutics 1982; 222:140-145.

Fischer W, Wictorin K, Bjorklund A, Williams LR, Varon S, Gage FH. Amelioration Of Cholinergic Neuron Atrophy And Spatial Memory Impairment In Aged Rats By Nerve Growth Factor. Nature 1987; 329:65-68.

Fisher SK, Agranoff BW. Receptor Activation And Inositol Lipid Hydrolysis In Neural Tissues. Journal Of Neurochemistry 1987; 48:999-1017.

Flynn DD, Ferraridileo G, Mash DC, Levey AI. Differential Regulation Of Molecular Subtypes Of Muscarinic Receptors in Alzheimer's Disease. Journal Of Neurochemistry 1995; 64:1888-1891.

Flynn DD, Potter LT. Different Effects Of N-Ethylmalemide On $M_1$ And $M_2$ Muscarine Receptors In Rat Brain. Proceedings Of The National Academy Of Science Of The United States Of America 1985; 82:580-583.

Fraser CM, Wang CD, Robinson DA, Gocayne JD, Venter JC. Site Directed Mutagenesis Of $M_1$ Muscarinic Acetylcholine Receptors-Conserved Aspartic Acids Play Important Roles In Receptor Function. Molecular Pharmacology 1989; 36:840-847.

Frey KA, Ehrenkaufer RL, Agranoff BW. Quantitative In Vivo Receptor Binding.II. Autoradiographic Imaging Of Muscarinic Cholinergic Receptors. Journal Of Neuroscience 1985; 5:2407-2414.

Frey KA, Ehrenkaufer RL, Beaucage S, Agranoff BW. Quantitative In Vivo Receptor Binding.I. Theory And Application To The Muscarinic Cholinergic Receptor. Journal Of Neuroscience 1985; 5:421-428.

Frey KA, Koeppe RA, Kilbourn MR, Snyder SE, Kuhl DE. PET Quantification Of Cortical Acetylcholinesterase Inhibition in Monkey And Human. Journal Of Nuclear Medicine 1997; 38:SS550.

Frey KA, Koeppe RA, Mulholland GK, et al. In Vivo Muscariic Cholinergic Receptor Imaging In Human Brain With [$^{11}$C] Scopolamine And Positron Emission Tomography. Journal Of Cerebral Blood Flow And Metabolism 1992; 12:147-154.

Frey KA, Kopppe RA, Jewett DM, et al. The In Vivo Distribution Of [$^{11}$C]-Scopolamine In Human Brain Determined By Positron Emmission Tomography. Society For Neuroscience Abstract 1987; 13:p1658.

Frost JJ, Mayberg HS, Fisher RS, et al. Mu Opiate Receptors Measured By Positron Emmission Tomography Are Increased In Temporal Lobe Epilepsy. Annals Of Neurology 1988; 23:231-237.

Frost JJ, Wagner HN, Dannals RF, et al. An In Vivo Study Of Central Serotonin Receptors In humans Using C-11-Labelled Ketanserin And Positron Emmission Tomography. Journal Of Computer Assisted Tomography 1985; 9:231-236.

Frost PT, Mintun MA, Raichle ME, Herscovitch P. A Non-invasive Approach To Quantitative Functional Brain Mapping With $H_2O^{15}$ And Positron Emmission Tomography. Journal Of Cerebral Blood Flow And Metabolism 1984; 4:329-33.

Furchgott RF, Zawadzki JV. The Obligatory Role Of Endothelial Cells In The Relaxation Of Arterial Smooth Muscle By Acetylcholine. Nature 1980; 288:373-376.

Gage FH, Wictorin K, Fischer W, Williams LR, Varon S, Bjorklund A. Retrograde Cell Changes In Medial Septum And Diagonal Band Following Fimbria Fornix Transection-Quantitative Temporal Analysis. Neuroscience 1986; 19:241-255.

Galzi JL, Changeux JP. Neuronal Nicotinic Receptors Molecular Organization And Regulation. Neuropharmacology 1995; 34:563-582.

Geula C, Mesulam MM. Cortical Cholinergic Fibres In Aging And Alzheimer's Disease A Morphometirc Study. Neuroscience 1989; 33:469-481.

Giachetti A, Mittman U, Brown JH, et al. Cardioselective Muscarinic Agonists. Federation Proceedings 1987; 46:2523-2535.

Giacobini E. Therapy Of Alzheimer's Disease-Symptomatic Or Neuroprotective?. Journal Of Neural Transmission 1994; 17:525-530.

Gibson RE, Moody T, Schneidau TA, Jagoda EM, Reba RC. The In Vitro Dissociation Kinetics Of (R,R)-[$^{125}$I] 4IQNB Is Reflected In The In Vivo Washout Of The Radioligand From Rat Brain. Life Sciences 1992; 50:629-637.

Gibson RE, Rzeszotarski WJ, Eckelman WC, Jagoda EM, Weckstein DJ, Reba RC. Differences In Affinities Of Muscarinic Acetylcholine Receptor Antagonists For Brain And Heart Receptors. Biochem Pharmacol 1983; 32:1851-1856.

Gibson RE, Rzeszotarski WJ, Jagoda EM, Francis BE, Reba RC, Eckelman WC. [$^{125}$I]-Quinuclidinyl 4-Iodobenzilate-A High Affinity, High Specific Activity Radioligand For The $M_1$ Acetylcholine And $M_2$ Acetylcholine Receptors. Life Sciences 1984; 34:2287-2296.

Gibson RE, Schneidau TA, Cohen VI, et al. In Vitro And In Vivo Characteristics Of [$^{125}$I] 3-(R)-Quinuclidinyl (S)-4-iodobenzilate. Journal Of Nuclear Medicine 1989; 30:1079-1087.

Gibson RE, Weckstein DJ, Jagoda EM, Rzeszotarski WJ, Reba RC, Eckelman WC. The Characteristics Of $^{125}$I 4-IQNB And $^{3}$H QNB In Vivo And In Vitro. Journal Of Nuclear Medicine 1984; 25:214-222.

Gibson RE, Zeeberg BR, Melograna JM, et al. In Vivo Dissociation Kinetics Of [$^{3}$H] Quinuclidinyl Benzilate: Relationship to Muscarini Receptor Concentration And In Vitro Kinetics. Brain Research 1991; 553:110-116.

Giraldo E, Hammer R, Ladinsky H. Disrtibution Of Muscarinic Receptor Subtypes In Rat Brain As Deermined In Binding Studies With AF-DX 116 And Pirenzepine. Life Sciences 1987; 40:833-840.

Gitler MS, Boulay SF, Virendar KS, et al. Characterization Of In Vivo Brain Muscarinic Acetylcholine Receptor Subtype Selectivity By Competition Studies Against (R,S)-[$^{125}$I]-QNB. Brain Research 1995; 687:71-78.

Gitler MS, Reba RC, Cohen VI, Rzeszotarski WJ, Baumgold J. A Novel $M_2$ Selective Muscarinic Antagonist-Binding Characteristics And Autoradiographic Distribution In Rat Brain. Brain Research 1992; 582:253-260.

Gjedde A, Wong DF. Modelling Neuroreceptor Binding Of Radioligands In Vivo. In: Frostt JJ, Wagner NH, eds. Quantitative Imaging: Neuroreceptors And Enzymes. New York: Raven Press, 1990:51-79.

Glenner GG, Wong CW. Alzheimer's Disease And Downs Syndrome-Sharing Of A Unique Cerebrovascular Amyloid Fibril Protein. Biochemical And Biophysical Research Communications 1984; 122:1131-1135.

Gnahn H, Hefti F, Heumann R, Schwab ME, Thoenen H. NGF Mediated Increase Of Choline Acetyltransferase (ChAT) In The Neonatal Rat Forebrain-Evidence For A Physiological Role Of NGF In The Brain. Developmental Brain Research 1983; 9:45-52.

Goldman H, Sapirstein LA. Brain Blood Flow In The Conscious And Anaesthetized Rat. American Journal Of Physiology 1973; 224:122-126.

Gordon I, Graver E, Genis I, Sehayek E, Michaelson DM. Memory Deficits And Cholinergic Impariments In Apolipoprotein E Deficit Mice. Neuroscience Letters 1995; 199:1-4.

Gray JA, Mitchell SN, Joseph MH, Grigoryan GA, Dawe S, Hodges H. Neurochemical Mechanisms Mediating The Behavioural And Cognitive Effects Of Nicotine. Drug Development Research 1994; 31:3-17.

Grundkeiqbal I, Iqbal K, Tung YC, Quinlan M, Wisniewski HM, Binder LI. Abnormal Phosphorylation Of The Microtubule Associated Protein Tau In Alzheimer Cytoskeletal Pathology. Proceedings Of The National Academy Of Sciences Of The United States OF America 1986; 83:4913-4917.

Gulyas AI, Gorcs TJ, Freund TF. Innervation Of Different Peptide Containing Neurons In The Hippocampus By GABAergic Septal Afferents. Neuroscience 1990; 37:31-44.

Gustavsson L, Hanson E. Stimulation Of Phospholipase D Activity By Phorbol Esters In Cultured Astrocytes. Journal Of Neurochemistry 1990; 54:737-742.

Hagan JJ, Jansen JHM, Broekkamp CLE. Blockade Of Spatial Learning By The $M_1$ Muscarinic Antagonist Pirenzepine. Psychopharmacology 1987; 93:470-476.

Hallanger AE, Levey AI, Lee HJ, Rye DB, Wainer BH. The Origins Of Cholinergic And Other Subcortical Afferents To The Thalamus In Rat. Journal Of Comparative Neurology 1987; 262:105-124.

Hallanger AE, Wainer BH. Ultrastructure Of ChAT Immunoreactive Terminals In The Reticular Nucleus Of The Rat. Journal Of Comparative Neurology 1988; 278:486-497.

Hammer R, Giachetti A. Muscarinic Receptor Subtypes M1 And M2 biochemical And Functional Characterization. Life Sciences 1982; 31:29991-2998.

Hanin I. AF64A Induced Cholinergic Hypofunction. Progress In Brain Research 1990; 84:289-299.

Hanin I, Jenden DJ, Cho AK. The Influence Of pH On The Muscarinic Action Of Oxotremorine, Arecoline, Pilocarpine, And Their Quaternary Ammonium Analogs. Molecular Pharmacology 1966; 2:352-359.

Hantraye P, loch C, Tacke U, et al. In Vivo Visulization By Positron Emmission Tomography Of The Progressive Striatal Dopamine Receptor Damage Occurring In MPTP Intoxicated Non-Human Primates. Life Sciences 1986; 39:1375-1382.

Hebb DO. Drives And The CNS (Conceptual Nervous System). Physiological Reviews 1955; 62:243-254.

Hefti F, Hartikka J, Salvatierra A, Weiner WJ, Mash DC. Localization Of Nerve Growth Factor Receptors In Cholinergic Neurons Of The Human Basal Forebrain. Neuroscience Letters 1986; 69:37-41.

Heidmann T, Changeux JP. Fast Kinetic Studies On The Allosteric Interactions Between Acetylcholine Receptor And The Local Anaexthetic Binding Sites. European Journal Of Biochemistry 1979; 94:281-296.

Helen P, London ED. Muscimol-Scopolamine Interactions in The Rat Brain. A Study With Deoxy-D-[$^{14}$C] Glucose. Journal Of Neuroscience 1984; 4:1405-1413.

Hempstead BL, Chleifer LS, Chao MV. Expression Of Functional Nerve Growth Factor Receptors After Gene Transfer. Science 1989; 243:373-375.

Hill TC, Magistretti PL, Holman BL, et al. Assessment Of Regional Cerebral Blood Flow (rCBF) In Stroke Using SPECT And N-Isopropyl-($^{123}$I)-para-iodoamphetamine (IMP). Stroke 1984; 15:40-45.

Holley LA, Wiley RG, Lappi DA, Sarter M. Cortical Cholinergic Deafferentiation Following The Intracortical Infusion Of Of 192IgG Saporin. A Quantitative Histochemical Study. Brain Research 1994; 663:277-286.

Holman BL, Gibson RE, Hill TC, Eckelman WC, Albert M, Reba RC. Muscarinic Acetylcholine Receptors In Alzheimer's Disease-In Vivo Imaging With Iodine 123 Labelled 3-Quinuclidinyl-4-iodobenzilate And Emission Tomography. Journal Of The American Medical Association 1985; 254:3063-3066.

Holman BL, Hellman RS, Goldsmith SJ, et al. Biodistribution, Dosimetry And Clinical Evaluation Of Technetium-99m Ethyl Cysteinate Dimer In Normal Subjects And In Patients With Chronic Cerebral Infarction. Journal Of Nuclear Medicine 1989; 30:1018-1024.

Hope BT, Michael GJ, Knigge JM, Vincent SR. Neuronal NADPH Diaphorase Is A Nitric Oxide Synthase . Proceedings Of The National Academy Of Science Of The United States Of America 1991; 88:2811-2814.

Horti A, Scheffel U, Dannals RF, et al. [$^{18}$F]-(+/-)-Exo-2-2(2-Fluoro-5-Pyridyl-)-7-Azabicyclo[2.2.1]He ptane, A Radioligand For In·Vivo Labelling And Imaging Of Central Nicotinic Acetylcholine Receptors. Journal Of Nuclear Medicine 1996; 37:SSp919.

Hu J, El-Fakahany EE. Selectivity Of McN-A-343 In Stimulating Phophoinisitide Hydrolysis Mediated By M$_1$ Muscarinic Receptors. Molecular Pharmacology 1990; 38:895-903.

Hughes AR, Harden TK. Adenosine And Muscarinic Cholinergic Receptors Attenuate Cyclic AMP Accumulation By Different Mechanisms In 1321N1 Astrocytoma Cells. Journal Of Pharmacology And Experimental Therapeutics 1986; 237:173-178.

Hulme EC, Birdsall NJM, Buckley NJ. Muscarinic Receptor Subtypes. Ann Rev Pharm Toxicol 1990; 30:633-673.

Hwang DR, Dence CS, McKinnon ZA, Mathias CJ, Welch MJ. Positron Labelled Muscarinic Acetylcholine Receptor Antagonist 2-[$^{18}$F] Fluorodexetimide And 4-[$^{18}$F] Fluorodexetimide Syntheses And Biodistribution. Nuclear Medicine And Biology 1991; 18:247-252.

Ingles JL, Beninger RJ, Jhamandas K, Boegman RJ. Scopolamine Injected Into The Rat Amygdala Impairs Working Memory In The Double Y-Maze. Brain Research Bulletin 1993; 32:339-344.

Innis RB, Malison RT, Altikriti M, et al. Amphetamine Stimulated Dopamine Release Competes In Vivo For [$^{123}$I] IBZM Binding To The $D_2$ Receptor In Non-Human Primates. Synapse 1992; 10:177-184.

Inoue M, Kuriyama H. Glucocorticoids Inhibit Acetylcholine Induced Current In Chromaffin Cells. American Journal Of Physiology 1989; 257:C906-C912.

Jakubik J, Backova L, Elfakahany EE, Tucek S. Subtype Selectivity Of the Positive Allosteric Action of Alcuronium At Cloned $M_1$-$M_5$ Muscarinic Acetylcholine Receptors. Journal Of Pharmacology And Experimental Therapeutics 1995; 274:1077-1083.

Jakubik J, Tucek S. Two Populations Of Muscarinic binding Sites In The Chick Heart Distinguished By Affinities For Ligands And Selective Inactivation. British Journal Of Pharmacology 1994; 113:1529-1537.

Jansson CC, Kukkonen J, Akerman KEO. Muscarinic Receptor Linked Elevation Of cAMP In SH-SY5Y Neuroblatoma Cells Is Mediated By $Ca^{2+}$ And Protein Kinase C. Biochemica Et Biophysica Acta 1991; 1095:255-260.

Jarrard LE, Kant GJ, Meyerhoff JL, Levy A. Behavioural And Neurochemical Effects Of Intraventricular AF64A Administration In Rats. Pharmacology Biochemistry And Behaviour 1984; 21:273-280.

Jope RS. High Affinity Choline Transport And AcetylCoA Production In Brain And Their Roles In The Regulation Of Acetylcholine Synthesis. Brain Research 1979; 180:313-343.

Kang J, Lemaire HG, Unterbeck A, et al. The Precursor Of Alzheimer's Disease Amyloid-A4 Protein Resembles A Cell Surface Receptor. Nature 1987; 325:733-736.

Kashikara K, Varga EV, Waite SL, Roeske WR, Yamamura HI. Cloning Of the Rat $M_3$, $M_4$ And $M_5$ Muscarinic Acetylcholine Receptor Genes By The Polymerase Chain Reaction (PCR) And the Pharmacological Characterization Of The Expressed Genes. Life Sciences 1992; 51:955-971.

Kassiou M, loch C, Strijkcmans V, et al. Synthesis Of [$Br^{76}$]4-Bromodexetimide And [$Br^{76}$] 4-Bromolevetimide. Radiotracers For Studying MuscarinicCholinergic receptors Using PET. Journal Of Labelled Compounds And Radiopharmaceuticals 1995; 36:259-266.

katz A, Wu DQ, Simon MI. Subunits Beta-Gamma Of Heterotrimeric G-Protein Activated $Beta_2$ Isoform Of Phosphlipase-C. Nature 1992; 360:686-689.

Kety SS. The Theory And Applications Of The Exchange Of Inert Gas At The Lungs And Tissues. Pharmacological Reviews 1951; 3:1-41.

Kew JNC, Sofroniew MV. Brain Derived Neurotrophic Factor, Acidic And Basic Fibroblast Growth Factors, Insulin-Like Growth Factor-I And Various Antioxidants Do Not Prevent The Apoptotic Death Of Developing Septal Cholinergic Neurons Following Nerve Growth Factor Withdrawal In Vivo. Neuroscience 1997; 76:809-820.

Kieswetter DO, Silverton JV, Eckelman WC. Synthesis And Biological Properties Of Chiral Fluoroalkyl Quinuclidinyl Benzilates. Journal Of Medicinal Chemistry 1995; 38:1711-1719.

Kim KD, Lernermarmarosh N, Wang DX, Kende AS, Abood LG. [$^3H$] Labelled Affinity And Photoaffinity Nicotine Analogs For Probing Brain Nicotinic Cholinergic Receptors. Medicinal Chemistry Research 1996; 6:40-51.

Kim SG, Ugurbil K. Functional Magnetic Resonance Imaging Of The Human Brain. Journal Of Neuroscience Methods 1997; 74:229-243.

Kirk RC, White KG, McNaughton N. Low Dose Scopolamine Affects Discriminability But Not Rate Of Forgetting In Delayed Conditional Discrimination. Psychopharmacology 1988; 96:541-546.

Knapp RJ, Hunt M, Wamsley JK, Yamamura HI. CNS Receptors For Opioods. In: London ED, ed. Imaging Drug Action In the Brain. CRC Press Inc., 1993:119-176.

Koelle LH, Friedenwald JS. A Histochemical Method For Localising Cholinesterase Activity. Proc Soc Exptl Biol Med 1949; 70:627-622.

Koeppe RA, Frey KA, Mulholland GK, et al. [$^{11}C$] Tropanyl Benzilate Binding To Muscarinic Cholinergic Receptors-Methodology And Kinetic Modelling Alternatives. Journal Of Cerebral Blood Flow And Metabolism 1994; 14:85-99.

Kowall NW, Kosik KS. Axonal Disruption And Aberrant Localization Of Tau Protein Characterize The Neuropil Pathology Of Alzheimer's Disease. Annals Of Neurology 1987; 22:639-643.

Krnjevic K, Silver A. A Histochemical Study Of Cholinergic Fibres In The Cerebral Cortex. Journal Of Anatomy 1965; 99:711-759.

Kromer LF. Nerve Growth Factor Treatment After Brain Injury Prevents Neuronal Death. Science 1987; 235:214-216.

Kubo T, Fukuda K, Mikami A, et al. Cloning, Sequencing And Expression Of Complementary DNA Encoding The Muscarinic Acetylcholine Receptor. Nature 1986; 323:411-416.

Kubo T, Maeda A, Sugimoto K, et al. Primary Structure Of Porcine Cardiac Muscarinc Acetylcholine Receptor Deduced From The cDNA Sequence. FEBS Letters 1986; 209:367-372.

Kuhar MJ, Murrin LC, Malouf AT, Klemm N. Dopamine Receptor Binding In Vivo: The Feasibility Of Autoradiographic Studies. Life Sciences 1978; 22:203-210.

Kuhar MJ, Yamamura HI. Light Autoradiographic Localisation Of Cholinergic Muscarinic Receptors In Rat Brain By Specific Binding Of A Potent Antagonist. Nature 1975; 253:560-561.

Kung HF, Alavi A, Chang W, et al. In Vivo SPECT Imaging Of CNS $D_2$ Dopamine Receptors. Initial Studies With Iodine-123 IBZM In Humans. Journal Of Nuclear Medicine 1990; 31:573-579.

Lai J, Mei L, Roeske WR, Chung FZ, Yamamura HI, Venter JC. The Cloned murine M1 muscarinic Receptor Is Associated With The Hydrolysis Of Phosphatidylinositols In Transfected murine B82 Cells. Life Sciences 1988; 42:2489-2502.

Lai J, Waite SL, Bloom JW, Yamamura HI, Roeske WR. The $M_2$ Muscarinic Acetylcholine Receptors Are Coupled To Multiple Signalling Pathways Via Pertusis Toxin Sensitive Guanine Nucleotide Regulatory Proteins. Journal Of Pharmacology And Experimental Therapeutics 1991; 258:938-944.

Lakher M, Wurtman RJ. In Vivo Synthesis Of Phosphatidylcholine In Rat Brain Via The Phospholipid Methylation Pathway. Brain Research 1987; 419:131-140.

Lambrecht G, Feifel R, Wagnerroder M, et al. Affinty Profiles Of Hexahydro-sila-difenidol Analogs At Muscarinc Receptor Subtypes. European Journal Of Pharmacology 1989; 168:71-80.

Lamy PP. The Role Of Cholinesterase Inhibitors In Alzheimer's Disease. CNS Drugs 1994; 1:146-165.

Landau WM, Freygang WHJr, Rowland LP, Sokoloff L, Kety SS. The Local Circulation Of The Living Brain, Values In The Unanesthetized And Anesthetized Cat. Transcripts Of The American Neurological Society 1955; 80:125-129.

Lee HJ, Rye DB, Hallanger AE, Levey AI, Wainer BH. Cholinergic Versus Non-Cholinergic Efferents From The Mespontine Tegmentum To The Extrapyramidal Motor System Nuclei. Journal Of Comparative Neurology 1988; 275:469-492.

Lee J, Paik C, Kiesewetter DO, Park SG, Eckelman WC. Evaluation Of Stereoisomers Of 4-Fluoroalkyl Analogues Of 3-Quinuclidinyl Benzilate In In Vivo Competition Studies Fo $M_1$, $M_2$ And $M_3$ Muscarinic Receptor Subtypes In Brain. Nuclear Medicine And Biology 1995; 22:773-781.

Lena C, Changeux JP. Allosteric Modulation Of The Nicotinic Acetylcholine Receptor. Trends In Neuroscience 1993; 16:181-186.

Levey AI. Muscarinic Acetylcholine Expression In Memory Circuits Implications For Treatment Of Alzheimer's Disease. Proceedings Of The National Academy Of Sciences Of The United States OF America 1996; 93:13541-13546.

Levey AI, Hallanger AE, Wainer BH. Cholinergic Nucleus Basalis Neurons May Influence The Cortex Via The Thalamus. Neuroscience Letters 1987; 74:7-13.

Levi-Montaclini R, Angeletti PU. Nerve Growth Factor. Physiology Reviews 1968; 48:534-569.

Levin ED. Nicotinic Systems And Cognitive Function. Psychopharmacology 1992; 108:417-431.

Lewis PR. The Effect Of Varying Conditions In The Koelle Technique. Bibliotheca Anat 1961; 2:11-20.

Liao C-F, Schilling WP, Birnbaumer M, Birnbaumer L. Cellular Responses To Stimulation Of The M5 muscarinic Acetylcholine Receptor As Seen in Murine L-Cells. Journal Of Biological Chemistry 1990; 265:11273-11284.

Linville DG, Giacobini E, Arneric SP. Heptylphysostigmine Enhances Basal Forebrain Control Of Cerebral Blood Flow. Journal Of Neuroscience Research 1992; 31:573-577.

Logan J, Dewey SL, Wolf AP, et al. Effects Of Endogenous Dopamine On Measures Of [$^{18}$F] N-Methylspiroperidol Binding in The Basal Ganglia. Comparison Of Simulations And Experimental Results From PET Studies In Baboons. Synapse 1991; 9:195-207.

London ED, Connolly RJ, Szikszay M, Wamsley JK, Dam M. Effects Of Nicotine On Local Cerebral Glucose Utilization In The Rat. Journal Of Neuroscience 1988; 8:3920-3928.

London ED, McKinney M, Dam M, Ellis A, Coyle JT. Decreased Cortical Glucose Utilization After Ibotenate Lesion Of The Rat Ventromedial Globus Pallidus. Journal Of Cerebral Blood Flow And Metabolism 1984; 4:381-390.

Longo VG. Behavioural And Electroencephalographic Effects Of Atropine And Related Compounds. Pharmacological Reviews 1966; 18:965-996.

Lopez MG, Fonteriz RI, Gandia L, et al. The Nicotinic Acetylcholine Receptor Of The Bovine Chromaffin Cell A New Target For Dihydropridines. European Journal Of Pharmacology Molecular Pharmacology Section 1993; 247:199-207.

Luetje CW, Patrick J. Both a and B Subunits Contribute To The Agonist Sensitivity Of Neuronal Nicotinic Acetylcholine Receptors. Journal Of Neuroscience 1991; 11:837-845.

Luetje CW, Wada K, Rogers S, et al. Neurotoxins Distinguish Between Different Neuronal Nicotinic Acetylcholine Receptor Subunit Combinations. Journal Of Neurochemistry 1990; 55:632-640.

Maeda A, Kubo T, Mishina M, Numa S. Tissue Distribution Of Messenger mRNAs Encoding Muscarinic Acetylcholine Receptor Subtypes. FEBS Letters 1988; 238:339-342.

Marien MR, Parsons SM, Altar CA. Quantitative Autoradiography Of Brain Binding Sites For The Vesicular Acetylcholine Transport Blocker 2-(40Phenylpiperidino)cyclohexanol (AH5183). Proceedings Of The National Academy Of Sciences Of The United States OF America 1987; 84:876-880.

Marshall IG. Studies on The Blocking Action Of 2-(-4-phenyl piperidino) cyclohexanol (AH5183). British Journal Of Pharmacology 1970; 38:503-516.

Martinez-Murillo R, Villalba RM, Rodrigo J. Immunocytochemical Localization Of Cholinergic Terminals In The Region Of The Nucleus Basalis Magnocellularis Of The Rat A Corrleated Light And Electron Microscopic Study . Neuroscience 1990; 36:362-376.

Mash DC, Flynn DD, Potter LT. Loss Of $M_2$ Muscarinic Receptors In The Cerebral Cortex In Alzheimer's Disease And Experimental Cholinergic Denervation. Science 1985; 228:1115-1117.

Mash DC, Potter LT. Autoradiographic Localization Of $M_1$ And $M_2$ Muscarine Receptors In Rat Brain. Neuroscience 1986; 19:551-564.

Massoulie J, Bon S. The Molecular Forms Of Cholinesterase And Acetylcholinesterase In Vertebrates. Annual Review Of Neuroscience 1982; 5:57-106.

Massoulie J, Sussman J, Bon S, Silman I. Structure And Functions Of Acetylcholinesterase And Butyrylcholinesterase. Progress In Brain Research 1993; 98:139-146.

Matuso Y, Seki A. Actions Of Pirenzepine Dihydrochloride (LS-519 Cl) On Gastric Juice Secretion, Gastric Moility And Experimental Gastric Ulcer. Arzneimittelforsch 1979; 29:1028-1035.

Maziere M. Cholinergic Neurotransmission Studied In Vivo Using Positron Emission Tomography Or Single Photon Emission Computerized Tomography. Pharmacology And Therapeutics 1995; 36:259-266.

McCormick DA. Cholinergic And Adrenergic Modulation Of Thalamocortical Processing. Trends In Neuroscience 1989; 12:215-221.

McCulloch J, Wallace MC, Laurie D, Angerson WJ, Burns HD, Gibson RE. Imaging Activation In The NMDA Receptor Complex With [$^{125}$I]-MK801. In: Krieglstein K, Oberpichler-Schwenk H, eds. Pharmacology Of Cerebral Ischaemia. Stuttgart: Wissenschaftliche Verlagsgesellschaft, 1992:159-163.

McPherson DW, Lambert CR, Knapp FF. In Vivo Metabolic Studies Of The Trans-(R,R) Isomer Of Radioiodinated IQNP-A New Ligand With High Affinity For The $M_1$ Muscarinic Cholinergic Receptor. European Journal Of Nuclear Medicine 1994; 21:1293-1297.

McRee RC, Boulay SF, Sood VK, et al. Autoradiographic Evidence That QNB Displays In Vivo Selectivity For The $m_2$ Subtype. Neuroimage 1995; 2:55-62.

Meeker RB, Harden TK. Muscarinic Cholinergic Receptor Mediated Activation Of Phosphodiesterase. Molecular Pharmacology 1982; 22:310-319.

Mei L, Lai J, Roeske WR, Fraser CM, Venter JC, Yamamura HI. Pharmacological Characterization Of The $M_1$ Muscarinic Receptors. Journal Of Pharmacology And Experimental Therapeutics 1989; 248:661-670.

Messamore E, Warpman U, Ogane N, Giacobini E. Cholinesterase Inhibitor Effects On Extracellular Acetylcholine In Rat Cortex. Neuropharmacology 1993; 32:745-750.

Messer WS, Thomas GJ, Hoss W. Selectivity Of Pirenzepine In The Central Nervous System 2. Differential Effects Of Pirenzepine And Scopolamine On Performance Of A Representational Memory Task. Brain Research 1987; 407:37-45.

Mesulam MM. Central Cholinergic Pathways: Neuroanatomy And Some Behavioural Implications. In: Avoli M, Reader TA, Dyles RW, Gloor P, eds. Neurotrasnmitters And Cortical Function. New York: Plenum Press, 1988:237-260.

Mesulam MM. Human Brain Cholinergic Pathways. Progress In Brain Research 1990; 84:231-241.

Mesulam MM. Structure And Function Of Cholinergic Pathways In The Cerebral Cortex, Limbic System, Basal Ganglia And Thalamus Of The Human Brain. In: Bloom FE, Koopfer DJ, eds. Psychopharmacolgy: The Fourth Generation Of Progress. New York: Raven Press, Ltd., 1995:

Mesulam MM, Geula C. Acetylcholineaterase Rich Neurons Of The Human Cerebral Cortex Cytoarchitectonic And Ontogenic Patterns Of Distribution. Journal Of Comparative Neurology 1991; 306:193-220.

Mesulam MM, Geula C, Bothwell MA, Hersh LB. Human Reticular Formation-Cholinergic Neurons Of The Pedunculopontine And Lateraldorsal Tegmental Nuclei And Some Cytochemical Comparisons To Forebrain Cholinergic Neurons. Journal Of Comparative Neurology 1989; 283:611-633.

Mesulam MM, Geula G. Nucleus Basalis (Ch4) And Cortical Innervation In The Human Brain-Observations Based On The Distribution Of Acetylcholinesterase And Choline Acetyltransferase. Journal Of Comparative Neurology 1988; 275:216-240.

Mesulam MM, Hersh LB, Mash DC, Geula C. Diffferential Cholinergic Innervation Within Functional Subdivisions Of The Human Cerebral Cortex A Choline Acertyltransferase Study. Journal Of Comparative Neurology 1992; 318:316-328.

Meyerhoff A. Absolute Configuration Of 3-Quinuclidinyl Benzilate And The Behavioural Effect In The Dog Of The Optical Isomers. Journal Of Medicinal Chemistry 1972; 15:994-995.

Michaelson DM, Angel I. Determination Of Delta pH In Cholinergic Synaptic Vesicles: It's Effect on Storage And Release Of Acetylcholine. Life Sciences 1980; 27:39-44.

Mintun MA, Raichle ME, Kilbourn MR, Wooten GF, Welch MJ. A Quantitative Model For The In Vivo Assessment Of Drug Binding Sites With Positron Emission Tomography. Annals Of Neurology 1984; 15:217-227.

Mitchelson F. Muscarinic Receptor Differentiation. Pharmacology And Therapeutics 1988; 37:357-423.

Moore PK, Evans R, Alswayeh OA. Rabbit Brain Contains An Endogenous Inhibitor Of Nitric Oxide Biosynthesis. European Journal Of Pharmacology 1990; 183:646-647.

Moroni F, Alesiani M, Leonardi P, Cherici G, Pelliccairi R, Lombardi G. Agonists Of Metabotropic Glutamate Receptors Differentially Modulate Transmitter Output. Journal Of Neurochemistry 1993; 61:S 266.

Moruzzi G, Magoun HW. Brain Stem Reticular Formation And Activation Of The Electroencephalogram. Clinical Neurophysiology 1949; 10:455-473.

Muir JL, Everitt BJ, Robbins TW. Reversal Of Visual Attention Dysfunction Following Lesions Of The Cholinergic Basal Forebrain By Physostigmine And Nicotine But Not By The 5-HT3 Receptor Antagonist Ondansetron. Psychopharmacology 1995; 118:82-92.

Muir JL, Everitt BJ, Robbins TW. The Cerebral Cortex Of The Rat And Visual Attention Function. Dissociable Effects Of Mediofrontal, Cingulate, Anterior, Dorsolateral And Parietal Cortex Lesions On A 5 Choice Serial Reaction Time Task. Cerebral Cortex 1996; 6:470-481.

Mulholland GK, Kilbourn MR, Sherman P, et al. Synthesis, In Vivo Biodistribution And Dosimetry Of [$^{11}$C] N-Methylpiperidyl Benzilate ([$^{11}$C] NMPB), A Muscarinic Acetylcholine Receptor Antagonist. Nuclear Medicine And Biology 1995; 22:13-17.

Mulle C, Lena C, Changeux JP. Potentiation Of Nicotinic Receptor Response By External Calcium In Rat Central Neurons. Neuron 1992; 8:937-945.

Musachio JL, Scheffel U, Stathis M, et al. Synthesis Of [$^{125}$I/$^{123}$I]-IPH: A Radiolabelled Analog Of Epibatidine For In Vivo Studies Of Nicotinic Acetylcholine Receptors. Journal Of Nuclear Medicine 1996; 37:SSp12.

Nakagawayagi Y, Saito Y, Takada Y, Nakamura H. Supressive Effect Of Carbachol On Forskolin Stimulated Neurite Outgrowth In Human Neuroblastoma NB-OK1 Cells. Biochemical And Biophysical Research Communications 1992; 182:45-54.

Nehls DG, Park CK, MacCormack AG, McCulloch J. The Effects Of N-Methyl-D-Aspartate Receptor Blockade With MK 801 Upon The Relationship Between Blood Flow And Glucose Utilization. Brain Research 1990; 511:271-279.

Neirinckx RD, Canning LR, Piper IM, et al. Technitium-99m D,1-HMPAO-A New Radiopharmaceutical For SPECT Imaging Of Regional Cerebral Blood Perfusion. Journal Of Nuclear Medicine 1987; 28:191-202.

Nilsson OG, Leanza G, Rosenblad C, Lappi DA, Wiley RG, Bjorklund A. Spatial Learning Impairments In Rats With Selective Immunolesion Of The Forebrain Cholinergic System. Neuroreport 1992; 3:1005-1008.

Nitsch RM, Slack BE, Wurtma RJ, Growdon JH. Release Of Alzheimer Amyloid Precursor Derivatives Stimulated by Activation Of Muscarinic Acetylcholine Receptors. Science 1992; 258:304-307.

Nonaka R, Moroji T. Quantitative Autoradioagraphy Of Muscarinic Cholinergic Receptors In The Rat Brain. Brain Research 1984; 296:295-303.

Nordberg A, Hartvig P, Lilja A, et al. Decreased Uptake And Binding Of $^{11}C$ Nicotine in Brain Of Alzheimer Patients As Visualized By Positron Emission Tomography. Journal Of Neural Transmission-Parkinsons Disease And Dementia 1990; 2:215-224.

Nordberg A, Hartvig P, Lundqvist H, Antoni G, Ulin J, Langstrom B. Uptake And regional Distribution Of (+)-(R)-N-[Mehtyl-C11]-Nicotine And (-)-)S)-N-[Methyl-C11]-Nicotine In the Brains Of Rhesus Monkey. An Attempt To Study Nicotinic Receptors In Vivo. Journal Of Neural Transmission 1989; 1:195-205.

Nyback H, Halldin C, Ahlin A, Curvall M, Eriksson L. PET Studies Of The Uptake Of (S)-[$^{11}C$] Nicotine And (R)-[$^{11}C$] Nicotine In The Human Brain. Difficulties In Visualizing Specific Receptor Binding In Vivo. Psychopharmacology 1994; 115:31-36.

Nyback H, Nordberg A, Langstrom B, et al. Attempts To Visualize Nicotinic Receptors In The Brain Of Monkey And Man By Positron Emission Tomography. Progress In Brain Research 1989; 79:313-319.

Octave JN. The Amyloid Precursor Peptide And Its Precursor In Alzheimer's Disease. Reviews In The Neurosciences 1995; 6:287-316.

Offermans S, Wieland T, Homann D, et al. Transfected Muscarinic Acetylcholine Receptors Selectively Couple To $G_i$ Type G-Proteins And $G_{q/11}$. Molecular Pharmacology 1994; 45:890-898.

Ohno M, Yamamoto T, Watanabe S. Blockade Of Hippocampal Nicotinic Receptors Impairs Working Memory But Not Reference Memory In Rats. Pharmacology Biochemistry And Behaviour 1993; 45:89-93.

Ohtake T, Heckers S, Wiley RG, Lappi DA, Mesulam MM, Geula C. Retrograde Degeneration And Colchicine Protection Of Basal Forebrain Cholinergic Neurons Following Hippocampal Injections Of An Immunotoxin Against The P75 Nerve Growth Factor Receptor. Neuroscience 1997; 78:123-133.

Olianas MC, Onali P. Properties Of Muscarinic Stimulated Adenylate Cyclase Activity In Rat Olfactory bulb. Journal Of Neurochemistry 1992; 58:1723-1729.

Orrison WW. Introduction To Neuroimaging. Boston: Little, Brown and Company, 1989:65-75.

Ortells MO, Lunt GG. Evolutionary History Of The Ligand Gated Ion-Channel Superfamily Of Receptors. Trends In Neuroscience 1995; 18:121-127.

Page KJ, Sirinathasinghji DJS, Everitt BJ. AMPA Induced Lesions Of the Basal Forebrain Differentially Affect Cholinergic And Non-cholinergic Neurons. Lesion Assessment Using Quantitative In-situ Hybridization Histochemistry. European Journal Of Neuroscience 1995; 7:1012-1021.

Palacios JM, Mengod G, Vilaro MT, et al. Cholinergic Receptors In The Rat And Human Brain: Microscopic Visualization. Progress In Brain Research 1990; 84:243-253.

Parker EM, Kameyama K, Higashijima T, Ross EM. Reconstitutively Active G-Protein Coupled Receptors Purified From Baculovirus Infected Insect Cells. Journal Of Biological Chemistry 1991; 266:519-527.

Parsons SM, Prior C, Marshall IG. Acetylcholine Transport, Storage And Release. International Review Of Neurobiology 1993; 35:279-390.

Patlak CS, Blasberg RG, Fenstermacher JD. An Evaluation Of Errors In The Determination Of Blood Flow By The Indicator Fractionation And Equilibrium (Kety) Methods. Journal Of Cerebral Blood Flow And Metabolism 1984; 4:47-60.

Paxinos G, Watson C. The Rat Brain In Stereotaxic Co-ordinates. 2nd ed. Sydney: Academic Press, 1986:

Pedder EK, Eveleigh P, poyner D, Hulme EC, Birdsall NJM. Modulation Of The Structure-Binding Relationship Of Antagonists For Muscarinic Acetylcholine Receptor Subtypes. British Journal Of Pharmacology 1991; 103:1561-1567.

Penney JB, Young AB. Quantitative Autoradiography Of Neurotransmitter Receptors In Huntington Disease. Neurology 1982; 32:1391-1395.

Pepeu G, Casamenti F, Giovanni MG, Vannuchi MG, Pedata F. Principal Aspects Of The Regulation Of Acetylcholine Release In The Brain. Progress In Brain Research 1990; 84:273-278.

Peralta EG, Ashkenazi A, Winslow JW, Ramachandran J, Capon DJ. Diffferential Regulation Of PI Hydrolysis And Adenyl Cyclase By Muscarinic Receptor Sbutypes. Nature 1988; 334:434-437.

Peralta EG, Ashkenazi A, Winslow JW, Smith DH, Ramachandran J. Distinct Primary Structures, Ligand Binding properties And Tissue Specific Expression Of 4 human Muscarinic Acetylcholine Receptors. EMBO Journal 1987; 13:3923-3929.

Peralta EG, Winslow JW, Peterson GL, et al. Primary Structure And Biochemical Properties Of An $M_2$ Muscarinc Receptor. Science 1987; 236:600-605.

Pereira EFR, Reinhardtmaelicke S, Schrattenholz A, Maelicke A, Albuquerque EX. Identification And Functional Characterizarion Of A New Agonist Site On Nicotinic Acetylcholine Receptors Of Cultured Hippocampal Neurons. Journal Of Pharmacology And Experimental Therapeutics 1993; 265:1471-1491.

Perry DC, Kellar KJ. [$^3$H] Epibatidine Labels Nicotinic Receptors In Rat Brain:An Autoradiographic Study. Journal Of Pharmacology And Experimental Therapeutics 1995; 275:1030-1034.

Perry EK, Court JA, Johnson M, Piggott MA, Perry RH. Autoradiographic Distribution Of [$^3$H] Nicotine Binding In Human Cortex Relative Abundance in Subicular Complex. Journal Of Chemical Neuroanatomy 1992; 5:399-405.

Perry EK, Kellar KJ. [$^3$H] Epibatidine Labels Nicotinic Receptors In Rat Brain An Autoradiographic Study. Journal Of Pharmacology And Experimental Therapeutics 1995; 275:1030-1034.

Perry EK, Smith CJ, Court JA, Perry RH. Cholinergic Nicotinc And Muscarinic ACetylcholine Receptors In Dementia Of Alzheimer, Parkinson And Lewy Body Dementia. Journal Of Neural Transmission 1990; 2:149-158.

Perry EK, Smith CJ, Perry RH, Whitford C, Johnson M, Birdsall NJ. Regional Distribution Of Muscarinic And Nicotinic Cholinergic Receptor Binding Activities In The Human Brain. Journal Of Chemical Neuroanatomy 1989; 2:189-199.

Perry EK, Tomilinson BE, Blessed G, Bergmann K, Gibson PH, Perry RH. Correlation Of Cholinergic Abnormalities With Senile Plaques And Mental Test Scores In Senile Dementia. British Medical Journal 1978; 2:1457-1459.

Pert CB, Kuhar MJ, Snyder SH. Autoradiographic Localization Of The Opiate Receptor In Rat Brain. Life Sciences 1975; 16:1849-1853.

Phelps ME, Maziotta JC, Kuhl DE, et al. Tomographic Mapping Of Human Cerebral Metabolism Visual Stimulation And Deprivation. Neurology 1981; 31:517-529.

Poirier J. Apolipoprotein E Polymorphism And Alzheimer's Disease. Lancet 1993; 261:921-923.

Poirier J. Apolipoprotein E In Aniaml Models Of CNS Injury And In Alzheimer's Disease. Trends In Neuroscience 1994; 17:525-530.

Poirier J, Hess M, May PC, Finch CE. Cloning Of Hippocampal Poly (A) RNA Sequences That Increase After Entorhinal Cortex Lesion In Adult Rat. Molecular Brain Research 1991; 9:191-195.

Potter LT. Synthesis,Storage And Release Of [$^{14}$C] Acetylcholine In Isolated Rat Diaphragm Muscles. Journal Of Physiology 1970; 206:145-166.

Potter LT, Flynn DD, Hanchett HE, Kalinoski DL, Lubernarod J, Mash DC. Independent $M_1$ And $M_2$ Receptors. Ligands, Autoradiography and Functions. Trends In Pharmacological Sciences 1984; S:22-31.

Preda L, Alberoni M, Bressi S, et al. Effects Of Acute Doses Of Oxiracetam In The Scopoalmine Model Of Human Amnesia. Psychopharmacology 1993; 110:421-426.

Prenant C, Barre L, Crouzel C. Synthesis Of [$^{11}$C] 3-Quinuclidinylbenzilate (QNB). Journal Of Labelled Compounds And Radiopharmaceuticals 1989; 27:1257-1265.

Price DL. New Perspectives On Alzheimer's Disease. Annual Review Of Neuroscience 1986; 9:489-512.

Proska J, Tucek S. Mechanisms Of Steric And Cooperative Actions Of Alcuronium On Cardiac Muscarinic Acetylcholine Receptors. Molecular Pharmacology 1994; 45:709-717.

Qian C, Li T, Shen TY, et al. Epibatidine Is A Nicotinic Analgesic. European Journal Of Pharmacology 1993; 250:R13-R14.

Quinn DM. Acetylcholinesterase: Enzymme Structure, Reaction Dynamics And Virtual Transition States. Chemical Reviews 1987; 87:955-979.

Quirion R, Boska P. Autoradiographic Distribution Of Muscarinic [$^3$H] Acetylcholine Receptors In Rat Brain: Comparison With Antagonists. European Journal Of Pharmacology 1986; 123:170-172.

Raiteri M, Leardi R, Marchi M. Heterogeneity Of Muscarinic Receptors Regulating Neurotransmitter Release In The Rat Brain . Journal Of Pharmacology And Experimental Therapeutics 1984; 228:209-214.

Raiteri M, Marchi M, Paudice P, Pittaluga A. Muscarinic Receptors Mediating Inhibition Of Gamma-amino-butyric-acid Release In Rat Corpus Striatum And Their Pharmacological Characterzation. Journal Of Pharmacology And Experimental Therapeutics 1990; 254:496-501.

Rapier C, Lunt GG, Wonnacott S. Stereoselective Nicotine Induced Release Of Dopamine From Striatal Synaptosomes Concentration Dependence And Repetitive Stimulation. Journal Of Neurochemistry 1988; 50:1123-1130.

Rapoport SI. Regulation Of Drug Entry Into The Nervous System. In: The Blood Brain Barrier In Physiology And Medicine. New York: Raven Press, 1976:153-176.

Rebois RV, Reynolds EE, Toll L, Howard BD. Storage Of Dopamine And ACetylcholine In Granules Of PC12, A Clonal Pheochromocytoma. Biochemistry 1980; 19:1240-1248.

Regenold W, Araujo D, Quirion R. Direct Visualization Of Brain $M_2$ Muscarinic Receptors Using The Selective Antagonist [$^3$H[ AF-DX 116. European Journal Of Pharmacology 1987; 144:417-419.

Regunathan S, Meeley MP, Reis DJ. Effect Of Clonidine on 2nd Messenger Systems In Rat Adrenal Gland. Life Sciences 1990; 47:2127-2133.

Reisine TD, Yammamura HI, Bird ED, Spokes E, Enna SJ. Pre- And Postsynaptic Neurochemical Alterations in Alzheimer's Disease. Brain Research 1978; 159:477-481.

Reynolds JA, Karlin A. Molecular Weight In Detergent Solution Of Acetylcholine Receptor From Torpedo Californica. Biochemistry 1978; 17:2035-2038.

Rhee SG, Choi KD. Regulation Of Inositol Phospholipid Specific Phospholipase C Isoenzymes. Journal Of Biological Chemistry 1992; 267:12393-12396.

Riekkinen P, Buzsaki G, Soininen H, Partanen J. The Cholinergic System And EEG Slow Waves. Electroencephalography And Clinical Neurophysiology 1991; 78:89-96.

Riker WF, Wescoe WC. The Pharmacolgy Of Flaxedil With Observations On Certain Analogs. Annals Of The New York Academy Of Sciences 1951; 54:373-394.

Robbins TW. Arousal Systems And Attentional Processes. Biological Physiology 1997; 45:57-71.

Robbins TW, Everitt BJ, Marston HM, Wilkinson J, Jones GH, Page KJ. Comparitive Effects Of Ibotenic Acid Induced And Quisqualic Acid Induced Lesions Of The Substantia Innominata On Attentional Function In Rat. Further Implications For The Role Of The Cholinergic Neurons Of the Nucleus Basalis In Cognitive Processes. Behavioural Brain Research 1989; 35:221-240.

Rossier J, Spantidakis Y, Benda P. The Effect Of $Cl^-$ On Choline Acetyltransferase Kinetic Parameters And A Proposed Role For $Cl^-$ In The Regulation Of Acetylcholine Synthesis. Journal Of Neurochemistry 1977; 29:1007-1012.

Ruggerio DA, Giuliano R, Anwar M, Stornetta R, Reis DJ. Anatomical Substrates Of Cholinergic Autonomic Regulation In The Rat. Journal Of Comparative Neurology 1990; 292:1-53.

Rupniak N,M.J., Samson NA, Tye SJ, Field MJ, Iversen SD. Evidence Against A Specific Effect Of Cholinergic Drugs On Spatial Memory In Primates. Behavioural Brain Research 1991; 43:1-6.

Rylett RJ, Schmidt BM. Regulation Of The Synthesis Of Acetylcholine. Progress In Brain Research 1993; 98:161-166.

Rzeszotarski WJ, Eckelman WC, Francis BE, et al. Synthesis And Evaluation Of Radioiodinated Derivatives Of 1-Azabicyclo [2.2.2] Oct-3-yl Alpha-hydroxy-(4-iodophenyl)-alpha Phenylacetate As Potential Radiopharmaceuticals. Journal Of Medicinal Chemistry 1984; 27:156-160.

Rzeszotarski WJ, Gibson RE, Simms DA, Jagoda EM, Ferreira NL, Reba RC. Analogs Of 3-Quinuclidinyl Benzilate. Journal Of Medicinal Chemistry 1982; 25:1103-1106.

Rzeszotarski WJ, McPherson DW, Ferkany DW, Kinnier WJ, Noronhablob L, Kirkienrzeszotarski A. Affinity And Selectivity Of The Optical Isomers of 3-Quninuclidinyl Benzilate And Related Muscarinic Antagonists. Journal Of Medicinal Chemistry 1988; 31:1463-1466.

Sahakian B, Jones G, Levy R, Gray J, Warburton D. The Effects Of Nicotine on Attention, Information Processing And Short Term Memory in Patients With Dementia Of The Alzheimer Type. British Journal Of Psychiatry 1989; 154:797-800.

Saji H, Magata Y, Tajima K, et al. Radioiodinated (S)-5-Iodonicotine: A New Radiopharmaceutical For SPECT Studies Of Brain Nicotine Receptors. Journal Of Nuclear Medicine 1993; 34:SSP234.

Sakurada O, Kennedy C, Jehle J, Brown JD, Carbin GL, Sokoloff L. Measurement Of Local Cerebral Blood Flow With Iodo [$^{14}C$] Antipyrine. American Journal Of Physiology 1978; 234:H59-H66.

Salvaterra PM, Vaughn JE. Regulation Of Choline Acetyltransferase. International Review Of Neurobiology 1989; 31:81-143.

Sandmann J, Peralta EG, Wurtman RJ. Coupling Of Transfected Muscarinic Acetylcholine Rceptor Subtypes To Phospholipase D. Journal Of Biological Chemistry 1991; 266:6031-6034.

Sargent PB. The Diversity Of Neuronal Nicotinic Acetylcholine Receptors. Annual Review Of Neuroscience 1993; 16:403-443.

Sawada Y, Hiraga BF, Patlak C, et al. Kinetic Analysis Of 3-Quinuclidinyl 4-[$^{125}I$] Iodobenzilate Transport And Specific Binding To Muscarinic Acetylcholine Receptor in Rat

Brain In Vivo: Implications For Human Studies. Journal Of Cerebral Blood Flow And Metabolism 1990; 10:781-807.

Sawada Y, Hiraga S, Patlak CS, Ito K, Pettigrew K, Blasberg RG. Cerebrovascular Transport Of [$^{125}$I] Quinuclidinyl Benzilate, [$^{3}$H] Cyclofoxy And [$^{14}$C] Iodoantipyrine. American Journal Of Physiology 1990; 258:H1585-H1598.

Schawb ME, Otten U, Agid Y, Thoenen H. Nerve Growth Factor (NGF) In The Rat CNS: Abscence Of Specific Retrograde Axonal Transport And Tyrosine Hydroxylase Induction In Locus Coeruleus And Substantia Nigra. Brain Research 1979; 168:473-483.

Scheffel U, Taylor GF, Kepler JA, Carrol FI, Kuhar MJ. In Vivo Labelling Of Neuronal Nicotinic Acetylcholine Receptors With Radiolabelled Isomers Of Norchloroepibatidine . Neuroreport 1995; 6:2483-2488.

Schrattenholz A, Pereira EFR, Roth U, Weber KH, Albuquerque EX. Agonist Responses Of Neuronal Nicotinic Receptors Are Potentiated by A Novel Class Of Allosterically Acting Ligands. Molecular Pharmacology 1996; 49:1-6.

Scremin OU, Scremin AME, Heuser D, Hudgell R, Romero E, Imbimbo BP. Prolonged Effects Of Cholinesterase Inhibition With Eptastigmine On Cerebral Blood Flow-Metabolism Ratio Of Normal Rats. Journal Of Cerebral Blood Flow And Metabolism 1993; 13:702-711.

Scremin OU, Sonnenschein RR, Rubinstein EH. Cholinergic Cerebral Vasodilatation In The Rabbit: Absence OF Concomitant Metabolic Activation. Journal Of Cerebral Blood Flow And Metabolism 1982; 2:241-247.

Seeman P, Niznik HB, Guan HC. Elevation Of Dopamine $D_2$ Receptors In Schizophrenia Is Underestimated By Radioactive Raclopride. Archives Of General Psychiatry 1990; 47:1170-1172.

Segre G, Cerretani D, Baldi A, Urso R. Pharmacokinetics Of Heptastigmine In Rats. Pharmacological Research 1992; 25:139-146.

Seguela P, Wadiche J, Dineleymiller K, Dani JA, Patrick JW. Molecular Cloning, Functional Properties And Distribution Of Rat Brain a7 A Nicotinic Cation Channel Highly Permeable To Calcium. Journal Of Neuroscience 1993; 13:596-604.

Shute CC, Lewis PR. The Ascending Cholinergic Reticular System:Neocortical, Olfactory And Subcortical Projections. Brain 1967; 90:497-520.

Silinsky EM. The BI Secretion. Pharmacological Reviews 1985; 37:81-132.

Silver A. The Biology Of Cholinesterases. Amsterdam: North-Holland, 1974:

Smith CD. Quantitative Computed Tomography And Magnetic Resonance Imaging In Aging And Alzheimer's Disease-Review. Journal Of Neuroimaging 1996; 1:44-53.

Smith G. Animal Models Of Alzheimer's Disease Experimental Cholinergic Denervation. Brain Research Reviews 1988; 13:103-118.

Smrcka AV, Hepler JR, Brown KO, Sternweis PC. Regulation Of Polyphosphoinositide Specific Phospholipase-C Activity by purified $G_q$. Science 1991; 251:804-807.

Sokoloff L, Reivich M, Kennedy C, et al. The [$^{14}$C] Deoxyglucose Method For The Measurement Of Local Cerebral Glucose Utilization: Theory, Procedure And Normal Values In The Conscious And Anaesthetized Albino Rat.. Journal Of Neurochemistry 1977; 28:897-916.

Soldatos CR, Kales JD, Scharf MB, Bixler EO, Kales A. Cigarette Smoking Associated With Sleep Difficulty. Science 1980; 207:551-553.

Soncrant TT, Holloway HW, Rappaport SI. Arecoline Induced Elevations Of Regional Cerebral Metabolism In the Conscious Rat. Brain Research 1985; 347:205-216.

Sood VK, Lee KS, Boulay SF, et al. In Vivo Autoradiography Of Radioiodinated (R)-3-Quinuclidinyl (S)-4-Iodobenzilate [(R,S)-IQNB] And (R)-3-Quinuclidinyl (R)-4-Iodobenzilate [(R,R)-IQNB].. Applied Radiation And Isotopes 1997; 48:27-35.

Spencer DG, Horvath E, Traber J. Direct Autoradiographic Determination Of $M_1$ And $M_2$ Muscarinic Acetylcholine Receptor Distribution In The Rat Brain: Relation To Cholinergic Nuclei And Projections. Brain Research 1986; 380:59-68.

Standaert DG, Saper CB, Rye DB, Wainer BH. Colocalization Of Atriopeptin-Like Immunoreactivity With Choline Acetyltransferase-Like And Substance P-Like Immunoreactivity In The Pedunculopontine And Lateraldorsal Tegmental Nuclei In The Rat. Brain Research 1986; 382:163-168.

Stein R, Pinkaskramarski R, Sokolovsky M. Cloned $M_1$ Muscarinic Receptors Mediate Both Adenylate Cyclase inhibition And Phosphoinositide Turnover. EMBO Journal 1988; 7:3031-3035.

Stern Y, Sano M, Mayeux R. Long Term Administration Of Oral Physostigmine In Alzheimer's Disease. Neurology 1988; 38:1837-1841.

Stockton JM, Birdsall NJM, Burgen ASV, Hulme EC. Modification Of The Binding Properties Of Muscarinic Receptors By Gallamine. Molecular Pharmacology 1983; 23:551-557.

Sugaya K, Giacobini E, Chiapinelli VA. Nicotinc Acetylcholine Receptor Subtypes In Human Frontal Cortex Changes In Alzheimer's Disease. Journal Of Neuroscience Research 1990; 27:349-359.

Sugaya K, McKinney M. The Rat Brain Examined By Combined Immunocytochemistry And In Situ Hybridization Histochemistry. Molecular Brain Research 1994; 23:111-125.

Suidan HS, Murrel RD, Tolkovsky AM. Carbachol And Bradykinin Elevate Cyclic AMP And Rapidly Deplete ATP In Cultured Neurons. Cell Regulation 1991; 2:13-35.

Svensson AL, Warpman U, HellstromLindahl E, Bogdanovic N, Lannfelt L, Nordberg A. Nicotinic Receptors, Muscarinic Receptors And Choline Acetyltransferase Activity In The Temporal Cortex Of Alzheimer Patients With Differing Apolipoprotein E Genotypes. Neuroscience Letters 1997; 232:37-40.

Talbot K, Woolf NJ, Butcher LL. Feline Islands Of Calleja Complex 2. Cholinergic And Cholinesterase Features. Journal Of Comparative Neurology 1988; 275:580-603.

Tandon R, Shipley JE, Greden JF, Mann NA, Esiner WH, Goodson JA. Muscarinic Cholinergic Hyperactivity In Schizophrenia. Relationship To Positive And Negative Symptoms. Schizophrenia Research 1991; 4:23-30.

Tavitian B, Pappata S, Bonnotlours S, et al. Positron Emission Tomography Study Of [C11] Methyl-Tertahydroaminoacridine (Methyl-Tacrine) In Baboon Brain. European Journal Of Pharmacology 1993; 236:229-238.

Torres EM, Perry TA, Blokland A, et al. Behavioural, Histochemical And Biochemical Consequences Of Selective Immunolesion In Discrete Regions Of The Basal Forebrain Cholinergic System. Neuroscience 1994; 63:95-122.

Tucek S, Musilkova J, nedoma J, Proska J, Shelkovnikova S, Vorlicek J. Positive Cooperativity In The Binding Of Alcuronium And N-MethylScopolamine To Muscarinc Acetylcholine Receptors. Molecular Pharmacology 1990; 38:674-680.

Tucek S, Proska J. Allosteric Modulation Of Muscarinic Acetylcholine Receptors. Trends In Pharmacological Sciences 1995; 16:205-212.

Tucek S, Proska J, Jakubik J. Mechanism Of Allosteric Interaction Between Alcuronium And Muscarinic Receptors And Location Of The Allosteric Binding Site. Journal Of Neurochemistry 1993; 61:S19.

Turner R, Lebihan D, Moonen CTW, Despres D, Frank J. Echo-Planar Time Course MRI Of Cat Brain Oxygenation Changes . Magnetic Resonance In Medicine 1991; 22:159-166.

Ulus IH, Wurtman RJ, Mauron C, Blusztajn JK. Choline Increases Acetylcholine Release And Protectes Against The Stimulation Induced Decrease In Phosphatide Levels Within Membranes Of Rat Corpus Striatum. Brain Research 1989; 484:217-227.

Valenzuela CF, Weign P, Yguerabide J, Johnson DA. Transverse Distance Between The Memebrane And The Agonist Binding Sites On The Torpedo ACetylcholine Receptor A Fluoresence Study. Biophysical Journal 1994; 66:674-682.

Valette H, Bottlaender M, Dolle F, Doci L, Syrota A, Crouzel C. An Attempt To Visualize Baboon Brain Nicotinic Receptors With N-[$^{11}$C] ABT-418 And N-[$^{11}$C]methyl-cytisine. Nuclear Medicine Communications 1997; 18:164-168.

Vandermeeran M, Mercken M, Vanmechelen E, et al. Detection Of Tau Proteins In Normal And Alzheimer's Disease Cerebrospinal Fluid With A Sensitive Sandwich Enzyme Linked Immunosorbent Assay. Journal Of Neurochemistry 1993; 61:1828-1834.

Varastet M, Brouillet E, Chavoix C, et al. In Vivo Visualization Of Central Muscarinic receptors Using [$^{11}$C] Quinuclidinyl Benzilate And Positron Emission Tomography In Baboons. European Journal Of Pharmacology 1992; 213:275-284.

Vaucher E, Hamel E. Cholinergic Basal Forebrain Neurons Project To Cortical Microvessels In The Rat: Electron Micorscopic Study With Anterogradely Transported Phaseolus Vulgaris Leucoagglutin And Choline Acetyltransferase Immunocytochemistry. Journal Of Neuroscience 1995; 15:7427-7441.

Vaucher E, Linville D, Hamel E. Cholinergic Basal Forebrain Projections To Nitric Oxide Synthase Containing Neurons In Rat Cerebral Cortex. Neuroscience 1997; 79:827-836.

Vincent SR, Satoh K, Armstrong DM, Fibiger HC. NADPH-Diaphorase A Selective Histochemical Marker For the Cholinergic Neurons Of The Pontine-Reticular Formation. Neuroscience Letters 1983; 43:31-36.

Vizi ES, Goldiner PL, Potter PE, Foldes FF. Heterogeneity Of Presynaptic Muscarinic Receptors Involved In Modulation Of Transmitter Release. Neuroscience 1989; 31:259-267.

Wada E, McKinnon D, Heinimann S, Patrick J, Swanson LW. The Distribution Of Messenger RNA Encoded By A New Member Of The Neuronal Nicotinic Acetylcholine Receptor Gene Family (a5) In The Rat Central Nervous System. Brain Research 1990; 526:45-53.

Wada E, Wada K, Boulter J, et al. Distribution Of a2, a3, a4 and b2 neuronal Nicotinic Receptor Subunit Messenger RNA In The Central Nervous System A Hybridization Hisotchemical Study In The Rat. Journal Of Comparative Neurology 1989; 284:314-335.

Wagner HN, Burns HD, Dannals RF, et al. Imaging Dopamine Receptors In The Human Brain By Positron Tomography. Science 1983; 221:1264-1266.

Wainer BH, Steininger TL, Roback JD, Burkewatson MA, Mufson EJ. Ascending Cholinergic Pathways-Functional Organization And Implications For Disease Models. Progress In Brain Research 1993; 98:9-30.

Waldemar G. Functional Brain Imaging With SPECT In Normal Aging And Dementia. Methodological, Pathophysiological And Diagnostic Aspects. Cerebrovascular And Brain Metabolism Reviews 1995; 7:89-130.

Walton FA. Flaxedil: A New Curarizing Agent. Canadian Medical Association Journal 1950; 63:123-129.

Wang JX, Roeske WR, Gulya K, Wang.W , Yamamura HI. [$^{3}$H] AF-X 116 Labels Subsets Of Muscarinic Cholinergic Receptors In Rat Brain And Heart. Life Sciences 1987; 41:1751-1760.

Watson EL, Singh JC, McPhee C, Beavo J, Jacobson KL. Regulation Of cAMP Metabolism In Mouse Parotid Gland By cGMP And Calcium. Molecular Pharmacology 1990; 38:547-553.

Weinberger DR, Gibson R, Coppola R, et al. The Distribution Of Cerebral Muscarinic Acetylcholine Receptors In Vivo In Patients With Dementia-A Controlled Study With $^{123}$IQNB And Single Photon Emission Computed Tomography. Journal Of Cerebral Blood Flow And Metabolism 1990; 10:781-807.

Weinberger DR, Gibson R, Coppola R, et al. The Distribution Of Cerebral Muscarinic Acetylcholine Receptors In Vivo In Patients With Dementia-A Controlled Study With $^{123}$IQNB And Single Photon Emission Computed Tomography. Archives Of Neurology 1991; 48:169-176.

Weinberger DR, Jones D, Reba RC, et al. A Comparison Of FDG PET And IQNB SPECT In Normal Subjects And In Patients With Dementia. Journal Of Neuropsychiatry And Clinical Neurosciences 1992; 4:239-248.

Weinberger DR, Mann U, Gibson RE, et al. Cerebral Muscarinic Receptors In Primary Degenerative Dementia As Evaluated By SPECT With Iodine-123-Labelled QNB. Advances In Neurology 1990; 51:147-150.

Wenk GL, Stoehr JD, Quintana G, Mobley S, Wiley RG. Beahvioural, Biochemical, Histological And Electrophysiological Effects Of 193 IgG Saporin Injections Into The Basal Forebrain Of Rats. Journal Of Neuroscience 1994; 14:5986-5995.

Wess J. Molecular Biology Of Muscarinic Acetylcholine Receptors. Critical Reviews In Neurobiology 1996; 10:69-99.

Wess J, Bonner TI, Dorje F, Brann MR. Delineation Of Muscarinic Receptor Domains Conferring Selectivity Of Coupling To Guanine Nucleotide Binding Proteins And 2nd Messengers. Molecular Pharmacology 1990; 38:517-523.

Wess J, Brann MR, Bonner TI. Identification of A Small Intracellular Region Of The Muscarinic M3 receptor As A Determinant Of Selective Coupling To PI Turnover. FEBS Letters 1989; 258:133-136.

Wess J, Gdula D, Brann MR. Site Directed Mutagenesis Of The M3-Muscarinic Receptor Identification Of A Series Of Threonine And Tyrosine Residues Invovlved In Agonist But Not Antagonist Binding. EMBO Journal 1991; 10:3729-3734.

Wess J, Maggio R, Palmer JR, Vogel Z. Role Of Conserved Threonine And Tyrosine Residues In Acetylcholine Binding And Muscarinic Receptor Activation A Study With M3-Muscarinic Receptor Point Mutants. Journal Of Biological Chemistry 1992; 267:19313-19319.

Whitehouse PJ, Martino AM, Antuono PG, et al. Nicotinic Acetylcholine Binding Sites In Alzheimer's Disease. Brain Research 1986; 371:146-151.

Whitehouse PJ, Price DL, Strubble RG, Clark AW, Coyle JT, Delong MR. Alzheimer's Disease And Senile Dementia: Loss Of Neurons In The Basal Forebrain. Science 1982; 215:1237-1239.

Whiting PJ, Lindstrom JM. Purification And Characterization Of Nicotinic Acetylcholine Receptor From Chick Brain. Biochemistry 1986; 25:2082-2093.

Wiley RG, Oeltmann TN, Lappi DA. Immunolesioning: Selective Destruction Of Neurons Using Immunotoxin To Rat NGF Receptor. Brain Research 1991; 562:149-153.

Wilson AA, Dannals RF, Ravert HT, Frost JJ, Wagner HN. Synthesis And Biological Evaluation Of [$^{125}$I]-4-Iododexetimide And [$^{123}$I]-4-Iododexetimide A Potent Muscarinic Cholinergic Receptor Antagonist. Journal Of Medicinal Chemistry 1989; 32:1057-1062.

Wong DF, Gjedde A, Wagner HN. Quantification Of Neuroreceptors In The Living Human Brain 1. Irreversible Binding Of Ligands. Journal Of Cerebral Blood Flow And Metabolism 1996; 6:137-146.

Wong DF, Gjedde A, Wagner HN. Quantification Of Neuroreceptors In The Living Human Brain 1. Irreversible Binding Of Ligands. Journal Of Cerebral Blood Flow And Metabolism 1996; 6:137-146.

Wong DF, Gjedde A, Wagner HN, et al. Quantification Of Neuroreceptors In The Living Human Brain 2. Inhibtion Studies Of Receptor Density And Affinity. Journal Of Cerebral Blood Flow And Metabolism 1986; 6:147-153.

Wong DF, Lever JR, Hartig PR, et al. Loclization Of Serotonin 5-HT2 Receptors In Living Human Brain By Positron Emmission Tomography Using N1-([C11]-Methyl)-2-Br-LSSSD. Synapse 1987; 1:393.

Wong SKF, Ross EM. Chimeric Muscarinic Cholinergic Beta Adrenergic Receptors That Are Functionally Promiscuous Among G-Proteins. Journal Of Biological Chemistry 1994; 269:18968-18976.

Wonnacott S, Soliakov L, Wilkie G, Redfern P, Marshall D. Presynaptic Nicotinic Acetylcholine Receptors In The Brain. Drug Development Research 1996; 38:149-159.

Woolf NJ. Cholinergic Systems In Neurobioogy. Progress In Neurobiology 1991; 37:475-524.

Woolf NJ. Cholinergic Systems In Mammalian Brain And Spinal Cord. Progress In Neurobiology 1991; 37:475-524.

Wurtman RJ. Alzheimer's Disease. Scientific American 1985; 252:62.

Wyper DJ, Brown D, Patterson J, Owens J, Hunter R, Teasdale E. Deficits In Iodine Labelled 3-Quinuclidinyl Benzilate Binding In Relation To Cerebral Blood Flow In Patients With ALzheimer's Disease. European Journal Of Nuclear Medicine 1993; 20:379-386.

Yamagata SK, Parsons SM. Cholinergic Synaptic Vesicles Contain A V-Type And A P-Type ATPase. Journal Of Neurochemistry 1989; 53:1354-1362.

Yamamura HI, Kuhar MJ, Snyder SH. In Vivo Identification Of Muscarinic Cholinergic Receptor Binding In Rat Brain. Brain Research 1974; 80:170-176.

Yamamura HI, Snyder SH. High Affinity Transport Of Choline Into Synaptosomes Of Rat Brain. Journal Of Neurochemistry 1973; 21:1355-1374.

Yasuda RP, Ciesla W, Flores LR, et al. Development Of Anitsera Selective For M4 And M5 Muscarinic Cholinergic Receptors-Distribution Of M4 And M5 Receptors In Rat Brain. Molecular Pharmacology 1993; 43:149-157.

Zeeberg BR, Boulay SF, Gitler MS, Sood VK, Reba RC. Correction Of The Stereochemical Assignment Of The Benzilic Acid Centre In (R)-(-)-3-Quinuclidinyl (S)-(+)-4-Iodobenzilate [(R,S)-4-IQNB]. Applied Radiation And Isotopes 1997; 48:463-467.

Zeeberg BR, Gitler MS, Baumgold J, de la Cruz RA, Reba RC. Binding Of Radioiodinated SPECT Ligands To Transfected Cell Membranes Expressing Single Muscarinic Receptor Subtypes. Biochemical And Biophysical Research Communications 1991; 179:768-775.

Zeman,W and Innes, J.R.M. The CNS and Its Topographical Relation To The Body. In Craigie's Neuroanatomy of the Rat. New York, Academic Press p11-41 1963.

# APPENDIX A

## Table A1

## (R,S)-[$^{125}$I]-QNB in the CNS of Conscious Rat

| Region | TIME FOLLOWING ADMINISTRATION OF TRACER 2 Hours | 6 Hours | 12 Hours | 24 Hours |
|---|---|---|---|---|
| ***Cerebellum*** | | | | |
| Cerebellar Cortex | 0.036 ± 0.012 | 0.03 ± 0.011 | 0.027 ± 0.027 | 0.018 ± 0.013 |
| ***Medulla/Pons*** | | | | |
| Pontine Grey | 0.250 ± 0.086 | 0.240 ± 0.055 | 0.095 ± 0.038 | 0.065 ± 0.017 |
| Nucleus of the Lateral Lemniscus | 0.123 ± 0.025 | 0.090 ± 0.015 | 0.050 ± 0.015 | 0.009 ± 0.009 |
| Lateral Dorsal Tegmental nucleus | 0.173 ± 0.059 | 0.120 ± 0.019 | 0.119 ± 0.024 | 0.039 ± 0.026 |
| ***Mesencephalon*** | | | | |
| Inferior Colliculus | 0.180 ± 0.045 | 0.140 ± 0.031 | 0.072 ± 0.012 | 0.042 ± 0.018 |
| Superior Colliculus | 0.235 ± 0.074 | 0.140 ± 0.029 | 0.075 ± 0.009 | 0.021 ± 0.011 |
| Substantia Nigra (pars compacta) | 0.160 ± 0.047 | 0.140 ± 0.025 | 0.083 ± 0.007 | 0.039 ± 0.016 |
| Substantia nigra (pars reticulata) | 0.153 ± 0.042 | 0.130 ± 0.029 | 0.070 ± 0.005 | 0.035 ± 0.018 |
| ***Diencepahlon*** | | | | |
| Hippocampus CA1 | 0.215 ± 0.070 | 0.240 ± 0.034 | 0.213 ± 0.041 | 0.254 ± 0.031 |
| Hippocampus CA2 | 0.275 ± 0.080 | 0.281 ± 0.035 | 0.234 ± 0.051 | 0.246 ± 0.027 |
| Hippocampus CA3 | 0.239 ± 0.067 | 0.250 ± 0.028 | 0.212 ± 0.039 | 0.235 ± 0.023 |
| Medial Geniculate Body | 0.260 ± 0.069 | 0.231 ± 0.035 | 0.147 ± 0.015 | 0.104 ± 0.015 |
| Sub Thalamic Nucleus | 0.183 ± 0.048 | 0.350± 0.201 | 0.102 ± 0.012 | 0.038 ± 0.014 |
| Lateral Geniculate Nucleus | 0.225 ± 0.065 | 0.203 ± 0.034 | 0.148 ± 0.020 | 0.071 ± 0.025 |
| Hypothalamus | 0.153 ± 0.053 | 0.167 ± 0.023 | 0.113 ± 0.021 | 0.069 ± 0.024 |
| Mediodorsal Thalamic Nucleus | 0.240 ± 0.069 | 0.224 ± 0.031 | 0.166 ± 0.029 | 0.105 ± 0.014 |
| Ventrolateral Thalamic Nucleus | 0.206 ± 0.063 | 0.195 ± 0.028 | 0.131 ± 0.024 | 0.067 ± 0.019 |
| ***Telencephalon*** | | | | |
| Visual Cortex (layer IV) | 0.349 ± 0.113 | 0.292 ± 0.055 | 0.254 ± 0.041 | 0.308 ± 0.026 |
| Dentate Gyrus | 0.267 ± 0.079 | 0.280 ± 0.060 | 0.223 ± 0.042 | 0.219 ± 0.007 |
| Auditory Cortex (layer IV) | 0.400 ± 0.085 | 0.370 ± 0.048 | 0.333 ± 0.074 | 0.350 ± 0.017 |
| Hippocampus Molecular Layer | 0.280 ± 0.077 | 0.290± 0.059 | 0.256 ± 0.049 | 0.236 ± 0.020 |
| Amygdala | 0.213 ± 0.055 | 0.207 ± 0.026 | 0.177 ± 0.040 | 0.161 ± 0.016 |
| Globus Pallidus | 0.117 ± 0.038 | 0.111 ± 0.026 | 0.082 ± 0.023 | 0.062 ± 0.026 |
| Caudate Nucleus | 0.301 ± 0.072 | 0.300 ± 0.053 | 0.291 ± 0.064 | 0.298 ± 0.037 |
| Septal Nuclei | 0.209 ± 0.054 | 0.19 ± 0.023 | 0.163 ± 0.030 | 0.125 ± 0.023 |
| Nucleus Basalis Magnocellularis | 0.124 ± 0.041 | 0.121 ± 0.025 | 0.102 ± 0.040 | 0.074 ± 0.021 |
| Nucleus Accumbens | 0.319 ± 0.089 | 0.322 ± 0.054 | 0.307 ± 0.086 | 0.328 ± 0.051 |
| Sensory Motor Cortex (layer IV) | 0.377 ± 0.085 | 0.302 ± 0.043 | 0.324 ± 0.070 | 0.315 ± 0.038 |
| Anterior Cingulate Cortex | 0.329 ± 0.090 | 0.333 ± 0.048 | 0.305 ± 0.090 | 0.311 ± 0.033 |
| Frontal Cortex | 0.362 ± 0.096 | 0.332 ± 0.049 | 0.316 ± 0.099 | 0.302 ± 0.030 |
| Parietal Cortex | 0.306 ± 0.103 | 0.323 ± 0.036 | 0.298 ± 0.066 | 0.305 ± 0.036 |
| ***Myelinated Fibre Tracts*** | | | | |
| Internal Capsule | 0.107 ± 0.033 | 0.090 ± 0.022 | 0.060 ± 0.011 | 0.043 ± 0.010 |
| Genu | 0.104 ± 0.029 | 0.111 ± 0.026 | 0.085 ± 0.035 | 0.071 ± 0.015 |

Table shows (R,S)-[$^{125}$I]-QNB in discrete brain regions of the conscious rat 2, 6, 12 and 24 h following iv administration of 200$\mu$Ci of tracer. Data are expressed as mean ± S.E.M $\mu$Ci per g brain , n= 3-5 animals for each time point.

## Table A2

## Effect of Heptylphysostigmine on (R,S)-[$^{125}$I]-QNB in Brain of Conscious Rat

| Region | TIME FOLLOWING ADMINISTRATION OF TRACER | | | |
|---|---|---|---|---|
| | 2 Hours | | 24 Hours | |
| | Vehicle | Heptyl. | Vehicle | Heptyl. |
| ***Cerebellum*** | | | | |
| Cerebellar Cortex | 0.080 ± 0.018 | 0.074 ± 0.009 | 0.007 ± 0.004 | 0.001 ± 0.001 |
| ***Medulla/Pons*** | | | | |
| Pontine Grey | 0.584 ± 0.023 | 0.593 ± 0.018 | 0.077 ± 0.012 | 0.045 ± 0.023 |
| Nucleus of the Lateral Lemniscus | 0.232 ± 0.024 | 0.218 ± 0.030 | 0.012 ± 0.006 | 0.018 ± 0.009 |
| Lateral Dorsal Tegmental nucleus | 0.197 ± 0.108 | 0.274 ± 0.034 | 0.039 ± 0.023 | 0.029 ± 0.019 |
| ***Mesencephalon*** | | | | |
| Inferior Colliculus | 0.389 ± 0.021 | 0.321 ± 0.049 | 0.038 ± 0.009 | 0.043 ±0.022 |
| Superior Colliculus | 0.351 ± 0.031 | 0.392 ± 0.098 | 0.030 ± 0.009 | 0.038 ± 0.011 |
| Substantia Nigra (pars compacta) | 0.283 ± 0.021 | 0.286 ± 0.102 | 0.028 ± 0.014 | 0.049 ± 0.011 |
| Substantia nigra (pars reticulata) | 0.259 ± 0.011 | 0.241 ± 0.075 | 0.031 ± 0.016 | 0.040 ± 0.007 |
| ***Diencepahlon*** | | | | |
| Hippocampus CA1 | 0.379 ± 0.045 | 0.350 ± 0.130 | 0.311 ± 0.086 | 0.302 ± 0.045 |
| Hippocampus CA2 | 0.486 ± 0.058 | 0.456 ± 0.142 | 0.295 ± 0.075 | 0.311 ± 0.052 |
| Hippocampus CA3 | 0.395 ± 0.041 | 0.393 ± 0.137 | 0.308 ± 0.069 | 0.316 ± 0.046 |
| Medial Geniculate Body | 0.453 ± 0.055 | 0.428 ± 0.122 | 0.126 ± 0.011 | 0.139 ± 0.034 |
| Sub Thalamic Nucleus | 0.355 ± 0.048 | 0.369 ± 0.104 | 0.039 ± 0.009 | 0.077 ± 0.035 |
| Lateral Geniculate Nucleus | 0.357 ± 0.048 | 0.393 ± 0.122 | 0.100 ± 0.013 | 0.108 ± 0.020 |
| Hypothalamus | 0.274 ± 0.027 | 0.276 ± 0.091 | 0.054 ± 0.007 | 0.051 ± 0.007 |
| Mediodorsal Thalamic Nucleus | 0.440 ± 0.046 | 0.403 ± 0.127 | 0.112 ± 0.010 | 0.113 ± 0.019 |
| Ventrolateral Thalamic Nucleus | 0.344 ± 0.043 | 0.328 ± 0.116 | 0.067 ± 0.008 | 0.064 ± 0.010 |
| ***Telencephalon*** | | | | |
| Visual Cortex (layer IV) | 0.536 ± 0.032 | 0.495 ± 0.149 | 0.365 ± 0.087 | 0.281 ± 0.141 |
| Dentate Gyrus | 0.479 ± 0.050 | 0.443 ± 0.146 | 0.321 ± 0.080 | 0.317 ± 0.058 |
| Auditory Cortex (layer IV) | 0.722 ± 0.071 | 0.925 ± 0.217 | 0.430 ± 0.085 | 0.521 ± 0.094 |
| Hippocampus Molecular Layer | 0.491 ± 0.042 | 0.451 ± 0.160 | 0.344 ± 0.089 | 0.303 ± 0.042 |
| Amygdala | 0.296 ± 0.075 | 0.324 ± 0.105 | 0.185 ± 0.041 | 0.165 ± 0.026 |
| Globus Pallidus | 0.215 ± 0.016 | 0.213 ± 0.079 | 0.053 ± 0.008 | 0.048 ± 0.008 |
| Caudate Nucleus | 0.478 ± 0.037 | 0.445 ± 0.164 | 0.331 ± 0.082 | 0.307 ± 0.048 |
| Septal Nuclei | 0.340 ± 0.040 | 0.311 ± 0.117 | 0.140 ± 0.018 | 0.147 ± 0.027 |
| Nucleus Basalis Magnocellularis | 0.262 ± 0.029 | 0.257 ± 0.095 | 0.071 ± 0.006 | 0.064 ± 0.009 |
| Nucleus Accumbens | 0.529 ± 0.048 | 0.528 ± 0.167 | 0.407 ± 0.105 | 0.376 ± 0.057 |
| Sensory Motor Cortex (layer IV) | 0.535 ± 0.019 | 0.628 ± 0.187 | 0.401 ± 0.076 | 0.381 ± 0.045 |
| Anterior Cingulate Cortex | 0.564 ± 0.030 | 0.532 ± 0.175 | 0.369 ± 0.104 | 0.392 ± 0.065 |
| Frontal Cortex | 0.593 ± 0.062 | 0.609 ± 0.182 | 0.382 ± 0.085 | 0.382 ± 0.053 |
| Parietal Cortex | 0.534 ± 0.053 | 0.606 ± 0.157 | 0.400 ± 0.092 | 0.394 ± 0.069 |
| ***Myelinated Fibre Tracts*** | | | | |
| Internal Capsule | 0.113 ± 0.014 | 0.119 ± 0.043 | 0.020 ± 0.002 | 0.031 ± 0.006 |
| Genu | 0.115 ± 0.010 | 0.137 ± 0.061 | 0.056 ± 0.014 | 0.038 ± 0.018 |

Table shows effect of heptylphysosigmine( 2mg /kg) on (R,S)-[$^{125}$I]-QNB in brain of consci
rat at 2 and 24 hours following iv administration of 200$\mu$Ci of tracer. Data are expressed as mea
S.E.M $\mu$Ci per g brain, n= 5 animals for each time point.

## Table A3

## Effect of Heptylphysostigmine on (R,R)-[$^{125}$I]-QNB in the Brain of Conscious Rat:

## VEHICLE TREATED ANIMALS

| Region | TIME FOLLOWING TRACER ADMINISTRATION 30 mins | 1 Hour | 2 Hours | 6 Hours |
|---|---|---|---|---|
| ***Cerebellum*** | | | | |
| Cerebellar Cortex | 0.050 ± 0.005 | 0.024 ± 0.003 | 0.023 ± 0.007 | 0.009 ± 0.002 |
| ***Medulla/Pons*** | | | | |
| Pontine Grey | 0.142 ± 0.015 | 0.101 ± 0.015 | 0.114 ± 0.023 | 0.026 ± 0.007 |
| Nucleus of the Lateral Lemniscus | 0.090 ± 0.009 | 0.057 ± 0.006 | 0.095 ± 0.021 | 0.019 ± 0.005 |
| Lateral Dorsal Tegmental nucleus | 0.101 ± 0.006 | 0.059 ± 0.007 | 0.072 ± 0.020 | 0.018 ± 0.006 |
| ***Mesencephalon*** | | | | |
| Inferior Colliculus | 0.097 ± 0.010 | 0.064 ± 0.009 | 0.077 ± 0.022 | 0.013 ± 0.003 |
| Superior Colliculus | 0.099 ± 0.008 | 0.068 ± 0.008 | 0.075 ± 0.022 | 0.017 ± 0.007 |
| Substantia Nigra (pars compacta) | 0.080 ± 0.008 | 0.056 ± 0.006 | 0.080 ± 0.021 | 0.018 ± 0.007 |
| Substantia nigra (pars reticulata) | 0.069 ± 0.007 | 0.051 ± 0.006 | 0.069 ± 0.018 | 0.014 ± 0.005 |
| ***Diencepahlon*** | | | | |
| Hippocampus CA1 | 0.084 ± 0.010 | 0.085 ± 0.011 | 0.186 ± 0.021 | 0.077 ± 0.008 |
| Hippocampus CA2 | 0.117 ± 0.018 | 0.096 ± 0.011 | 0.181 ± 0.048 | 0.058 ± 0.008 |
| Hippocampus CA3 | 0.109 ± 0.017 | 0.090 ± 0.008 | 0.185 ± 0.021 | 0.068 ± 0.007 |
| Medial Geniculate Body | 0.113 ± 0.013 | 0.087 ± 0.009 | 0.114 ± 0.031 | 0.022 ± 0.005 |
| Sub Thalamic Nucleus | 0.103 ± 0.015 | 0.067 ± 0.009 | 0.086 ± 0.011 | 0.025 ± 0.008 |
| Lateral Geniculate Nucleus | 0.110 ± 0.015 | 0.079 ± 0.008 | 0.107 ± 0.017 | 0.014 ± 0.005 |
| Hypothalamus | 0.080 ± 0.008 | 0.054 ± 0.006 | 0.079 ± 0.018 | 0.011 ± 0.004 |
| Mediodorsal Thalamic Nucleus | 0.109 ± 0.015 | 0.079 ± 0.008 | 0.113 ± 0.017 | 0.014 ± 0.005 |
| Ventrolateral Thalamic Nucleus | 0.079 ± 0.009 | 0.051 ± 0.05 | 0.073 ± 0.016 | 0.010 ± 0.004 |
| ***Telencephalon*** | | | | |
| Visual Cortex (layer IV) | 0.145 ± 0.016 | 0.106 ± 0.016 | 0.224 ± 0.031 | 0.065 ± 0.016 |
| Dentate Gyrus | 0.125 ± 0.014 | 0.099 ± 0.014 | 0.205 ± 0.033 | 0.059 ± 0.015 |
| Auditory Cortex (layer IV) | 0.183 ± 0.017 | 0.142 ± 0.016 | 0.289 ± 0.032 | 0.077 ± 0.014 |
| Hippocampus Molecular Layer | 0.161 ± 0.047 | 0.107 ± 0.012 | 0.195 ± 0.036 | 0.60 ± 0.012 |
| Amygdala | 0.092 ± 0.008 | 0.076 ± 0.006 | 0.132 ± 0.017 | 0.040 ± 0.007 |
| Globus Pallidus | 0.065 ± 0.006 | 0.043 ± 0.006 | 0.086 ± 0.022 | 0.018 ± 0.006 |
| Caudate Nucleus | 0.127 ± 0.014 | 0.106 ± 0.010 | 0.209 ± 0.024 | 0.064 ± 0.011 |
| Septal Nuclei | 0.092 ± 0.013 | 0.079 ± 0.009 | 0.132 ± 0.024 | 0.031 ± 0.008 |
| Nucleus Basalis Magnocellularis | 0.070 ± 0.007 | 0.053 ± 0.007 | 0.098 ± 0.013 | 0.023 ± 0.007 |
| Nucleus Accumbens | 0.136 ± 0.014 | 0.118 ± 0.015 | 0.224 ± 0.030 | 0.072 ± 0.007 |
| Sensory Motor Cortex (layer IV) | 0.169 ± 0.022 | 0.127 ± 0.013 | 0.261 ± 0.024 | 0.070 ± 0.012 |
| Anterior Cingulate Cortex | 0.147 ± 0.017 | 0.123 ± 0.012 | 0.243 ± 0.027 | 0.075 ± 0.009 |
| Frontal Cortex | 0.152 ± 0.019 | 0.125 ± 0.013 | 0.244 ± 0.023 | 0.070 ± 0.010 |
| Parietal Cortex | 0.155 ± 0.022 | 0.116 ± 0.012 | 0.231 ± 0.030 | 0.064 ± 0.007 |
| ***Myelinated Fibre Tracts*** | | | | |
| Internal Capsule | 0.036 ± 0.008 | 0.035 ± 0.002 | 0.044 ± 0.015 | 0.003 ± 0.002 |
| Genu | 0.038 ± 0.006 | 0.033 ± 0.002 | 0.046 ± 0.013 | 0.012 ± 0.003 |

Table shows (R,R)-[$^{125}$I]-QNB in discrete brain regions of the conscious rat in vehicle (0.7 m
0.9% saline) treated animals 30 mins, 1, 2 and 6 hours following iv administration of 200$\mu$Ci
tracer. Data are expressed as mean ± S.E.M $\mu$Ci per g brain , n= 5 animals for each time point.

## Table A4

## Effect of Heptylphysostigmine on (R,R)-[$^{125}$I]-QNB in the Brain of Conscious Rat:

## HEPTYLPHYSOSTIGMINE TREATED ANIMALS

| Region | TIME FOLLOWING TRACER ADMINISTRATION 30 mins | 1 Hour | 2 Hours | 6 Hours |
|---|---|---|---|---|
| ***Cerebellum*** | | | | |
| Cerebellar Cortex | 0.047 ± 0.006 | 0.046 ± 0.012 | 0.026 ± 0.009 | 0.016 ± 0.005 |
| ***Medulla/Pons*** | | | | |
| Pontine Grey | 0.123 ± 0.007 | 0.114 ± 0.008 | 0.106 ± 0.005 | 0.032 ± 0.006 |
| Nucleus of the Lateral Lemniscus | 0.077 ± 0.007 | 0.087 ± 0.019 | 0.077 ± 0.015 | 0.033 ± 0.012 |
| Lateral Dorsal Tegmental nucleus | 0.089 ± 0.009 | 0.070 ± 0.010 | 0.064 ± 0.012 | 0.024 ± 0.006 |
| ***Mesencephalon*** | | | | |
| Inferior Colliculus | 0.085 ± 0.007 | 0.080 ± 0.010 | 0.069 ± 0.014 | 0.024 ± 0.005 |
| Superior Colliculus | 0.108 ± 0.010 | 0.097 ± 0.007 | 0.079 ± 0.011 | 0.025 ± 0.004 |
| Substantia Nigra (pars compacta) | 0.069 ± 0.012 | 0.080 ± 0.006 | 0.074 ± 0.011 | 0.027 ± 0.003 |
| Substantia nigra (pars reticulata) | 0.058 ± 0.010 | 0.073 ± 0.009 | 0.065 ± 0.012 | 0.024 ± 0.002 |
| ***Diencepahlon*** | | | | |
| Hippocampus CA1 | 0.072 ± 0.010 | 0.104 ± 0.011 | 0.108 ± 0.014 | 0.071 ± 0.022 |
| Hippocampus CA2 | 0.102 ± 0.014 | 0.123 ± 0.016 | 0.126 ± 0.013 | 0.065 ± 0.011 |
| Hippocampus CA3 | 0.090 ± 0.012 | 0.114 ± 0.015 | 0.110 ± 0.012 | 0.070 ± 0.011 |
| Medial Geniculate Body | 0.112 ± 0.014 | 0.109 ± 0.012 | 0.101 ± 0.009 | 0.036 ± 0.004 |
| Sub Thalamic Nucleus | 0.095 ± 0.015 | 0.088 ± 0.008 | 0.068 ± 0.010 | 0.018 ± 0.006 |
| Lateral Geniculate Nucleus | 0.089 ± 0.013 | 0.102 ± 0.016 | 0.073 ± 0.009 | 0.018 ± 0.005 |
| Hypothalamus | 0.066 ± 0.009 | 0.073 ± 0.012 | 0.051 ± 0.008 | 0.032 ± 0.015 |
| Mediodorsal Thalamic Nucleus | 0.088 ± 0.012 | 0.099 ± 0.011 | 0.078 ± 0.008 | 0.020 ± 0.006 |
| Ventrolateral Thalamic Nucleus | 0.065 ± 0.011 | 0.076 ± 0.014 | 0.055 ± 0.009 | 0.015 ± 0.004 |
| ***Telencephalon*** | | | | |
| Visual Cortex (layer IV) | 0.136 ± 0.013 | 0.133 ± 0.012 | 0.166 ± 0.010 | 0.099 ± 0.019 |
| Dentate Gyrus | 0.113 ± 0.013 | 0.112 ± 0.009 | 0.146 ± 0.010 | 0.080 ± 0.008 |
| Auditory Cortex (layer IV) | 0.254 ± 0.035 | 0.223 ± 0.026 | 0.146 ± 0.012 | 0.147 ± 0.011 |
| Hippocampus Molecular Layer | 0.107 ± 0.014 | 0.109 ± 0.008 | 0.265 ± 0.017 | 0.081 ± 0.006 |
| Amygdala | 0.078 ± 0.008 | 0.094 ± 0.014 | 0.086 ± 0.010 | 0.030 ± 0.010 |
| Globus Pallidus | 0.055 ± 0.010 | 0.066 ± 0.011 | 0.052 ± 0.007 | 0.016 ± 0.005 |
| Caudate Nucleus | 0.104 ± 0.016 | 0.115 ± 0.015 | 0.126 ± 0.012 | 0.076 ± 0.008 |
| Septal Nuclei | 0.079 ± 0.016 | 0.091 ± 0.013 | 0.088 ± 0.010 | 0.035 ± 0.010 |
| Nucleus Basalis Magnocellularis | 0.063 ± 0.011 | 0.074 ± 0.012 | 0.063 ± 0.008 | 0.022 ± 0.008 |
| Nucleus Accumbens | 0.113 ± 0.015 | 0.133 ± 0.012 | 0.149 ± 0.11 | 0.076 ± 0.016 |
| Sensory Motor Cortex (layer IV) | 0.174 ± 0.256 | 0.166 ± 0.024 | 0.173 ± 0.013 | 0.071 ± 0.014 |
| Anterior Cingulate Cortex | 0.137 ± 0.018 | 0.142 ± 0.016 | 0.164 ± 0.011 | 0.080 ± 0.012 |
| Frontal Cortex | 0.171 ± 0.030 | 0.149 ± 0.025 | 0.178 ± 0.012 | 0.090 ± 0.007 |
| Parietal Cortex | 0.154 ± 0.025 | 0.152 ± 0.022 | 0.176 ± 0.014 | 0.088 ± 0.017 |
| ***Myelinated Fibre Tracts*** | | | | |
| Internal Capsule | 0.030 ± 0.006 | 0.042 ± 0.008 | 0.034 ± 0.011 | 0.014 ± 0.006 |
| Genu | 0.020 ± 0.006 | 0.043 ± 0.008 | 0.042 ± 0.009 | 0.023 ± 0.007 |

Table shows (R,R)-[$^{125}$I]-QNB in discrete brain regions of the conscious rat in heptylphysostigmine (2 mg/kg) treated animals 30 mins, 1, 2 and 6 hours following iv administration of 200$\mu$Ci of tracer. Data are expressed as mean ± S.E.M $\mu$Ci per g brain, n= 5 animals for each time point.

# APPENDIX B

## (R,S)-[$^{125}$I]-QNB in Rat Brain

**Table B1**

**Physiologic Variables-2 Hour Animals**

| | Sample Time (Hours) | | |
|---|---|---|---|
| | **0** | **1** | **2** |
| **pH** | 7.1 ± 0.02 | 7.42 ± 0.01 | 7.43 ± 0.01 |
| **$pCO_2$ (mmHg)** | 42.3 ± 1.9 | 38.6 ± 4.7 | 38.6 ± 2.1 |
| **$pO_2$ (mmHg)** | 90.8 ± 5.4 | 90.8 ± 5.5 | 94.0 ± 6.2 |
| **Temp. ($^oC$)** | 37.5 ± 0.3 | 37.7 ± 0.2 | 37.6 ± 0.2 |
| **MABP (mmHg)** | 121 ± 4 | 122 ± 5 | 124 ± 3 |
| **Plasma Glucose (mM)** | 4.7 ± 0.2 | 5.3 ± 0.3 | 5.6 ± 0.4 |
| **n** | 5 | 5 | 5 |

**Table B2**

**Physiologic Variables-6 Hour Animals**

| | Sample Time (Hours) | | | |
|---|---|---|---|---|
| | **0** | **2** | **4** | **6** |
| **pH** | 7.4 ± 0.1 | 7.4 ± 0.1 | 7.4 ± 0.1 | 7.4 ± 0.1 |
| **$pCO_2$(mmHg)** | 37.0 ± 5.1 | 37.7 ± 0.3 | 36.7 ± 0.7 | 36.0 ± 2.0 |
| **$pO_2$ (mmHg)** | 97.7 ± 3.1 | 99.3 ± 3.9 | 111.3 ± 17.1 | 103.7 ± 2.2 |
| **Temp.($^oC$)** | 37.1 ± 0.1 | 37.1 ± 0.1 | 37.0 ± 0.1 | 37.2 ± 0.3 |
| **MABP (mmHg)** | 122 ± 4 | 108 ± 7 | 115 ± 5 | 115 ± 3 |
| **Plasma Glucose(mM)** | 6.3 ± 0.3 | 6.0 ± 0.5 | 6.2 ± 0.5 | 6.1 ± 0.1 |
| **n** | 3 | 3 | 3 | 3 |

Tables show physiologic variables measured in 2 and 6 hour animals following intravenous administration of 200 $\mu$Ci (R,S)-[$^{125}$I]-QNB. Samples were taken immediately prior to (0), 1, and 6 hours following (R,S)-[$^{125}$I]-QNB administration. Brains were removed and processed f autoradiography at 2 and 6 hours post-administration of tracer. There were no statistically significant differences in any of the variables measured at any of the time points between animal the 2, 6, 12 and 24 hour groups (ANOVA). Data are presented as mean ± S.E.M.

**Table B3**

**Physiologic Variables-12 Hours**

| | Ssmple Time (Hours) | | | | |
|---|---|---|---|---|---|
| | **0** | **2** | **4** | **8** | **12** |
| **pH** | 7.4 ± 0.1 | 7.4 ± 0.1 | 7.4 ± 0.1 | 7.4 ± 0.1 | 7.5 ± 0.02 |
| **$pCO_2$(mmHg)** | 40.9 ± 1.8 | 42.2 ± 0.5 | 41.3 ± 0.9 | 42.7 ± 1.8 | 41.7 ± 0.3 |
| **$pO_2$ (mmHg)** | 101.1 ± 3.8 | 93.9 ± 6.6 | 99.7 ± 2.7 | 107.0 ± 6.2 | 105.3 ± 4.1 |
| **Temp.($^oC$)** | 37.5 ± 0.2 | 37.5 ± 0.2 | 37.5 ± 0.1 | 37.6 ± 0.2 | 37.1 ± 0.2 |
| **MABP (mmHg)** | 115 ± 2 | 120 ± 4 | 121 ± 3 | 119 ± 4 | 115 ± 4 |
| **Plasma Glucose(mM)** | 6.9 ± 1.3 | 5.5 ± 0.8 | 5.3 ± 0.9 | 6.4 ± 0.4 | 7.2 ± 0.1 |
| **n** | 3 | 3 | 3 | 3 | 3 |

**Table B4**

**Physiologic Variables-24 Hour Animals**

| | Sample Time (Hours) | | | | | |
|---|---|---|---|---|---|---|
| | **0** | **2** | **4** | **8** | **12** | **24** |
| **pH** | 7.4 ± 0.1 | 7.4 ± 0.1 | 7.4 ± 0.1 | 7.4 ± 0.1 | 7.4 ± 0.1 | 7.5 ± 0.1 |
| **$pCO_2$(mmHg)** | 36.9 ± 3.4 | 39.8 ± 2.4 | 41.4 ± 1.5 | 40.8 ± 0.8 | 41.3 ±3.0 | 41.5 ±2.4 |
| **$pO_2$ (mmHg)** | 95.7 ± 4.2 | 96.8 ± 5.6 | 92.6 ± 45 | 96.5 ± 4.3 | 103.5±7.8 | 102.8±6.7 |
| **Temp.($^oC$)** | 37.3 ± 0.2 | 37.4 ± 0.2 | 37.7 ± 0.3 | 37.6 ± 0.3 | 37.4 ± 0.2 | 37.5 ± 0.4 |
| **MABP (mmHg)** | 111 ± 6 | 129 ± 9 | 112 ± 4 | 108 ± 8 | 107 ± 8 | 114 ± 5 |
| **Plasma Glucose(mM)** | 5.3 ± 0.5 | 7.2 ± 0.1 | 6.5 ± 0.2 | 44. ± 0.6 | 6.1 ± 0.2 | 5.7 ± 0.7 |
| **n** | 5 | 5 | 5 | 5 | 5 | 5 |

Tables show physiologic variables measured in 12 and 24 hour animals following intravenous administration of 200 $\mu$Ci (R,S)-[$^{125}$I]-QNB. Samples were taken immediately prior to (0) and 4 , 8 , 12 and 24 hours following (R,S)-[$^{125}$I]-QNB administration. Brains were removed and processed for autoradiography at 12 and 24 hours post-administration of tracer. There were no statistically significant differences in any of the variables measured at any of the time points between animals in the 2, 6, 12 and 24 hour groups (ANOVA). Data are presented as mean ± S.E.M.

**Table B5**

**Physiologic Variables-30 min Animals**

| | Sample Time (Mins) | |
|---|---|---|
| | 0 | 30 |
| pH | 7.4 ± 0.1 | 7.4 ± 0.1 |
| $pCO_2$ (mmHg) | 33.5 ± 3.5 | 31.0 ± 2.7 |
| $pO_2$ (mmHg) | 123.0 ± 13.2 | 113.7 ± 6.8 |
| Temp. (°C) | 37.4 ± 0.1 | 37.4 ± 0.1 |
| MABP (mmHg) | 118 ± 4 | 126 ± 4 |
| Plasma Glucose (mM) | 4.6 ± 0.5 | 5.1 ± 0.3 |
| n | 5 | 5 |

**Table B6**

**Physiologic Variables-1 Hour Animals**

| | Sample Time (Hours) | |
|---|---|---|
| | 0 | 1 |
| pH | 7.4 ± 0.1 | 7.39 ± 0.1 |
| $pCO_2$ (mmHg) | 37.6 ± 4.7 | 39.6 ± 2.5 |
| $pO_2$ (mmHg) | 115.6 ± 8.0 | 116.8 ± 3.3 |
| Temp. (°C) | 37.2 ± 0.1 | 37.3 ± 0.1 |
| MABP (mmHg) | 123 ± 7 | 131 ± 7 |
| Plasma Glucose (mM) | 8.2 ± 0.9 | 8.2 ± 0.3 |
| n | 5 | 5 |

Tables show physiologic variables measured in 30 mins and 1 hour animals following intravenc administration of (R,R)-[$^{125}$I]-QNB. Samples were taken immediately prior to (0), 30 mins anc hour following (R,R)-[$^{125}$I]-QNB administration. Brains were removed and processed for autoradiography 30 mins and 1 hour post-administration of tracer. There were no statistically significant differences in any of the variables measured at any of the time points between animal the 30 min , 1, 2 and 6 hour groups.Data are presented as mean ± S.E.M.

**Table B7**

**Physiologic Variables-2 Hour Animals**

| | Sample Time (Hours) | | |
|---|---|---|---|
| | 0 | 1 | 2 |
| pH | 7.43 ± 0.1 | 7.40 ± 0.1 | 7.43 ± 0.1 |
| $pCO_2$ (mmHg) | 36.4 ± 4.2 | 33.8 ± 3.3 | 34.8 ± 2.3 |
| $pO_2$ (mmHg) | 136.0 ± 6.0 | 140.2 ± 4.8 | 133.4 ± 8.6 |
| Temp. ($^oC$) | 37.3 ± 0.1 | 37.3 ± 0.1 | 37.3 ± 0.1 |
| MABP (mmHg) | 124 ± 1.3 | 121 ± 2 | 132 ± 6 |
| Plasma Glucose (mM) | 5.1 ± 0.5 | 5.9 ± 0.3 | 5.5 ± 0.8 |
| n | 5 | 5 | 5 |

**Table B8**

**Physiologic Variables-6 Hour Animals**

| | Sample Time (Hours) | | | |
|---|---|---|---|---|
| | 0 | 2 | 4 | 6 |
| pH | 7.43 ± 0.1 | 7.41 ± 0.1 | 7.43 ± 0.1 | 7.4 ± 0.1 |
| $pCO_2$(mmHg) | 34.4 ± 3.2 | 33.4 ± 3.7 | 36.0 ± 3.0 | 38.2 ± 2.6 |
| $pO_2$ (mmHg) | 122.6 ± 10.2 | 117.2 ± 7.8 | 128.2 ± 3.1 | 132.8 ± 10.4 |
| Temp. ($^oC$) | 37.3 ± 0.1 | 37.3 ± 0.1 | 37.3 ± 0.1 | 37.4 ± 0.1 |
| MABP (mmHg) | 120 ± 5 | 122 ± 8.4 | 120 ± 3.9 | 120 ± 2.8 |
| Plasma Glucose (mM) | 6.0 ± 1.1 | 5.2 ± 0.4 | 5.6 ± 0.7 | 5.1 ± 0.3 |
| n | 5 | 5 | 5 | 5 |

Tables show physiologic variables measured in 2 and 6 hour animals following intravenous administration of (R,R)-[$^{125}$I]-QNB. Samples were taken immediately prior to (0) , 1, 2, 4 and hours following (R,R)-[$^{125}$I]-QNB administration. Brains were removed and processed for autoradiography at 2 and 6 hours post-administration of tracer. There were no statistically significant differences in any of the variables measured at any of the time points between animal the 0.5, 1, 2 and 6 hour groups (ANOVA). Data are presented as mean ± S.E.M.

## Table B9

## (R,S)-[$^{125}$I]-QNB in Rat Brain
## Following Heptylphysostigmine (2mg/kg) Administration
## Physiologic Variables-2 Hour Animals

| | | Sample Time (Hours) | | | |
|---|---|---|---|---|---|
| | | Pre Infusion | 0 | 1 | 2 |
| pH | Veh | 7.5 ± 0.1 | 7.5 ± 0.1 | 7.5 ± 0.1 | 7.5 ± 0.1 |
| | HEP | 7.5 ± 0.1 | 7.4 ± 0.1 | 7.4 ± 0.1 | 7.4 ± 0.1 |
| $pCO_2$ (mmHg) | Veh | 37.0 ± 1.7 | 38.7 ± 1.5 | 37.0 ± 1.4 | 38.7 ± 1.2 |
| | HEP | 41.7 ± 1.2 | 37.7 ± 1.4 | 37.7 ± 1.7 | 45.7 ± 10 |
| $pO_2$ (mmHg) | Veh | 85.0 ± 3.7 | 89.7 ± 1.7 | 97.7 ± 1.9 | 96.7 ± 1.8 |
| | HEP | 86.0 ± 0.8 | 95.7 ± 4.5 | 109 ± 2.1 | 99.3 ± 1.5 |
| Temp. ($^0$C) | Veh | 37.0 ± 0.1 | 37.1 ± 0.2 | 37.1 ± 0.1 | 37.2 ± 0.2 |
| | HEP | 37.0 ± 0.1 | 37.0 ± 0.2 | 37.1 ± 0.2 | 37.0 ± 0.1 |
| MABP (mmHg) | Veh | 110 ± 1 | 110 ± 1 | 108 ± 8 | 112 ± 2 |
| | HEP | 113 ± 2 | 120 ± 1.3 | 128 ± 1 ** | 127 ± 2 |
| Plasma Glucose (mM) | Veh | 4.8 ± 0.7 | 4.9 ± 0.9 | 5.2 ± 1.1 | 5.7 ± 0.9 |
| | HEP | 5.2 ± 0.5 | 6.1 ± 0.8 | 7.3 ± 0.3 | 5.5 ± 0.6 |
| n | | 5 | 5 | 5 | 5 |

Samples were taken before vehicle/heptylphysostigmine administration (Pre-Infusion), immedia
prior to (0) and 1 and 2 hours following (R,S)-[$^{125}$I]-QNB administration. Brains were remove
and processed for autoradiography at 2 hours post-administration of tracer. **P <0.01 denotes
significant difference for statistical comparison between variables for vehicle and
heptylphysostigmine treated animals (ANOVA, Student's t-test with Bonferroni correction).Data
are presented as mean ± S.E.M.

**Table B10**

**(R,S)-[$^{125}$I]-QNB in Rat Brain**

**Following Heptylphysostigmine (2mg/kg) Administration**

**Physiologic Variables-24 Hour Animals**

| | | Sample Time (Hours) | | | | | | | |
|---|---|---|---|---|---|---|---|---|---|
| | | **Pre Infusion** | **0** | **1** | **2** | **4** | **8** | **12** | **24** |
| **pH** | **Veh** | 7.4 ± 0.1 | 7.4 ± 0.1 | 7.5 ± 0.1 | 7.5 ± 0.1 | 7.5 ± 0.1 | 7.5 ± 0.1 | 7.5 ± 0.1 | 7.5 ± 0.1<br>7.5 ± 0.1 |
| | **HEP** | 7.4 ± 0.1 | 7.5 ± 0.1 | 7.4 ± 0.1 | 7.5 ± 0.0 | 7.4 ± 0.1 | 7.5 ± 0.1 | 7.5 ± 0.1 | |
| **$pCO_2$ (mmHg)** | **Veh** | 42.7 ± 1.2 | 41.0 ± 0.5 | 41.0 ± 0.5 | 39.0 ± 0.8 | 35.3 ± 0.8 | 39.0 ± 1.2 | 40.1 ±0.9 | 42.5 ± 0.8<br>44.7 ± 0.7 |
| | **HEP** | 38.7 ± 1.6 | 32.5 ± 1.18 | 39.0 ± 1.78 | 36.0 ± 1.7 | 40.0 ± 0.7 | 43.7 ± 0.7 | 45.7 ± 0.9 | |
| **$pO_2$ (mmHg)** | **Veh** | 85.0 ± 2.3 | 97.7 ±1.9 | 97.7 ± 1.9 | 92.0 ± 0.6 | 100.0 ± 1.1 | 99.3 ± 1.4 | 98.7 ± 0.8 | 99.0 ± 0.7<br>96. ± 1.9 |
| | **HEP** | 88.0 ± 0.18 | 93.0 ± 1.4 | 107.0 ±1.6 | 101.0 ± 1.4 | 97.5 ± 0.5 | 92.3 ± 1.5 | 97.3 ± 1.5 | |
| **Temp. ($^oC$)** | **Veh** | 37.2 ± 0.3 | 37.2 ± 0.3 | 37.2 ± 0.3 | 37.1 ± 0.1 | 37.0 ± 0.2 | 37.1 ± 03 | 37.0 ± 0.1 | 37.0 ± 0.2<br>37.0 ± 0.1 |
| | **HEP** | 37.2 ± 0.3 | 37.3 ± 0.4 | 37.2 ± 0.4 | 37.3 ± 0.4 | 37.2 ± 0.2 | 37.0 ± 0.1 | 37.2 ± 0.3 | |
| **MABP** | **Veh** | 120 ± 0.1 | 118 ± 2 | 118 ± 2 | 118± 2 | 120 ± 1 | 118 ± 1 | 123 ± 1 | 117 ± 1<br>111 ± 2 |
| **(mmHg)** | **HEP** | 103 ± 1 | 105 ± 2 | 120 ± 2 | 120 ± 1 | 118 ± 2 | 120 ± 1 | 115 ± 2 | |
| **Plasma** | **Veh** | 5.3 ± 1.1 | 4.7 ±0.8 | 4.7 ± 0.8 | 5.7 ± 0.8 | 5.0 ± 0.6 | 5.2 ± 0.6 | 4.0 ± 0.2 | 4.3 ± 0.3<br>7.0 ± 0.8 |
| **Glucose (mM)** | **HEP** | 5.4 ± 0.6 | 5.0 ± 0.6 | 6.1 ± 0.8 | 5.0 ± 0.4 | 6.0 ± 1 | 5.6 ± 0.9 | 5.2 ± 0.6 | |
| **n** | | 5 | 5 | 5 | 5 | 5 | 5 | 5 | 5 |

Samples were taken before vehicle/ heptylphysostigmine administration (Pre-Infusion), immediately prior to (0) and 1, 2, 4, 8, 12 and 24 hours following (R,S)-[$^{125}$I]-QNB administration. Brains were removed and processed for autoradiography at 24 hours post-administration of tracer. Data are presented as mean ± S.E.M. There were no statistically significant differences in any of the variables measured at any of the time points between animals in the vehicle and heptylphysostigmine groups (ANOVA, Student's t-test with Bonferroni correction).

## Table B11

## (R,,R)-[$^{125}$I]-QNB in Rat Brain
## Following Heptylphysostigmine (2mg/kg) Administration

### Physiologic Variables-30min Animals

| | | Sample Time (Mins) | | |
|---|---|---|---|---|
| | | Pre Infusion | 0 | 30 |
| pH | Veh | 7.42 ± 0.1 | 7.42 ± 0.1 | 7.42 ± 0.1 |
| | HEP | 7.43 ± 0.1 | 7.42 ± 0.1 | 7.41 ± 0.1 |
| $pCO_2$ (mmHg) | Veh | 33.5 ± 3.5 | 40.7 ± 4.3 | 31.0 ± 2.7 |
| | HEP | 39.2 ± 1.9 | 32.0 ± 3.1 | 34.6 ± 3.5 |
| $pO_2$ (mmHg) | Veh | 123.0 ± 13.2 | 113 ± 8.1 | 113.7 ± 6.8 |
| | HEP | 131.0 ± 10.0 | 126.0 ± 3.6 | 139.8 ± 8.2 |
| Temp. ($^oC$) | Veh | 37.4 ± 4.7 | 37.4 ± 0.1 | 37.4 ± 0.1 |
| | HEP | 37.4 ± 0.1 | 37.4 ± 0.1 | 37.3 ± 0.1 |
| MABP (mmHg) | Veh | 118 ± 1 | 115 ± 4.8 | 126 ± 4 |
| | HEP | 121 ± 6 | 132 ± 3.4 | 138 ± 3.9 |
| Plasma Glucose (mM) | Veh | 4.6 ± 0.5 | 6.1 ± 0.7 | 5.1 ± 0.3 |
| | HEP | 5.7 ± 0.9 | 8.9 ± 1.8 | 8.6 ± 1.1 |
| n | | 5 | 5 | 5 |

Samples were taken before vehicle/ heptylphysostigmine administration (Pre-Infusion), immediately prior to (0) and 30 mins following (R,R)-[$^{125}$I]-QNB administration. Brains were removed and processed for autoradiography at 30 mins post-administration of tracer. There wer statisitcally significant differences between vehicle and heptylphyostigmine treated animals in the variables measured at any of the time points (ANOVA, Student's t-test with Bonferroni correction).Data are presented as mean ± S.E.M(n=5).

## Table B12

## (R,R)-[$^{125}$I]-QNB in Rat Brain
## Following Heptylphysostigmine (2mg/kg) Administration

### Physiologic Variables-1 Hour Animals

| | | Sample Time (Hours) | | |
|---|---|---|---|---|
| | | Pre Infusion | 0 | 1 |
| pH | Veh | 7.40 ± 0.1 | 7.40 ± 0.1 | 7.39 ± 0.1 |
| | HEP | 7.41 ± 0.1 | 7.41 ± 0.1 | 7.42 ± 0.1 |
| $pCO_2$ (mmHg) | Veh | 45.0 ± 3.0 | 37.6 ± 4.7 | 39.6 ± 2.5 |
| | HEP | 34.2 ± 5.0 | 34.4 ± 1.7 | 35.4 ± 1.2 |
| $pO_2$ (mmHg) | Veh | 118.0 ± 7.5 | 115.6 ± 8.1 | 116.8 ± 3.3 |
| | HEP | 120.4 ± 5.8 | 117.4 ± 2.5 | 131.8 ± 8.5 |
| Temp. ($^oC$) | Veh | 37.2 ± 0.1 | 37.2 ± 0.1 | 37.3 ± 0.1 |
| | HEP | 37.2 ± 0.1 | 37.2 ± 0.1 | 37.2 ± 0.1 |
| MABP (mmHg) | Veh | 124 ± 6 | 123 ± 7 | 131 ± 7 |
| | HEP | 107 ± 5 | 117 ± 3.7 | 126 ± 4 |
| Plasma Glucose (mM) | Veh | 5.8 ± 0.8 | 8.2 ± 0.9 | 8.2 ± 0.3 |
| | HEP | 4.2 ± 0.3 | 7.6 ± 1.1 * | 8.1 ± 0.4 ** |
| n | | 5 | 5 | 5 |

Samples were taken before vehicle/ heptylphysostigmine administration (Pre-Infusion), immediately prior to (0) and 1 hour following (R,R)-[$^{125}$I]-QNB administration. Brains were removed and processed for autoradiography at 1 hour post-administration of tracer.

*P < 0.05, **P <0.01 denotes significant difference for statistical comparison between pre- and post drug variables and comparision of pre-drug variables and variables measured 1 hour after tracer administration in heptylphysotigmine treated animals (ANOVA, Student's t-test with Bonferroni correction).Data are presented as mean ± S.E.M(n=5).

## Table B13

## (R,R)-[$^{125}$I]-QNB in Rat Brain Following Heptylphysostigmine (2mg/kg) Administration

### Physiologic Variables-2 Hour Animals

| | | Sample Time (Hours) | | | |
|---|---|---|---|---|---|
| | | Pre Infusion | 0 | 1 | 2 |
| pH | Veh | 7.44 ± 0.1 | 7.43 ± 0.1 | 7.44 ± 0.1 | 7.43 ± 0.1 |
| | HEP | 7.45 ± 0.1 | 7.43 ± 0.1 | 7.42 ± 0.1 | 7.42 ± 0.1 |
| $pCO_2$ (mmHg) | Veh | 43.0 ± 3.0 | 36.4 ± 4.2 | 33.8 ± 3.3 | 39.0 ± 2.3 |
| | HEP | 37.0 ± 4.2 | 29.0 ± 1.6 | 36.6 ± 2.1 | 29.8 ± 3.3 |
| $pO_2$ (mmHg) | Veh | 183.0 ± 9.0 | 136.0 ± 6.0 | 140.0 ± 4.8 | 147.0 ± 8.6 |
| | HEP | 128.0 ± 8.4 | 136.8 ±11.6 | 127.4 ± 7.4 | 128.4 ± 7.4 |
| Temp. ($^{o}$C) | Veh | 37.3 ± 0.1 | 37.3 ± 0.1 | 37.3 ± 0.1 | 37.2 ± 0.1 |
| | HEP | 37.2 ± 0.1 | 37.3 ± 0.1 | 37.2 ± 0.1 | 37.2 ± 0.1 |
| MABP (mmHg) | Veh | 120 ± 3 | 124 ± 1.3 | 124 ± 1.3 | 132 ± 5.6 |
| | HEP | 116 ± 7 | 124 ± 2 | 126 ± 1.8 | 117 ± 5 |
| Plasma Glucose (mM) | Veh | 5.9 ± 0.4 | 5.9 ± 1.1 | 5.9 ± 0.3 | 5.5 ± 0.8 |
| | HEP | 5.7 ± 0.7 | 9.0 ± 1 | 7.3 ± 1.3 | 7.8 ± 1.3 |
| n | | 5 | 5 | 5 | 5 |

Samples were taken before vehicle/ heptylphysostigmine administration (Pre-Infusion), immediately prior to (0), 1 and 2 hours following (R,R)-[$^{125}$I]-QNB administration. Brains we removed and processed for autoradiography at 2 hours post-administration of tracer. There were statistically significant differences between vehicle and heptylphyostigmine treated animals in the variables measured at any of the time points (ANOVA, Student's t-test with Bonferroni correction).Data are presented as mean ± S.E.M(n=5).

**Table B14**

**(R,R)-[$^{125}$I]-QNB in Rat Brain**

**Following Heptylphysostigmine (2mg/kg) Administration**

**Physiologic Variables-6 Hour Animals**

| | | Sample Time (Hours) | | | | | |
|---|---|---|---|---|---|---|---|
| | | **Pre Infusion** | **0** | **1** | **2** | **4** | **6** |
| **pH** | **Veh** | 7.43 ± 0.1 | 7.4 ± 0.1 | 7.41 ± 0.1 | 7.4 0± 0.1 | 7.43 ± 0.1 | 7.42 ± 0.1 |
| | **HEP** | 7.42 ± 0.1 | 7.42 ± 0.1 | 7.51 ± 0.11 | 7.40 ± 0.01 | 7.43 ± 0.1 | 7.43 ± 0.1 |
| **$pCO_2$ (mmHg)** | **Veh** | 38.6 ± 2.6 | 34.4 ± 3.2 | 33.4 ± 6.7 | 36.0 ± 3.0 | 38.2 ± 2.6 | 39.6 ± 3.0 |
| | **HEP** | 33.8 ± 1.7 | 32.0 ± 0.3 | 28.6 ± 3.0 | 40.4 ± 2.5 | 40.8 ± 1.4 | 31.8 ± 1.6 |
| **$pO_2$ (mmHg)** | **Veh** | 129.0 ± 5.4 | 122.6 ± 10.2 | 117.2 ± 7.7 | 128.2 ± 3.1 | 132.8 ± 10.4 | 119.0 ± 4.4 |
| | **HEP** | 123.4 ± 6.6 | 121.0 ± 8.6 | 126.6 ± 5.0 | 132.0 ± 3.3 | 129.8 ± 4.1 | 118.2 ± 3.2 |
| **Temp. ($^oC$)** | **Veh** | 37.4 ± 0.1 | 37.3 ± 0.1 | 37.3 ± 0.1 | 37.3 ± 0.1 | 37.4 ± 0.1 | 37.3 ± 0.1 |
| | **HEP** | 37.3 ± 0.1 | 37.2 ± 0.1 | 37.3 ± 0.1 | 37.4 ± 0.1 | 37.3 ± 0.1 | 37.3 ± 0.1 |
| **MABP** | **Veh** | 116 ± 5.3 | 120 ± 5 | 122 ± 8.4 | 120 ± 3.9 | 120 ± 2.8 | 122 ± 3 |
| **(mmHg)** | **HEP** | 118 ± 5.3 | 129 ± 8.7 | 131 ± 8.6 | 124 ± 5.5 | 130 ± 3.8 | 124 ± 3.8 |
| **Plasma** | **Veh** | 5.0 ± 0.4 | 6.0 ± 1.1 | 5.2 ± 0.4 | 5.6 ± 0.7 | 5.1 ± 0.3 | 5.1 ± 0.5 |
| **Glucose (mM)** | **HEP** | 6.5 ± 1.1 | 10.1 ± 0.9 * | 9.8 ± 1.6 ** | 7.6 ± 0.7 | 6.0 ± 0.4 | 5.5 ± 0.6 |
| **n** | | 5 | 5 | 5 | 5 | 5 | 5 |

Samples were taken before vehicle/ heptylphysostigmine administration (Pre-Infusion), immediately prior to (0), 1, 2, 4 and 6 hours following (R,R)-[$^{125}$I]-QNB administration. Brains were removed and processed for autoradiography at 6 hours post-administration of tracer.

*$P < 0.05$, **$P < 0.01$ denotes significant difference for statistical comparison between variables for vehcle and heptylphysostigmine treated animals (ANOVA, Student's t-test with Bonferroni correction).Data are presented as mean ± S.E.M(n=5).

## Table B15

## Regional Cerebral Blood Flow In The Conscious Rat Following Heptylphysostigmine Administration

### Physiologic Variables

| | Pre-Infusion | | Pre-CBF | |
|---|---|---|---|---|
| | **Vehicle** | **Heptyl.** | **Vehicle** | **Heptyl.** |
| **pH** | 7.43 ± 0.10 | 7.41 ± 0.023 | 7.47 ± 0.02 | 7.42 ± 0.1 |
| **pCO2 (mmHg)** | 44.7 ± 1.4 | 47.6 ± 1.0 | 37.8 ± 1.2 | 43.8 ± 1.9 |
| **pO2 (mmHg)** | 85.0 ± 2.8 | 88.8 ± 5.8 | 94.8 ± 4.6 | 109.8 ± 6.1 |
| **Temp. (0C)** | 36.7 ± 0.1 | 36.6 ± 0.2 | 37.0 ± 0.1 | 35.4 ± 0.6* |
| **MABP (mmHg)** | 121 ± 2 | 124 ± 1 | 129 ± 2 | 146 ± 6* †† |
| **Plasma Glucose (mM)** | 8.1 ± 0.5 | 10.0 ± 1.6 | 7.8 ± 0.3 | 20.2 ± 1.2*** ††† |
| **n** | *5* | *5* | *5* | *5* |

Samples were taken before vehicle/heptylphysostigmine administration (Pre-Infusion),and immediately prior to blood flow measurement (Pre-CBF). Brains were removed and processed for autoradiography at 2 hours post-administration of vehicle/heptylphysostigmine. Heptylphysostigmine produced a moderate fall in body temperature as well as significant increases in both mean artereial blood pressure and plasma glucose levels. *P <0.05, ***P <0.001 for statistical comaprison between heptylphysostigmine and vehicle treated animals. †† P <0.01, †††P <0.001 for statistical comparison between Pre-Infusion and Pre-CBF measurements in heptylphysostigmine treated animals. (ANOVA, Student's t-test with Bonferroni correction).Data are presented as mean ± S.E.M(n=5).

# APPENDIX C

**Heptylphysotigmine Produces a Prolonged Inhibition of AChE Activity in the Brain of Conscious Rat**

**Table C1**

**(R,S)-[$^{125}$I]-QNB: Semi-quantitative Histochemistry In Rat Brain Sections**

| | AChE ACTIVITY (Optical Density) | | | |
|---|---|---|---|---|
| **Region** | **2 Hours** | | **24 Hours** | |
| | Vehicle | Heptyl. | Vehicle | Heptyl. |
| **Frontal Cortex** | 0.039 ± 0.003 | 0.024 ± 0.008 | 0.043 ± 0.005 | 0.027 ± 0.008 |
| **Parietal Cortex** | 0.038 ± 0.002 | 0.016 ± 0.002*** | 0.042 ± 0.003 | 0.023 ± 0.006* |
| **Hippocampus CA 1** | 0.060 ± 0.003 | 0.023 ± 0.007** | 0.067 ± 0.050 | 0.050 ± 0.019 |
| **Cerebellar Cortex** | 0.017 ± 0.003 | 0.013 ± 0.001 | 0.018 ± 0.001 | 0.037 ± 0.023 |
| **n** | 5 | 5 | 5 | 5 |

**Table 1:** AChE enzyme activity measured by semi-quantitative histochemistry in sections of rat brain from vehicle and heptylphysotigmine treated animals at 2 and 24 hours in studies with (R,S)-[$^{125}$I]-QNB. Heptylphysostigmine administration reduces AChE activity in all regions analysed, with statistically significant reduction observed in the parietal cortex and CA1 of the hippocampus.

*P <0.05, **P <0.01 and ***P <0.001 Student's unpaired *t*-Test [n= 5 sections ].Data are expressed as mean ± S.E.M Optical Density as a measure of staining intensity.

**Heptylphyostigmine Produces a Prolonged Inhibition of AChE Activity in the Brain of Conscious Rat**

**Table C2**

**(R,R)-[$^{125}$I]-QNB: Semi-quantitative Histochemistry In Rat Brain Sections**

**ACHE ACTIVITY (Optical Density)**

| | 0.5 Hours | | 1 Hour | | 2 Hours | | 6 Hours | |
|---|---|---|---|---|---|---|---|---|
| **Region** | **Vehicle** | **Heptyl.** | **Vehicle** | **Heptyl.** | **Vehicle** | **Heptyl.** | **Vehicle** | **Heptyl.** |
| | | | | | | | | |
| **Frontal Cortex** | 0.042 ± 0.02 | 0.018 ± 0.03 *** | 0.046 ± 0.006 | 0.024 ± 0.005 * | 0.040 ± 0.006 | 0.024 ± 0.008 | 0.039 ± 0.004 | 0.034 ± 0.007 |
| **Parietal Cortex** | 0.039 ± 0.02 | 0.012 ± 0.010 * | 0.044 ± 0.009 | 0.018 ± 0.006 * | 0.043 ± 0.004 | 0.027 ± 0.003 * | 0.039 ± 0.007 | 0.029 ± 0.003 |
| **Hippocampus CA 1** | 0.066 ± 0.003 | 0.021 ± 0.006 *** | 0.069 ± 0.007 | 0.023 ± 0.008 ** | 0.064 ± 0.003 | 0.031 ± 0.008 ** | 0.067 ± 0.004 | 0.042 ± 0.010 * |
| **Cerebellar Cortex** | 0.019 ± 0.004 | 0.019 ± 0.008 * | 0.023 ± 0.003 | 0.017 ± 0.003 | 0.022 ± 0.007 | 0.016± 0.003 | 0.020 ± 0.009 | 0.019 ± 0.008 |
| **n** | 5 | 5 | 5 | 5 | 5 | 5 | 5 | 5 |

AChE enzyme activity measured by semi-quantitative histochemistry in sections of rat brain from vehicle and heptylphysotigmine treated animals at 0.5, 1, 2 and 6 hours in studies with (R,R)-[$^{125}$I]-QNB. Heptylphysostigmine administration reduces AChE activity in all regions analysed. Data are expressed as mean ± S.E.M Optical Density as a measure of staining intensity. *P <0.05, **P <0.01 and ***P <0.001 Student's unpaired *t*-Test [n= 5 sections ].

**Table C3**

**Effect of Heptylphysostigmine on AChE Activity *In Vitro***

| Region | (R,S)-[$^{125}$I]-QNB | | (R,R)-[$^{125}$I]-QNB | |
|---|---|---|---|---|
| | Control | Heptyl. (10-6M) | Control | Heptyl. (10-6M) |
| **Frontal Cortex** | 0.023 ± 0.002 | 0.0095 ± 0.002*** | 0.071 ± 0.028 | 0.011 ± 0.001*** |
| **Parietal Cortex** | 0.032 ± 0.003 | 0.0085 ± 0.002*** | 0.052 ± 0.019 | 0.002 ± 0.001* |
| **Cerebelar Cortex** | 0.018 ± 0.002 | 0.008 ± 0.002** | 0.031 ± 0.013 | 0.018 ± 0.003 |
| **n** | 6 | 6 | 6 | 6 |

Table shows AChE enzyme activity measured by semi-quantitative histochemistry in untreated (control) and heptylphysostigmine ($10^{-6}$M) treated sections of rat brain taken from *in vitro* displacement studies with (R,S)- and (R,R)-[$^{125}$I]-QNB. Heptylphysostigmine produces a profound reduction in enzyme activity at this concentration in all regions analysed. *P <0.05, **P <0.01 and ***P <0.001 for the statistical comparison between control and heptylphysostigmine treated sections (Student's unpaired t-test). Data are expressed as mean ± S.E. M Optical Density as a measure of staining intensity. n= number of sections analysed per region.

# APPENDIX D

## Table D1

## (R,,S)-[$^{125}$I]-QNB *In Vitro* Association Data

| | Total Binding (nM/g) | Non-specific Binding (nM/g) | Specific Binding (nM/g) |
|---|---|---|---|
| **Frontal Cortex** | | | |
| **1 min** | 10.58 ± 0.94 | 7.50 ± 0.76 | 3.00 ± 0.25 |
| **2 mins** | 12.08 ± 1.73 | 10.00 ± 2.18 | 2.80 ± 0.98 |
| **5 mins** | 14.75 ± 2.27 | 13.42 ± 1.58 | 1.33 ± 0.96 |
| **10 mins** | 21.33 ± 1.17 | 18.33 ± 1.39 | 2.85 ± 1.43 |
| **20 mins** | 39.40 ± 3.82 | 25.58 ± 2.97 | 13.83 ± 1.21 |
| **40 mins** | 66.08 ± 14.01 | 33.30 ± 1.31 | 31.92 ± 12.72 |
| **60 mins** | 85.58 ± 18.28 | 43.58 ± 6.01 | 42.00 ± 12.34 |
| **90 mins** | 109.00 ± 5.94 | 38.58 ± 8.30 | 70.50 ± 10.49 |
| **120 mins** | 96.58 ± 1.71 | 36.75 ± 1.28 | 59.83 ± 1.76 |
| | | | |
| **Parietal Cortex** | | | |
| **1 min** | 7.33 ± 0.08 | 4.09 ± 0.52 | 1.09 ± 0.46 |
| **2 mins** | 10.25 ± 1.38 | 6.83 ± 1.08 | 0.67 ± 0.30 |
| **5 mins** | 14.33 ± 2.34 | 9.67 ± 1.97 | 0.75 ± 0.38 |
| **10 mins** | 23.42 ± 0.71 | 12.33 ± 3.31 | 5.08 ± 2.60 |
| **20 mins** | 40.25 ± 6.39 | 20.67 ± 4.55 | 14.58 ± 2.90 |
| **40 mins** | 71.00 ± 18.90 | 38.33 ± 7.32 | 38.50 ± 12.13 |
| **60 mins** | 87.43 ± 23.91 | 41.77 ± 6.39 | 47.37 ± 17.9 |
| **90 mins** | 96.33 = 17.00 | 39.67 ± 6.67 | 57.5 ± 12.06 |
| **120 mins** | 90.42 ± 6.68 | 42.08 ± 6.45 | 53.33 ± 0.83 |
| | | | |
| **Caudate Nucleus** | | | |
| **1 min** | 6.92 ± 0.46 | 4.08 ± 0.79 | 0.83 ± 0.83 |
| **2 mins** | 9.33 ± 0.96 | 5.84 ± 0.68 | 1.18 ± 0.91 |
| **5 mins** | 13.33 ± 1.40 | 9.17 ± 1.170 | 1.42 ± 0.51 |
| **10 mins** | 17.88 ± 0.68 | 10.83 ± 0.22 | 1.75 ± 0.630 |
| **20 mins** | 24.25 ± 1.46 | 14.34 ± 1.160 | 4.33 ± 0.51 |
| **40 mins** | 34.08 ± 4.08 | 20.170 ± 1.30 | 8.92 ± 2.87 |
| **60 mins** | 45.42 ± 6.57 | 26.25 ± 3.11 | 11.17 ± 3.48 |
| **90 mins** | 58.25 ± 4.63 | 26.75 ± 5.67 | 24.02 ± 1.90 |
| **120 mins** | 59.83 ± 4.21 | 32.75 ± 3.67 | 21.25 ± 2.32 |
| | | | |
| **Cerebellar Cortex** | | | |
| **1 min** | 9.17 ± 1.42 | 4.17 ± 1.80 | 1.50 ± 0.52 |
| **2 mins** | 11.08 ± 1.76 | 3.17 ± 2.68 | 5.50± 2.65 |
| **5 mins** | 19.15 ± 2.08 | 12.42 ± 1.12 | 3.92 ± 2.65 |
| **10 mins** | 20.17 ± 3.47 | 7.58 ± 4.8 | 2.37 ± 1.30 |
| **20 mins** | 34.75 ± 9.72 | 30.42 ± 6.02 | 13.33 ± 7.7 |
| **40 mins** | 78.92 ± 22.96 | 51.17 ± 16.76 | 25.25 ± 13.65 |
| **60 mins** | 92.33 ± 23.49 | 36.85 ± 14.23 | 41.42 ± 15.31 |
| **90 mins** | 94.85 ± 28.49 | 44.17 ± 23.25 | 27.35 ± 5.55 |
| **120 mins** | 94.33 ± 16.61 | 46.75 ± 6.16 | 53.42 ± 10.67 |
| | | | |
| **n** | 3 | 3 | 3 |

*In vitro* association data for 0.1 nM (R,S)-[$^{125}$I]-QNB binding to rat brain sections over 120 mins. Table shows total, non-specific and specific binding to frontal cortex, parietal cortex, caudate nucleus and cerbellar cortex. Data are expressed as mean + S.E.M. nmols per g Brain. n= number of experiments.

## Table D2

## (R,R)-[$^{125}$I]-QNB *In Vitro* Association Data

| | Total Binding (nM/g) | Non-specific Binding (nM/g) | Specific Binding (nM/g) |
|---|---|---|---|
| **Frontal Cortex** | | | |
| **1 min** | 1.79 ± 130 | 1.58 ± 1.07 | 0.21 ± 0.21 |
| **2 mins** | 2.96 ± 1.08 | 2.33 ± 0.77 | 0.63 ± 0.34 |
| **5 mins** | 4.65 ± 0.80 | 3.45 ± 0.57 | 1.20 ± 0.36 |
| **10 mins** | 6.65 ± 0.50 | 5.74 ± 0.72 | 0.91 ± 0.28 |
| **20 mins** | 11.53 ± 1.55 | 7.07 ± 0.63 | 4.46 ± 1.88 |
| **40 mins** | 15.07 ± 7.54 | 7.69 ± 4.02 | 7.38 ± 3.91 |
| **60 mins** | 28.14 ± 3.04 | 11.91 ± 0.40 | 16.22 ± 3.17 |
| **90 mins** | 32.48 ± 4.59 | 12.88 ± 1.52 | 19.60 ± 5.77 |
| **120 mins** | 35.40 ± 2.85 | 13.83 ± 1.24 | 21.57 ± 4.00 |
| | | | |
| **Parietal Cortex** | | | |
| **1 min** | 1.58 ± 1.02 | 14.5 ± 0.91 | 0.13 ± 0.12 |
| **2 mins** | 2.84 ± 0.07 | 2.40 ± 0.50 | 0.44 ± 0.18 |
| **5 mins** | 4.63 ± 0.88 | 3.54 ± 0.60 | 1.08 ± 0.28 |
| **10 mins** | 7.02 ± 0.68 | 5.15 ± 0.07 | 1.87 ± 0.64 |
| **20 mins** | 8.99 ± 4.54 | 4.96 ± 2.49 | 4.03 ± 2.20 |
| **40 mins** | 15.46 ± 7.77 | 7.31 ± 3.67 | 8.14 ± 4.10 |
| **60 mins** | 27.61 ± 1.74 | 9.21 ± 1.00 | 18.40 ± 2.02 |
| **90 mins** | 34.96 ± 5.81 | 11.05 ± 1.78 | 23.9 ± 6.37 |
| **120 mins** | 38.38 ± 5.61 | 13.10 ± 2.53 | 25.28 ± 6.66 |
| | | | |
| **Caudate Nucleus** | | | |
| **1 min** | 1.55 ± 1.10 | 1.40 ± .92 | 0.15 ± 0.09 |
| **2 mins** | 2.77 ± 1.10 | 2.47 ± 0.72 | 0.29 ± 0.15 |
| **5 mins** | 4.74 ± 0.86 | 4.22 ± 0.68 | 0.51 ± 0.24 |
| **10 mins** | 6.94 ± 0.88 | 6.18 ± 0.95 | 0.75 ± 0.33 |
| **20 mins** | 9.98 ± 0.82 | 7.01 ± 0.67 | 2.97 ± 1.03 |
| **40 mins** | 9.50 ± 1.70 | 6.51 ± 3.29 | 2.99 ± 1.49 |
| **60 mins** | 16.53 ± 4.78 | 10.07 ± 0.17 | 6.47 ± 1.45 |
| **90 mins** | 20.80 ± 1.41 | 12.00 ± 1.58 | 8.83 ± 1.56 |
| **120 mins** | 23.40 ± 1.05 | 13.16 ± 1.45 | 10.24 ± 0.43 |
| | | | |
| **Cerebellar Cortex** | | | |
| **1 min** | 1.57 ± 0.95 | 1.43 ± 0.84 | 0.14 ± 0.12 |
| **2 mins** | 2.88 ± 0.95 | 2.44 ± 0.84 | 0.44 ± 0.12 |
| **5 mins** | 4.52 ± 0.44 | 3.56 ± 0.40 | 0.66 ± 0.08 |
| **10 mins** | 5.99 ± 0.64 | 4.86 ± 0.31 | 1.13 ± 0.40 |
| **20 mins** | 6.54 ± 0.36 | 4.65 ± 0.19 | 1.89 ± 0.18 |
| **40 mins** | 12.64 ± 3.30 | 7.98 ± 2.36 | 4.66 ± 0.95 |
| **60 mins** | 16.78 ± 6.42 | 10.52 ± 4.00 | 6.27 ± 2.49 |
| **90 mins** | 16.55 ± 0.44 | 10.54 ± 0.57 | 6.00 ± 0.86 |
| **120 mins** | 21.52 ± 0.92 | 12.28 ± 0.27 | 9.24 ± 1.04 |
| | | | |
| ***n*** | 3 | 3 | 3 |

*In vitro* association data for 0.2 nM (R,R)-[$^{125}$I]-QNB binding to rat brain sections over 120 mins. Table shows total, non-specific and specific binding to frontal cortex, parietal cortex, caudate nucleus and cerebellar cortex. Data are expressed as mean + S.E.M. nmols per g Brain. n= number of experiments.

## Table D3

## (R,S)-[$^{125}$I]-QNB *In Vitro* Saturation Data

| | Total Binding (nM/g) | Non-specific Binding (nM/g) | Specific Binding (nM/g) |
|---|---|---|---|
| **Frontal Cortex** | | | |
| **0.007 nM QNB** | 1.08 ± 0.20 | 0.82 ± 0.02 | 026 ± 0.06 |
| **0.01 nM QNB** | 1.93 ± 0.17 | 1.33 ± 0.18 | 0.60 ± 0.28 |
| **0.03 nM QNB** | 4.39 ± 0.39 | 2.56 ± 0.19 | 1.84 ± 0.29 |
| **0.05 nM QNB** | 5.89 ± 0.54 | 3.48 ± 0.21 | 2.41 ± 0.56 |
| **0.07 nM QNB** | 5.71 ± 0.97 | 3.37 ± 0.24 | 2.3 ± 0.95 |
| **0.1 nM QNB** | 6.47 ± 1.07 | 4.69 ± 0.84 | 1.78 ± 0.55 |
| | | | |
| **Parietal Cortex** | | | |
| **0.007 nM QNB** | 1.50 ± 0.29 | 0.79 ± 0.03 | 0.74 ± 0.27 |
| **0.01 nM QNB** | 2.16 ± 0.14 | 1.30 ± 0.21 | 0.86 ± 0.17 |
| **0.03 nM QNB** | 4.19 ± 0.36 | 2.25 ± 0.21 | 1.94 ± 0.42 |
| **0.05 nM QNB** | 5.98 ± 0.49 | 3.32 ± 0.13 | 2.66 ± 0.25 |
| **0.07 nM QNB** | 7.34 ± 2.74 | 3.34 ± 0.34 | 1.00 ± 1.2 |
| **0.1 nM QNB** | 7.50 ± 2.15 | 4.80 ± 1.37 | 2.70 ± 0.92 |
| | | | |
| **Caudate Nucleus** | | | |
| **0.007 nM QNB** | 1.00 ± 0.12 | 0.73 ± 0.05 | 0.27 ± 0.09 |
| **0.01 nM QNB** | 1.45 ± 0.10 | 0.88 ± 0.09 | 0.57 ± 0.11 |
| **0.03 nM QNB** | 2.83 ± 0.36 | 1.86 ± 0.20 | 0.97± 0.16 |
| **0.05 nM QNB** | 4.58 ± 0.23 | 3.05 ± 0.16 | 1.53 ± 0.12 |
| **0.07 nM QNB** | 5.03 ± 0.35 | 3.02 ± 0.03 | 2.00 ± 0.36 |
| **0.1 nM QNB** | 5.08 ± 0.46 | 3.65 ± 0.27 | 1.43 ± 0.47 |
| | | | |
| **Cerebellar Cortex** | | | |
| **0.007 nM QNB** | 0.88 ± 0.014 | 0.66 ± 0.15 | 0.22 ± 0.06 |
| **0.01 nM QNB** | 1.29 ± 0.13 | 0.91 ± 0.08 | 0.39 ± 0.06 |
| **0.03 nM QNB** | 2.82 ± 0.59 | 2.06 ± 0.27 | 0.77 ± 0.45 |
| **0.05 nM QNB** | 4.29 ± 0.24 | 2.98 ± 0.17 | 1.31 ± 0.12 |
| **0.07 nM QNB** | 4.77 ± 0.28 | 3.32 ± 0.25 | 1.45 ± 0.46 |
| **0.1 nM QNB** | 6..36 ± 1.28 | 4.00 ± 0.79 | 2.66 ± 0.58 |
| | | | |
| **n** | 3-4 | 3-4 | 3-4 |

*In vitro* saturation data for 0.007 nM to 0.1 nM (R,S)-[$^{125}$I]-QNB binding to rat brain sections. Table shows total, non-specific and specific binding to frontal cortex, parietal cortex, caudate nucleus and cerebellar cortex. Data are expressed as mean + S.E.M. nmols per g Brain. n= number of experiments.

## Table D4

## (R,R)-[$^{125}$I]-QNB *In Vitro* Saturation Data

| | Total Binding (nM/g) | Non-specific Binding (nM/g) | Specific Binding (nM/g) |
|---|---|---|---|
| **Frontal Cortex** | | | |
| **0.007 nM QNB** | 1.21 ± 0.11 | 0.50 ± 0.04 | 0.55 ± 0.05 |
| **0.01 nM QNB** | 2.38 ± 0.22 | 0.92 ± 0.14 | 1.61 ± 0.36 |
| **0.03 nM QNB** | 3.84 ±1.13 | 2.23 ± 0.29 | 2.36 ± 0.91 |
| **0.05 nM QNB** | 8.70 ± 1.63 | 2.93 ± 0.31 | 6.80 ± 1.50 |
| **0.07 nM QNB** | 8.19 ± 0.74 | 4.04 ± 0.23 | 4.86 ± 0.15 |
| **0.1 nM QNB** | 13.21 ± 2.45 | 6.91 ± 0.12 | 9.00 ± 1.27 |
| | | | |
| **Parietal Cortex** | | | |
| **0.007 nM QNB** | 1.05 ± 0.01 | 0.51 ± 0.02 | 0.54 ± 0.02 |
| **0.01 nM QNB** | 2.27 ± 0.15 | 0.71 ± 0.17 | 1.56 ± 0.32 |
| **0.03 nM QNB** | 5.32 ± 0.33 | 2.39 ± 0.33 | 2.92 ± 0.01 |
| **0.05 nM QNB** | 6.91 ± 0.76 | 4.78 ± 0.77 | 2.13 ± 1.53 |
| **0.07 nM QNB** | 10.43 ± 1.40 | 4.41 ± 0.69 | 6.01 ± 0.71 |
| **0.1 nM QNB** | 15.02 ± 0.70 | 6.70 ± 0.60 | 8.33 ± 1.29 |
| | | | |
| **Caudate Nucleus** | | | |
| **0.007 nM QNB** | 0.453 ± 0.03 | 0.39 ± 0.01 | 0.14 ± 0.04 |
| **0.01 nM QNB** | 0.96 ± 0.04 | 0.45 ± 0.07 | 0.51 ± 0.03 |
| **0.03 nM QNB** | 3.37 ± 0.43 | 2.10 ± 0.08 | 1.27 ± 0.35 |
| **0.05 nM QNB** | 6.25 ± 0.58 | 2.60 ± 0.01 | 3.65 ± 0.60 |
| **0.07 nM QNB** | 5.11 ± 0.38 | 2.92 ± 0.29 | 2.18 ± 0.09 |
| **0.1 nM QNB** | 10.45 ± 1.34 | 5.00 ± 0.36 | 5.45 ± 1.70 |
| | | | |
| **Cerebellar Cortex** | | | |
| **0.007 nM QNB** | 0.74 ± 0.02 | 0.59 ± 0.01 | 0.59 ± 0.01 |
| **0.01 nM QNB** | 0.80 ± 0.03 | 0.57 ± 0.03 | 0.57 ± 0.03 |
| **0.03 nM QNB** | 2.84 ± 0.32 | 2.61 ± 0.26 | 2.61 ± 0.26 |
| **0.05 nM QNB** | 4.86 ± 0.47 | 3.28 ± 0.64 | 3.28 ± 0.64 |
| **0.07 nM QNB** | 5.03 ± 1.25 | 3.61 = 0.63 | 3.61 ± 0.63 |
| **0.1 nM QNB** | 8.76 ± 1.60 | 5.67 ± 1.85 | 5.67 ± 1.85 |
| | | | |
| **n** | 3 | 3 | 3 |

*In vitro* saturation data for 0.007 nM to 0.1 nM (R,R)-[$^{125}$I]-QNB binding to rat brain sections. Table shows total, non-specific and specific binding to frontal cortex, parietal cortex, caudate nucleus and cerbellar cortex. Data are expressed as mean + S.E.M. nmols per g Brain. n= number of experiments.

## Table D5

## (R,S)-[$^{125}$I]-QNB In *Vitro* Displacement Data
## Effect of Acetyl choline On Binding to Rat Brain Sections
## In The Presence Of Heptylphysostigmine

| | Total Binding (nM/g) | Non-specific Binding (nM/g) | Specific Binding (nM/g) |
|---|---|---|---|
| **Frontal Cortex** | | | |
| Control | 120.6 ± 12.9 | 76.33 ± 21.88 | 50.0 ± 16.2 |
| $10^{-5}$M Ach | 115.6 ± 12.66 | 6.3.1 ± 8.77 | 58.8 ± 13.3 |
| $10^{-4}$M Ach | 106.3 ± 20.3 | 5.1.3 ± 13.22 | 55.0 ± 11.9 |
| $10^{-3}$M ACh | 109.4 ± 15.0 | 61.3 ± 7.5 | 48.1 ± 7.7 |
| $10^{-2}$M ACh | 14.4 ± 21.1 | 70.0 ± 14.0 | 45.6 ± 10.5 |
| | | | |
| **Parietal Cortex** | | | |
| Control | 91.3 ± 11.4 | 5.2.5 ± 5.9 | 38.8 ± 16.5 |
| $10^{-5}$M Ach | 92.5 ± 17.3 | 5.13 ± 10.7 | 41.3 ± 7.4 |
| $10^{-4}$M Ach | 93.1 ± 10.8 | 61.3 ± 11.0 | 21.3 ± 8.6 |
| $10^{-3}$M ACh | 96.9 ± 12.8 | 53.1 ± 4.3 | 33.8 ± 9.9 |
| $10^{-2}$M ACh | 107.5 ± 15.0 | 51.3 ± 3.9 | 56.3 ± 11.7 |
| | | | |
| **Cerebellar Cortex** | | | |
| Control | 108.8 ± 22.3 | 78.8 ± 11.6 | 30.0 ± 11.9 |
| $10^{-5}$M Ach | 157.5 ± 10.5 | 91.9 ± 16.9 | 64.4 ± 11.1 |
| $10^{-4}$M Ach | 113.1 + 11.4 | 73.8 + 9.9 | 39.4 + 9.4 |
| $10^{-3}$M ACh | 139.4 ± 15.1 | 90.0 ± 13.7 | 49.4 ± 12.6 |
| $10^{-2}$M ACh | 126.3 ± 9.4 | 93.1 ± 15.8 | 35.0 ± 11.7 |
| n | 4 | 4 | 4 |

Effect of $10^{-5}$ to $10^{-2}$ M Acetylcholine on the binding of (R,S)-[ $^{125}$I]-QNB to 20$\mu$m coronal rat brain sections in vitro, in the presence of $10^{-6}$M heptylphysostigmine. Table shows Total, Non-specific and Specific binding for frontal, parietal and cerebellar cortices. Acetylcholine failed to displace specicifc binding over this concentration range in any of the regions analysed. Data are expressed as mean ± S.E.M. nM per g brain, n= number of experiments performed.

## Table D6

### (R,R)-[$^{125}$I]-QNB In *Vitro* Displacement Data
### Effect of Acetyl choline On Binding to Rat Brain Sections
### In The Presence Of Heptylphysostigmine

| | Total Binding (nM/g) | Non-specific Binding (nM/g) | Specific Binding (nM/g) |
|---|---|---|---|
| **Frontal Cortex** | | | |
| Control | 83.54 ± 25.89 | 48.68 ± 17.41 | 34.86 ± 11.35 |
| $10^{-6}$M Ach | 102.86 ± 44.43 | 58.96 ± 21.21 | 43.90 ± 23.95 |
| $10^{-4}$M Ach | 102.66 ± 44.61 | 50.44 ± 18.69 | 52.22 ± 25.97 |
| $10^{-3}$M ACh | 88.07 ± 31.75 | 54.74 ± 18.78 | 33.33 ± 13.25 |
| | | | |
| **Parietal Cortex** | | | |
| Control | 74.22 ± 20.71 | 33.11 ± 14.91 | 41.11 ± 14.99 |
| $10^{-6}$M Ach | 78.62 ± 26.06 | 47.92 ± 16.15 | 30.70 ± 11.11 |
| $10^{-4}$M Ach | 103.91 ± 8.93 | 64.84 ± 1.91 | 39.07 ± 7.02 |
| $10^{-3}$M ACh | 72.37 ± 24.77 | 42.81 ± 15.39 | 29.56 ± 9.72 |
| | | | |
| **Cerebellar Cortex** | | | |
| Control | 105.91 ± 42.56 | 85.70 ± 43.81 | 20.21 ± 9.58 |
| $10^{-6}$M Ach | 128.21 ± 43.41 | 97.60 ± 41.78 | 30.61 ± 7.78 |
| $10^{-4}$M Ach | 124.58 ± 46.90 | 57.97 ± 22.80 | 66.61 ± 24.19 |
| $10^{-3}$M ACh | 94.64 ± 30.49 | 52.24 ± 18.07 | 42.40 ± 14.18 |
| n | 3 | 3 | 3 |

Effect of $10^{-6}$ to $10^{-3}$ M Acetylcholine on the binding of (R,R)-[ $^{125}$I]-QNB(0.2 nM) to 20$\mu$m coronal rat brain sections in vitro, in the presence of $10^{-6}$M heptylphysostigmine. Table shows Total, Non-specific and Specific binding for frontal, parietal and cerebellar cortices. Acetylcholine failed to displace specific binding over this concentration range in any of the regions analysed. Data are expressed as mean ± S.E.M. nM per g brain, n= number of experiments performed.

## Table D7

### (R,R)-[$^{125}$I]-QNB In *Vitro* Displacement Data
### Effect of Heptylphysostigmine On Binding to Rat Brain Sections

| | Total Binding (nM/g) | Non-specific Binding (nM/g) | Specific Binding (nM/g) |
|---|---|---|---|
| **Frontal Cortex** | | | |
| Control | 83.54 ± 25.89 | 48.68 ± 17.41 | 34.86 ± 11.35 |
| $10^{-6}$M HEP | 89.22 ± 22.31 | 50.89 ± 16.60 | 38.33 ± 7.21 |
| $10^{-4}$M HEP | 64.48 ± 18.11 | 48.59 ± 15.28 | 15.89 ± 2.86 |
| $10^{-3}$M HEP | 26.98 ± 10.15 | 25.68 ± 9.34 | 1.30 ± 1.01* |
| | | | |
| **Parietal Cortex** | | | |
| Control | 74.22 ± 20.71 | 33.11 ± 14.91 | 41.11 ± 14.99 |
| $10^{-6}$M HEP | 69.92 ± 17.71 | 40.34 ± 10.47 | 29.58 ±7.77 |
| $10^{-4}$M HEP | 50.42 ± 13.91 | 35.55 ± 10.02 | 14.87 ± 3.91 |
| $10^{-3}$M HEP | 24.06 ± 8.19 | 23.03 ± 8.19 | 1.03 ± 0.51* |
| | | | |
| **Cerebellar Cortex** | | | |
| Control | 105.91 ± 42.56 | 85.70 ± 43.81 | 20.21 ± 9.58 |
| $10^{-6}$M HEP | 75.82 ± 16.05 | 40.40 ± 13.72 | 35.42 ± 9.27 |
| $10^{-4}$M HEP | 55.84 ± 18.98 | 48.62 ± 21.89 | 7.22 ± 3.88 |
| $10^{-3}$M HEP | 23.34 ± 9.52 | 21.46 ± 7.86 | 1.88 ± 1.79 |
| n | 3 | 3 | 3 |

Effect of $10^{-6}$ to $10^{-3}$ M Heptylphysostigmine on the binding of (R,R)-[ $^{125}$I]-QNB (0.2 nM) to 20$\mu$m coronal rat brain sections *in vitro*. Table shows Total, Non-specific and Specific binding for frontal, parietal and cerebellar cortices. Heptylphysostigmine produces profound reductions in (R,R)-[ $^{125}$I]-QNB binding at $10^{-3}$ M. *P <0.05 for the statisitcal comparison between specific binding in control and heptylphysostigmine treated sections (ANOVA, Student's unpaired t-test with Bonferroni correction). Data are expressed as mean ± S.E.M. nM per g brain, n= number of experiments performed.

## PUBLISHED ABSRACTS

Effect Of Heptylphysostigmine Administration On (R,S)-[$^{125}$I]-QNB Binding In Vivo (1997). Paterson, D.S., Owens, J., Tebbutt, A.A. and McCulloch, J. *XVIII International Symposium On Cerebral Blood Flow And Metabolism*, Baltimore, U.S.A. 112 Supplement 1 S1